



PACIFIC EARTHQUAKE ENGINEERING RESEARCH CENTER

Performance-Based Earthquake Engineering Design Evaluation Procedure for Bridge Foundations Undergoing Liquefaction-Induced Lateral Ground Displacement

Christian A. Ledezma

and

Jonathan D. Bray

University of California, Berkeley

Performance-Based Earthquake Engineering Design Evaluation Procedure for Bridge Foundations Undergoing Liquefaction-Induced Lateral Ground Displacement

Christian A. Ledezma

and

Jonathan D. Bray, Ph.D., P.E.

Department of Civil and Environmental Engineering
University of California, Berkeley

PEER Report 2008/05
Pacific Earthquake Engineering Research Center
College of Engineering
University of California, Berkeley

August 2008

ABSTRACT

Liquefaction-induced lateral ground displacement has caused significant damage to pile foundations during past earthquakes. Ground displacements due to liquefaction can impose large forces on the overlying structure and large bending moments in the laterally displaced piles. Pile foundations, however, can be designed to withstand the displacement and forces induced by lateral ground displacement. Piles may actually “pin” the upper layer of soil that would normally spread atop the liquefied layer below it into the stronger soils below the liquefiable soil layer. This phenomenon is known as the “pile-pinning” effect. Piles have been designed as “pins” across liquefiable layers in a number of projects, and this design methodology was standardized in the U.S. bridge design guidance document MCEER/ATC-49-1. A number of simplifying assumptions were made in developing this design procedure, and several of these assumptions warrant re-evaluation. In this report, some of the key assumptions involved in evaluating the pile-pinning effect are critiqued, and a simplified probabilistic design framework is proposed for evaluating the effects of liquefaction-induced displacement on pile foundations of bridge structures. Primary sources of uncertainty are incorporated in the proposed procedure so that it is compatible with the Pacific Earthquake Engineering Research (PEER) Center performance-based earthquake engineering (PBEE) framework.

A detailed description of the problem and of the current approach to evaluating liquefaction-induced bridge damage is first presented. The PEER-PBEE methodology is described, with emphasis on the components of the method that are more pertinent to the problem under study. Several preliminary evaluations are performed before the proposed simplified procedure is applied. These preliminary assessments include the estimation of the seismic hazard at the site, a liquefaction triggering assessment, and an evaluation of the liquefaction-induced flow failure potential at the site.

The details of the application of the PEER-PBEE methodology to the case of bridges founded on piles affected by liquefaction-induced lateral ground displacement are then provided. A procedure to estimate residual lateral displacements at the abutments for a given intensity of the ground motion is described, followed by a discussion of the structural models that can be used to evaluate how these displacements influence the response of the bridge superstructure. With these assessments of bridge response, which are couched in probabilistic terms with key sources of uncertainty characterized, well-defined damage states of the bridge system and its

components can be estimated. Lastly, procedures for the final estimates of repair costs and downtimes for the most likely damage conditions are presented.

The proposed procedure is applied to a realistic bridge example that was developed by PEER and Caltrans engineers to illustrate the use of the method and the insights that can be garnered from its application to a bridge evaluation at a site with potentially liquefiable soil. Three alternative models are available in the estimation of repair cost ratios and downtimes for the different hazard levels included in the analysis. They are the first-order reliability method, the point estimate method, and the simplified coupled model. Some of the most useful insights developed through the application of the proposed method are the identification and quantification of the parameters most affecting the uncertainty in the assessment of the seismic performance of a bridge. The ground motion hazard, which was defined by the spectral acceleration at the degraded period of the potential sliding mass at the abutments, is the most important source of uncertainty. It is followed by the uncertainty in estimating seismic displacement at a specific ground motion hazard level and the uncertainty in estimating the residual undrained shear strength of the liquefied soil.

The proposed simplified procedure is validated through its application to three important “case” histories: Landing Road bridge (1987 Edgecumbe earthquake), Showa bridge (1964 Niigata earthquake), and one centrifuge model test performed at UC Davis. The results from this procedure compare well with the observations from these cases, and they are also consistent with the results from an advanced finite element analyses performed by the University of Washington research team. Lastly, a procedure to incorporate ground motion time histories is described, and findings from the study and recommendations for future work are summarized.

A simplified “user’s guide” that summarizes the proposed procedure follows this abstract.

ACKNOWLEDGMENTS

This work was supported by the Earthquake Engineering Research Centers Program of the National Science Foundation under NSF Award Number EEC-9701568 through the Pacific Earthquake Engineering Research Center (PEER) under subaward Project ID: 2422006. Partial funding of this project through PEER by Caltrans was also provided. Any opinions, findings, and conclusion or recommendations expressed in this material are those of the authors and do not necessarily reflect those of the National Science Foundation.

Discussions on the application of the PEER-PBEE methodology with Professor Armen Der Kiureghian of UC Berkeley and with Professor Kevin Mackie of the University of Central Florida were invaluable. Additionally, discussions with other fellow PEER researchers Professors Ross Boulanger of UC Davis, Geoff Martin of USC, Pedro Arduino and Steve Kramer of the University of Washington, Scott Ashford of Oregon State University, Ahmed Elgamal of UCSD, and Božidar Stojadinović of UC Berkeley were also invaluable. Caltrans engineers Tom Shantz, Steve Sahs, Michael Keever, and Mark Yashinsky were of great help in reviewing this work and in developing estimates of the expected damage and consequences at specified levels of residual seismic displacement.

CONTENTS

ABSTRACT.....	iii
ACKNOWLEDGMENTS.....	v
TABLE OF CONTENTS.....	vii
LIST OF FIGURES.....	xiii
LIST OF TABLES.....	xvii
USER’S GUIDE TO AN EVALUATION PROCEDURE FOR ASSESSING BRIDGE DAMAGE DUE TO LIQUEFACTION-INDUCED LATERAL GROUND DISPLACEMENT.....	G1
1 OVERVIEW.....	G1
2 ASSUMPTIONS AND LIMITATIONS.....	G1
3 INPUT PARAMETERS.....	G2
4 OUTPUT PARAMETERS.....	G2
5 PRELIMINARY ASSESSMENT.....	G2
5.1 Liquefaction Evaluation.....	G2
5.2 Flow Failure Evaluation.....	G3
5.3 Passive Forces versus Structural Capacity.....	G4
6 PRIMARY ASSESSMENT.....	G5
6.1 Relationship between Yield Coefficient and Equivalent Undrained Shear Strength.....	G7
6.2 Shear Force in Piles.....	G7
6.3 Passive Reaction at the Abutment.....	G8
6.4 Base Area.....	G8
7 INCORPORATION OF UNCERTAINTY.....	G9
8 EVALUATION OF DOWNTIMES AND REPAIR COSTS.....	G9
9 EXCEL SPREADSHEET.....	G11
1 INTRODUCTION.....	1
1.1 Problem Studied.....	1
1.2 Current Approach to Evaluating Liquefaction-Induced Bridge Damage.....	3
1.3 PEER-PBEE Methodology.....	6
2 PRELIMINARY ASSESSMENT.....	9
2.1 Seismic Hazard.....	9
2.1.1 Uniform Hazard Spectra.....	11
2.1.2 De-aggregation of Hazard.....	12
2.2 Liquefaction Evaluation.....	12

2.2.1	Overburden Corrected SPT Value	15
2.2.2	Influence of Fines Content.....	15
2.2.3	Magnitude Scaling Factor	16
2.2.4	Correction for Low and High Overburden Stresses.....	16
2.2.5	Other Correction Factors.....	17
2.3	Flow Failure	18
2.4	Passive Soil Forces versus Ultimate Structural Resistance.....	21
3	PROBABILISTIC EVALUATION OF SEISMIC LATERAL DISPLACEMENT	21
3.1	Lateral Displacement as Engineering Demand Parameter.....	21
3.1.1	Estimation of Residual Lateral Displacement.....	22
3.1.1.1	Deterministic Estimation of Residual Lateral Displacement at Abutments.....	22
3.1.1.2	Sources and Characterization of Uncertainty	27
3.1.1.3	Procedures to Calculate Probability of Exceeding Engineering Parameter Threshold, Given Intensity Measure	32
3.2	Derived Engineering Demand Parameters.....	35
3.2.1	Decoupled Models	35
3.2.2	Coupled Model.....	37
4	PROBABILISTIC EVALUATION OF BRIDGE DAMAGE.....	39
4.1	Damage to Abutments.....	39
4.2	Damage to Columns.....	40
4.3	Damage to Piles	41
5	PROBABILISTIC EVALUATION OF CONSEQUENCES.....	43
5.1	Repair Costs	43
5.1.1	Simplified Approach	43
5.1.2	Component-Based Approach	47
5.2	Downtimes	49
5.2.1	Simplified Approach	49
5.2.2	Component-Based Approach	49
6	BRIDGE EVALUATION EXAMPLE	51
6.1	General.....	51

6.2	Assumptions.....	53
6.3	Calculations.....	54
6.3.1	Seismic Hazard.....	54
6.3.2	Liquefaction Assessment	57
6.3.3	Flow Failure Assessment	57
6.3.4	Passive Soil Forces versus Ultimate Structural Resistance.....	59
6.3.4.1	Intermediate Piers	59
6.3.4.2	Abutment	60
6.3.5	Vertical Stresses	60
6.3.6	Initial Fundamental Period of Potential Sliding Mass	61
6.3.7	Yield Coefficient as a Function of Equivalent Undrained Shear Strength of Critical Layer	63
6.3.8	Size of Potential Failure Surface.....	65
6.3.9	Ground Motion Intensity.....	66
6.3.10	Passive Reaction	66
6.3.11	Probability of Liquefaction	67
6.4	Results Using First-Order Reliability Method (FORM).....	67
6.5	Results Using Point Estimate Method (PEM).....	72
6.6	Results Using Simplified Coupled Model	74
6.6.1	Properties	74
6.6.2	Input	75
6.6.3	Results.....	76
7	SENSITIVITY ANALYSIS	81
7.1	Results.....	83
7.2	Comments	87
8	VALIDATION OF SIMPLIFIED APPROACH	89
8.1	Landing Road Bridge during 1987 Edgecumbe Earthquake.....	89
8.1.1	1987 Edgecumbe Earthquake.....	89
8.1.2	Landing Road Bridge	93
8.1.3	Soil Profile	94
8.1.4	Preliminary Calculations.....	94

8.1.4.1	Passive Reaction at Abutment	95
8.1.4.2	Shear Force in Piles	95
8.1.4.3	Residual Undrained Shear Strength of Liquefied Soil	95
8.1.4.4	Equivalent Undrained Shear Strength from Passive Reaction and Piles Shear Force	96
8.1.4.5	Stability Analysis.....	96
8.1.5	Results Using Simplified Approach.....	97
8.1.5.1	Initial Fundamental Period of Potential Sliding Mass.....	97
8.1.6	Results.....	99
8.1.6.1	Damage Estimation.....	99
8.1.6.2	Sensitivity Analysis	100
8.2	Showa Bridge during 1964 Niigata, Japan, Earthquake	101
8.2.1	1964 Niigata, Japan, Earthquake.....	101
8.2.2	Showa Bridge.....	103
8.2.3	Soil Profile	105
8.2.4	Results Using Simplified Approach.....	106
8.3	Centrifuge Tests	110
8.3.1	Introduction.....	110
8.3.2	Foundation Properties	110
8.3.3	Soil Properties	111
8.3.4	Input Motions.....	112
8.3.5	Results Using Simplified Approach.....	112
9	OTHER ISSUES.....	117
9.1	Comparison with Results from Advanced Finite Element Analysis.....	117
9.2	Incorporation of Ground Motion Time Histories.....	121
10	CONCLUSIONS.....	123
10.1	Summary	123
10.2	Principal Findings	123
10.3	Future Research.....	125
	REFERENCES.....	127
	APPENDIX A: REPRESENTATIVE MATLAB ROUTINES	133

APPENDIX B: PILES DESIGN.....141
APPENDIX C: ULTIMATE CAPACITY CALCULATION SHEET—PYCAPSI.....161

LIST OF FIGURES

Figure 1.....	G1
Figure 2.....	G5
Figure 3.....	G6
Figure 4.....	G8
Figure 5.....	G11
Fig. 1.1 “Pile-pinning” effect for case of pile locked into both soil above and below liquefiable soil layer	2
Fig. 2.1 SPT clean-sand base curve for magnitude 7.5 earthquakes with data from liquefaction case histories (after Youd et al. 2001, modified from Seed et al. 1985).....	14
Fig. 2.2 Passive soil forces versus ultimate structural resistance at piers (modified from Berrill et al. 2001).....	19
Fig. 2.3 Passive soil forces versus ultimate structural resistance at abutments	19
Fig. 3.1 Estimation of initial fundamental period of potential sliding mass (T_s).....	23
Fig. 3.2 Passive reaction versus deflection at abutments (after Caltrans 2006).....	26
Fig. 3.3 Mean estimates of S_{ur} / σ_{vc}' ratios from different methods	28
Fig. 3.4 Dispersion in estimates of S_{ur} / σ_{vc}' ratios from different methods.....	29
Fig. 3.5 Structural model to estimate lateral displacement of intermediate piers’ pile caps from displacement of abutment pile caps	35
Fig. 3.6 Structural model to estimate pile-cap rotation as function of lateral deformation	36
Fig. 3.7 Simplified 2D structural model	37
Fig. 3.8 Schematic representation of simplified coupled model.....	37
Fig. 4.1 Abutment damage states as function of residual relative lateral deformation in longitudinal direction.....	40
Fig. 4.2 Column repair decisions as function of residual tangential drift.....	41
Fig. 4.3 Piles damage states as function of pile cap lateral displacement.....	42
Fig. 5.1 Bridge damage as function of residual lateral displacement	44
Fig. 5.2 Repair cost ratio distribution given damage state considering low (gray bars) and high (black bars) uncertainty	46
Fig. 5.3 Repair cost ratio cumulative distribution given damage state considering low (continuous line) and high (dashed lines) uncertainty.....	47

Fig. 6.1	Example bridge profile	52
Fig. 6.2	Piles at interior bents—dimensions and properties	52
Fig. 6.3	Piles at abutments—dimensions and properties	52
Fig. 6.4	Left abutment—soil profile and dimensions (not to scale)	53
Fig. 6.5	Right abutment—soil profile and dimensions (not to scale)	53
Fig. 6.6	Uniform hazard spectra, 5% damping, at site	56
Fig. 6.7	Factors of safety against liquefaction	57
Fig. 6.8	Post-liquefaction stability analysis of left abutment ($FS = 1.37, k_y = 0.11$)	58
Fig. 6.9	Post-liquefaction stability analysis of right abutment ($FS = 1.21, k_y = 0.055$)	59
Fig. 6.10	Representative soil column of potential sliding mass at left abutment	61
Fig. 6.11	Representative soil column of potential sliding mass at right abutment	62
Fig. 6.12	Yield coefficient (k_y) versus equivalent total residual undrained shear strength (S_{ur}) relationship for cases with liquefaction	64
Fig. 6.13	Yield coefficient (k_y) versus equivalent total residual undrained shear strength (S_u) relationship for cases without liquefaction	64
Fig. 6.14	Effect of residual undrained shear strength on base length of potential sliding mass	65
Fig. 6.15	Passive reaction versus displacement	66
Fig. 6.16	Probability of exceeding lateral displacement threshold (d) for different hazard levels. In top figures, black symbols denote cases with liquefaction and white symbols denote cases without liquefaction	68
Fig. 6.17	Damage states using FORM	69
Fig. 6.18	Repair cost ratios using FORM—low uncertainty	70
Fig. 6.19	Repair cost ratios using FORM—high uncertainty	71
Fig. 6.20	Damage states using PEM	73
Fig. 6.21	Deformed shape of bridge from OpenSees model	76
Fig. 6.22	Repair cost ratios using simplified coupled model	79
Fig. 6.23	Contribution to expected cost of repair actions for different hazard levels	79
Fig. 7.1	Relative importance of random variables for different hazard and displacement levels. Upper and bottom figures correspond to results for left and right abutments, respectively	84

Fig. 7.2	Normalized relative sensitivity ($\hat{\delta}$) of probability $p_f = P(D > d)$ to variations in mean of random variables for different hazard and displacement levels. Upper and bottom figures correspond to results for left and right abutments, respectively	85
Fig. 7.3	Normalized relative sensitivity ($\hat{\eta}$) of probability $p_f = P(D > d)$ to variations in standard deviation of random variables for different hazard and displacement levels. Upper and bottom figures correspond to results for left and right abutments, respectively.....	86
Fig. 8.1	Epicenter of 1987 Edgecumbe earthquake, Landing Road bridge, and Matahina dam.	90
Fig. 8.2	Acceleration time series and 5%-damping response spectrum of Matahina dam station (Source: PEER NGA database).....	91
Fig. 8.3	Landing Road bridge—simplified SPT and shear wave velocity profiles	92
Fig. 8.4	Distance and site condition correction factor as function of period	93
Fig. 8.5	Schematic elevation of Landing Road bridge (after Berrill et al. 2001)	94
Fig. 8.6	Potential failure mass at north abutment, considering contribution of passive reaction and piles shear force	96
Fig. 8.7	Equivalent residual undrained shear strength versus yield coefficient.....	98
Fig. 8.8	Probability of exceeding threshold residual lateral displacement (d) at north abutment of Landing Road bridge, given intensity of 1987, $M_w=6.6$ Edgecumbe earthquake in New Zealand	99
Fig. 8.9	Probability of bridge being in damage states of Negligible (N), Small (S), Moderate (M), Large (L), and Collapse (C)	100
Fig. 8.10	Relative importance of, and $P(D > d)$'s sensitivity with respect to, three random variables, as function of expected level of residual lateral displacement. Continuous line is for S_{ur} , dotted line for α , and dash-dotted line for ε	101
Fig. 8.11	Epicenter of 1964 Niigata earthquake, and Showa bridge	102
Fig. 8.12	Strong-motion earthquake records during Niigata earthquake; (A) Roof, (B) Basement of 4-story apartment building (after Iwasaki 1974)	103
Fig. 8.13	Collapse of Showa bridge (Photo by Penzien, J., 1964; Source: earthquake Engineering Online Archive, NISEE, http://nisee.berkeley.edu/elibrary/)	104
Fig. 8.14	Schematic diagram of collapse of Showa bridge (after Takata et al. 1965).....	105

Fig. 8.15	Soil profile and estimated liquefied layer (after Hamada et al. 1986).....	106
Fig. 8.16	Post-earthquake recovery and deformation of pile from Showa bridge. Note absence of an upper non-liquefiable crust (after Fukuoka 1966)	107
Fig. 8.17	Idealized pressure distribution for pile foundations affected by liquefaction-induced lateral ground displacement (after JRA 1996).....	108
Fig. 8.18	Schematic diagram showing predicted loading based on JRA code (after Bhattacharya 2003).....	109
Fig. 8.19	Deformed shape and bending moment diagram (units are kN and m).....	109
Fig. 8.20	SJB03 model layout—accelerometer instrumentation. Dimensions in mm (after Brandenberg et al. 2003).....	111
Fig. 8.21	Representative time series from SJB03 for medium Santa Cruz motion (after Brandenberg et al., 2005).....	113
Fig. 8.22	Soil displacement versus pile cap displacement for SJB03 test	114
Fig. 8.23	Simplified foundation structural model.....	115
Fig. 9.1	Bridge example finite element mesh (after Shin 2007).....	117
Fig. 9.2	Main components of analytical model (after Shin 2007)	117
Fig. 9.3	Comparison of results—residual pile cap displacement at abutments	118
Fig. 9.4	Comparison of results—residual pile cap displacement at piers	119
Fig. 9.5	Comparison of results—residual tangential drift ratio at columns.....	120
Fig. 9.6	Comparison of results—residual long. relative deck-end/abutment displacement ..	120
Fig. 9.7	(a) Problem analyzed; (b) Newmark rigid model; (c) linear elastic, modal, coupled sliding model; (d) nonlinear, lumped mass, coupled sliding model (after Rathje and Bray 2000).....	122

LIST OF TABLES

Table 1	Characteristics of selected random variables	G9
Table 2	Damage State as function of seismic displacement	G10
Table 3	Expected Downtimes as function of damage level	G10
Table 4	Repair cost ratio distribution given damage state	G10
Table 4.1	Abutment damage states as function of residual relative lateral deformation in longitudinal direction	39
Table 4.2	Column repair decisions as function of residual tangential drift	40
Table 4.3	Piles damage states as function of pile cap lateral displacement	42
Table 5.1	Bridge damage as function of residual lateral displacement	44
Table 5.2	Repair cost ratio distribution given damage state considering low and high uncertainty (values in parenthesis correspond to high uncertainty)	45
Table 5.3	Expected downtimes given bridge damage level	49
Table 6.1	Uniform hazard spectra, 5% damping, at site	56
Table 6.2	Probability of $D > d$ given IM (FORM results)	68
Table 6.3	Expected repair cost ratios using FORM—low uncertainty	70
Table 6.4	Expected repair cost ratios using FORM—high uncertainty	71
Table 6.5	Expected downtimes using FORM	72
Table 6.6	Probability of $D > d$ given IM (PEM results)	72
Table 6.7	Expected repair cost ratios using PEM—low uncertainty	73
Table 6.8	Expected repair cost ratios using PEM—high uncertainty	73
Table 6.9	Expected downtimes using PEM	74
Table 6.10	Equivalent pile length under each pier	74
Table 6.11	Stiffness of soil springs	75
Table 6.12	Input displacements	76
Table 6.13	Residual tangential column drifts	77
Table 7.1	Characteristics of selected random variables	82
Table 8.1	Soil properties (after Kashighandi and Brandenberg, 2006)	94

USER'S GUIDE TO AN EVALUATION PROCEDURE FOR ASSESSING BRIDGE DAMAGE DUE TO LIQUEFACTION-INDUCED LATERAL GROUND DISPLACEMENT

1. OVERVIEW

This guide presents a method to estimate the effects of liquefaction-induced lateral ground displacement on bridges founded on piles. In this simplified approach, the amount of residual lateral displacements at the bridge abutments is assumed to define the performance of the bridge (see Fig. 1). The bridge performance is expressed in terms of repair costs and downtimes. This procedure is appropriate as a screening tool to identify bridges where the effects of liquefaction-induced lateral displacement are important.

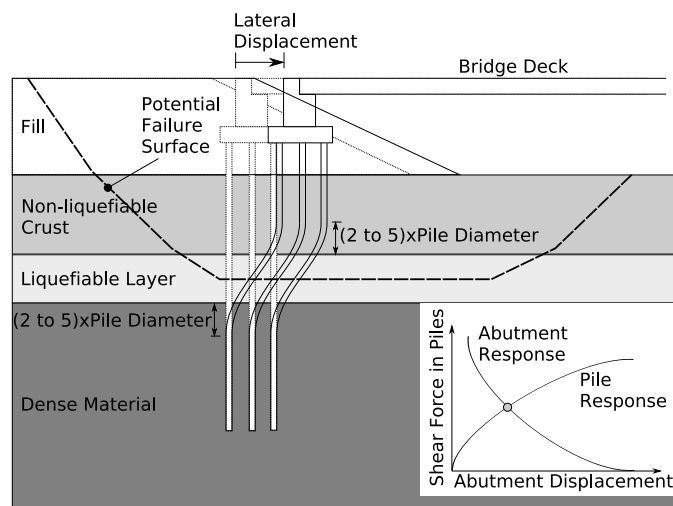


Figure 1

2. ASSUMPTIONS AND LIMITATIONS

It is assumed that the pile cap and the upper non-liquefiable crust will move together. It is also assumed that residual lateral displacement at the abutments is an appropriate index of bridge performance. The post-liquefaction static factor of safety at the abutments is assumed to be larger than 1 (i.e., no flow failure), and inertial effects from the structural response of the bridge are neglected. It is assumed that the bridge superstructure restrains the horizontal movement of the abutment through the compression of the deck. It is assumed that the piles are fixed against

rotation at some distance above and below the liquefiable material. For the case of a thin non-liquefiable upper crust and pinned pile connection it could be assumed that the piles are pinned at the pile/pile-cap connection, and some equations will need to be modified (see Section 3.1.1.1 in the main report). This simplified method is applicable to cases with groups of vertical piles, and serves as a reasonable approximation for the case of groups of vertical piles with only a few battered piles. In situations where all the piles are inclined, the results of this method are only approximate and probably overly conservative.

3. INPUT PARAMETERS

Information required to use this simplified method are the uniform hazard spectra at the site, i.e., the 5%-damped acceleration response spectrum, and its de-aggregation with respect to the controlling event's magnitude and distance; the soil profile, i.e., thickness of the different layers, and SPT (or CPT) profiles; and foundation properties, such as number and configuration of piles, and their mechanical properties (i.e., Young's modulus, moment of inertia, and plastic moment).

4. OUTPUT PARAMETERS

The results of this evaluation are the median and dispersion of residual lateral displacement at the abutments and the repair costs and downtimes associated with the estimated displacement.

5. PRELIMINARY ASSESSMENT

5.1 Liquefaction Evaluation

The probability of liquefaction can be evaluated using the expression developed by Seed et al. (2003):

$$P_L(N_{1,60}, CSR, M_w, \sigma_v, \sigma'_v, FC) = \Phi \left(- \frac{\left(N_{1,60} \cdot (1 + 0.004FC) - 13.32 \cdot \ln(CSR) - 29.53 \cdot \ln(M_w) - 3.70 \cdot \ln(\sigma'_v) + 0.05 \cdot FC + 44.97 \right)}{2.70} \right) \quad (1)$$

where P_L is the probability that liquefaction occurs; $N_{1,60}$ is the standard penetration test (SPT) blow-count normalized to an overburden pressure of approximately 100 kPa (1 ton/ft²) and a hammer energy ratio or hammer efficiency of 60%; CSR is the cyclic stress ratio, $CSR = 0.65(a_{\max}/g)(\sigma_v/\sigma'_v)r_d$, where a_{\max} is the peak horizontal ground surface acceleration, g is the acceleration of gravity, σ_v is total vertical stress, σ'_v is effective vertical stress, and r_d is the nonlinear shear mass participation factor (see Eq. 2.5 in the main body of the report); M_w is moment magnitude, FC is percent fines content (by dry weight) expressed as an integer (i.e., 12% fines is expressed as $FC=12$), and Φ is the standard normal cumulative distribution function (e.g., the NORMSDIST function in Excel).

5.2 Flow Failure Evaluation

The second step in the preliminary assessment is to verify that the static post-liquefaction factor of safety at the abutments is larger than 1. The residual undrained shear strengths (S_{ur}) are assigned to the potentially liquefiable layers identified in the previous step, and a conventional pseudostatic slope stability analysis is performed. The value of S_{ur} can be estimated using the expression:

$$\bar{S}_{ur} \approx \exp\left(\frac{\bar{N}_{1,60-CS}}{8} - 3.5\right) \times \left(1 + \frac{(0.3\bar{N}_{1,60-CS})^2}{128}\right), \quad 0 \leq \bar{N}_{1,60-CS} \leq 20 \quad (2)$$

where the top bar denotes the mean value of the respective variable. This expression is based on the combination of five of the most commonly used procedures to estimate the residual

undrained shear strength of the liquefiable layer, S_{ur} which are: Seed and Harder (1990), Olson and Stark (2002), and Kramer (2007), and the two correlations of S_{ur} with $N_{1,60-CS}$, and S_{ur} / σ_{vc}' with $N_{1,60-CS}$ proposed by Idriss and Boulanger (2007). Expressions to estimate $N_{1,60-CS}$ are shown in sections 2.2.1 and 2.2.2 of the report.

If information from cone penetration tests (CPTs) is available, the following CPT-SPT correlation proposed by Kulhawy and Mayne (1990) may be used to convert tip resistances into SPT blow-counts:

$$\frac{(q_c / P_a)}{N} = 5.44 (D_{50})^{0.26} \quad (3)$$

where q_c is tip resistance, P_a is atmospheric pressure (~ 100 kPa), N is the measured SPT value, and D_{50} is the particle size that 50% passes by weight. Additionally, direct CPT correlations for evaluating liquefaction triggering and residual undrained shear strength may be used.

5.3 Passive Forces versus Structural Capacity

An assessment is made whether soil flows around the foundation or movement of the foundation occurs in concert with the soil. The assessment requires a comparison between the estimated passive soil forces that can be exerted on the foundation system and the ultimate structural resistance that can be developed by the structure itself (see Fig. 2). The passive reaction of the upper non-liquefiable crust against the pile cap can be estimated using the procedure developed by Mokwa (1999). The reaction of the liquefied material can be estimated using the recommendations by JRA (1996), i.e., to assume that the lateral pressure distribution is 0.3 times the overburden pressure. The simplified procedure described in this guide assumes that movement of the foundation occurs in concert with the soil, i.e., that the structural resistance is smaller than the soil's capacity. If this condition is not satisfied, the recommendation is to design the foundations to withstand the passive pressures created by the soil flowing around the structure.

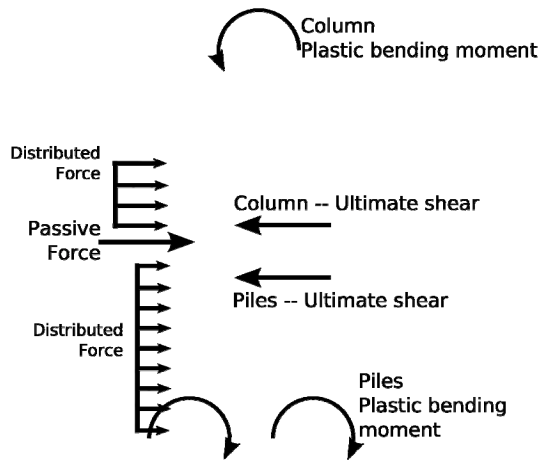


Figure 2

6. PRIMARY ASSESSMENT

When the analysis in Section 5.3 indicates that the soil forces are less than the total structural resistance, the amount of seismically induced permanent slope displacement is estimated using the expression developed by Bray and Travararou (2007):

$$\ln(D) = -1.10 - 2.83 \ln(k_y) - 0.333 (\ln(k_y))^2 + 0.566 \ln(k_y) \ln(Sa) + 3.04 \ln(Sa) + \dots - 0.244 (\ln(Sa))^2 + 1.5T_s + 0.278(M_w - 7) \pm \varepsilon \quad (4)$$

where M_w is moment magnitude, T_s is the initial fundamental period of the potential sliding mass, Sa represents the spectral acceleration at $1.5T_s$, and ε is a normally-distributed random variable with zero mean and standard deviation $\sigma = 0.66$. To eliminate a potential bias in the model for very low values of T_s , the first term of this equation, i.e., the term -1.10, should be replaced with the term -0.22 when $T_s < 0.05$ s.

The initial fundamental period of the sliding mass (T_s) is estimated using the expression: $T_s = 4H/V_s$ for the case of a relatively wide potential sliding mass that is either shaped like a trapezoid or segment of a circle where its response is largely 1D (Bray, 2007), where H = the average height of the potential sliding mass, and V_s is the average shear wave velocity of the sliding mass. Figure 3 shows how to estimate T_s for the case of a soil mass, underlain by a stiff

crust, sliding on top of liquefied material. In those cases, the location of the equivalent 1D soil column should be estimated as the weighted average of the location of the slices used in the slope stability analysis, where the weighting factor would be the total weight of the respective slice.

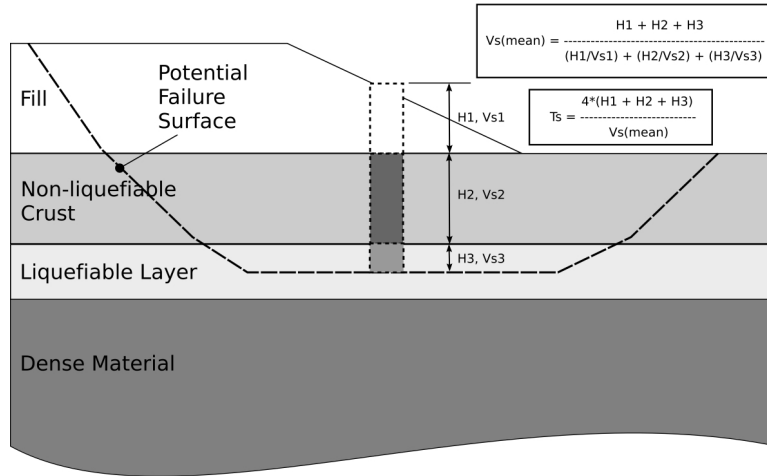


Figure 3

In Equation 4, the estimated displacement is strongly dependent on the slope's dynamic resistance, i.e., its yield coefficient, k_y . Since k_y itself is dependent on the displacement D due to pile-pinning and other effects, one must use iteration to solve for D . The value of the yield coefficient k_y that goes into the Bray and Travasarou (2007) expression can be calculated as follows:

$$k_y = p \left(S_{ur} + \frac{N \cdot V_p(D/2)}{A} + \frac{F_p(D/2)}{A} \right) \quad (5)$$

where p represents the relationship between k_y and S_u , N is the number of piles under the abutment, $V_p(D/2)$ is the shear force on any abutment pile, $F_p(D/2)$ represents the passive reaction at the abutment, and A is the area of the horizontal portion of the failure surface. See Section 3.1.1.1 of the main report for more details.

6.1 Relationship between Yield Coefficient and Equivalent Undrained Shear Strength

A relationship between k_y and S_u can be obtained by solving the pseudostatic slope stability problem at the abutment with different “reasonable” values of S_u , between S_{\min} and S_{\max} . Let \bar{S}_{ur} be the mean residual undrained shear strength of the liquefiable layer, M_p the plastic bending moment of each pile, H the thickness of the liquefiable layer, and F_p^{\max} the total maximum passive reaction at the abutment. A reasonable lower limit for S_u is the mean residual undrained shear strength of the liquefiable layer, i.e., $S_u = S_{\min} \approx \bar{S}_{ur}$. An upper limit for S_u can be estimated considering that the piles have reached their plastic limit, that the distance between points of fixity is equal to the thickness of the critical layer, and that the passive reaction at the abutments has reached its maximum, in that case $S_u = S_{\max} \approx \bar{S}_{ur} + N \times 2M_p / (H \times A) + F_p^{\max} / A$. Preliminary results for a series of sensitivity analysis indicate that for cases when there is a distinct weak layer where sliding is localized, the relationship between k_y and S_u is approximately linear.

6.2 Shear Force in Piles

The shear force in any pile, V_p , is estimated by assuming that the piles are fixed against rotation at some distance above and below the critical layer. Then, the shear force in any pile is calculated as

$$V_p(D) = \frac{2M(D)}{H + (\alpha_{top} + \alpha_{bottom}) \cdot 2R} \quad (6)$$

where $M(D)$ is the bending moment at the ends of the pile, $M(D) = 6E_{pile}I_{pile}D / L_{pile}^2 <$ plastic moment of pile, where E_{pile} is Young’s modulus, I_{pile} is the moment of inertia of the pile, D is the relative lateral displacement between the ends of the pile, and L_{pile} is the equivalent length of the pile, i.e., $L_{pile} = H + (\alpha_{top} + \alpha_{bottom}) \cdot 2R$; H is the total thickness of the critical layer, $2R$ is the diameter of the pile, and α_{top} and α_{bottom} are factors that indicate how many diameters above and below the critical layer the piles are fixed against rotation.

6.3 Passive Reaction at the Abutment

The passive reaction at the abutment, F_p , is estimated using the recommendations from Section 7.8.1. of Caltrans' Seismic Design Criteria (2006), where for seat abutments (see Fig. 4):

$$\begin{aligned}
 K_{abut} &= K_i \times w \times \left(\frac{h}{5.5} \right) \\
 K_i &= 20 \frac{\text{kip/in}}{\text{ft}} \\
 P_{bw} &= A_e \times 5.0 \text{ ksf} \times \frac{h}{5.5} \\
 A_e &= h \times w \text{ (area of the backwall)}
 \end{aligned}
 \tag{7}$$

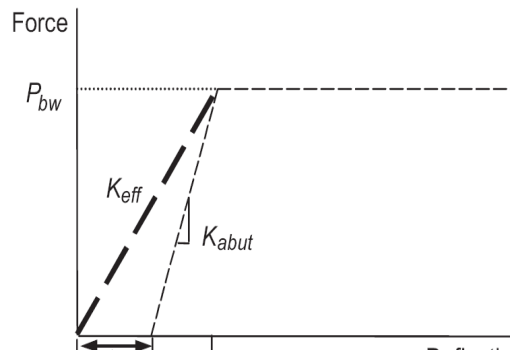


Figure 4

where w and h are the width and height of the backwall (in feet), respectively. For details see Section 3.1.1.1 of the main report.

6.4 Base Area

The horizontal part of the base of the potential sliding surface can be assumed to be rectangular in shape, i.e., $A = l \times t$, where l and t are its plan dimensions in the longitudinal and transverse directions, respectively. Two effects should be considered in the estimation of l and t . First, because the overall size of the potential sliding mass varies as the equivalent undrained shear strength of the critical layer changes, the value of l (from the 2D pseudostatic seismic stability problem at the abutment) should be considered, in general, a function of S_u . Because the size of the potential sliding mass usually increases as the value S_u increases, a conservative approach

that would lead to a smaller increase in resistance due to the pile-pinning effect would be for l to be for the case in which $S_u = S_{\max}$. Second, as Boulanger et al. (2006) have stated, the tributary width t will be greater than the abutment crest width, because there will be some influence of the abutment side slope masses in the abutment response. Their recommendation of assuming that one half of the slide slope masses is restrained by the piles is adopted in this procedure.

For given values of S_{ur} , α , ε , T_s , M_w , and S_a , the expression for k_y is a function of only the lateral displacement D , which can be replaced in the Bray and Travararou (2007) expression. The result is a nonlinear, implicit equation in D that can be solved iteratively.

7. INCORPORATION OF UNCERTAINTY

The uncertainty in the estimation of D is captured at a specified hazard level using the point estimate method (PEM) with the parameters S_{ur} and ε , which have the characteristics given in Table 1.

Table 1. Characteristics of selected random variables

Random Variable	Description	Probability Density Function	Uncertainty Measure
S_{ur}	Residual undrained shear strength of the liquefied material	Log-normal	Coefficient of Variation = 0.40
ε	Error term in the estimation of the residual lateral displacement	Normal	Standard Deviation = 0.66

8. EVALUATION OF DOWNTIMES AND REPAIR COSTS

Based on the results of the previous section, Tables 2, 3 and 4 can be used to estimate the expected damage state of the bridge, and its associated downtime and repair costs.

Table 2. Damage state as function of seismic displacement

Seismic Displacement (in.)	Damage Level
0 – 1”	Negligible
1” – 4”	Small
4” – 20”	Moderate
20” – 80”	Large
> 80”	Collapse

Table 3. Expected downtimes as function of damage level

Damage Level	Median downtime (and likely range)
Negligible	0
Small	0
Moderate	0
Large	1day (0.5 to 1.5 days)
Collapse	60 days (25 to 95 days)

Table 4. Repair cost ratio distribution given damage state

	Damage State				
	Negligible	Small	Moderate	Large	Collapse
$\Pr(RCR = 0.0 ds)$	1	1	0	0	0
$\Pr(RCR = 0.1 ds)$	0	0	1	0	0
$\Pr(RCR = 0.2 ds)$	0	0	0	0	0
$\Pr(RCR = 0.3 ds)$	0	0	0	0	0
$\Pr(RCR = 0.4 ds)$	0	0	0	0.15	0
$\Pr(RCR = 0.5 ds)$	0	0	0	0.70	0
$\Pr(RCR = 0.6 ds)$	0	0	0	0.15	0.20
$\Pr(RCR = 0.7 ds)$	0	0	0	0	0.55
$\Pr(RCR = 0.8 ds)$	0	0	0	0	0.20
$\Pr(RCR = 0.9 ds)$	0	0	0	0	0.05
$\Pr(RCR = 1.0 ds)$	0	0	0	0	0

9. EXCEL SPREADSHEET

An Excel spreadsheet is provided to perform the calculations indicated in steps 7 and 8, using the point estimate method, assuming a constant value for α and A , and considering that S_{ur} and ϵ are the only random variables in the estimation of the seismic displacement D . A sample layout of the spreadsheet is shown in Figure 5.

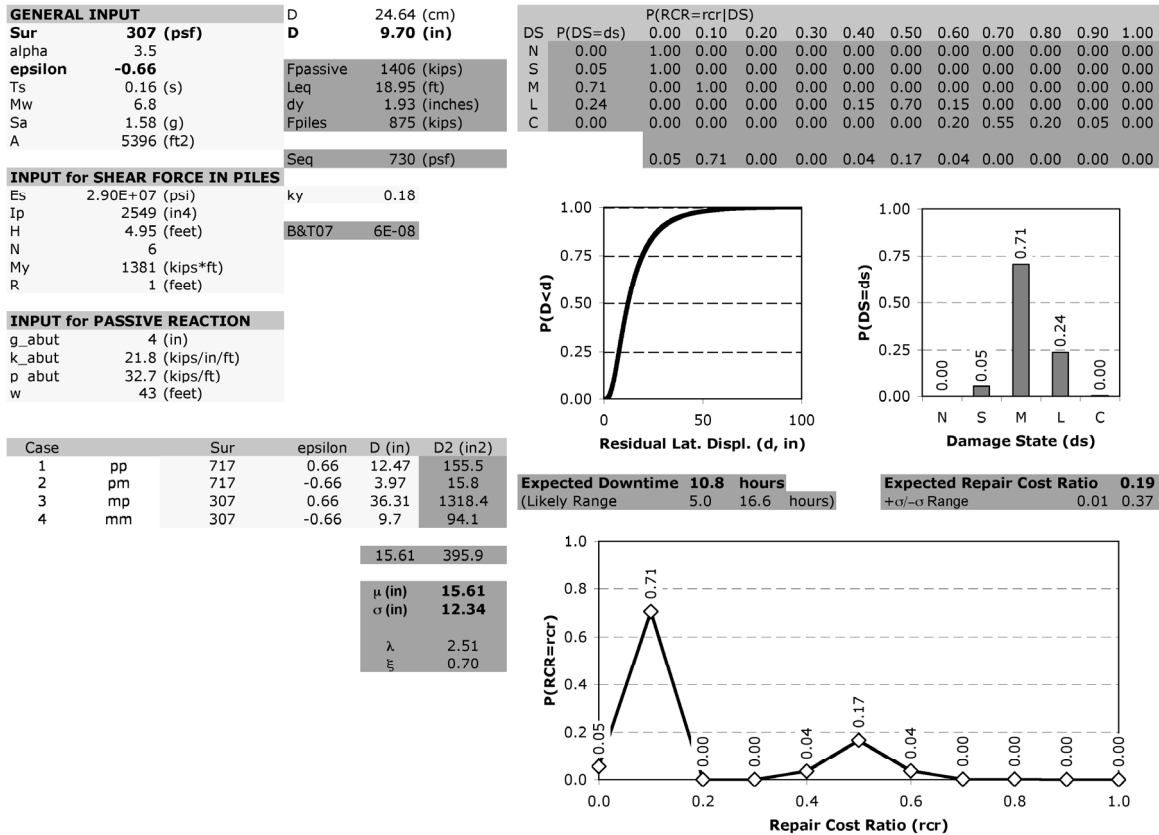


Figure 5

1 Introduction

1.1 PROBLEM STUDIED

Past earthquakes have shown that pile foundations can be vulnerable to liquefaction-induced ground failures. In cases where the post-liquefaction static factor of safety is less than one, flow slides may occur and induce large lateral and vertical deformations causing extensive damage. For example, the Showa bridge failed catastrophically in part due to liquefaction-induced lateral spreading produced by the 1964 Niigata, Japan earthquake (e.g., Hamada 1992). Compressional forces in the structure, additional shear forces in connections, and significant relative ground displacements across the supporting piles, which induce large bending moments, may all result due to liquefaction-induced displacement. Each of these additional loads may lead to severe damage or collapse of structures. Even if flow slides do not occur, earthquake-induced seismic displacements of the ground may progressively develop and damage piles and the overlying structure.

When liquefaction-induced displacements threaten the performance of an engineered structure, soil remediation techniques may be considered to minimize the expected damage. These techniques usually involve ground modification, ground improvement, or stabilizing measures that significantly reduce the liquefaction hazard or reduce the level of ground deformations to an acceptable level. However, mitigation may be difficult and costly at some sites, and it may not be necessary if the structure's foundation piles can be designed to withstand the displacement and forces induced by the liquefaction. Moreover, if the foundation piles can be designed to "pin" the upper layer of soil, that would normally spread atop the liquefied layer below it, into the stronger soils below the liquefiable soil layer, then other ground remediation techniques may not be required to achieve satisfactory performance. This technique has been coined the "pile-pinning" effect, which is illustrated in Figure 1.1.

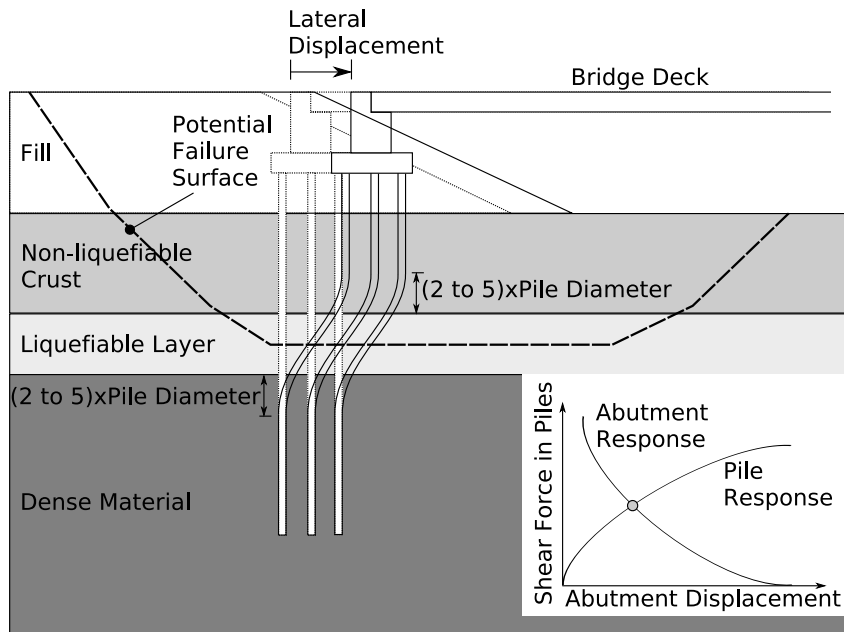


Fig. 1.1 “Pile-pinning” effect for case of a pile locked into both soil above and below liquefiable soil layer.

Case histories have shown that piles have developed plastic hinges without leading to structural collapse. As Martin (2004) indicates, in the Kobe earthquake, field investigations using borehole cameras and slope indicators showed that pile damage in lateral spread zones concentrated at the interface between liquefied and non-liquefied layers, as well as near pile heads. Also, lateral analyses using p-y interface springs together with pile-deformations induced by estimated ground displacement profiles were consistent with observed pile performance. Considerable cost savings could result by including structural resistance in displacement demand estimates (i.e., by including the pile-pinning effect) and allowing increased displacement corresponding to limited plastic hinge rotation (Martin 2004).

The pile-pinning effect was first implemented in the United States as a result of the seismic safety evaluation of Sardis dam (Finn et al. 1991). Sardis dam was judged to be potentially unstable due to excessive seismic deformations resulting from liquefaction of a thin layer of silt in the foundation of the dam. The liquefiable silt layer was located between stronger soil strata above and below the potentially weak soil layer. Dynamic effective stress–large-strain finite element analyses (Finn et al. 1997) indicated that the potentially large seismic displacements due to laterally spreading atop the liquefiable silt layer could be arrested by

“pinning” the competent soils above the weak layer into the strong soils below the weak layer. A total of nearly 2600 prestressed reinforced concrete piles (60 cm in diameter and spaced 2.4 to 3.7 m apart) were installed in the mid-1990s to remediate Sardis dam.

The pile-pinning effect is now recognized as a legitimate remediation option when bridge or wharf structures built on pile foundations are located in areas susceptible to liquefaction-induced lateral spreading (e.g., Martin and Lam 2000; Martin et al. 2002). Work by Martin and others led to the development of a simplified design procedure for evaluating the effects of liquefaction-induced lateral spreads as proposed in the MCEER/ATC-49-1-recommended seismic design document of bridges (ATC/MCEER Joint Venture 2003).

1.2 CURRENT APPROACH TO EVALUATING LIQUEFACTION-INDUCED BRIDGE DAMAGE

A simplified design procedure for evaluating the effects of liquefaction-induced lateral spreads on bridge performance, which includes the “pile-pinning effect,” is delineated in the MCEER/ATC-49-1 document (ATC/MCEER Joint Venture 2003). The steps involved in the current MCEER/ATC (2003) design procedure are:

- Step 1: The soil layers that are likely to liquefy are identified.
- Step 2: A stability analysis is executed to determine the likelihood of soil movements, and to determine the extent of such movements. This would include the depths of soil likely to move and the plan extent of the likely soil failure block. Assessment of the impacts to a bridge structure can then be made by considering the proximity of the failure block to the foundation system.
- Step 3: The maximum displacement of the soil is estimated. This may be accomplished using the simplified Newmark charts, Newmark time history analysis, or more advanced techniques.
- Step 4: An assessment is made whether soil flows around the foundation or movement of the foundation will occur. The assessment requires a comparison between the estimated passive soil forces that can be exerted on the foundation system and the ultimate structural resistance that can be developed by the structure itself. This assessment requires estimating the forces that can develop if soil is to actually flow around the foundation system and comparing

them with the likely resistance that the structure will provide. In cases where a crust of non-liquefied material may exist at or near the ground surface, the full structural resistance is likely to be less than the flow-induced passive forces, and in such cases the foundation is likely to move with the soil. In many cases, it may be immediately obvious which condition, soil flow or foundation movement, is more likely.

Step 5: If flow of soil around the structure is likely, the foundation is designed to withstand the passive pressures created by the soil flowing around the structure. The induced forces are effectively the largest forces that the structure will experience, and for this reason it is conservative to design a structure for such forces.

Step 6: If on the other hand, the assessment indicates that movement of the foundation is likely, then the structure must be evaluated for adequacy at the maximum expected displacement. This is the mechanism illustrated in Figure 1.1. The implication of this assessment is that for relatively large ground movements, soil displacements are likely to induce similar magnitude movements of the foundation. In this context, “large” is taken relative to the structural yield resistance. The resulting induced movements of the foundations may produce substantial plastic hinging in the foundations, and may induce relatively large reactions in the superstructure.

The recommended acceptance criteria are the same as for the Seismic Analysis and Design Procedure E (SDAP E), i.e., the pushover method. Plastic hinge rotation limits of 0.05 radians are used for an upper level event, and the allowance of plasticity in the foundation is believed to be reasonable, even though plasticity may be below grade, because such damage in the foundation is not likely to pose a collapse hazard.

Step 7: If such deformations are not acceptable, there are realistically only two ways to restrict the foundation and substructure forces to acceptable values. The first method is to design the foundations to resist the forces that would accompany passive flow of the soil around the foundations. The other method would be to limit the ground movement by providing either ground or structural remediation. It is the structural option that provides the most

rational first path, and this makes use of the “pinning” or dowel action that pile or shaft foundations contribute as they cross the potential failure plane of the moving soil mass.

Step 8: The determination of the plastic mechanism that is likely to occur in the presence of spreading should be done in a reasonable manner. Due to the range of inherent uncertainties, great precision in the determination may not produce more accuracy. Thus, simple estimates of the mechanism and its corresponding lateral resistance capability are often adequate. For instance, one method is to use the upper bound method of plasticity and postulate potential mechanisms, then, assess the mechanism that is likely to control using judgment. The acceptance criteria are basically the structural deformation criteria for SDAP E, which uses the pushover method. In fact, the piles are elements that limit the acceptable displacements of the system.

The lateral shear that produces the plastic mechanism can be decreased to account for the P- Δ effect. Because the lateral soil force that produces a plastic mechanism in the foundation/substructure system is required, the reduction in shear required to produce a mechanism due to P- Δ should be considered.

A more precise method of determining the plastic mechanism would be to use an approach that ensures compatibility of deformations between the soil and piles, which accounts for plastic deformations in the piles themselves. This second requirement could be satisfied by using software that is capable of performing pushover analysis, then using p-y curves from a program such as LPILE (Reese et al. 2000) to produce boundary support elements that ensure compatibility.

Step 9: The system then must be assessed for a prescribed displacement field to represent the likely soil spreading deformation. From this analysis, an estimate of the likely shear resistance that the foundation will provide is estimated, and this shear can then be incorporated back into the stability analysis.

Step 10: If substantial resistance is provided, then its effect on limiting the instability-driven movement of the soil block should be introduced into the analysis. This step is typically not included in current assessments of potential foundation

movements, although inclusion of such resistance may often improve the structure's expected performance.

Steps 11&12: The overall displacement is re-calculated with the revised resistance levels considered. Once a realistic displacement is calculated, then the foundation and structural system can be assessed for this movement. It is at this point that more permissive displacements than for substructure design can be relied upon. This implies that plastic rotations, and potentially large ones, may be allowed to occur in the foundation under such conditions.

Step 13: If the structure's behavior is acceptable, then the design is complete; if not, then the engineer must assess whether to try to produce adequacy either through additional piles or shafts, and these may not need to connect to the foundation (passive piles). Alternately, ground improvement approaches may be considered, for instance, stone columns. The selection of structural or geotechnical remediation methods is based on the relative economy of the system being used.

The process is repeated by returning to Step 8 and modifying the available resistance until the slope is stabilized.

Although the MCEER/ATC methodology provides a useful framework for analyzing this type of problem, it does not offer a systematic way of evaluating the performance of existing and proposed bridge designs at sites that could undergo liquefaction-induced lateral ground displacement. The performance-based earthquake engineering (PBEE) framework developed by PEER provides a systematic procedure and it also allows the incorporation of relevant sources of uncertainty in the performance evaluation.

1.3 PEER-PBEE METHODOLOGY

As opposed to judging that a design is satisfactory or unsatisfactory based on compliance with defined standards, performance-based earthquake engineering (PBEE) provides a comprehensive methodology for assessing the likely performance of a design for an array of seismic loadings. The likely seismic performance and the consequences of that performance in terms of quantities that a client understands, such as the number of deaths and injuries, repair cost, and downtime, is

estimated for a sliding scale of seismic hazard levels from frequent to rare earthquake events. The Pacific Earthquake Engineering Research (PEER) Center PBEE methodology is based on the premise that the overall bridge performance assessment can be divided into a series of discrete steps that, although related, can be analyzed independently. In general terms, these steps are:

1. Defining the seismic hazard in terms of the intensity of ground motions
2. Evaluating the dynamic response of the system for each intensity level
3. Estimating the damage produced for each calculated dynamic response
4. Assessing the consequences for each damage state

In mathematical terms, the PEER-PBEE methodology is expressed through a framework equation that estimates the mean annual frequency of events where a specified decision variable exceeds a given threshold. The PEER-PBEE equation is (Cornell and Krawinkler 2000):

$$\lambda(dv) = \int_{dm} \int_{edp} \int_{im} G(dv | dm) |dG(dm | edp)| |dG(edp | im)| |d\lambda(im)| \quad (1.1)$$

in which im is the ground motion intensity measure, edp is an engineering demand/response parameter, dm denotes a damage measure, dv denotes a decision variable such as repair cost or downtime, $G(x|y) = \Pr(X > x | Y = y)$ is the conditional complementary cumulative distribution function of the random variable X given $Y = y$, $dG(x|y)$ is the differential of $G(x|y)$ with respect to x , and $\lambda(x)$ is the mean frequency of $\{X > x\}$ events per year. Der Kiureghian (2005) provides a comprehensive review of the PEER-PBEE framework.

To evaluate Equation 1.1, it is necessary to define the conditional complementary cumulative distribution functions $G(x|y)$. The following sections present procedures to define those functions for the case of bridges with foundations that respond to liquefaction-induced lateral ground displacement, which includes the pile-pinning effect. Initially, the bridge/foundation system is evaluated to identify the governing mechanisms.

2 Preliminary Assessment

2.1 SEISMIC HAZARD

Seismic hazard analyses involve the quantitative estimation of the ground shaking hazard at a particular site (e.g., see Kramer 1996 for more information). This estimation can be performed deterministically, assuming a particular earthquake scenario, or probabilistically, in which uncertainties in earthquake size, location, and time of occurrence are explicitly considered. The following is a short summary of the paper by Abrahamson (2000), which briefly describes both approaches, with emphasis on the probabilistic approach.

In a deterministic seismic hazard analysis, earthquake scenarios are evaluated separately. For each source, a scenario earthquake is defined (i.e., magnitude, distance, style of faulting, and in some cases rupture direction). The ground motion for the scenario earthquake is usually estimated using attenuation relations, but is sometimes estimated using seismological simulations of the ground motion. For faults, at least five attributes need to be considered in developing a deterministic design earthquake: classification of active or inactive, the earthquake magnitude, the distance to the site, the tectonic regime, and the fault type. To estimate the ground motion for the scenario earthquake requires selecting the appropriate site condition, ground motion model, number of standard deviations, and in some cases rupture directions.

Probabilistic seismic hazard analysis follows the basic approach developed by Cornell (1968), with the addition that the variability in the ground motion (for a given magnitude and distance) is included. The basic methodology involves computing how often a suite of specified levels of ground motion will be exceeded at the site. The hazard analysis computes the annual number of events that produce a ground motion parameter that exceeds a specified level. This number of events per year is also called the “annual probability of exceedance.” The inverse of this parameter is called the “return period.” The calculation of the annual frequency of exceedance involves several probability distributions for each seismic source, i.e., the frequency of earthquakes of various magnitudes, the rupture dimension and location of the earthquakes, and

the attenuation of the ground motion from the earthquake rupture to the site. The occurrence rates of the earthquakes of various magnitudes are estimated by magnitude recurrence relations. The location of the earthquake depends on the geometry of the seismic source. The distance from the rupture to the site is computed from the earthquake location and rupture dimension. The ground motion at the site is estimated from the attenuation relation.

For point sources, the rate at which the ground motion from the i -th source exceeds the test level z at the site is given by:

$$\nu_i(A > z) = N_i(M_{\min}) \int_{\varepsilon=\varepsilon_{\min}}^{\varepsilon=\varepsilon_{\max}} \int_{r=0}^{\infty} \int_{m=M_{\min,i}}^{m=M_{\max,i}} f_{m_i}(m) f_{r_i}(r) f_{\varepsilon}(\varepsilon) P(A > z | m, r, \varepsilon) dm dr d\varepsilon \quad (2.1)$$

where $N_i(M_{\min})$ is the rate of earthquakes with magnitude greater than M_{\min} from the i -th source, r is the distance measure, m is magnitude, ε is the number of standard deviations of the ground motions from the median ground motion, $M_{\max,i}$ is the maximum magnitude for the i -th source, $f_{m_i}(m)$ and $f_{r_i}(r)$ are the probability density function for the magnitude and the distance, respectively, that describe the relative likelihood of different earthquake scenarios, $f_{\varepsilon}(\varepsilon)$ is the probability density function for a ground motion variability, and $P(A > z | m, r, \varepsilon)$ is the probability that the ground motion exceeds the test level z for magnitude m , distance r , and number of standard deviations ε . Because in the context of attenuation relationships, the magnitude, distance, and number of standard deviations fully define the intensity of the ground motion, $P(A > z | m, r, \varepsilon)$ is either 0 or 1.

For planar sources (e.g., known faults) the finite dimension and location of the rupture should be considered to compute the closest distance. Specifically, the randomness in the rupture length, rupture width, rupture location along strike, and rupture location dip should be considered. For planar sources Equation 2.1 becomes:

$$\begin{aligned} \nu_i(A > z) = N_i(M_{\min}) \int_{W=0}^{\infty} \int_{RA=0}^{\infty} \int_{Ex=0}^1 \int_{Ey=0}^1 \int_{m=M_{\min,i}}^{M_{\max,i}} \int_{\varepsilon=\varepsilon_{\min}}^{\varepsilon_{\max}} f_{m_i}(m) f_{W_i}(m, W) f_{RA_i}(m, RA) \dots \\ \dots f_{Ex_i}(x) f_{Ey_i}(y) f_{\varepsilon}(\varepsilon) P(A > z | m, r_i(x, y, RA, W), \varepsilon) dW dRA dx dy dm d\varepsilon \end{aligned} \quad (2.2)$$

where $f_{W_i}(m, W)$, $f_{RA_i}(m, RA)$, $f_{Ex_i}(x)$, and $f_{Ey_i}(y)$ are probability density functions for the rupture width, rupture area, location of the center of rupture along strike and location of the center of rupture down dip, respectively. In Equation 2.2, x and y give the location of the center of the rupture in terms of the fraction of the fault length and fault width, respectively (e.g., $x=0$ is one end of the fault and $x=1$ is the other end of the fault).

The hazard integral in Equation 2.2 may appear to be complicated, but most of the computations are related to finding the distribution of the closest distance. Equation 2.2 defines a complete set of possible earthquake scenarios (i.e., magnitude and distance combinations) with the full range of possible ground motion levels for each scenario while keeping track of which scenarios lead to ground motions that exceed the test value z .

For multiple seismic sources, the total annual rate of events with ground motions that exceed z at the site is just the sum of the annual rate of events from the individual sources (assuming that the sources are independent):

$$v(A > z) = \sum_{i=1}^{N_{source}} v_i(A > z) \quad (2.3)$$

where N_{source} is the total number of fault and areal sources.

2.1.1 Uniform Hazard Spectra

A common method for developing design spectra based on the probabilistic approach is through the uniform (or equal) hazard spectra. A uniform hazard spectrum is developed by first computing the hazard at various spectral periods using response spectral attenuation relations. That is, the hazard is computed independently for each spectral period. For a selected return period, the ground motion for each spectral period is measured from the hazard curves. These ground motions are then plotted at their respective spectral periods to form the uniform hazard spectrum. The term “uniform hazard spectrum” is used because there is an equal probability of exceeding the ground motion at any period. Since the hazard is computed independently for each period, in general, a uniform hazard spectrum does not represent the response spectrum of any single earthquake.

2.1.2 De-aggregation of Hazard

The hazard curve gives the combined effect of all magnitudes and distances on the probability of exceeding a specified ground motion level. Because all of the sources, magnitudes, and distances are mixed together, it is difficult to get an intuitive understanding of what is controlling the hazard from the hazard curve itself. A common practice is to break down the hazard back into its contributions from different magnitude and distance pairs to provide insight into what events are the most important for the hazard, at a given ground motion level. This process is called de-aggregation. With de-aggregation, the fractional contribution of different subsets of the events to the total hazard is computed. The most common form of de-aggregation is a two-dimensional de-aggregation in magnitude and distance bins. The de-aggregation by magnitude and distance bins allows the dominant scenario earthquake (magnitude and distance pairs) to be identified. A de-aggregation by seismic source allows the dominant seismic source to be identified. The results of the de-aggregation will be different for different probability levels (e.g., 100 year- versus 1000 year return periods) and for different spectral periods.

2.2 LIQUEFACTION EVALUATION

Liquefaction is defined as the transformation of a granular material from a solid to a liquefied state as a consequence of increased pore-water pressure and reduced effective stress (Marcuson 1978). Increased pore-water pressure is induced by the tendency of loose to moderately dense granular materials with poor drainage to compact when subjected to cyclic shear deformations. As liquefaction occurs, the soil stratum softens, allowing large cyclic deformations to occur. In loose materials, the softening is also accompanied by a loss of shear strength, to a residual level known as the residual undrained shear strength (S_{ur}), that may lead to large shear deformations or even flow failure under moderate to high shear stresses, such as beneath a foundation or sloping ground. Beneath gently sloping to flat ground, liquefaction may lead to ground oscillation or lateral spread as a consequence of either flow deformation or cyclic mobility. Loose soils may also compact after liquefaction with reconsolidation leading to ground settlement.

Estimation of two variables is required for evaluation of liquefaction resistance of soils:
(1) the seismic demand on a soil layer, expressed in terms of the induced cyclic stress ratio

(CSR) and (2) the capacity of the soil to resist liquefaction, expressed in terms of the cyclic stress ratio required to generate liquefaction (CRR).

Seed and Idriss (1971) formulated the following equation for the calculation of CSR:

$$CSR = \frac{\tau_{av}}{\sigma'_{vo}} = 0.65 \left(\frac{a_{max}}{g} \right) \left(\frac{\sigma_{vo}}{\sigma'_{vo}} \right) r_d \quad (2.4)$$

where a_{max} is the peak horizontal acceleration at the ground surface generated by the earthquake; g is the acceleration of gravity; σ_{vo} and σ'_{vo} are the total and effective vertical overburden stresses, respectively; and r_d is the stress reduction coefficient. The latter coefficient accounts for the flexibility of the soil profile. For routine engineering practice the following equation may be used to estimate the average values of r_d (Youd et al. 2001):

$$r_d = \frac{1.000 - 0.4113z^{0.5} + 0.04052z + 0.001753z^{1.5}}{1.000 - 0.4177z^{0.5} + 0.05729z - 0.006205z^{1.5} + 0.001210z^2} \quad (2.5)$$

where z is the depth below ground surface in meters.

A plausible method for evaluating CRR is to retrieve and test undisturbed soil specimens in the laboratory. Unfortunately, in-situ stress states generally cannot be reestablished in the laboratory, and specimens of granular soils retrieved with typical drilling and sampling techniques are too disturbed to yield meaningful results. Only through specialized sampling techniques, such as ground freezing, can sufficiently undisturbed specimens be obtained. The cost of such procedures is generally prohibitive for all but the most critical projects. To avoid the difficulties associated with sampling and laboratory testing, field tests have become the state of practice for routine liquefaction investigations. Several field tests have gained common usage for evaluation of liquefaction resistance, including the standard penetration test (SPT) and the cone penetration test (CPT). In the remaining part of this section the evaluation of liquefaction resistance using the standard penetration test is presented.

Criteria for evaluation of liquefaction resistance based on the SPT have become relatively robust over the years. Those criteria are largely embodied in the CSR versus $N_{1,60}$ plot reproduced in Figure 2.1. $N_{1,60}$ is the SPT blow count normalized to an overburden pressure of approximately 100 kPa (1 ton/ft²) and a hammer energy ratio or hammer efficiency of 60%. Figure 2.1 is a graph of calculated CSR and corresponding $N_{1,60}$ from sites where liquefaction effects were or were not observed following past earthquakes with magnitudes of approximately 7.5. CRR curves on this graph were conservatively positioned to separate regions with data

indicative of liquefaction from regions with data indicative of non-liquefaction. Curves were developed for granular soils with the fines contents of 5% or less, 15%, and 35% or more as shown on the plot. The CRR curve for fines contents <5% is the basic penetration criterion for the simplified procedure and is referred to as the “SPT clean sand base curve.” The CRR curves in Figure 2.1 are valid only for magnitude 7.5 earthquakes.

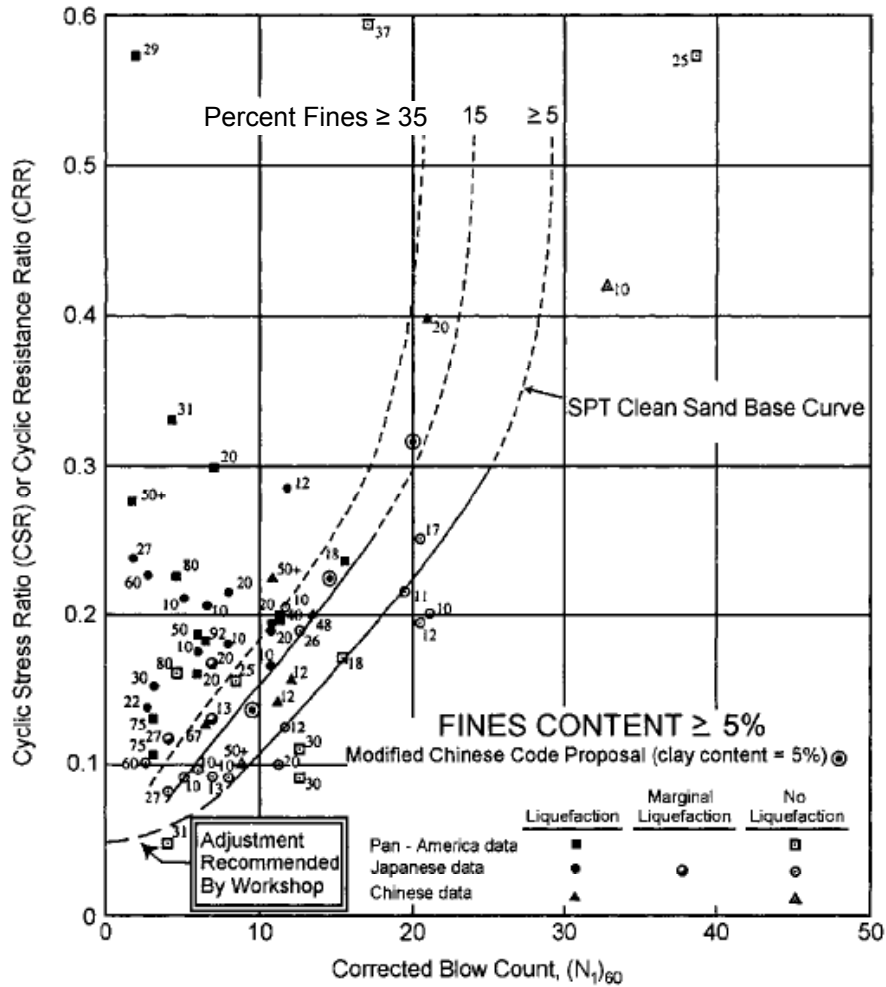


Fig. 2.1 SPT clean-sand base curve for magnitude 7.5 earthquakes with data from liquefaction case histories (after Youd et al. 2001, modified from Seed et al. 1985).

In personal communication to Youd et al. (2001), A. F. Rauch approximated the clean-sand base curve plotted in Figure 2.1 by the following equation:

$$CRR_{7.5} = \frac{1}{34 - N_{1,60-CS}} + \frac{N_{1,60-CS}}{135} + \frac{50}{(10 \cdot N_{1,60-CS} + 45)^2} - \frac{1}{200} \quad (2.6)$$

This equation is valid for $N_{1,60-CS} < 30$. For $N_{1,60-CS} \geq 30$, clean granular soils are often classified as being too dense to liquefy and are labeled as “non-liquefiable.” Similar types of relationships are available to estimate $CRR_{7.5}$ based on normalized CPT penetration resistances.

2.2.1 Overburden Corrected SPT Value

Because SPT N-values increase with increasing effective overburden stress, an overburden stress correction factor is applied (Seed and Idriss 1982). This factor is commonly calculated from the following equation (Liao and Whitman 1986):

$$N_{1,60} = C_N N_{60}, \text{ where } C_N = \sqrt{\frac{P_a}{\sigma'_{vo}}} \quad (2.7)$$

where C_N normalizes the measured standard penetration resistance N_m to an effective overburden pressure of approximately $P_a = 100$ kPa (1 atm). C_N should not exceed a value of 1.7.

2.2.2 Influence of Fines Content

Youd et al. (2001) recommend Equations 2.8–2.10 as approximate corrections for the influence of fines content (FC) on CRR. These equations were developed by I. M. Idriss with the assistance of R. B. Seed for correction of $N_{1,60}$ to an equivalent clean sand value, $N_{1,60-CS}$:

$$N_{1,60-CS} = \alpha + \beta \cdot N_{1,60} \quad (2.8)$$

$$\begin{aligned} \alpha &= 0 && \text{for } FC \leq 5\% \\ \alpha &= \exp\left[1.76 - (190/FC^2)\right] && \text{for } 5\% < FC < 35\% \\ \alpha &= 5.0 && \text{for } FC \geq 35\% \end{aligned} \quad (2.9)$$

$$\begin{aligned} \beta &= 1.0 && \text{for } FC \leq 5\% \\ \beta &= \left[0.99 + (FC^{1.5}/1000)\right] && \text{for } 5\% < FC < 35\% \\ \beta &= 1.2 && \text{for } FC \geq 35\% \end{aligned} \quad (2.10)$$

2.2.3 Magnitude Scaling Factor

The clean-sand base or CRR curves in Figure 2.1 apply only to magnitude 7.5 earthquakes. To adjust the clean-sand curves to magnitudes smaller or larger than 7.5, Seed and Idriss (1982) introduced correction factors termed “magnitude scaling factors (MSFs).” These factors are used to scale the CRR base curves upward or downward on CRR versus $N_{1,60}$ plot.

To illustrate the influence of magnitude scaling factors on calculated hazard, the equation for the factor of safety (FS) against liquefaction is written in terms of CRR, CSR, and MSF as follows:

$$FS = \left(\frac{CRR_{7.5}}{CSR} \right) MSF \quad (2.11)$$

where CSR is the calculated cyclic stress ratio generated by the earthquake shaking and $CRR_{7.5}$ is the cyclic resistance ratio for magnitude 7.5 earthquakes. $CRR_{7.5}$ is determined from Equation 2.6.

Several relations have been proposed to estimate MSF (e.g., Seed and Idriss 1982; Ambraseys 1988; and Andrus and Stokoe 1997). In this report the relation recommended by Youd et al. (2001) is used, i.e.,

$$MSF = \frac{10^{2.24}}{M_w^{2.56}} = \left(\frac{7.5}{M_w} \right)^{2.56} \quad (2.12)$$

2.2.4 Correction for Low and High Overburden Stresses

Cyclically loaded laboratory test data indicate that liquefaction resistance increases with increasing confining stress. The rate of increase, however, is nonlinear. To account for the nonlinearity between CRR and effective overburden pressure, Seed (1983) introduced the correction factor K_σ to extrapolate the simplified procedure to soil layers with effective overburden pressures different than 100 kPa. Cyclically loaded, isotropically consolidated triaxial compression tests on sand specimens were used to measure CRR for high-stress conditions and to develop K_σ values. By taking the ratio of CRR for various confining pressures to the CRR determined for approximately 100 kPa (1 atm), Seed (1983) developed the original

K_σ correction curve. Other investigators have added data and suggested modifications to better define K_σ for engineering practice. Hynes and Olsen (1999) compiled and analyzed an enlarged data set to provide guidance and formulate equations for selecting K_σ . The equation they derived for calculating K_σ is:

$$K_\sigma = \left(\frac{\sigma'_{vo}}{P_a} \right)^{(f-1)} \leq 1.4 \quad (2.13)$$

where σ'_{vo} , effective overburden pressure; and P_a , atmospheric pressure, are measured in the same units; and f is an exponent that is a function of site conditions, including relative density, stress history, aging, and overconsolidation ratio. NCEER's recommendation for the values for f are for relative densities between 40% and 60%, $f = 0.8-0.7$; and for relative densities between 60% and 80%, $f = 0.7-0.6$.

2.2.5 Other Correction Factors

The correction factors presented in the previous sections are the most relevant for the application discussed in this report; however, in general, there are other important factors that should be evaluated, e.g., SPT corrections due to energy ratio, borehole diameter, rod length, and sampling method; and correction for sloping ground (K_α).

2.3 FLOW FAILURE

If after assigning undrained residual shear strengths (S_{ur}) to the layers that are likely to liquefy and calculating the post-liquefaction static factor of safety, the post-liquefaction static factor of safety is found to be less than or equal to unity (i.e., step 2 of the MCEER/ATC (2003) design procedure), it is reasonable (and conservative) to assume that large ground deformations will be imposed on the bridge foundations. This case is termed the liquefaction flow case. Case histories suggest that when the post-liquefaction factor of safety is less than one, ground deformations on the order of several meters are possible. Such large ground deformations will likely induce large damage to the bridge and may even lead to a partial or complete collapse of the bridge. In these situations, if the bridge cannot be relocated, the "pile-pinning" effects procedure presented in this

document cannot be applied, and significant ground improvement and/or stabilizing measures are required to ensure that the post-liquefaction factor of safety is greater than one. Otherwise, significant, uncontrolled bridge deformations and damage are likely to occur, which are difficult to assess with confidence.

2.4 PASSIVE SOIL FORCES VERSUS ULTIMATE STRUCTURAL RESISTANCE

The methodology that is presented in the next sections assumes that the pile cap and surrounding soil move together. To verify this, the reaction capacity of the soil must be compared to the maximum lateral capacity of the piles and columns (see Figs. 2.2–2.3). If the soil capacity is smaller than the structural capacity, the soil will continue to displace or flow around the stable foundation, and the foundation should be designed to resist the pressures created by the flowing soil; otherwise, the movement of the foundation will likely occur in concert with the soil. The pressures created by the flowing soil can be estimated using the procedure developed by Mokwa (1999) for the passive soil resistance of the non-liquefied upper crust reacting against the pile cap, and the recommended pressure distributions given by JRA (1996) for the liquefied material. It is important to note that according to Boulanger et al. (2003) for beam on nonlinear Winkler foundation models where the lateral ground displacement loads are modeled as limit pressures (with the p-y springs removed in the lateral displacement interval), the limit pressure for liquefied sand may be roughly represented as $p \approx 0.6 \cdot \sigma_{vc}' \cdot b$. Since $\sigma_{vc}' \approx 0.5 \cdot \sigma_{vc}$, then, for liquefied sand, the lateral pressure can be approximately represented as $p \approx 0.3 \cdot \sigma_{vc} \cdot b$, which is the approach proposed by JRA (1996).

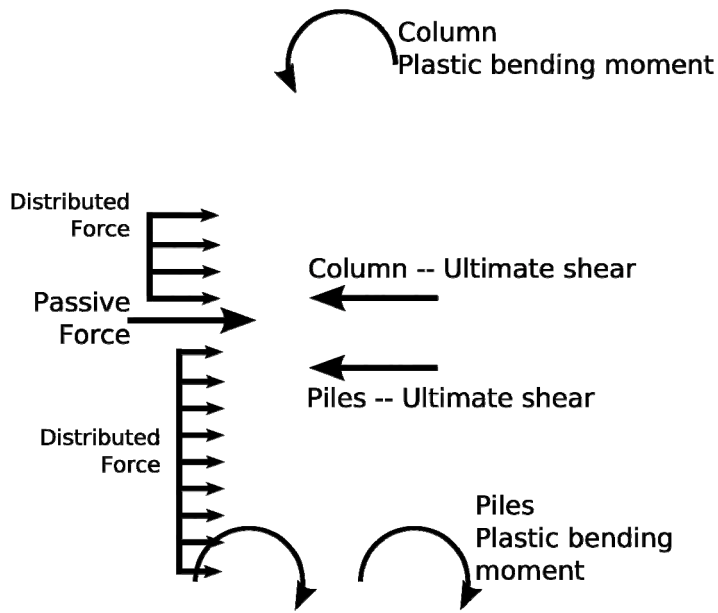


Fig. 2.2 Passive soil forces versus ultimate structural resistance at piers (modified from Berrill et al. 2001).

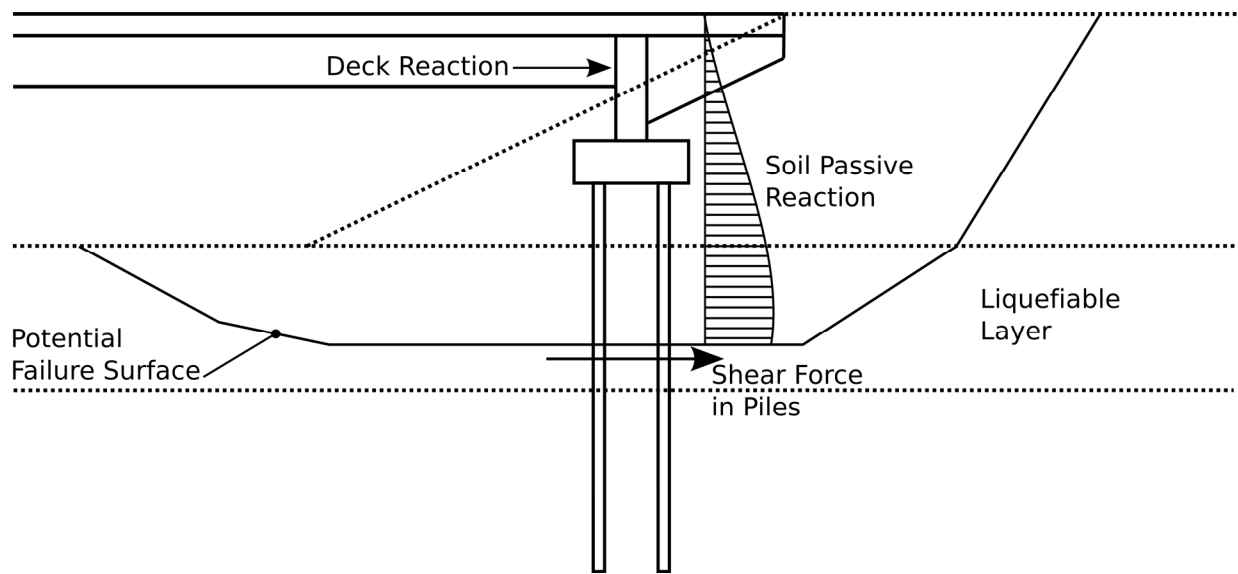


Fig. 2.3 Passive soil forces versus ultimate structural resistance at abutments.

3 Probabilistic Evaluation of Seismic Lateral Displacement

3.1 LATERAL DISPLACEMENT AS ENGINEERING DEMAND PARAMETER

After an exhaustive examination of the problem at hand (i.e., bridge undergoing lateral ground displacement wherein the soil crust moves with the pile cap), seismically induced permanent lateral displacement (D) of the ground undergoing liquefaction-induced lateral displacement was judged to be the most representative engineering demand/response parameter (edp). Any resulting bridge damage could be best tied to the amount of lateral ground displacement for this problem. Although the amount of vertical settlement at the abutments can also influence the performance of a bridge, its effect is usually much more localized and it has not been incorporated in the simplified approach proposed in this study. If liquefaction-induced vertical settlements need to be estimated, it is recommended to use the methods by Ishihara and Yoshimine (1990) and Tokimatsu and Seed (1984) for volumetric compression, and the procedure developed by FMSM Engineers (2007) for settlements induced by deviatoric deformations.

The probability that the liquefaction-induced lateral ground displacement exceeds a specified threshold for a given ground motion intensity measure is required to implement the PEER-PBEE methodology. In this chapter, a procedure to estimate the function $G(edp|im)$, which is required to evaluate Equation (1.1), is presented. The probability that the residual lateral seismic displacement, which is denoted as D , exceeds a certain threshold of seismic displacement, d , given a provided ground motion intensity measure, im , which is described by the relationship $\Pr(D > d | im)$, is presented.

3.1.1 Estimation of Residual Lateral Displacement

The total probability theorem is used to estimate the required conditional probability $\Pr(D > d | im)$. Let L be the event that liquefaction occurs, and let \bar{L} be the event that liquefaction does not occur. The probability that the residual lateral deformation exceeds a certain threshold given an intensity measure, $\Pr(D > d | im)$, can be estimated as:

$$\Pr(D > d | im) = \Pr(D > d | im, L) \Pr(L | im) + \Pr(D > d | im, \bar{L}) \Pr(\bar{L} | im) \quad (3.1)$$

The remaining parts of this chapter show how the terms of Equation (3.1) can be estimated.

3.1.1.1 Deterministic Estimation of Residual Lateral Displacement at Abutments

In general, the amount of residual lateral displacement will be a function of the intensity of the ground motion and the dynamic resistance of the earth slopes that impact the bridge system. This dynamic resistance is represented by the yield coefficient, k_y . In the proposed procedure, the expected level of residual longitudinal displacement at the abutments, D , is estimated using the relationship developed by Bray and Travararou (2007):

$$\begin{aligned} \ln(D) = & -1.10 - 2.83 \ln(k_y) - 0.333 (\ln(k_y))^2 + 0.566 \ln(k_y) \ln(Sa) + 3.04 \ln(Sa) + \dots \\ & - 0.244 (\ln(Sa))^2 + 1.5T_s + 0.278(M_w - 7) \pm \varepsilon \end{aligned} \quad (3.2)$$

where M_w is moment magnitude, T_s is the initial fundamental period of the potential sliding mass, Sa represents the spectral acceleration at $1.5T_s$, and ε is a normally-distributed random variable with zero mean and standard deviation $\sigma = 0.66$. To eliminate a potential bias in the model for very low values of T_s , the first term of Equation (3.2), i.e., the term -1.10, should be replaced with the term -0.22 when $T_s < 0.05$ s. For these seismic stability calculations, the initial fundamental period of the sliding mass (T_s) can be estimated using the expression: $T_s = 4H/V_s$ for the case of a relatively wide potential sliding mass that is either shaped like a trapezoid or segment of a circle where its response is largely 1D (Bray 2007), where H = the average height of the potential sliding mass, and V_s is the average shear wave velocity of the sliding mass. For the case of a triangular-shaped sliding mass that largely has a 2D response, the expression $T_s = 2.6H/V_s$ should be used. Figure 3.1 shows how to estimate T_s for the case of a soil mass, underlain by a stiff crust, sliding on top of liquefied material. In those cases, the location of the

equivalent 1D soil column should be estimated as the weighted average of the location of the slices used in the slope stability analysis, where the weighting factor would be the total weight of the respective slice.

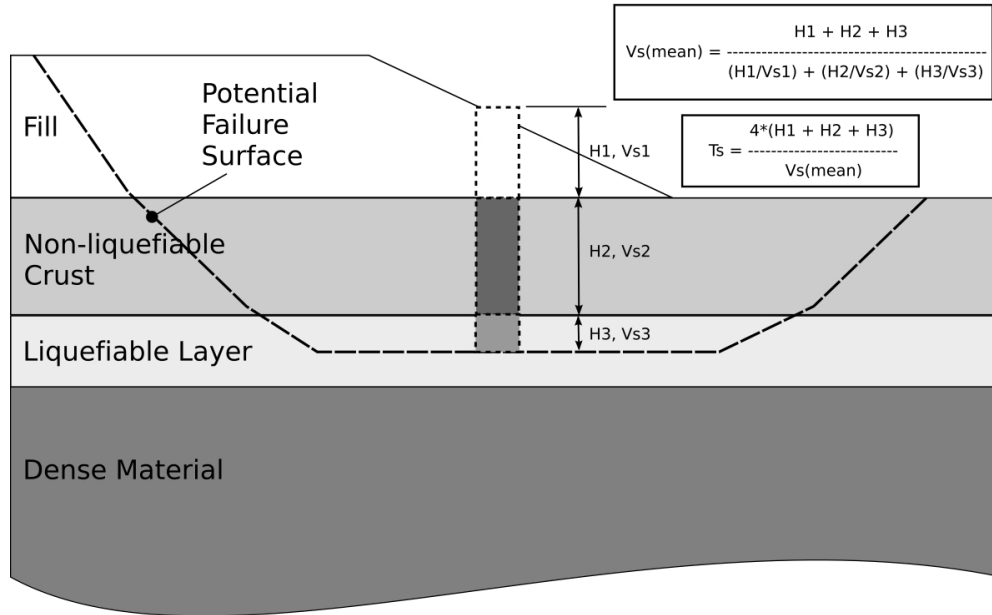


Fig. 3.1 Estimation of initial fundamental period of potential sliding mass (T_s).

The lateral resistance of the slope is principally derived from three sources: the residual undrained shear strength of the critical layer (S_{ur}), the forces induced by the pile-pinning effect, and the passive reaction at the abutment. These three forces can be combined and expressed in terms of an equivalent undrained shear strength (S_u):

$$S_u = S_{ur} + \frac{N \cdot V_p(D/2)}{A} + \frac{F_p(D/2)}{A} \quad (3.3)$$

where N is the number of piles under the abutment, $V_p(D/2)$ is the shear force on any abutment pile, $F_p(D/2)$ represents the passive reaction at the abutment, and A is the area of the horizontal portion of the failure surface. The terms $V_p(D/2)$ and $F_p(D/2)$ indicate that: (i) the shear force in the piles and the passive reaction at the abutment are a function of the lateral displacement of the abutment, D , and (ii) as recommended by Boulanger et al. (2006), the resistant forces are calculated using half of the maximum residual lateral deformation, recognizing that in these cases the maximum residual displacement usually occurs at the end of the ground motion and not at the beginning.

Let p be a function that relates the value of the yield coefficient (k_y) and the total equivalent undrained shear strength of the critical layer (S_u), i.e., $k_y = p(S_u)$, then:

$$k_y = p \left(S_{ur} + \frac{N \cdot V_p(D/2)}{A} + \frac{F_p(D/2)}{A} \right) \quad (3.4)$$

If this expression is replaced in Equation 3.2, the result is an implicit equation for D , which needs to be solved iteratively. The remainder of this subsection shows how the required terms p , V_p , F_p , and A can be estimated.

The function $p(S_u)$ can be estimated by solving the pseudostatic seismic stability problem at the abutment with different “reasonable” values of S_u , between S_{\min} and S_{\max} . Let \bar{S}_{ur} be the mean residual undrained shear strength of the liquefiable layer, M_p the plastic bending moment of each pile, H the thickness of the liquefiable layer, and F_p^{\max} the total maximum passive reaction at the abutment. A reasonable lower limit for S_u is the mean residual undrained shear strength of the liquefiable layer, i.e., $S_u = S_{\min} \approx \bar{S}_{ur}$. An upper limit for S_u can be estimated considering that the piles have reached their plastic limit, that the distance between the points of fixity is equal to the thickness of the critical layer, and that the passive reaction at the abutments has reached its maximum, in that case $S_u = S_{\max} \approx \bar{S}_{ur} + N \times 2M_p / (H \times A) + F_p^{\max} / A$. Preliminary results for a series of sensitivity analysis indicate that for cases when there is a distinct weak layer where sliding is localized, the function $p(S_u)$ is roughly linear.

The shear force in any pile, V_p , can be estimated assuming that the piles are fixed against rotation at some distance above and below the critical layer. This idea follows the approach proposed in the document MCEER/ATC-49-1 (2003) where the assumed plastic mechanism for the piles considers the formation of plastic hinges at some distance above and below the liquefiable material. Then, the shear force in any pile can be calculated as:

$$V_p(D) = \frac{2M(D)}{H + (\alpha_{top} + \alpha_{bottom}) \cdot 2R} \quad (3.5)$$

where $M(D)$ is the bending moment at the ends of the pile; $M(D) = 6E_{pile}I_{pile}D/L_{pile}^2 <$ plastic moment of pile, where E_{pile} is Young’s modulus, I_{pile} is the moment of inertia of the pile, D is the relative lateral displacement between the ends of the pile, and L_{pile} is the equivalent length of the pile, i.e., $L_{pile} = H + (\alpha_{top} + \alpha_{bottom}) \cdot 2R$; H is the total thickness of the critical layer, $2R$ is the

diameter of the pile, and α_{top} and α_{bottom} are factors that indicate how many diameters above and below the critical layer the piles are fixed against rotation. In this simplified approach it has been assumed that $\alpha_{top} \approx \alpha_{bottom} = \alpha$.

For the case of a thin nonliquefiable crust and pinned pile connection, a reasonable assumption would be to consider that the piles are fixed at a $\alpha_{bottom} \cdot 2R$ below the liquefiable material (as before), and pinned at the pile/pile-cap connection. In such case, the shear force in any pile can be calculated as:

$$V_p(D) = \frac{M(D)}{H + \alpha_{bottom} \cdot 2R + d^*} \quad (3.6)$$

where d^* is the vertical distance between the top of the liquefiable layer and the bottom of the pile cap.

Strictly speaking, the previous recommendations for the estimation of $V_p(D)$ are only valid for groups of vertical piles. However, they are a valid approximation for pile groups with only a few battered piles, and they also work as a lower bound (i.e., conservative) approximation for the less common case of pile groups consisting of only inclined piles.

The passive reaction at the abutment, $F_p(D)$, can be estimated using the recommendations from Section 7.8.1 of Caltrans' Seismic Design Criteria (2006), where for seat abutments (see Fig. 3.2):

$$\begin{aligned} K_{abut} &= K_i \times w \times \left(\frac{h}{5.5} \right) \\ K_i &= 20 \frac{\text{kip/in}}{\text{ft}} \\ P_{bw} &= A_e \times 5.0 \text{ ksf} \times \frac{h}{5.5} \\ A_e &= h \times w \text{ (area of the backwall)} \end{aligned} \quad (3.7)$$

where w and h are the width and height of the backwall (in feet), respectively.

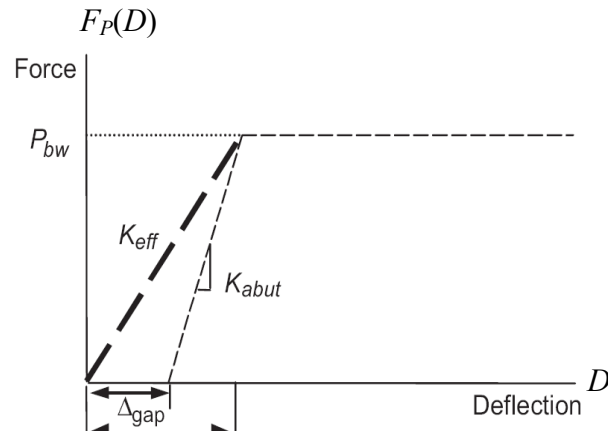


Fig. 3.2 Passive reaction versus deflection at abutments (after Caltrans 2006).

In the context of a simplified approach like the one proposed in this study, it is considered reasonable to use the abutment's passive resistance without reductions. However, it is important to note that the MCEER/ATC-49-1 (2003) procedure recommends reducing the prescribed passive capacity by 50%, a “reasonable” factor according to this document, assuming that the abutment fill has slumped “somewhat” due to the movement of the soil block. Also, it might be argued that a reduction factor should be applied to account for the fact that this force usually acts well above the potential failure plane and is less effective in resisting the rotation of the soil mass. Nevertheless, it is still questionable how much this force should be modified in a more general case.

The horizontal part of the base of the potential sliding surface can be assumed to be rectangular in shape, i.e., $A=l \times t$, where l and t are its plan dimensions in the longitudinal and transverse directions, respectively. Two effects should be considered in the estimation of l and t . First, because the overall size of the potential sliding mass varies as the equivalent undrained shear strength of the critical layer changes, the value of l (from the 2D pseudostatic seismic stability problem at the abutment) should be considered, in general, a function of S_u . Because the size of the potential sliding mass usually increases as the value of S_u increases, a conservative approach that would lead to a smaller increase in resistance due to the pile-pinning effect would be for l to be for the case in which $S_u = S_{u\max}$. Second, as Boulanger et al. (2006) have stated, the tributary width t will be greater than the abutment crest width because there will be some influence of the abutment side slope masses in the abutment response. Their recommendation of assuming that one half of the slide slope masses is restrained by the piles is adopted in the proposed procedure.

3.1.1.2 Sources and Characterization of Uncertainty

Three important parameters are treated as random variables in the proposed soil-foundation model used to estimate the engineering demand/response parameter: the error term from the model by Bray and Travasarou (2007), ε ; the distance, expressed in terms of number of pile diameters, from the limits of the liquefiable layer to the points of fixity of the piles, α_{top} and α_{bottom} ; and the residual undrained shear strength of the liquefiable layers, S_{ur} . It is important to note that above the liquefiable layer the assumption of fixity of the piles against rotation might be unconservative in situations where the upper crust is too thin or weak.

The characterization of the uncertainty of ε , α_{top} , and α_{bottom} is relatively straightforward. From the model by Bray and Travasarou (2007), the variable ε is a normally distributed random variable with zero mean and standard deviation $\sigma = 0.66$. The parameters α_{top} and α_{bottom} are assumed to have a uniform distribution between 2 and 5, with the restriction that $\alpha_{top} \cdot 2R$ cannot be greater than the vertical distance between the top of the liquefiable layer and the bottom of the respective pile cap.

The uncertainty in S_{ur} can be estimated if the probability density function (PDF) of the normalized standard penetration test blow count ($N_{1,60}$) and the PDF of S_{ur} for a given SPT value are assumed to be known. In that case, by the total probability theorem:

$$f_{S_{ur}}(s_{ur}) = \int_{-\infty}^{+\infty} f_{S_{ur}}(s_{ur} | n_{1,60}) f_{N_{1,60}}(n_{1,60}) dn_{1,60} \quad (3.8)$$

where $f_{S_{ur}}(s_{ur})$ is the resultant PDF of S_{ur} , and $f_{N_{1,60}}(n_{1,60})$ and $f_{S_{ur}}(s_{ur} | n_{1,60})$ are the given probability density functions.

In the proposed approach it is assumed that $N_{1,60}$ has a lognormal distribution and a coefficient of variation (c.o.v.) of 0.3. The selected c.o.v. is based on Table 3 of Duncan (2000), wherein 0.15 to 0.45 is given as the typical range for the coefficient of variation of $N_{1,60}$.

The probability density function of the S_{ur}/σ_{vc} ratio given a corrected standard penetration test (SPT) blow-count ($N_{1,60-CS}$) is also assumed to be lognormal. Five of the most commonly used procedures to estimate the residual undrained shear strength of the liquefiable layer, S_{ur} , are combined to estimate its mean and coefficient of variation. Figure 3.3 shows the

mean estimates from the methods proposed by Seed and Harder (1990), Olson and Stark (2002), and Kramer (2007), and the correlations of S_{ur} with $N_{1,60-CS}$, and S_{ur} / σ_{vc}' with $N_{1,60-CS}$ proposed by Idriss and Boulanger (2007). These models were linearly combined using relative weights of 2:3:3:2:5, respectively, to estimate the mean of $(S_{ur} / \sigma_{vc}') | N_{1,60-CS}$. Preference was given to methods that estimate the ratio S_{ur} / σ_{vc}' as opposed to just S_{ur} and to the most recent method of Idriss and Boulanger (2007). The result is shown in Figure 3.3 with black X's.

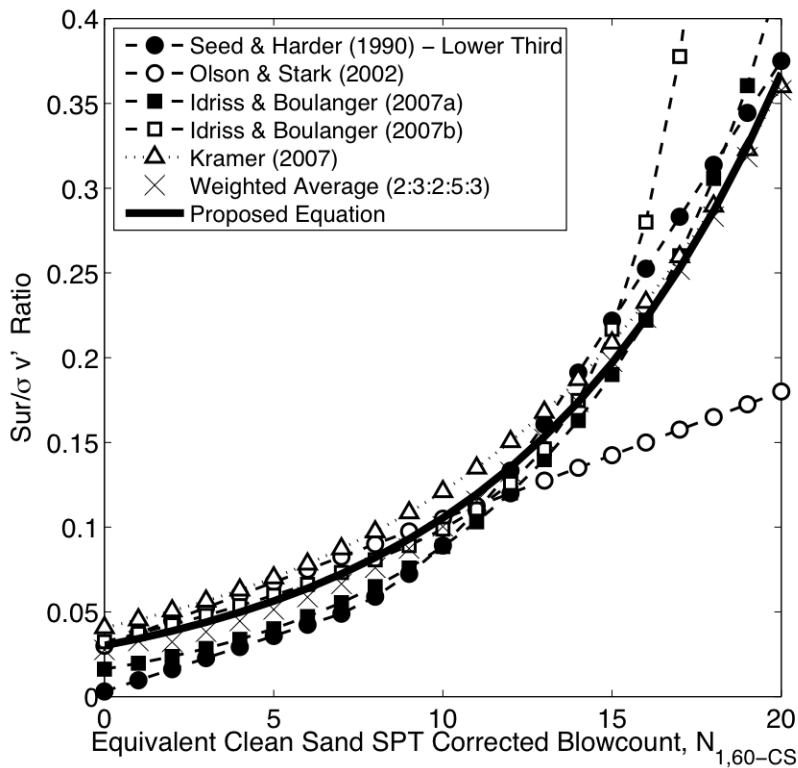


Fig. 3.3 Mean estimates of S_{ur} / σ_{vc}' ratios from different methods.

The relationship that was fitted to the combined results expressed by the black X's, shown as the thick black line in Figure 3.3 is:

$$E[(S_{ur} / \sigma_{vc}') | N_{1,60-CS}] = \exp\left(\frac{N_{1,60-CS}}{8} - 3.5\right) \quad 0 \leq N_{1,60-CS} \leq 20 \quad (3.9)$$

The upper and lower limits of the Seed and Harder (1990) relationship, and the plus and minus one standard deviations of the models proposed by Olson and Stark (2002) and Kramer (2007), which are shown in Figure 3.4, were used to estimate the coefficient of variation of this random variable.

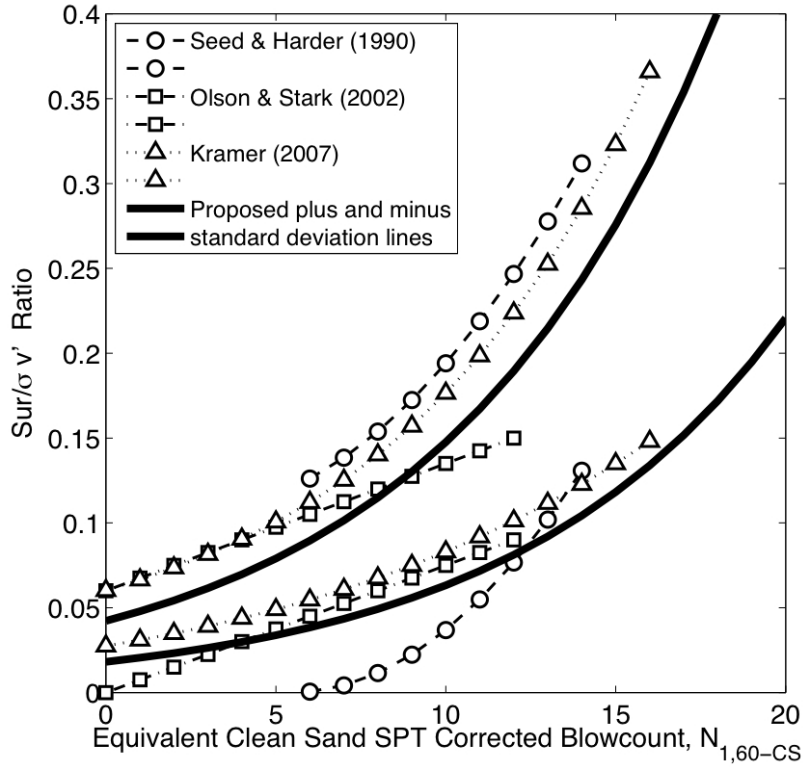


Fig. 3.4 Dispersion in estimates of S_{ur} / σ_{vc}' ratios from different methods.

Based on these results, a reasonable assumption is to consider that the c.o.v. of S_{ur} / σ_{vc}' given $N_{1,60-CS}$ is equal to 0.40 (constant), i.e.,

$$c.o.v. [(S_{ur} / \sigma_{vc}') | N_{1,60-CS}] = 0.40 \quad 0 \leq N_{1,60-CS} \leq 20 \quad (3.10)$$

The result of this assumption is shown with thick black lines in Figure 3.4. Note that every pair of curves is shifted with respect to the others because every pair is centered on different mean values.

If it is assumed that $(S_{ur} / \sigma_{vc}') | N_{1,60-CS}$ has the mean and c.o.v. shown in Equations 3.8 and 3.9, and that $cov_{N_{1,60}} = 0.3$ (constant), the second-order approximation for the first moment of $(S_{ur} / \sigma_{vc}') | N_{1,60-CS}$ gives the following recommended mean and standard deviation for (S_{ur} / σ_{vc}') :

$$\mu_{S_{ur}/\sigma_{v'}} \approx \exp\left(\frac{\mu_{N_{1,60-CS}}}{8} - 3.5\right) \times \left(1 + \frac{(0.3\mu_{N_{1,60-CS}})^2}{128}\right) \quad (3.11)$$

$$\sigma_{S_{ur}/\sigma_{v'}} \approx 0.4\mu_{S_{ur}/\sigma_{v'}}$$

If information from cone penetration tests (CPTs) is provided, the following CPT-SPT correlation proposed by Kulhawy and Mayne (1990) may be used:

$$\frac{(q_c/P_a)}{N} = 5.44(D_{50})^{0.26} \quad (3.12)$$

where q_c is tip resistance, P_a is atmospheric pressure (~ 100 kPa), N is the measured SPT value, and D_{50} is the particle size that 50% passes by weight. Alternatively, one could use expressions that directly estimate S_{ur} from CTP results. Equations (3.13) and (3.14) were developed by Olson and Stark (2002) and Idriss and Boulanger (2007), respectively, for this purpose:

$$\frac{S_{ur}}{\sigma_{v'}} = 0.03 + 0.0143(q_{c1}) \pm 0.03 \quad (\text{for } q_{c1} \leq 6.5 \text{ MPa}) \quad (3.13)$$

$$\frac{S_{ur}}{\sigma_{v'}} = \exp\left(\frac{q}{24.5} - \left(\frac{q}{61.7}\right)^2 + \left(\frac{q}{106}\right)^3 - 4.42\right) \times \left(1 + \exp\left(\frac{q}{11.1} - 9.82\right)\right) \leq \tan \phi' \quad (3.14)$$

where $\sigma_{v'}$ is the effective overburden stress, q_{c1} is the normalized tip resistance (MPa), $q \equiv q_{c1Ncs-Sr}$ is the equivalent clean-sand CPT normalized corrected tip resistance, and ϕ' is the effective stress friction angle.

The last source of uncertainty in the proposed model is the occurrence of liquefaction. Let L be the event that liquefaction occurs, and \bar{L} be the event that liquefaction does not occur. The probability of occurrence of liquefaction given an intensity measure, $\Pr(L|im)$, can be estimated making use of the expression developed by Seed et al. (2003):

$$P_L(N_{1,60}, CSR, M_w, \sigma_{v'}, FC) = \Phi \left(- \frac{\left(\begin{array}{l} N_{1,60} \cdot (1 + 0.004FC) - 13.32 \cdot \ln(CSR) - \\ 29.53 \cdot \ln(M_w) - 3.70 \cdot \ln(\sigma_{v'}) \\ + 0.05 \cdot FC + 44.97 \end{array} \right)}{2.70} \right) \quad (3.15)$$

where P_L is the probability that liquefaction occurs; $N_{1,60}$ is the normalized standard penetration test blow-count; CSR is the cyclic stress ratio, $CSR = 0.65(a_{\max}/g)(\sigma_v/\sigma'_v)r_d$, where a_{\max} is the peak horizontal ground surface acceleration, g is the acceleration of gravity, σ_v is the total vertical stress, σ'_v is the effective vertical stress, and r_d is the nonlinear shear mass participation factor; M_w is the moment magnitude; FC is the percent fines content (by dry weight) expressed as an integer (i.e., 12% fines is expressed as $FC = 12$); and Φ is the standard normal cumulative distribution function (e.g., the NORMSDIST function in Excel).

If CPT results are available, the probability of liquefaction occurrence given an intensity measure can be estimated using the following expression (Moss et al. 2005):

$$P_L = \Phi \left[- \frac{\left(q_{c,1}^{1.045} + q_{c,1} (0.110 \cdot R_f) + (0.110 \cdot R_f) + c (1 + 0.850 \cdot R_f) + \dots \right)}{1.632} \right] \quad (3.16)$$

where $q_{c,1}$ is the normalized tip resistance (MPa), $q_{c,1} = q_c \cdot C_q$, where q_c is the raw tip resistance (MPa), $C_q = (P_a/\sigma'_v)^c$ is the tip normalization factor, P_a is the reference stress (~ 100 kPa), σ'_v is the effective overburden stress (kPa), and c is the normalization exponent (a value typically between 0.35 and 1.00); $R_f = (f_s/q_c) \cdot 100$ is the friction ratio, i.e., the sleeve to tip resistance expressed as percentage; CSR is the equivalent uniform cyclic stress ratio; M_w is moment magnitude; and Φ is the cumulative normal distribution.

If the values of σ'_v and FC are assumed to be deterministic, Equation (3.15) provides an estimation of the probability of liquefaction given the values of $N_{1,60}$, CSR , and M_w . The values of CSR and M_w are part of the earthquake ground motion intensity measures, so this relation can provide an estimate of $\Pr(L | im, n_{1,60})$. Let $f_{N_{1,60}}(n_{1,60})$ be the PDF of the random variable $N_{1,60}$. The total probability theorem can be used to estimate the probability of liquefaction given an intensity measure through:

$$\begin{aligned} \Pr(L | im) &= \int_{-\infty}^{+\infty} \Pr(L | im, n_{1,60}) f_{N_{1,60}}(n_{1,60} | im) dn_{1,60} \\ &= \int_0^{+\infty} \Pr(L | im, n_{1,60}) f_{N_{1,60}}(n_{1,60}) dn_{1,60} \end{aligned} \quad (3.17)$$

where it has been assumed that $N_{1,60}$ is independent of the intensity measure (im). The probability that liquefaction does not occur given an intensity measure can be calculated as:

$$\Pr(\bar{L} | im) = 1 - \Pr(L | im) \quad (3.18)$$

3.1.1.3 Procedures to Calculate Probability of Exceeding Engineering Parameter Threshold, Given Intensity Measure

At this point a pseudoprobabilistic model to estimate the residual lateral seismic displacement, D , and an associated set of random variables have been identified. The pseudoprobabilistic model is a modification of the one developed by Bray and Travararou (2007), and the random variables that have been selected and characterized are: S_{ur} , α , and ε . Once these two components of the problem are defined, several methods are available to numerically calculate the required probabilities, $\Pr(D > d | im, L)$ or $\Pr(D > d | im, \bar{L})$. Two of these methods are appropriate in the context of the proposed simplified design procedure: the first-order reliability method (FORM) and the point estimate method (PEM).

In the first of these two methods, FORM, the evaluation of $\Pr(D > d | im, L)$ or $\Pr(D > d | im, \bar{L})$ is thought of as the estimation of the probability of failure of a component, where “failure” is defined as the event $\{D > d\}$ given an intensity measure and that liquefaction has (or has not) occurred. In reliability theory terms, the limit-state function of the problem is $g(\underline{x}) = d - D(\underline{x})$, where \underline{x} represents a vector of random variables, and $D(\underline{x})$ comes from Equation (3.2). The vector of random variables in this case is $\underline{x} = [S_{ur} \quad \alpha \quad \varepsilon]^T$, and the probability of failure is defined as a three-fold integral:

$$p_f = \int_{\Omega} f(\underline{x}) d\underline{x} \quad (3.19)$$

where $f(\underline{x})$ is the joint probability density function (PDF) of \underline{x} , and $\Omega \equiv \{g(\underline{x}) \leq 0\}$. The evaluation of this integral is usually difficult, because for most nontrivial selections of $f(\underline{x})$ and Ω , no closed-form solution of the integral exists. In FORM, an approximation to the probability integral in Equation 3.14 is obtained by transforming the set of random variables \underline{x} to standard normal space \underline{u} , and by linearizing the limit-state function in the standard normal space $G(\underline{u})$ at

an optimal point \underline{u}^* . The fundamental assumption is that the limit-state function is continuous and differentiable, at least in the neighborhood of the optimal point. Then:

$$p_f = \int_{g(\underline{x}) \leq 0} f(\underline{x}) d\underline{x} = \int_{G(\underline{u}) \leq 0} \varphi_n(\underline{u}) d\underline{u} \quad (3.20)$$

where $\varphi_n(\underline{u})$ is the multivariate standard normal probability density function, and

$$\begin{aligned} G(\underline{u}) &\approx G_1(\underline{u}) = \nabla G(\underline{u}^*)(\underline{u} - \underline{u}^*) = \|\nabla G(\underline{u}^*)\|(\beta - \alpha \underline{u}) \\ \underline{u}^* &= \arg \min \{\|\underline{u}\| \mid G(\underline{u}) = 0\} \end{aligned} \quad (3.21)$$

In essence, FORM replaces the failure domain $G(\underline{u}) \leq 0$ by the halfspace $\beta - \alpha \underline{u} \leq 0$. The first-order approximation of the failure probability is given by the probability content of the halfspace in the standard normal space, which is completely defined by the parameter β , i.e.,

$$p_f \approx \Phi(-\beta) \quad (3.22)$$

where Φ is the standard normal cumulative density function.

Preliminary results indicate that FORM gives reasonably accurate results when compared to Monte Carlo Simulations or the results from second-order reliability methods (SORM). The program FERUM was used to evaluate the required probability $\Pr(g(\underline{x}) \leq 0)$ using FORM (Der Kiureghian et al. 2006; <http://www.ce.berkeley.edu/~haukaas/ FERUM/ferum.html>).

The second method, PEM, was first proposed by Rosenblueth in 1975. With PEM the first moments of the function $D(\underline{x})$ are computed in terms of the first few moments of the random variable \underline{x} . No information is required (nor obtained) about the probability density function of the different parameters. This means that to estimate the required probabilities, an assumption must be made about the PDF of $D(\underline{x})$, e.g., lognormal. For a detailed explanation of PEM, the reader is referred to Christian and Baecher (1999). This method indicates that if $\underline{X} = [X_1 \ X_2 \ \dots \ X_n]^T$ is a vector of n random variables, and Y a deterministic scalar function of \underline{X} , $Y = g(\underline{X})$, the low-order moments of $f_Y(y)$ can be estimated as:

$$E[Y^m] = \sum P_{s_1 s_2 \dots s_n} (y_{s_1 s_2 \dots s_n})^m \quad (3.23)$$

where m is the moment order and:

$$s_i = \begin{cases} + & \text{if } X_i = \mu_{X_i} + \sigma_{X_i} \\ - & \text{if } X_i = \mu_{X_i} - \sigma_{X_i} \end{cases} \quad (3.24)$$

$$P_{s_1 s_2 \dots s_n} = \frac{1}{2^n} \left[1 + \sum_{i=1}^{n-1} \sum_{j=i+1}^n s_i s_j \rho_{ij} \right] \quad (3.25)$$

$$y_{s_1 s_2 \dots s_n} = Y(X_{s_1 s_2 \dots s_n}) \quad (3.26)$$

For the case of three uncorrelated random variables Equation 3.18 reduces to:

$$E[Y] = \frac{1}{8} \begin{bmatrix} Y(\mu_{X_1} + \sigma_{X_1}, \mu_{X_2} + \sigma_{X_2}, \mu_{X_3} + \sigma_{X_3}) + Y(\mu_{X_1} + \sigma_{X_1}, \mu_{X_2} + \sigma_{X_2}, \mu_{X_3} - \sigma_{X_3}) + \dots \\ Y(\mu_{X_1} + \sigma_{X_1}, \mu_{X_2} - \sigma_{X_2}, \mu_{X_3} + \sigma_{X_3}) + Y(\mu_{X_1} - \sigma_{X_1}, \mu_{X_2} + \sigma_{X_2}, \mu_{X_3} + \sigma_{X_3}) + \dots \\ Y(\mu_{X_1} + \sigma_{X_1}, \mu_{X_2} - \sigma_{X_2}, \mu_{X_3} - \sigma_{X_3}) + Y(\mu_{X_1} - \sigma_{X_1}, \mu_{X_2} + \sigma_{X_2}, \mu_{X_3} - \sigma_{X_3}) + \dots \\ Y(\mu_{X_1} - \sigma_{X_1}, \mu_{X_2} - \sigma_{X_2}, \mu_{X_3} + \sigma_{X_3}) + Y(\mu_{X_1} - \sigma_{X_1}, \mu_{X_2} - \sigma_{X_2}, \mu_{X_3} - \sigma_{X_3}) \end{bmatrix} \quad (3.27)$$

$$E[Y^2] = \frac{1}{8} \begin{bmatrix} Y^2(\mu_{X_1} + \sigma_{X_1}, \mu_{X_2} + \sigma_{X_2}, \mu_{X_3} + \sigma_{X_3}) + Y^2(\mu_{X_1} + \sigma_{X_1}, \mu_{X_2} + \sigma_{X_2}, \mu_{X_3} - \sigma_{X_3}) + \dots \\ Y^2(\mu_{X_1} + \sigma_{X_1}, \mu_{X_2} - \sigma_{X_2}, \mu_{X_3} + \sigma_{X_3}) + Y^2(\mu_{X_1} - \sigma_{X_1}, \mu_{X_2} + \sigma_{X_2}, \mu_{X_3} + \sigma_{X_3}) + \dots \\ Y^2(\mu_{X_1} + \sigma_{X_1}, \mu_{X_2} - \sigma_{X_2}, \mu_{X_3} - \sigma_{X_3}) + Y^2(\mu_{X_1} - \sigma_{X_1}, \mu_{X_2} + \sigma_{X_2}, \mu_{X_3} - \sigma_{X_3}) + \dots \\ Y^2(\mu_{X_1} - \sigma_{X_1}, \mu_{X_2} - \sigma_{X_2}, \mu_{X_3} + \sigma_{X_3}) + Y^2(\mu_{X_1} - \sigma_{X_1}, \mu_{X_2} - \sigma_{X_2}, \mu_{X_3} - \sigma_{X_3}) \end{bmatrix} \quad (3.28)$$

Equation 3.27 gives an estimation of the mean of Y . Its standard deviation can be estimated from the results of Equations 3.27 and 3.28 as $\sigma_Y = \sqrt{E[Y^2] - E^2[Y]}$.

For the bridge problem discussed in this report, the estimated level of displacement D can be written as a linear combination of the displacements that would occur with and without liquefaction for a given intensity measure of the ground motion. Let P_L be the probability of the occurrence of liquefaction, and D_L and D_{NL} be the displacements with and without liquefaction, respectively, then:

$$D = P_L D_L + (1 - P_L) D_{NL} \quad (3.29)$$

It can be shown that in this case the expectation of D and D^2 are:

$$\begin{aligned} E[D] &= P_L E[D_L] + (1 - P_L) E[D_{NL}] \\ E[D^2] &= P_L^2 E[D_L^2] + (1 - P_L)^2 E[D_{NL}^2] + 2P_L(1 - P_L) E[D_L] E[D_{NL}] \end{aligned} \quad (3.30)$$

from where $\mu_D = E[D]$ and $\sigma_D = \sqrt{E[D^2] - E^2[D]}$.

3.2 DERIVED ENGINEERING DEMAND PARAMETERS

The amount of lateral displacement at the ends of the bridge will directly affect the local response of the abutments and their foundation, but it will also affect the lateral displacements and rotations of the other pile caps, and ultimately it will influence the amount of drift that the bridge columns will experience and hence, overall bridge damage.

3.2.1 Decoupled Models

In this section, three simple structural models are proposed to estimate the lateral displacement of the intermediate piers' pile caps, the pile-cap rotation, and the effect that these displacements and rotations will have on column drift.

A simple structural model is proposed to estimate the lateral displacement of the intermediate piers' pile caps from the displacement of the abutments' pile caps (see Fig. 3.5). The adopted concept is that as the embankments displace toward the center of the bridge, the abutments' pile caps will move in concert with the upper non-liquefiable crust. Then, a fraction of that lateral movement will get transferred to the next pile caps through the compression of the non-liquefiable crust.

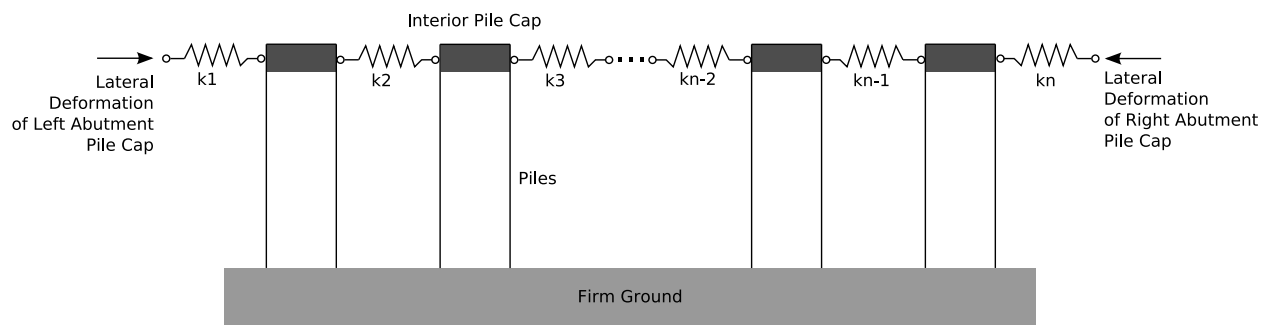


Fig. 3.5 Structural model to estimate lateral displacement of intermediate piers' pile caps from displacement of abutment pile caps.

The stiffness k of the springs used in this model can be estimated considering the *pile cap passive earth pressure spring* model (Mokwa 1999). The stiffness of these springs is based on y_{50} which is the displacement that corresponds to half of the ultimate passive resistance of the

pile cap ($P_{ult, cap}$). The value of $P_{ult, cap}$ is estimated using the $\phi = 0$ sliding wedge method (Mokwa 1999):

$$P_{ult, cap} = \frac{S_u b H}{2} \left(4 + \frac{\gamma H}{S_u} + 0.25 \frac{H}{b} + 2\alpha \right) \quad (3.31)$$

Pile-cap rotation can have an important effect on column drift. Figure 3.6 shows the simple structural model that is proposed to estimate pile-cap rotation as a function of its lateral deformation. The pile cap is assumed to be infinitely rigid compared to the piles; each column of this model represents one row of piles, so their area and moment of inertia need to be specified accordingly; finally, the height of the columns needs to be consistent to what has been assumed previously, i.e.,

$$H_{eq} \approx H_{Liquefiable\ Layer} + 3.5 \cdot (2R) + Min\{3.5 \cdot (2R), d^*\} \quad (3.32)$$

where the factors of 3.5 correspond to the mean of α_{top} or α_{bottom} , R is pile radius, and d^* is the vertical distance between the top of the liquefiable layer and the bottom of the respective pile cap.

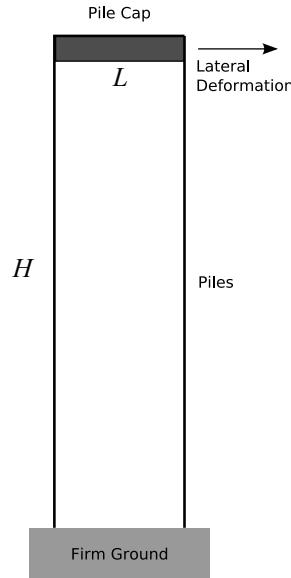


Fig. 3.6 Structural model to estimate pile-cap rotation as a function of lateral deformation.

If the response of the piles is assumed to be linear elastic, the relationship between pile-cap rotation (θ) and lateral displacement (D) is:

$$\theta = \frac{24}{\left(\frac{A_{pile} L^2}{I_{pile}} + 16 \right)} \cdot \frac{D}{H} \text{ clockwise} \quad (3.33)$$

where H and L are defined in Figure 3.6; and A_{pile} and I_{pile} are, respectively, the area and moment of inertia of one pile. For other situations (e.g., flexible pile cap, or nonlinear behavior of piles), programs such as SAP2000, OpenSees, and RISA can be used.

To evaluate the potential effects that foundation deformations may have on bridge column drifts, it is proposed to use a structural model as shown in Figure 3.7. Given the potential levels of deformations involved, the model used to represent the superstructure's elements has to capture geometric and material nonlinearity. The inputs for this model are the abutments' lateral displacements applied at both ends of the bridge, and the lateral displacements and rotations of the intermediate pile caps.

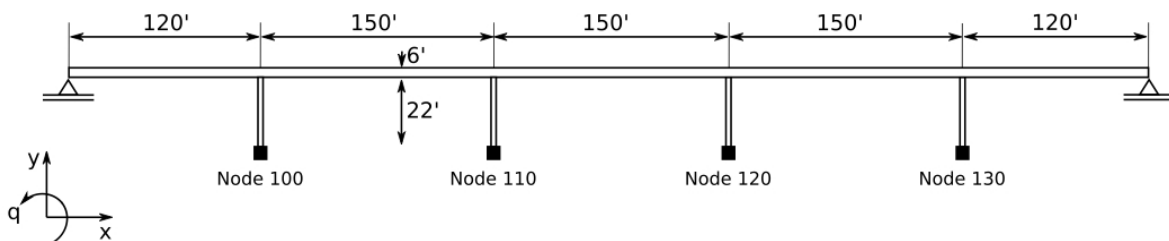


Fig. 3.7 Simplified 2D structural model.

3.2.2 Coupled Model

Figure 3.8 shows a simple structural model that is proposed to estimate column drift given the amount of residual lateral displacement at the embankments of the bridge.

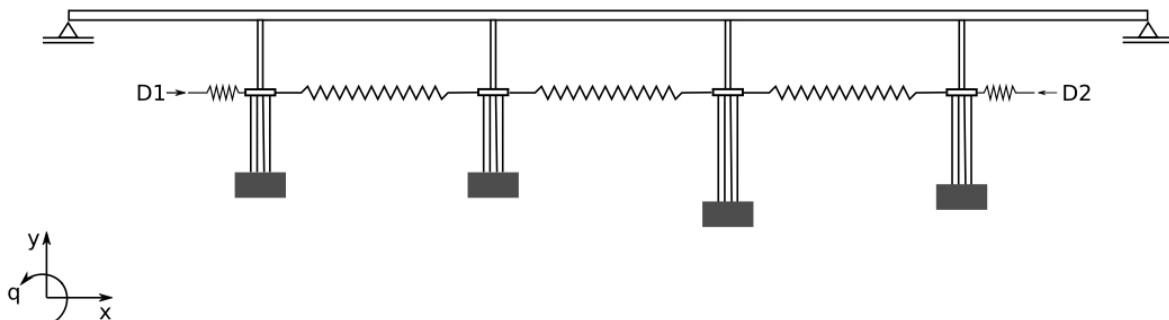


Fig. 3.8 Schematic representation of simplified coupled model.

In this model, the equivalent length (L_{eq}) of the piles tries to represent the lateral stiffness they provide to the system, $L_{eq} = H_{liq} + 2 \times 3.5(2R)$, where H_{liq} is the thickness of the liquefiable material at the location of the respective pier, and R is the pile radius.

The springs shown in Figure 3.8 try to model the interaction that occurs, through the compression of the upper non-liquefiable layer, between pile caps, and between the embankment and the first pile cap. The stiffness of these springs can be estimated considering the *pile cap passive earth pressure spring* model (Mokwa 1999). It is proposed to consider that the stiffness of the intermediate springs is half of the stiffness of the end springs, because there are two springs acting in series between the pile caps.

4 Probabilistic Evaluation of Bridge Damage

Based on the assumptions made by Dr. Kevin Mackie, on discussions with other engineers, and engineering judgment, the following models have been adopted for the estimation of damage (or repair decisions) to the abutments, columns, and piles.

4.1 DAMAGE TO ABUTMENTS

Four damage states (repair decisions) were identified for the abutments: cleaning, assembly, backwall spalling, and backwall failure. As Table 4.1 shows, these states were considered to be a function of the residual relative lateral displacement between the abutment and deck structure. Figure 4.1 is the graphical representation of the values given in Table 4.1.

Table 4.1 Abutment damage states as function of residual relative lateral deformation in longitudinal direction.

Damage State/ Repair Decision	Median Residual Lateral Deformation	Dispersion Log-units
Cleaning	2 in (0.05 m)	0.25
Assembly	4 in (0.10 m)	0.25
Backwall spalling	4.3 in (0.11 m)	0.30
Backwall failure	5.5 in (0.14 m)	0.40

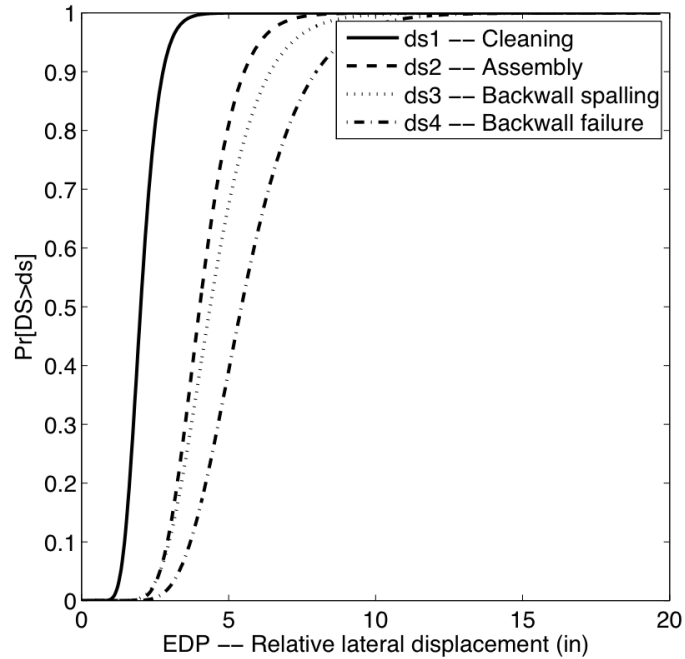


Fig. 4.1 Abutment damage states as function of residual relative lateral deformation in longitudinal direction.

4.2 DAMAGE TO COLUMNS

Four repair decisions have been identified for the piers: do nothing, thicken pier, re-center column, and allow failure. As Table 4.2 shows, the repair decisions were considered to be a function of the residual tangential drift of the columns. Figure 4.2 is the graphical representation of the values given in Table 4.2.

Table 4.2 Column repair decisions as function of residual tangential drift.

Repair Decisions	Median Residual Tangential Drift	Dispersion Log-units
Do nothing	0.50%	0.30
Thicken pier	1.25%	0.40
Re-center column	2.00%	0.40
Failure	6.72%	0.35

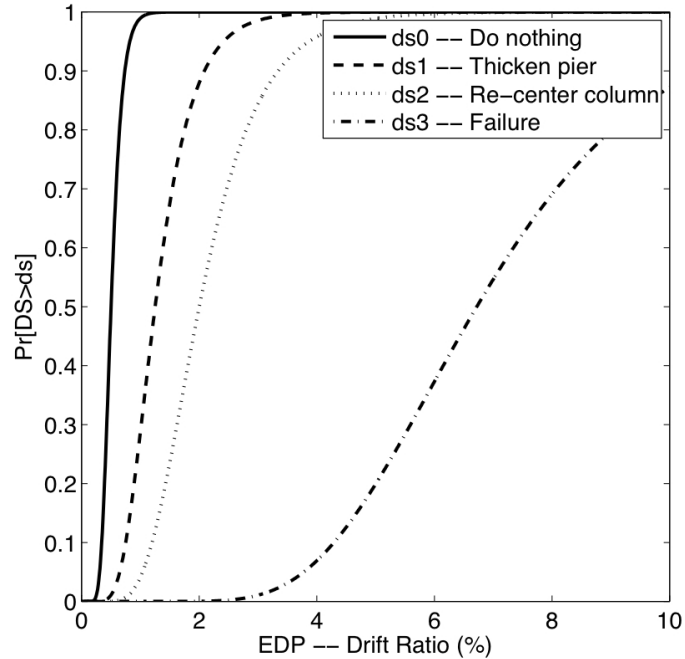


Fig. 4.2 Column repair decisions as function of residual tangential drift.

4.3 DAMAGE TO PILES

Without sufficient case histories and experimental data, analytical models or engineering judgment based on recommendations from a panel of experts are the only ways to estimate the amount of damage induced in a pile as a function of pile deformation or distortion. Using the analytical approach, the most straightforward estimation would be to utilize the allowable limiting plastic rotation of 0.05 radians that is given in the MCEER/ATC-49-1 (2003) document. Consequently, if the plastic rotation in the pile is calculated to be less than 0.05 radians, the expected level of damage to the pile would be estimated to be negligible or small. If the plastic rotation in the pile is calculated to be greater than 0.05 radians, the expected damage state for the pile would be estimated to be moderate, large, or collapse.

Another alternative is to make use of the estimations made by Dr. Kevin Mackie for the assessment of pile damage. Two repair decisions have been identified for the piles: add pile, and enlarge and add piles. As Table 4.3 shows, the repair decisions are a function of the pile cap lateral displacement and the thickness of the potentially liquefiable layer. A constant dispersion of 0.4 (log-units) has been assumed in this case. Figure 4.3 is the graphical representation of the values given in Table 4.3.

Table 4.3 Piles damage states as function of pile cap lateral displacement.

Piles	Median displacement required to “add piles”	Median displacement required to “enlarge and add piles”
Left Abutment	12 in (0.3 m)	20 in (0.5 m)
Column 1	12 in (0.3 m)	20 in (0.5 m)
Column 2	16 in (0.4 m)	28 in (0.7 m)
Column 3	28 in (0.7 m)	47 in (1.2 m)
Column 4	31 in (0.8 m)	55 in (1.4 m)
Right Abutment	31 in (0.8 m)	55 in (1.4 m)

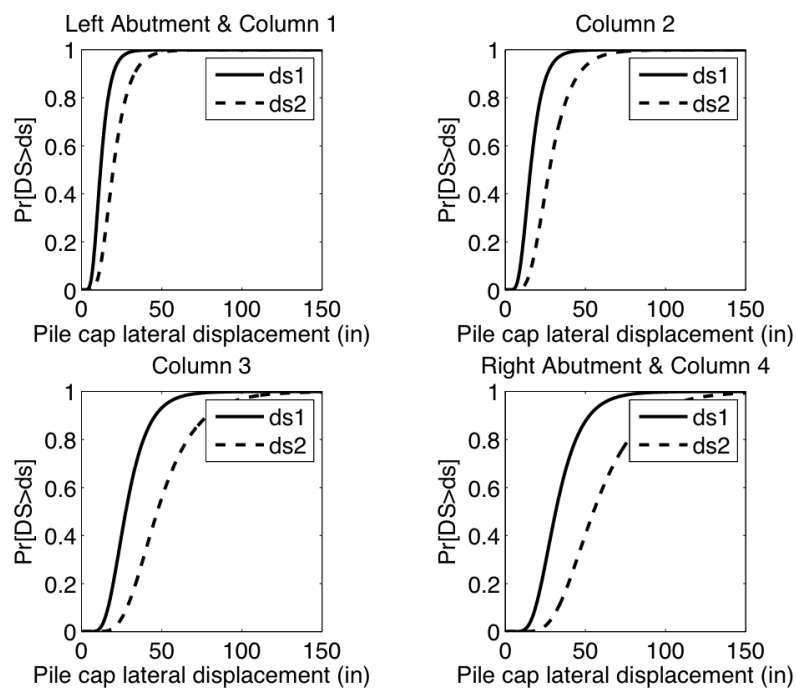


Fig. 4.3 Piles damage states as function of pile cap lateral displacement.

5 Probabilistic Evaluation of Consequences

5.1 REPAIR COSTS

5.1.1 Simplified Approach

In this simplified approach, it is assumed that the amount of seismically induced permanent lateral displacement (D) at the bridge abutments, which is modified to reflect the restraint provided by the bridge deck and pile-pinning effect (when it is appropriate to do so), has the primary effect on the overall performance of the entire bridge system. Depending on the level of seismically induced residual lateral displacement calculated at the bridge abutments, it is proposed to consider that the bridge can reach five potential levels of damage: negligible, small, moderate, large, and collapse (see Table 5.1). Figure 5.1 shows the resultant fragility curves for these damage states, given a seismic displacement.

Table 5.1 Bridge damage as a function of residual lateral displacement.

Seismic Displacement (in.)	Damage Level
0 – 1”	Negligible
1” – 4”	Small
4” – 20”	Moderate
20” – 80”	Large
> 80”	Collapse

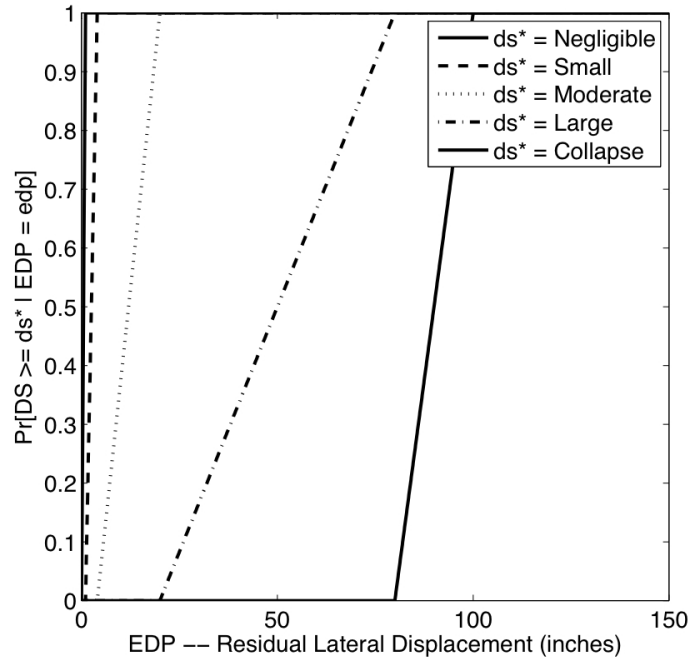


Fig. 5.1 Bridge damage as function of residual lateral displacement.

The potential repair costs of a bridge are a function of the level of damage the bridge has experienced. For every damage state, it is assumed that there is a certain probability of reaching specific repair cost ratios, which have been discretized in bins of 0.1 (see Table 5.2 and Fig. 5.2). The resultant fragility curves for Repair Cost Ratios are shown in Figure 5.3, which has been subdivided into eleven subplots for the sake of clarity. Each subplot corresponds to one specific repair cost ratio, where the five damage states (Negligible, Small, Moderate, Large, and Collapse) are listed across the x-axis, and the probability of exceeding a specific repair cost ratio for a given damage state is provided along the y-axis. The level of uncertainty in the estimation of repair cost ratios as a function of damage state may have an important effect on the results of the proposed approach. That is why it is recommended to apply this simplified approach considering at least two different levels of uncertainty, which for this case are categorized as low (gray bars/continuous line) and high (black bars/dashed lines).

Table 5.2 Repair cost ratio distribution given damage state considering low and high uncertainty (values in parenthesis correspond to high uncertainty).

	Damage State				
	Negligible	Small	Moderate	Large	Collapse
$\Pr(RCR = 0.0 ds)$	1 (1)	1 (1)	0	0	0
$\Pr(RCR = 0.1 ds)$	0	0	1 (0.95)	0	0
$\Pr(RCR = 0.2 ds)$	0	0	0 (0.05)	0	0
$\Pr(RCR = 0.3 ds)$	0	0	0	0 (0.05)	0
$\Pr(RCR = 0.4 ds)$	0	0	0	0.15 (0.25)	0 (0.05)
$\Pr(RCR = 0.5 ds)$	0	0	0	0.70 (0.30)	0 (0.15)
$\Pr(RCR = 0.6 ds)$	0	0	0	0.15 (0.25)	0.20 (0.20)
$\Pr(RCR = 0.7 ds)$	0	0	0	0 (0.1)	0.55 (0.25)
$\Pr(RCR = 0.8 ds)$	0	0	0	0 (0.05)	0.20 (0.20)
$\Pr(RCR = 0.9 ds)$	0	0	0	0	0.05 (0.1)
$\Pr(RCR = 1.0 ds)$	0	0	0	0	0 (0.05)

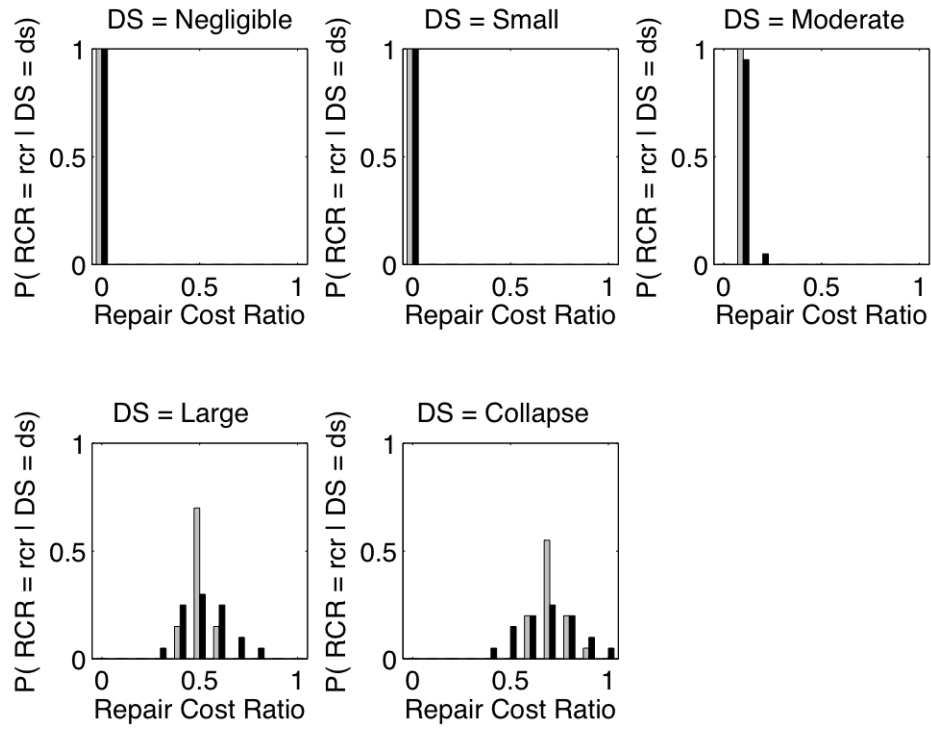


Fig. 5.2 Repair cost ratio distribution given damage state considering low (gray bars) and high (black bars) uncertainty.

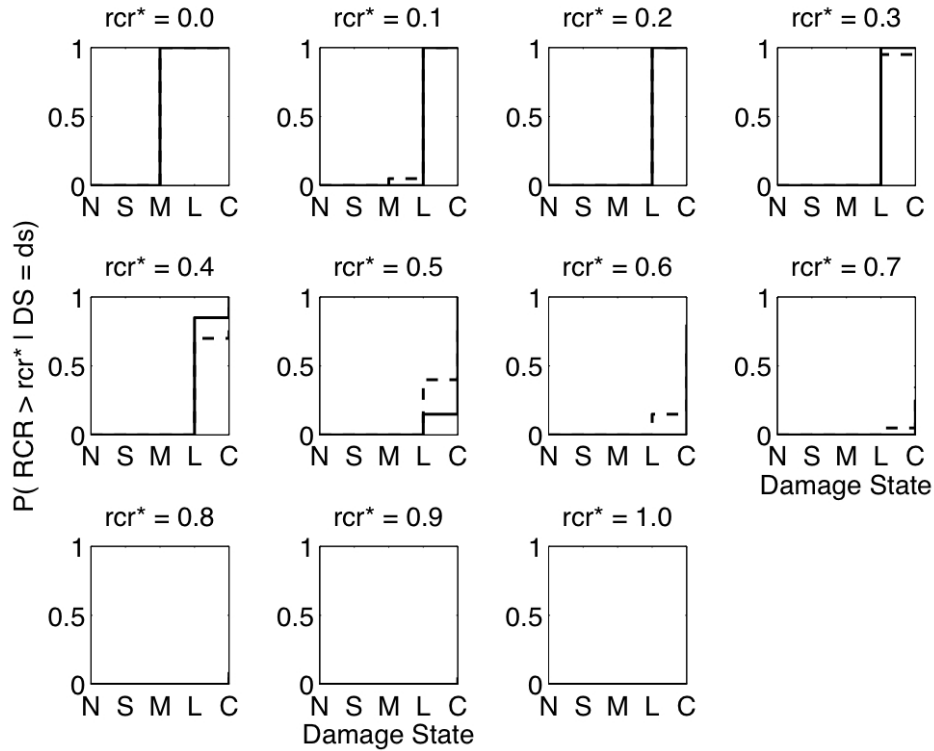


Fig. 5.3 Repair cost ratio cumulative distribution given damage state considering low (continuous line) and high (dashed lines) uncertainty.

5.1.2 Component-Based Approach

The method proposed by Mackie et al. (2007) is selected to estimate the total repair cost ratio from the repair cost of different components of the bridge. In this method the repair cost probability distribution is derived using first and second moments from a simple graphical tool called “Fourway.” This tool uses three probabilistic models to evaluate repair costs based on the Pacific Earthquake Engineering Research Center’s performance-based earthquake engineering framework: (1) a probabilistic seismic demand model relating earthquake intensity measure to bridge response parameters, (2) a probabilistic damage model relating bridge demand to discrete damage states of key bridge components, and (3) a cost model relating damage states to the cost of available repair methods.

In this simplified approach, the results from the coupled model (see Section 3.2.2) are used to estimate EDPs versus IM relationships. Damage states are defined for 19 bridge components to relate DMs to EDPs. Each damage state is associated with several repair quantities, and each repair quantity has a unit cost that is used to relate DVs to DMs. Repair cost

data in Mackie et al. (2007) is taken from different sources including Caltrans Construction Statistics, Caltrans Bridge Design Aids, and information based on case histories of Caltrans bridges in previous earthquakes.

According to Mackie et al. (2007), the Fourway method is based on the first and second (central) probabilistic moments and is a generalization of the closed-form solution to a single DV-DM-EDP-IM analysis. The simplified Fourway solution requires certain conditions on each of the demand, damage, and loss models in order to obtain a relationship between intensity and loss. Three specific conditions must be valid: (1) the distribution of EDP is lognormal when conditioned on IM (and so forth for DM and DV when conditioned on EDP and DM, respectively); (2) the conditional dispersion of EDP given IM is constant across the range of intensities considered; and (3) that the median relationships in each probabilistic model follow a power-law relationship. When these three assumptions hold, the expected loss and accompanying variance can be obtained in closed form. However, even in the case of arbitrary conditional probability distributions and non-power-law median relationships, the Fourway method still provides an exact value for the expected loss and a variance approximation.

In order to completely define the Fourway process, seismic demand, damage, and loss models must be formulated. As indicated before, the seismic demand model is formulated from simplified coupled analysis of the example bridge. Performance groups are defined in terms of different EDPs to quantify damage to different bridge components. The loss model by Mackie et al. (2007) used repair quantity (Q) as the DV. Uncertainty in the repair quantity and unit cost models were incorporated into the analysis. A single Fourway analysis is performed for each performance group in the bridge and repair quantity. Each Fourway analysis predicts the repair quantity distribution (based on the moments of the distribution) associated with each performance group and repair method. The repair quantities are combined between performance groups taking into account the correlation between performance groups. Finally, total repair costs (TC) are derived from a relationship between the total repair quantities (Q) and a unit cost (C) for the repair items. The two probabilistic moments derived from the method can be used as lognormal or normal distribution parameters to describe both the probability of exceeding different repair costs at a given IM, as well as the probability of exceeding a single repair cost at varying levels of intensity.

5.2 DOWNTIMES

5.2.1 Simplified Approach

In the simplified approach, it is assumed that if the damage state of the bridge is moderate or less, no downtime will occur; that if large damage occurs, the median downtime of the bridge would be 1 day; and that if collapse occurs, the median downtime would be 60 days. The uncertainty around the median number of days has been assumed to be similar to the coefficient of variation of the HAZUS estimates for downtimes (add reference), i.e., $c.o.v. = 42 \text{ days} / 75 \text{ days} \approx 0.56$, then:

Table 5.3 Expected downtimes given bridge damage level.

Damage Level	Median downtime (and likely range)
Negligible	0
Small	0
Moderate	0
Large	1day (0.5 to 1.5 days)
Collapse	60 days (25 to 95 days)

5.2.2 Component-Based Approach

This approach follows the same ideas described in Mackie et al. (2007) (see Section 5.1.2), but where repair cost ratios have been replaced by repair times.

6 Bridge Evaluation Example

6.1 GENERAL

The methodology that has been presented in the previous sections will be applied to the general bridge example described in Figures 6.1–6.5 to illustrate how the proposed methodology can be applied in engineering practice. The bridge that has been selected for the analysis is a typical Caltrans highway bridge underlain by liquefiable soil susceptible to lateral ground displacement. The bridge consists of a five-span reinforced concrete structure with a post-tensioned reinforced concrete box girder deck section and monolithic piers. The three middle spans are 150 ft long and the two end spans are 120 ft long. The deck is 6 ft deep, and the four piers are 22 ft high. The pier columns are 4 ft in diameter with a 2% longitudinal steel reinforcing ratio.

Each bridge pier is supported by a group of 3×2 open-ended steel piles with a diameter of 2 ft, thickness of 0.5 in., and yield strength of 60 ksi. The same type and number of piles was used at the abutments but distributed in only one row.

The soil below the left abutment consists of a medium stiff clay crust underlain by a thin, loose to medium dense sand, a layer of stiff clay, and a dense sand layer underlain by rock. The soil beneath the right abutment consists of the same clay crust underlain by a thicker layer of the loose sand, followed by a dense sand layer underlain by rock. The lower clay layer below the left abutment becomes thinner toward the center of the bridge, and it does not exist below the right embankment. The embankments are 28 ft high and have 2:1 (H:V) slopes. The groundwater is located at the bottom of the surface clay layer. The properties of the loose and medium sand layers across the bridge were aimed to induce liquefaction under moderate ground shaking so that lateral ground displacement, especially in the vicinity of the right abutment, triggered broad bridge damage.

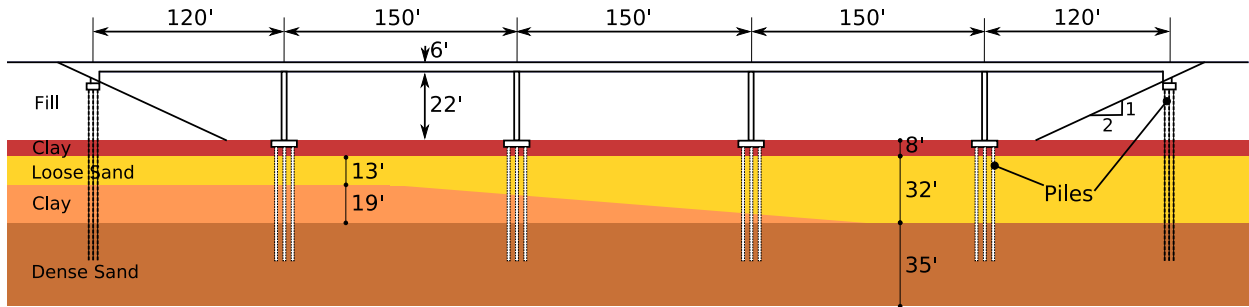


Fig. 6.1 Example bridge profile.

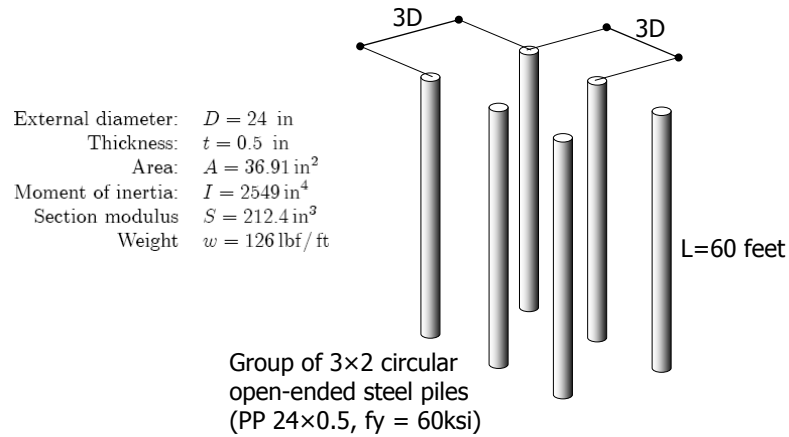


Fig. 6.2 Piles at interior bents—dimensions and properties.

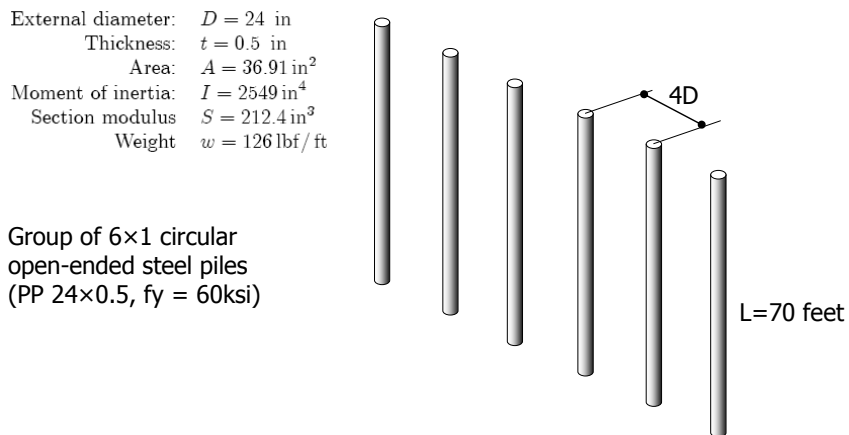


Fig. 6.3 Piles at abutments—dimensions and properties.

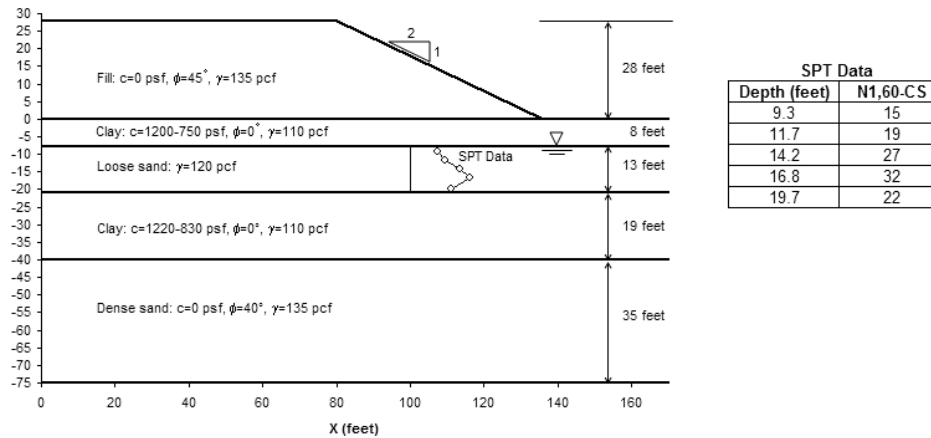


Fig. 6.4 Left abutment—soil profile and dimensions (not to scale).

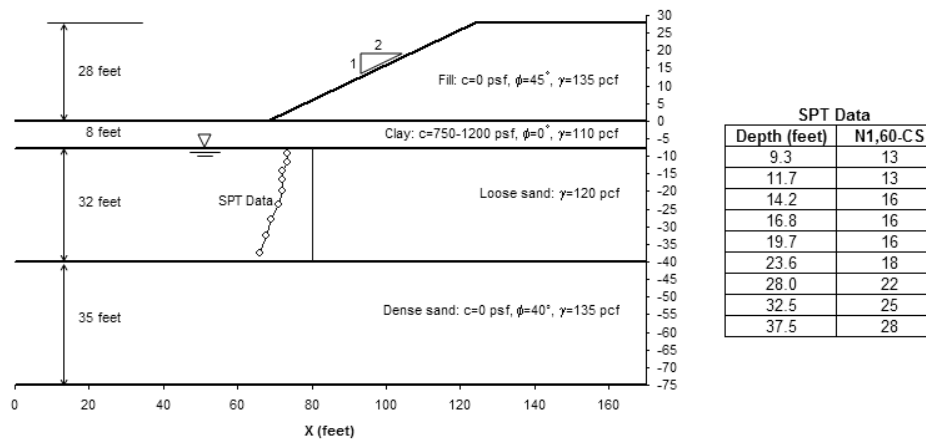


Fig. 6.5 Right abutment—soil profile and dimensions (not to scale).

6.2 ASSUMPTIONS

1. There is only one critical sliding surface at each abutment.
2. At the left abutment, the slope stability analysis performed using SLOPE/W (GEO-SLOPE/W 2004) shows that the base of the potential failure surface goes through the bottom of the layer with an SPT blow-count of $N_{1,60-CS} = 15$. Since it has been assumed that c.o.v.= 0.3, the SPT blow-count at the critical layer of the left abutment has a *lognormal* distribution with mean 15, and a standard deviation of 4.5.

3. At the right abutment, the slope stability analysis shows that the base of the potential failure surface goes through the bottom of bottom layer with an SPT blow-count of $N_{1,60-CS} = 13$. Two liquefiable layers are involved in the potential failure surface. The two layers have the same SPT blow-count, i.e., $N_{1,60-CS} = 13$. Again, assuming a c.o.v.= 0.3, the SPT blow-count at the equivalent critical layer of the right abutment has a *lognormal* distribution with mean 13, and a standard deviation of 3.9.
4. Based on the results of Section 3.1.1.2 assume that the undrained residual shear strength to effective vertical stress ratio (S_{ur} / σ_{vc}') given that a value of $\mu_{N_{1,60-CS}}$ has a *lognormal* distribution with mean and standard deviation given by

$$\mu_{S_{ur} / \sigma_{vc}'} \approx \exp\left(\frac{\mu_{N_{1,60-CS}} - 3.5}{8}\right) \times \left(1 + \frac{(0.3\mu_{N_{1,60-CS}})^2}{128}\right) \quad (6.1)$$

$$\sigma_{S_{ur} / \sigma_{vc}'} \approx 0.4\mu_{S_{ur} / \sigma_{vc}'}$$

6.3 CALCULATIONS

6.3.1 Seismic Hazard

The 5%-damping uniform hazard spectra for a free-field soil condition from Somerville and Collins (2002) was used in this analysis. These spectra were derived from a probabilistic seismic hazard analysis using the ground motion model of Abrahamson and Silva (1997) for a site in Oakland, California; it contains rupture directivity effects, which were represented in the probabilistic ground motion hazard analysis using the empirical model of Somerville et al. (1997). The hazard levels considered by Somerville and Collins (2002) were those of events with probabilities of exceedance of 50%, 10%, and 2% in 50 years. Only the strike-normal component (parallel to the longitudinal direction of the bridge) is considered in this 2D analysis.

The de-aggregation of the hazard at a period of 1 second shows that at all three hazard levels, the hazard is dominated by earthquakes on the Hayward fault, which is located about 7 km east of the site. The Hayward fault is a strike-slip fault that has the potential to generate earthquakes having magnitudes as large as 7. According to Somerville and Collins (2002), the

largest contributions come from events with magnitudes 6.6, 6.8, and 7.0 for the hazard levels corresponding to events with probabilities of exceedance of 50%, 10%, and 2% in 50 years, respectively.

As the next sections of this report will show, the probability of liquefaction for the three hazard levels analyzed by Somerville and Collins (2002) is high ($> 80\%$). Then, a fourth hazard level, which would not likely cause liquefaction, was added for this design example to illustrate the effects that liquefaction has on the likely seismic performance of the bridge. The uniform hazard spectra for the smallest hazard level was estimated by making a linear extrapolation in the $S_a(soil)/MSF$ versus $\ln(T_R)$ space, where T_R is the return period, for every period of vibration. For PGA (soil) the result of the linear regression was:

$$\frac{PGA(soil)}{MSF} \approx -0.3776 + 0.1411 \cdot \ln(T_R) \quad (6.2)$$

Following the procedure given in Youd et al. (2001), a peak ground acceleration of 0.14g would not cause liquefaction at the site. Assuming that for this case $M_w \approx 6.6$, then $MSF \approx (7.5/6.6)^{2.95} = 1.458$ and

$$\begin{aligned} \frac{0.14}{1.458} &\approx -0.3776 + 0.1411 \cdot \ln(T_R) \\ \Rightarrow T_R &\approx 29 \text{ years} \end{aligned} \quad (6.3)$$

A similar linear regression was performed for each period of vibration, and the S_a / MSF ratio for each period was estimated assuming $T_R = 29 \text{ years}$ (82% in 50 years event). Table 6.1 and Figure 6.6 show the 5%-damping uniform hazard spectra for the free-field soil condition and the four hazard levels considered in the analysis.

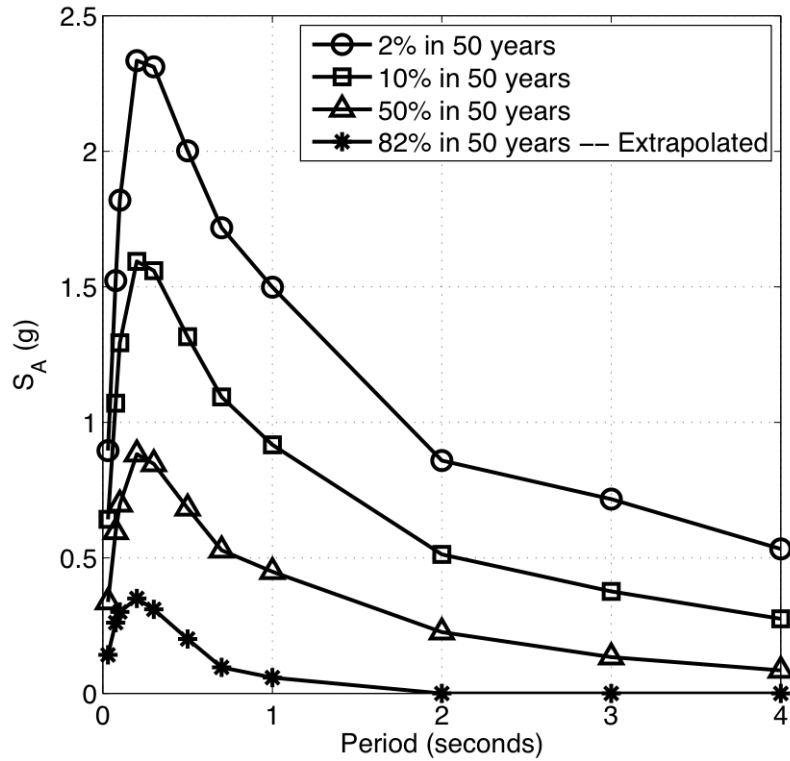


Fig. 6.6 Uniform hazard spectra, 5% damping, at site.

Table 6.1 Uniform hazard spectra, 5% damping, at site.

Period (s)	Probability of Exceedance in 50 years			
	82%	50%	10%	2%
0.03	0.142	0.337	0.642	0.896
0.075	0.261	0.596	1.071	1.523
0.10	0.301	0.698	1.294	1.820
0.20	0.350	0.883	1.594	2.335
0.30	0.310	0.847	1.560	2.312
0.50	0.201	0.683	1.316	2.002
0.70	0.096	0.528	1.094	1.718
1.00	0.058	0.449	0.917	1.499
2.00	0	0.226	0.513	0.859
3.00	0	0.134	0.376	0.717
4.00	0	0.085	0.275	0.533

6.3.2 Liquefaction Assessment

The procedure recommended in Youd et al. (2001) was used to estimate the factor of safety against liquefaction of the different sublayers of the loose sand layers present at both ends of the bridge. Figure 6.7 shows the estimated factors of safety against liquefaction for the two abutments, and the four hazard levels considered. This figure shows that for the 50%, 10%, and 2% in 50-years events, liquefaction is (very) likely to occur at both ends of the bridge. On the other hand, for the 82% in 50 years event, the factor of safety against liquefaction is rather high (~2 or higher), which indicates that chances of liquefaction for this event are low.

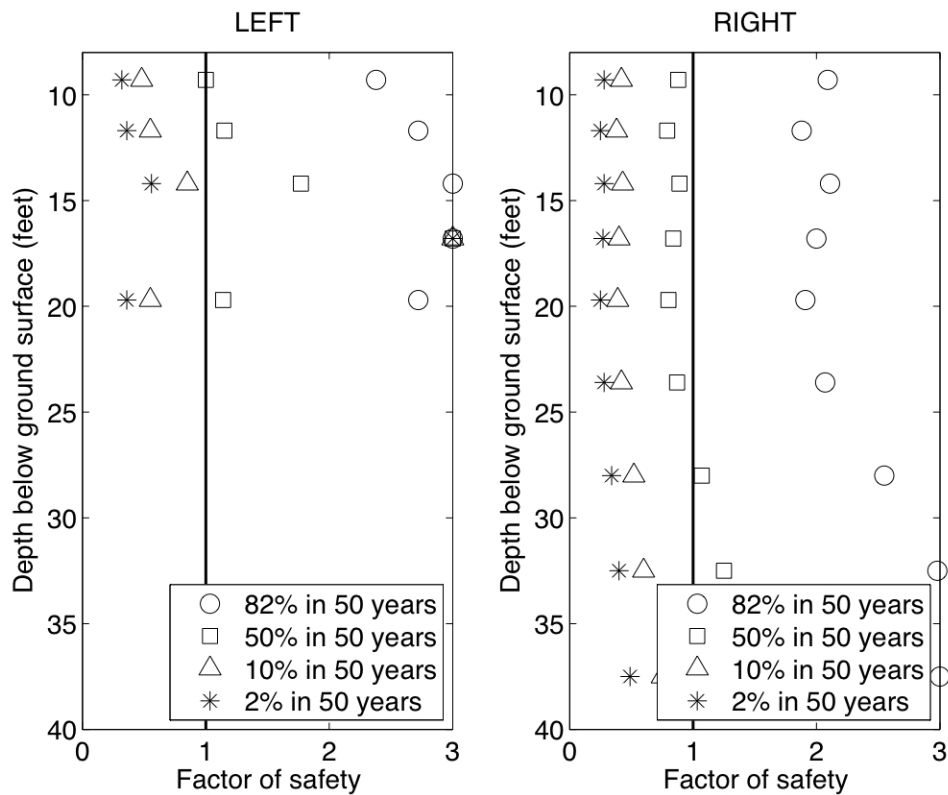


Fig. 6.7 Factors of safety against liquefaction.

6.3.3 Flow Failure Assessment

The next step is to evaluate if flow failure is likely to occur at any of the abutments, i.e., to estimate the post-liquefaction static factor of safety at the abutments. The program SLOPE/W (GEO-SLOPE 2004) was used to perform the slope stability analyses, where the expected

residual undrained shear strength was assigned to the sublayers of loose sand where $N_{1,60-CS} \leq 20$, i.e.,

$$S_{ur} \approx \exp\left(\frac{N_{1,60-CS}}{8} - 3.5\right) \quad \text{if } 0 \leq N_{1,60-CS} \leq 20 \quad (6.4)$$

Figures 6.8 and 6.9 show the results of the post-liquefaction stability analysis, where it can be seen that the static factor of safety at both abutments is larger than 1, indicating that in this case flow failure is not likely to occur.

Left Abutmet
No Piles
kh=0

Fill - gamma=135 pcf, c=0 psf, phi=45 degrees
 Shallow clay - gamma=110 pcf, c=1200-750 psf, phi=0 degr
 Deep clay - gamma=110 pcf, c=1220-830 psf, phi=0 degree
 Dense sand - gamma=135 pcf, c=0 psf, phi=40 degrees
 Loose sand 1 - gamma=120 pcf, c=560 psf, phi=0 degrees
 Loose sand 2 - gamma=120 pcf, c=968 psf, phi=0 degrees
 Loose sand 3 - gamma=120 pcf, c=0 psf, phi=40 degrees
 Loose sand 4 - gamma=120 pcf, c=0 psf, phi=42 degrees
 Loose sand 5 - gamma=120 pcf, c=0 psf, phi=39 degrees

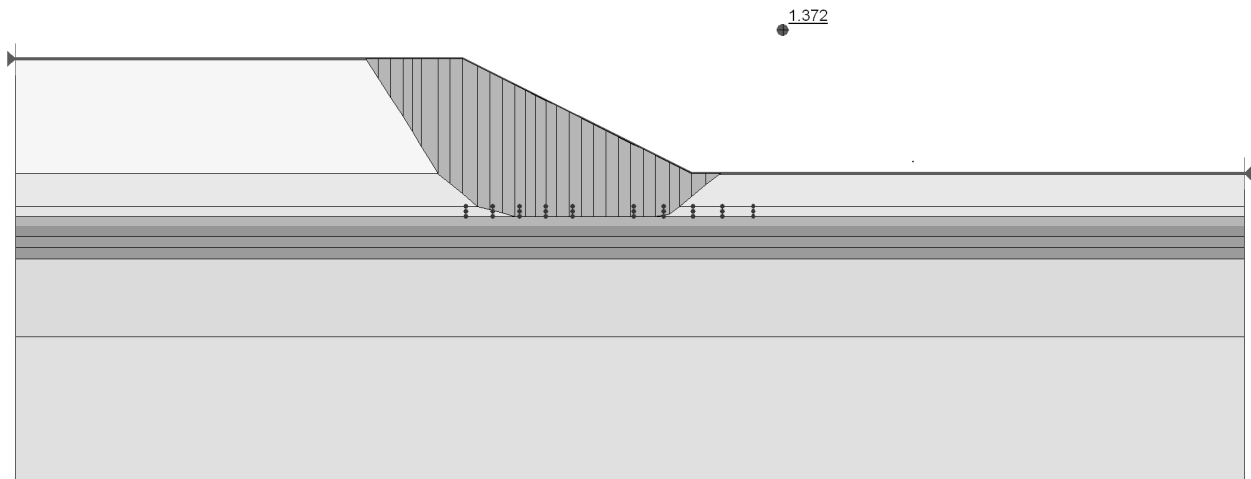


Fig. 6.8 Post-liquefaction stability analysis of left abutment ($FS = 1.37, k_y = 0.11$).

Right Abutment
No Piles
kh = 0

Fill - gamma=135 pcf, c=0 psf, phi=45 degrees
 Shallow clay - gamma=110 pcf, c=750-1200 psf, phi=0 degree
 Dense sand - gamma=135 pcf, c=0 psf, phi=40 degrees
 Loose sand 1 - gamma=120 pcf, c=436 psf, phi=0 degrees
 Loose sand 2 - gamma=120 pcf, c=457 psf, phi=0 degrees
 Loose sand 3 - gamma=120 pcf, c=698 psf, phi=0 degrees
 Loose sand 4 - gamma=120 pcf, c=731 psf, phi=0 degrees
 Loose sand 5 - gamma=120 pcf, c=768 psf, phi=0 degrees
 Loose sand 6 - gamma=120 pcf, c=1051 psf, phi=0 degrees
 Loose sand 7 - gamma=120 pcf, c=0 psf, phi=39 degrees
 Loose sand 8 - gamma=120 pcf, c=0 psf, phi=40 degrees
 Loose sand 9 - gamma=120 pcf, c=0 psf, phi=42 degrees

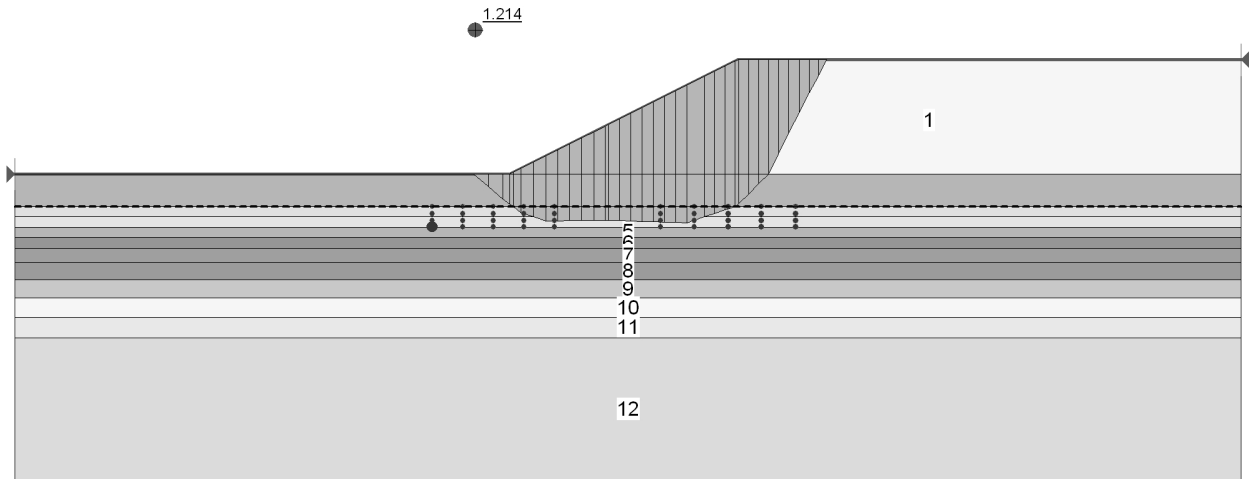


Fig. 6.9 Post-liquefaction stability analysis of right abutment ($FS = 1.21, k_y = 0.055$).

6.3.4 Passive Soil Forces versus Ultimate Structural Resistance

6.3.4.1 Intermediate Piers

The Excel spreadsheet *pultSI2.xls* developed by Professors Mokwa and Duncan (which is provided in Appendix B) was used to estimate the passive capacity of the pile cap, $P_{PileCap} = 213 \text{ kips}$. The 1996 JRA-recommended pressures against piles in laterally flowing liquefied soils were used to estimate the additional forces exerted against the piles. The result of this estimation is $P_{NonLiqLayer} = 26 \text{ kips}$, and $P_{LiqLayer} = 80 \text{ kips}$, and $P_{LiqLayer} = 328 \text{ kips}$ for the left and right ends of the bridge, respectively. Then, $P_{ult,Soil}(left) = 319 \text{ kips}$ and $P_{ult,Soil}(right) = 567 \text{ kips}$.

The structural capacity at the intermediate piers is:

$$P_{ult,Structural} = \frac{2 \times 5674 \text{ kips} \cdot \text{feet}}{22 \text{ feet}} + \frac{2 \times (6 \times 1381) \text{ kips} \cdot \text{feet}}{H_{eq}} \quad (6.5)$$

where $H_{eq} \approx 25 \text{ feet}$ and $H_{eq} \approx 44 \text{ feet}$ for the left and right ends of the bridge, respectively.

Then, $P_{ult,Structural}(\text{left}) = 1179 \text{ kips}$ and $P_{ult,Structural}(\text{right}) = 893 \text{ kips}$. This means that at the intermediate piers the soil will continue to displace or flow around the stable foundation in case of lateral ground displacement.

6.3.4.2 Abutment

The Excel spreadsheet *pultSI2.xls* developed by Prof. Mokwa and Prof. Duncan was used to estimate the passive capacity of the pile cap, $P_{ult,Passive} = 5842 \text{ kips}$. The structural capacity at the abutment is:

$$P_{ult,Structural} = \frac{2 \times (6 \times 1381) \text{ kips} \cdot \text{feet}}{H_{eq}} \quad (6.6)$$

where $H_{eq} = 27 \text{ feet}$ and $H_{eq} = 46 \text{ feet}$ for the left and right ends of the bridge, respectively.

Then, $P_{ult,Structural}(\text{left}) = 613 \text{ kips}$ and $P_{ult,Structural}(\text{right}) = 360 \text{ kips}$. Considering only the pile cap passive capacity we have that $P_{ult,Structural} < P_{ult,Soil}$, which means that in case of lateral ground displacement, the abutment structure will move in concert with the soil.

6.3.5 Vertical Stresses

The effective and total vertical stresses, σ_v' and σ_v , evaluated at the center of the equivalent critical layer are:

Left Abutment	$\sigma_v' = 135 \times 14 + 110 \times 8 + (120 - 62.428) \times 2.5 / 2 = 2842 \text{ psf}$
	$\sigma_v = 135 \times 14 + 110 \times 8 + 120 \times 2.5 / 2 = 2920 \text{ psf}$
Right Abutment	$\sigma_v' = 135 \times 14 + 110 \times 8 + (120 - 62.428) \times 3.73 / 2 = 2877 \text{ psf}$
	$\sigma_v = 135 \times 14 + 110 \times 8 + 120 \times 3.73 / 2 = 2994 \text{ psf}$

6.3.6 Initial Fundamental Period of Potential Sliding Mass

The initial fundamental period (T_s) of the potential sliding mass at the left abutment (see Fig. 6.10) can be calculated as follows. From Imai and Tonouchi (1982) for cohesionless materials $G_{\max} \approx 325(N_{60})^{0.68}$ (ksf).

The fill material has $\phi = 45^\circ$, i.e., $N_{60} \approx 50$, then $G_{\max} \approx 325(50)^{0.68} = 4647 \text{ ksf}$, and since $\gamma = 135 \text{ pcf}$, then:

$$V_s(\text{fill}) = \sqrt{G_{\max} / \rho} = \sqrt{32.2 \text{ feet/s}^2 \times 4,647,000 \text{ psf} / 135 \text{ pcf}} \approx 1,050 \text{ ft/s} \quad (6.7)$$

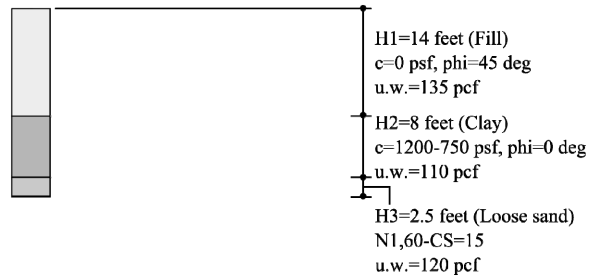


Fig. 6.10 Representative soil column of potential sliding mass at left abutment.

The loose sand has $\sigma_{v0}' = 2842 \text{ psf}$ and $C_N = \sqrt{2,116.2 / 2,842} = 0.86$, then $N_{60} \approx 15 / 0.86 \approx 17$ and $G_{\max} = 325(17)^{0.68} = 2,230 \text{ ksf}$, and since $\gamma = 120 \text{ pcf}$, then

$$V_s(\text{Loose Sand}) = \sqrt{G_{\max} / \rho} = \sqrt{32.2 \text{ feet/s}^2 \times 2,230,000 \text{ psf} / 120 \text{ pcf}} \approx 770 \text{ ft/s} \quad (6.8)$$

According to Weiler (1988), for cohesive materials with $PI \approx 20-25$, and $OCR \approx 2$, the ratio G_{\max} / S_u is about 600. The clay material has $c \approx (1200 + 750) / 2 = 975 \text{ psf}$, then $G_{\max} \approx 585 \text{ ksf}$, and since $\gamma = 110 \text{ pcf}$, then:

$$V_s = \sqrt{G_{\max} / \rho} = \sqrt{32.2 \text{ feet/s}^2 \times 585,000 \text{ psf} / 110 \text{ pcf}} \approx 410 \text{ ft/s} \quad (6.9)$$

and

$$\bar{V}_s = \frac{H_1 + H_2 + H_3}{\frac{H_1}{V_{s1}} + \frac{H_2}{V_{s2}} + \frac{H_3}{V_{s3}}}$$

$$\bar{V}_s = \frac{14 + 8 + 2.5}{\frac{14}{1,050} + \frac{8}{410} + \frac{2.5}{770}} = 680 \text{ ft/s} \quad (6.10)$$

$$\Rightarrow T_s = \frac{4(H_1 + H_2 + H_3)}{\bar{V}_s} \approx 0.14 \text{ seconds (left abutment)}$$

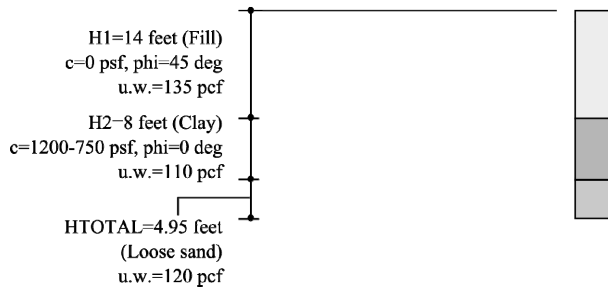


Fig. 6.11 Representative soil column of potential sliding mass at right abutment.

The initial fundamental period (T_s) of the potential sliding mass at the right abutment (see Fig. 6.11) can be calculated using the same procedure used for the left abutment. With respect to the left abutment, the only difference is the loose sand material. There are two sublayers involved with thicknesses (from top to bottom) of 2.50 ft and 2.45 ft, and N_{60} values equal to 15 blows/ft (value already corrected by C_N). Using the relation by Imai and Tonouchi (1982), the

maximum shear modulus G_{\max} of these layers is about 2,050 ksf, and their shear wave velocities are around 740 ft/s. Then:

$$\bar{V}_s = \frac{\sum_i H_i}{\sum_i \frac{H_i}{V_{si}}}$$

$$\bar{V}_s = \frac{14+8+2.50+2.45}{\frac{14}{1050} + \frac{8}{410} + \frac{2.50}{740} + \frac{2.45}{740}} = 680 \text{ ft/s} \quad (6.11)$$

$$\Rightarrow T_s = \frac{4 \times 26.95}{680} \approx 0.16 \text{ seconds (right abutment)}$$

6.3.7 Yield Coefficient as a Function of Equivalent Undrained Shear Strength of Critical Layer

Figure 6.12 shows the nearly linear relationship between k_y and S_u for both of the bridge abutments considered in this design example if liquefaction occurs. If liquefaction does not occur, the potential failure surface goes through the bottom of the shallow clay layer. Figure 6.13 shows the relationship between k_y and S_u for this case (same for both abutments).

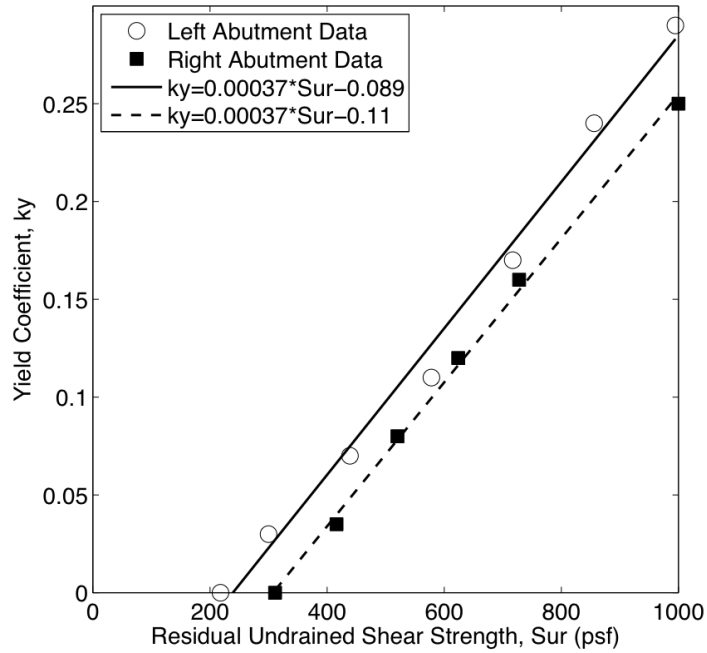


Fig. 6.12 Yield coefficient (k_y) versus equivalent total residual undrained shear strength (S_{ur}) relationship for cases with liquefaction.

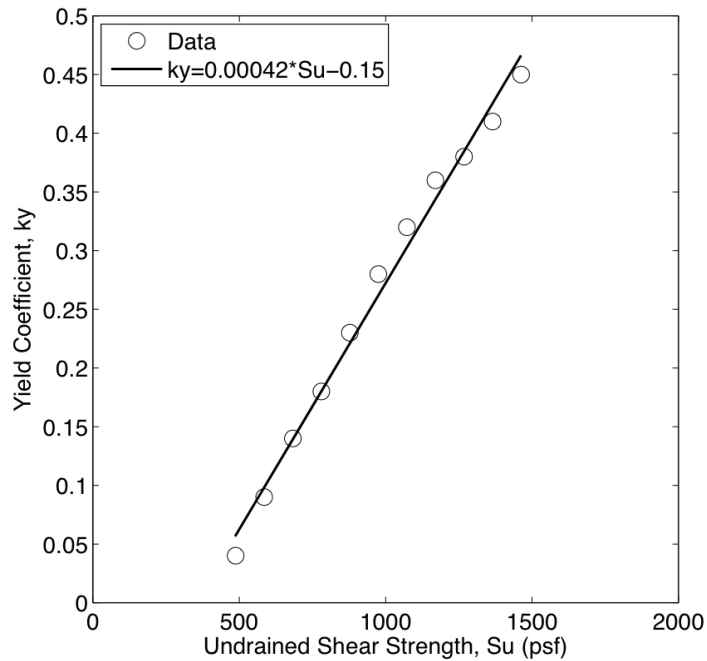


Fig. 6.13 Yield coefficient (k_y) versus equivalent total residual undrained shear strength (S_u) relationship for cases without liquefaction.

6.3.8 Size of Potential Failure Surface

To study the effect of S_u on the size of the potential failure surface, the length of the base of the critical slip surface was tracked as the equivalent undrained shear strength of the critical layer varied. As Figure 6.14 shows, there is a ~30% increase in the size of the base area of the critical slip surface for the right abutment as S_u increases. However, for value of S_u higher than 600 psf the value of l remained constant. For the left abutment, there was no distinct change in the size of the l with changes in S_u . The latter finding does not mean that the overall size of the potential sliding mass did not increase with S_u . It actually did slightly. It indicates only that the longitudinal dimension of the base of the potential failure surface, l , did not increase significantly.

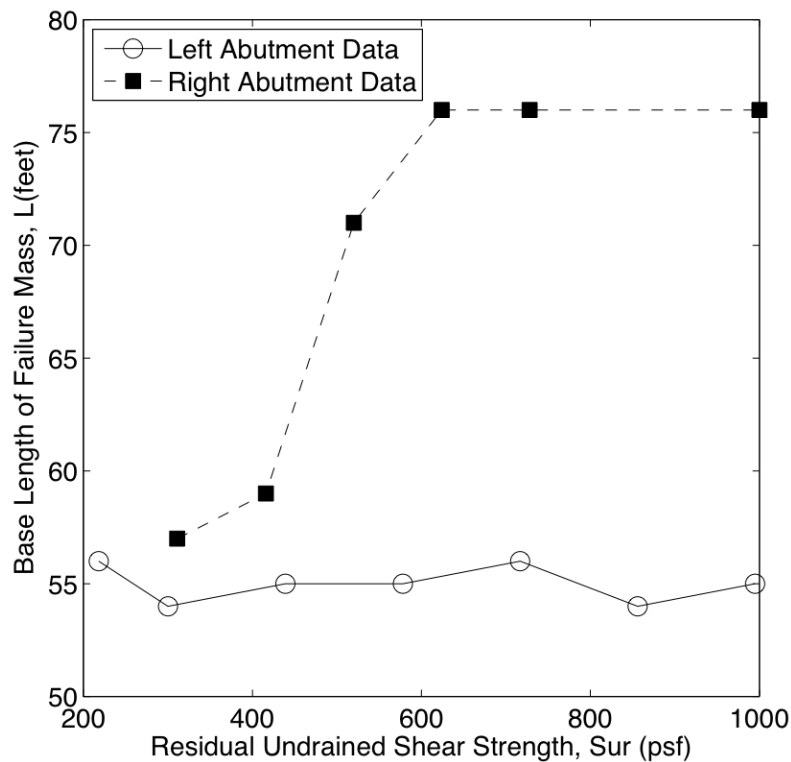


Fig. 6.14 Effect of residual undrained shear strength on base length of potential sliding mass.

Based on these results it is assumed that for the left abutment $l = 55$ feet (constant), and for the right abutment $l = 60$ feet if $S_u \leq 500$ psf, and $l = 75$ feet if $S_u > 500$ psf.

Finally, assuming that one half of the slide slope masses must be restrained by the piles (Boulanger et al. 2006), the resulting tributary width in this case is $t = 70$ feet .

6.3.9 Ground Motion Intensity

The peak ground accelerations for the 82%, 50%, 10%, and 2% in 50 years events are 0.14 g, 0.34 g, 0.64 g, and 0.90 g, respectively (Somerville and Collins 2002); and the spectral accelerations at $1.5T_s$ are 0.35 g, 0.88 g, 1.59 g, and 2.33 g, respectively for the left abutment with liquefaction ($T_s = 0.14$ s); 0.33 g, 0.87 g, 1.58 g, and 2.33 g, respectively for the right abutment with liquefaction ($T_s = 0.16$ s); and 0.35 g, 0.87 g, 1.58 g, and 2.31 g, respectively for the left and right abutments without liquefaction ($T_s = 0.13$ s).

6.3.10 Passive Reaction

According to Caltrans Design Criteria, the longitudinal stiffness of the abutment is 20 (kip/in)/ft $\times 43$ ft $\times 6 / 5.5 \approx 940$ kips/in , and the total passive capacity is 6 ft $\times 43$ ft $\times 5$ ksf $\times 6 / 5.5 \approx 1,410$ kips . The assumed gap was 4 in. (see Fig. 6.15).

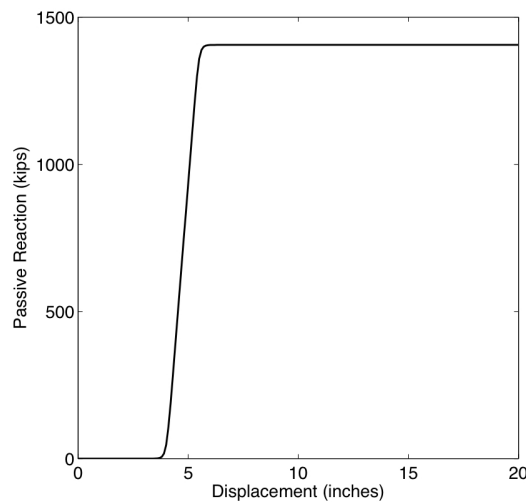


Fig. 6.15 Passive reaction versus displacement.

6.3.11 Probability of Liquefaction

Recalling that the in-situ cyclic shear stress ratio is defined as $CSR = 0.65(a_{\max} / g)(\sigma_v / \sigma'_v)r_d$, where a_{\max} is the peak horizontal ground surface acceleration, g is the acceleration of gravity, σ_v is total vertical stress, σ'_v is the effective vertical stress, and r_d is the nonlinear shear mass participation factor, in this case the values of CSR are:

$$\text{Left Abutment (} z = 9.25 \text{ feet): } CSR = 0.65 \times PGA \times 2920 \times 0.96 / 2842 = 0.64 \cdot PGA$$

$$\text{Right Abutment (} z = 9.86 \text{ feet): } CSR = 0.65 \times PGA \times 2994 \times 0.96 / 2877 = 0.65 \cdot PGA$$

The probabilities of liquefaction for the 82%, 50%, 10%, and 2% in 50 years events are 8%, 83%, 99%, and ~100%, respectively, for the left abutment, and 17%, 92%, ~100%, and ~100%, respectively, for the right abutment.

6.4 RESULTS USING FIRST-ORDER RELIABILITY METHOD (FORM)

Figure 6.16 and Tables 6.2–6.5 show the results of applying the proposed simplified approach using the first-order reliability method (FORM).

In Figure 6.16, the upper figures in each column represent the probability of displacement being greater than the threshold given in the x-axis for each liquefaction case, where the lines with white symbols correspond to the case without liquefaction and the lines with black symbols represent the cases with liquefaction. The bottom figures in each column show the final result, where the cases with and without liquefaction have been combined using the total probability theorem.

Table 6.2 is a summary of the results given in Figure 6.16. Figure 6.17 shows the estimated damages for the different hazard levels. Figures 6.18 and 6.19, Tables 6.3 and 6.4, show the expected repair cost ratios for different hazard levels, and two levels of uncertainty in the estimation of repair cost ratios as a function of damage state.

Finally, Table 6.5 shows the expected bridge downtimes for the different hazard levels analyzed.

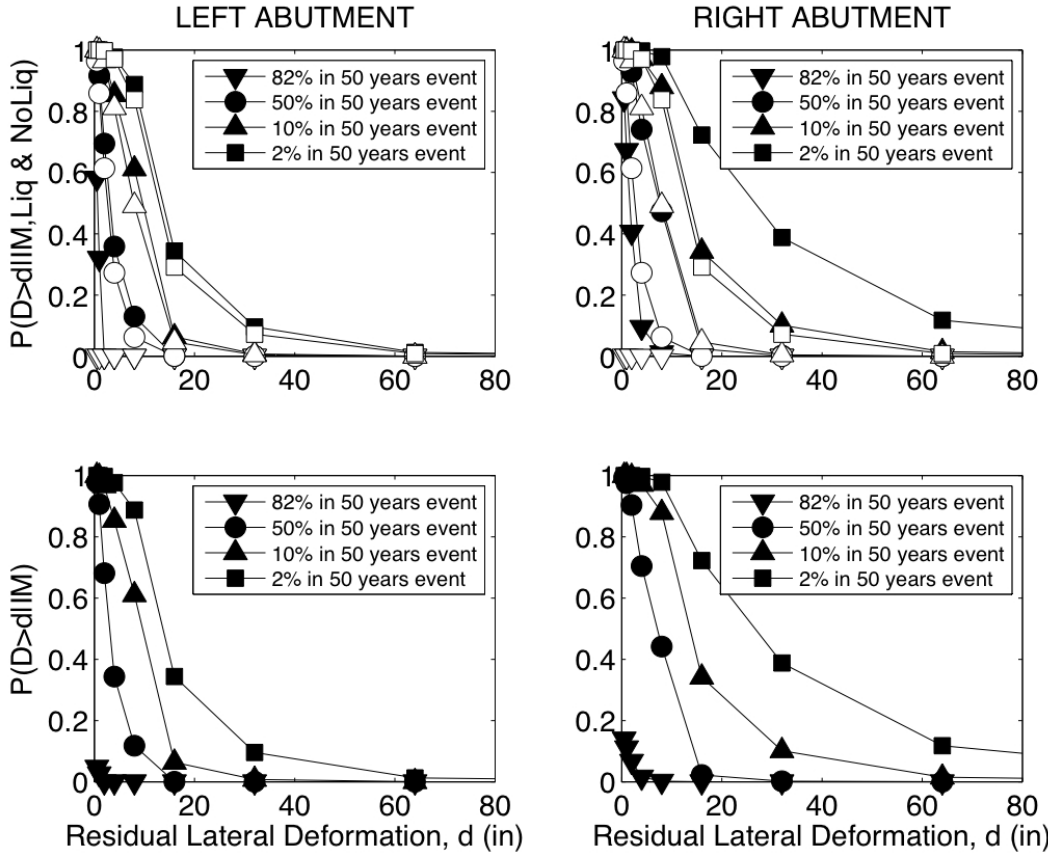


Fig. 6.16 Probability of exceeding a lateral displacement threshold (d) for different hazard levels. In top figures, black symbols denote cases with liquefaction and white symbols denote cases without liquefaction.

Table 6.2 Probability of $D > d$ given IM (FORM results).

	Left Abutment				Right Abutment			
	Prob. of Exceedance in 50 yrs.				Prob. of Exceedance in 50 yrs.			
	82%	50%	10%	2%	82%	50%	10%	2%
16th Percentile	< 0.5"	1"	4"	9"	< 0.5"	3"	9"	12"
Median	< 0.5"	3"	10"	14"	< 0.5"	7"	14"	27"
84th Percentile	< 0.5"	7"	15"	28"	< 0.5"	13"	28"	59"

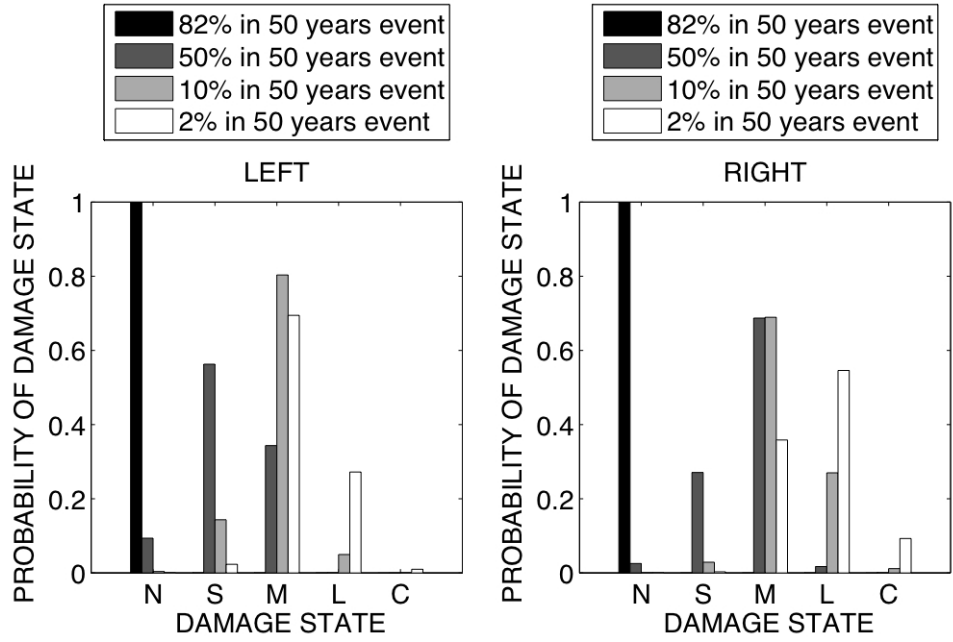


Fig. 6.17 Damage states using FORM.

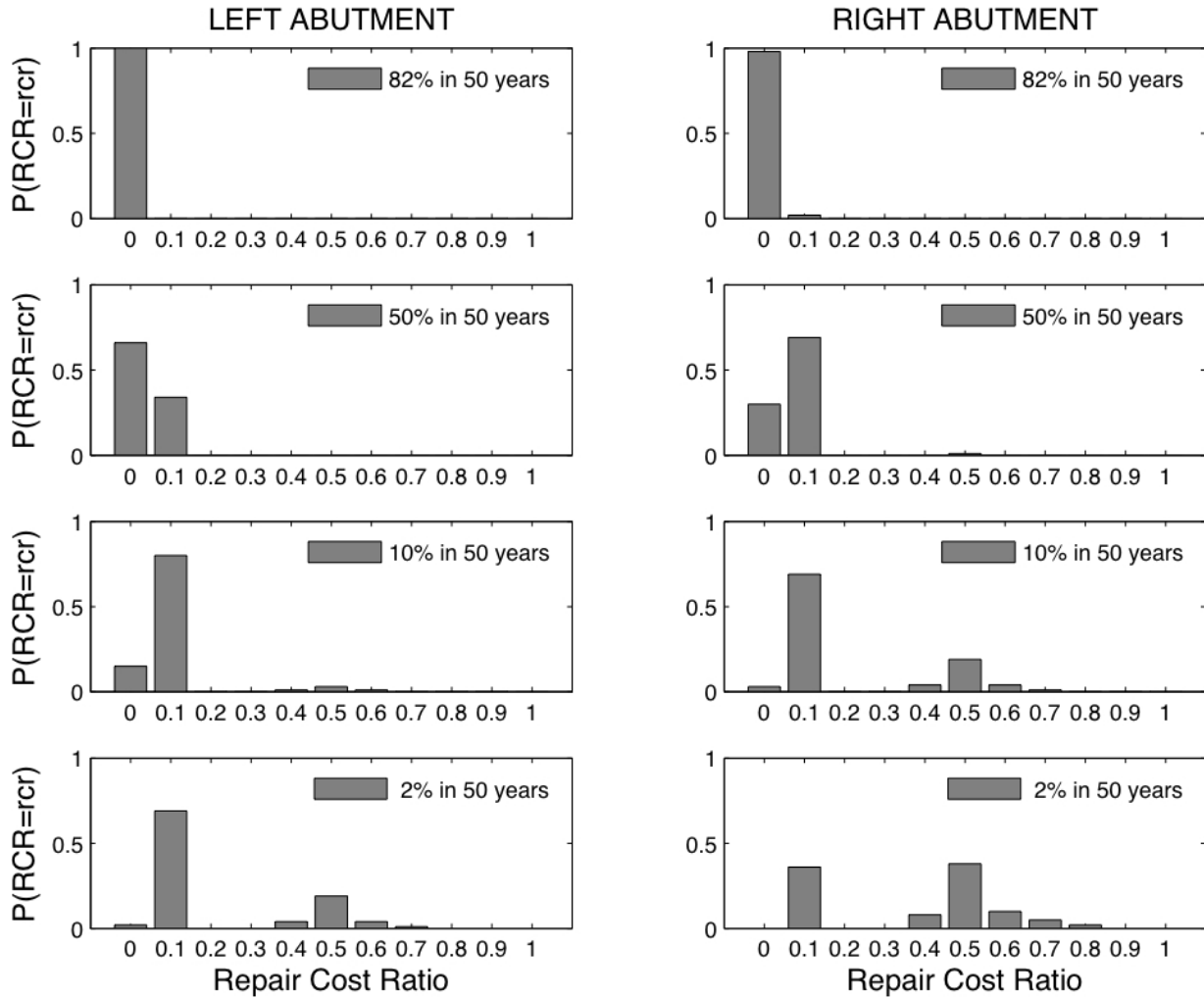


Fig. 6.18 Repair cost ratios using FORM—low uncertainty.

Table 6.3 Expected repair cost ratios using FORM—low uncertainty.

	Left Abutment				Right Abutment			
	Probability of Exceedance in 50 years				Probability of Exceedance in 50 years			
	82%	50%	10%	2%	82%	50%	10%	2%
μ	~0	0.03	0.11	0.21	~0	0.08	0.21	0.37
σ	~0	0.05	0.10	0.19	0.01	0.07	0.19	0.22

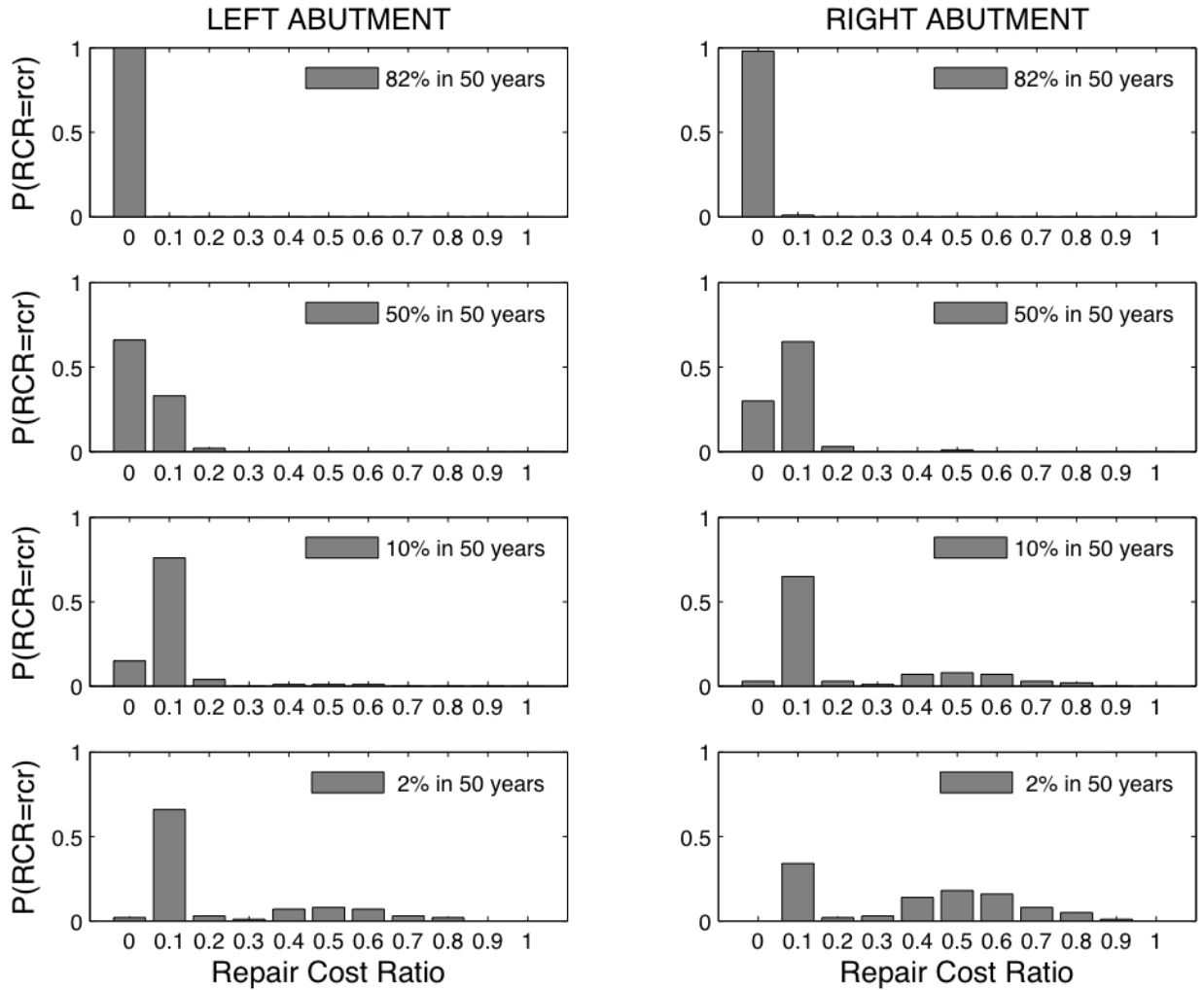


Fig. 6.19 Repair cost ratios using FORM—high uncertainty.

Table 6.4 Expected repair cost ratios using FORM—high uncertainty.

	Left Abutment				Right Abutment			
	Probability of Exceedance in 50 years				Probability of Exceedance in 50 years			
	82%	50%	10%	2%	82%	50%	10%	2%
μ	~ 0	0.04	0.11	0.22	~ 0	0.08	0.22	0.39
σ	~ 0	0.05	0.11	0.21	0.01	0.08	0.21	0.24

Table 6.5 Expected downtimes using FORM.

	Left Abutment				Right Abutment			
	Probability of Exceedance in 50 years				Probability of Exceedance in 50 years			
	82%	50%	10%	2%	82%	50%	10%	2%
μ	0	Negligible	1.5 hours	1 day	0	0.5 hours	1 day	6 days
σ	n/a	n/a	~1 hour	0.5 day	n/a	~0.5 hours	0.5 days	3.5 days

6.5 RESULTS USING POINT ESTIMATE METHOD (PEM)

Tables 6.6–6.9 show the results of applying the proposed simplified approach using the point estimate method (PEM). Table 6.6 is a summary of the results in terms of residual lateral displacements at the abutments. Tables 6.7 and 6.8 show the expected repair cost ratios for different hazard levels, and two levels of uncertainty in the estimation of repair cost ratios as a function of damage state. Table 6.9 shows the expected bridge downtimes using PEM for the different hazard levels analyzed.

Table 6.6 Probability of $D > d$ given IM (PEM results).

	Left Abutment				Right Abutment			
	Prob. of Exceedance in 50 years				Prob. of Exceedance in 50 years			
	82%	50%	10%	2%	82%	50%	10%	2%
$\mu - \sigma$	0.3"	1"	2"	4"	0.4"	2"	3"	8"
μ	0.6"	2"	7"	15"	0.7"	4"	15"	33"
$\mu + \sigma$	0.9"	3"	11"	26"	1"	7"	27"	58"

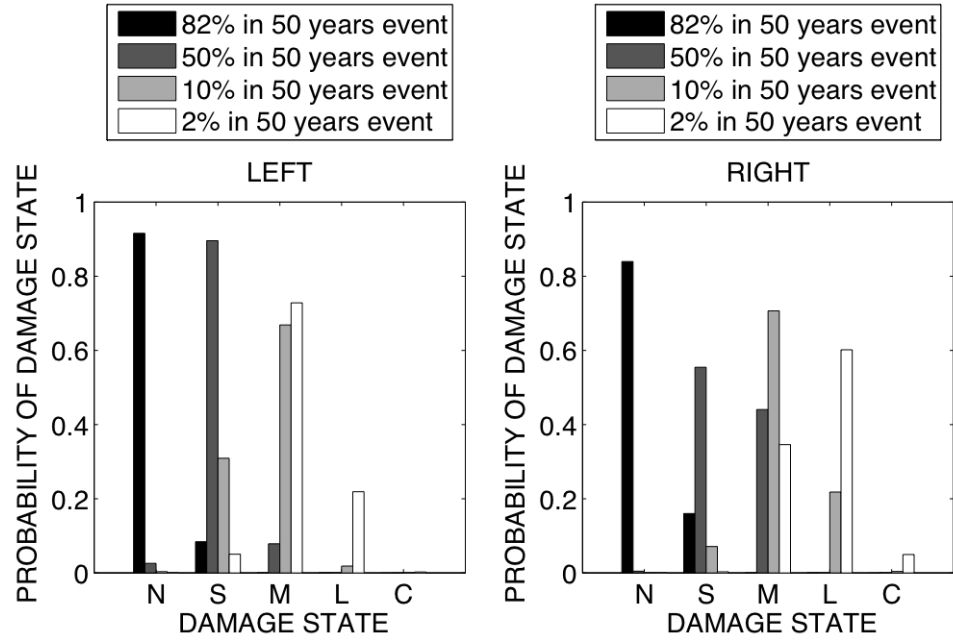


Fig. 6.20 Damage states using PEM.

Table 6.7 Expected repair cost ratios using PEM—low uncertainty.

	Left Abutment				Right Abutment			
	Prob. of Exceedance in 50 years				Prob. of Exceedance in 50 years			
	82%	50%	10%	2%	82%	50%	10%	2%
μ	~0	0.01	0.08	0.18	~0	0.04	0.18	0.37
σ	~0	0.03	0.07	0.17	~0	0.05	0.18	0.21

Table 6.8 Expected repair cost ratios using PEM—high uncertainty.

	Left Abutment				Right Abutment			
	Prob. of Exceedance in 50 years				Prob. of Exceedance in 50 years			
	82%	50%	10%	2%	82%	50%	10%	2%
μ	~0	0.01	0.08	0.19	~0	0.05	0.19	0.39
σ	~0	0.03	0.08	0.19	~0	0.05	0.19	0.23

Table 6.9 Expected downtimes using PEM.

	Left Abutment				Right Abutment			
	Probability of Exceedance in 50 years				Probability of Exceedance in 50 years			
	82%	50%	10%	2%	82%	50%	10%	2%
μ	0	0	0.5 hours	0.5 days	0	0	0.5 days	3.5 days
σ	n/a	n/a	~0.5 hours	~0.5 days	n/a	n/a	~0.5 days	~2 days

6.6 RESULTS USING SIMPLIFIED COUPLED MODEL

This analytical model was prepared by Dr. Kevin Mackie of the University of Central Florida, and it is a modified and simplified version of a fully nonlinear 3D model of the PEER bridge using OpenSees (Mackie and Stojadinović 2006). Figure 3.8 shows the main components of the bridge model.

6.6.1 Properties

The properties of the superstructure can be found in Mackie and Stojadinović (2006). Under each pier there is a group of 3×2 circular open-ended steel piles (PP 24”×0.5”, $f_y = 60$ ksi), with a center-to-center spacing of 6 ft. In this model, the equivalent length (L_{eq}) of the piles tries to represent the lateral stiffness they provide to the system, $L_{eq} = H_{liq} + 2 \times 3.5(2R)$, where H_{liq} is the thickness of the liquefiable material at the location of the respective pier, and R is the pile radius ($R = 1$ ft). Table 6.10 shows the estimated values of L_{eq} under each pier.

Table 6.10 Equivalent pile length under each pier.

Column	Equivalent length L_{eq}
1 (left most pier)	27 ft (8.2 m)
2	32 ft (9.7 m)
3	41 ft (12.6 m)
4 (right most pier)	46 ft (14.0 m)

The springs shown in Figure 3.8 try to model the interaction that occurs, through the compression of the upper non-liquefiable layer, between pile caps, and between the embankment and the first pile cap. The stiffness of these springs was estimated assuming that the ultimate passive capacity of the soil reacting against the pile cap is reached at a deformation of 0.01 m. The value of P_{ult} was calculated using the $\phi=0$ *sliding wedge method* developed by Mokwa (1999). Table 6.11 shows the stiffnesses that were used.

Table 6.11 Stiffness of soil springs.

Spring	Stiffness
1 (left)	273 kips/in (47810 kN/m)
2	137 kips/in (23904 kN/m)
3	137 kips/in (23904 kN/m)
4	137 kips/in (23904 kN/m)
5 (right)	273 kips/in (47810 kN/m)

The stiffness of the intermediate springs 2, 3, and 4 is half of the stiffness of any of the end springs because that is the equivalent stiffness of the two springs that are acting in series between the pile caps.

6.6.2 Input

Horizontal deformations, consistent with the different hazard levels under consideration, were applied to the free ends of the end springs, and to the two ends of the bridge. Table 6.12 shows the displacements that were imposed, which are the mean displacements from Table 6.2.

Table 6.12 Input displacements.

Return Period	Nodes	Horizontal Deformation
$T_R=29$ years	Left end	Negligible
	Right end	
$T_R=72$ years	Left end	0.08 m
	Right end	0.18 m
$T_R=475$ years	Left end	0.25 m
	Right end	0.36 m
$T_R=2475$ years	Left end	0.36 m
	Right end	0.69 m

6.6.3 Results

Figure 6.21 shows the deformed shape of the bridge after the application of the deformation pattern indicated in the previous section. Table 6.13 presents a summary of the results obtained using this analysis.

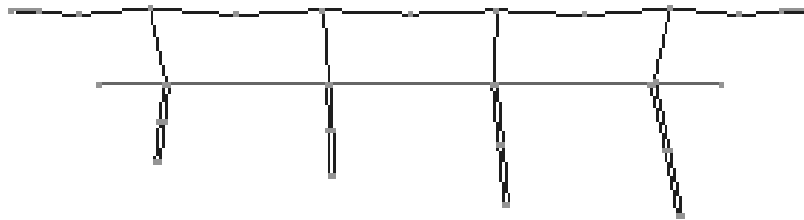


Fig. 6.21 Deformed shape of bridge from OpenSees model.

Table 6.13 Residual tangential column drifts.

Return Period of Event	Column	Column Drift
$T_R=29$ years	1	Negligible
	2	
	3	
	4	
$T_R=72$ years	1	0.5%
	2	0.2%
	3	0.1%
	4	0.5%
$T_R=475$ years	1	2.4%
	2	0.3%
	3	0.3%
	4	2.5%
$T_R=2475$ years	1	4.9%
	2	1.4%
	3	0.7%
	4	5.5%

From this analysis, using linear regressions in the log-log space, the following intensity measure (IM)–engineering demand parameter (EDP) relationships could be estimated:

For column drift:

$$\begin{aligned}
 \ln(\delta_1) &= 2.3504 \ln(Sa) - 0.3246 \pm c \\
 \ln(\delta_2) &= 1.8695 \ln(Sa) - 1.5535 \pm c \\
 \ln(\delta_3) &= 1.9695 \ln(Sa) - 2.0545 \pm c \\
 \ln(\delta_4) &= 2.4638 \ln(Sa) - 0.3166 \pm c
 \end{aligned}
 \tag{6.12}$$

where δ_i is the residual tangential drift of column i (in %), Sa is the 5% spectral acceleration (in g's) at $T = 0.5 \cdot (1.5T_{s,Left} + 1.5T_{s,Right}) = 0.23$ s, and $c = 0.75$ (i.e., same as the input displacements).

For the residual pile head displacements at the left and right abutments, D_{Left} and D_{Right} (in inches):

$$\begin{aligned}\ln(D_{Left}) &= 1.6073 \ln(Sa) + 1.3876 \pm c \\ \ln(D_{Right}) &= 1.3563 \ln(Sa) + 2.0989 \pm c\end{aligned}\quad (6.13)$$

For the residual longitudinal relative deck-end/abutment displacements at the left and right ends of the bridge, ΔD_{Left} and ΔD_{Right} (in meters):

$$\begin{aligned}\ln(\Delta D_{Left}) &= 1.1165 \ln(Sa) - 3.0924 \pm c \\ \ln(\Delta D_{Right}) &= 1.1353 \ln(Sa) - 3.0188 \pm c\end{aligned}\quad (6.14)$$

And, for the residual pile cap displacements at the columns, D_i ($i = 1, 2, 3, 4$) (in meters):

$$\begin{aligned}\ln(D_1) &= 2.9602 \ln(Sa) - 4.1108 \pm c \\ \ln(D_2) &= 0.5006 \ln(Sa) - 3.7418 \pm c \\ \ln(D_3) &= 1.2889 \ln(Sa) - 2.8652 \pm c \\ \ln(D_4) &= 1.5281 \ln(Sa) - 2.1031 \pm c\end{aligned}\quad (6.15)$$

Figure 6.22 shows the estimated total repair cost ratios using these relationships and the procedure described in Section 5.1.2 for the case when liquefaction occurs. The circles in Figure 6.22 show the expected repair cost ratios for return periods of 72, 475, and 2475 years. Using the simplified coupled model the expected repair cost ratios are 1%, 21%, and 49% for these three hazard levels, respectively. Using the simplified approach, which is based only on the amount of residual lateral displacement at the abutments, the expected repair cost ratios are 8%, 21%, and 37%. Although both methods estimate similar mean repair cost ratios, their level of dispersion is different. The coefficient of variation in the simplified approach is ~ 0.8 , while in the simplified coupled model the c.o.v. is ~ 0.45 .

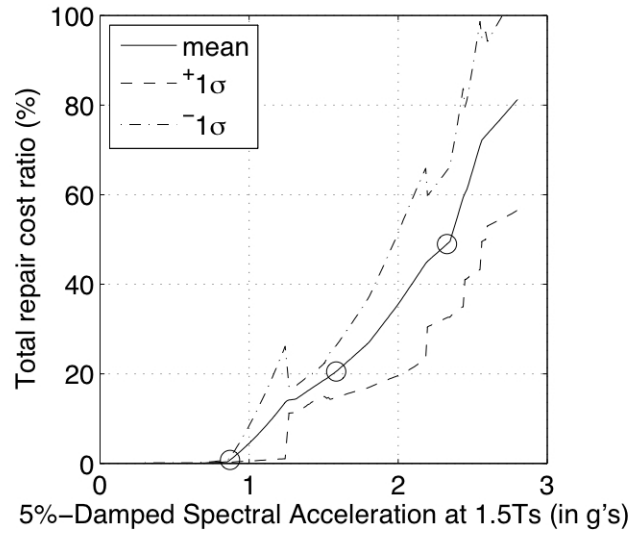


Fig. 6.22 Repair cost ratios using simplified coupled model.

Figure 6.23 shows the contribution of the different repair tasks to the total repair cost for different hazard levels.

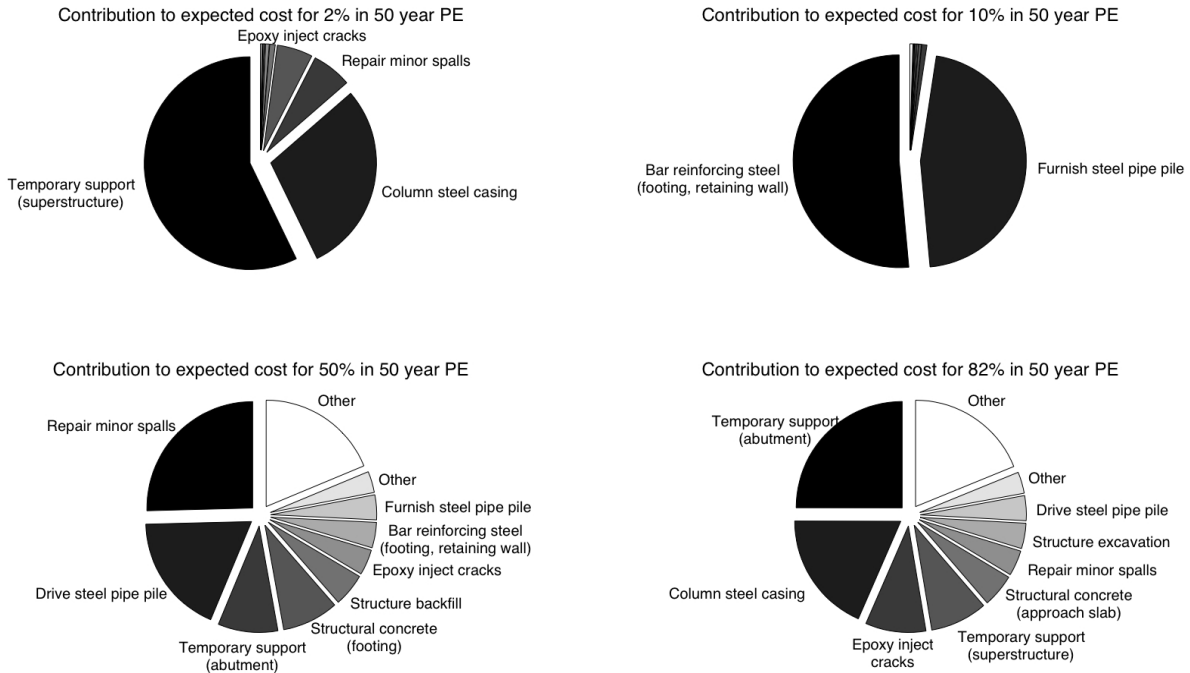


Fig. 6.23 Contribution to expected cost of repair actions for different hazard levels.

7 Sensitivity Analysis

The Pacific Earthquake Engineering Research (PEER) Center performance-based earthquake engineering (PBEE) approach can provide important insights through de-aggregation of the results to identify those components that impact the results most significantly. Additionally, sensitivity analyses may be performed that provide information about the relative importance of the random variables and the sensitivities of the first-order approximation of the failure probability with respect to parameters in the probability distributions. The first-order reliability method provides a useful set of importance and sensitivity measures. In this paper, seven random variables were considered in the estimation of the probability of exceeding a specified level of displacement for a given intensity measure. The random variables that were considered are: S_{ur} , the residual undrained shear strength of the liquefied material; α , the normalized distance to the points of fixity of the piles; ε , the error term in the estimation of the residual lateral displacement from the model by Bray and Travararou (2007); T_s , the initial fundamental period of the potential sliding mass; S_a , the spectral acceleration at $1.5T_s$; H , thickness of the liquefiable material; and P_a , the passive reaction of the embankment against the backwall.

The characteristics of the S_{ur} , α , and ε variables had already been presented in previous sections. The uncertainty in the parameter T_s was estimated recalling that $T_s = c \cdot H / V_s$ (where c is a constant), and considering that the uncertainty in H is small. In that case, the first-order approximations for the mean and standard deviation of T_s are:

$$\begin{aligned} \mu_{T_s} &\approx \frac{cH}{\mu_{V_s}} \\ \sigma_{T_s} &\approx \sqrt{\left(\left. \frac{dT_s}{dV_s} \right|_{\mu_{V_s}} \right)^2} \sigma_{V_s}^2 = \sqrt{\left(-\frac{cH}{\mu_{V_s}^2} \right)^2} \sigma_{V_s}^2 = \frac{cH}{\mu_{V_s}^2} \sigma_{V_s} \end{aligned} \quad (7.1)$$

Then, the coefficient of variation of T_s would be:

$$c.o.v.[T_s] = \frac{\sigma_{T_s}}{\mu_{T_s}} = \frac{cH}{\mu_{V_s}^2} \sigma_{V_s} \cdot \frac{\mu_{V_s}}{cH} = \frac{\sigma_{V_s}}{\mu_{V_s}} = c.o.v.[V_s] \quad (7.2)$$

This means that the coefficient of variation of T_s and V_s should be similar. According to Jones et al. (2002), the Electric Power Research Institute undertook an investigation of appropriate methods for estimating earthquake ground motion in eastern North America. This work, which involved numerous investigators, included extensive, high-quality field and laboratory testing of soils at more than 200 different sites. The measured shear wave velocities were shown to be lognormally distributed with $\sigma_{\ln V} = 0.39$. Then, for the analysis that follows, it is assumed that the coefficient of variation of T_s is 0.4.

The uncertainty in the value of the spectral acceleration at $1.5T_s$ (S_a) was estimated by averaging the error terms in the attenuation relationships by Chiou and Youngs (2006) and Campbell and Bozorgnia (2007) for periods between 0 and 1 second. The result was a coefficient of variation of about 0.6. The coefficient of variation of the variables H and P_a was assumed to be 0.3.

Table 7.1 summarizes the estimated characteristics of the seven random variables used in this section.

Table 7.1 Characteristics of selected random variables.

Random Variable	Description	Probability Density Function	Coefficient of Variation
S_{ur}	Residual undrained shear strength of the liquefied material	Log-normal	0.40
α	Normalized distance to the points of fixity of the piles	Uniform	0.87
ε	Error term in the estimation of the residual lateral displacement	Normal	0.66 (Standard Deviation)
T_s	Initial fundamental period of the potential sliding mass	Log-normal	0.40
S_a	Spectral acceleration at $1.5T_s$.	Log-normal	0.60
H	Thickness of liquefiable material	Log-normal	0.30
P_a	Passive reaction against the abutment's backwall	Log-normal	0.30

7.1 RESULTS

The order of importance of the random variables is identified by their relative contribution to the variance of the linearized limit-state function. This contribution is reflected in the unit vector $\hat{\gamma}$ (Der Kiureghian 1999), which, in our case, changes from hazard level to hazard level, and it is also different for each threshold level of lateral displacement. Figure 7.1 shows the absolute value of the terms in $\hat{\gamma}$ for each level of displacement and hazard level. The most important random variable was S_a , for all hazard and displacement levels, i.e., an important fraction of the uncertainty involved in this problem is due to the uncertainty in the estimation of the intensity measure, which in this case is the spectral acceleration at the fundamental degraded period of vibration of the potential sliding mass. The parameters ε and S_{ur} were also important, i.e., the overall uncertainty was also affected by the uncertainty in the estimation of the residual lateral displacement given an intensity measure, and the residual undrained shear strength of the liquefiable material. For small lateral displacements, S_{ur} is more important than ε , while for larger displacements the opposite is true. Lastly, Figure 7.1 shows that for all cases the importance of the parameters α , T_s , H , and P_a was rather small.

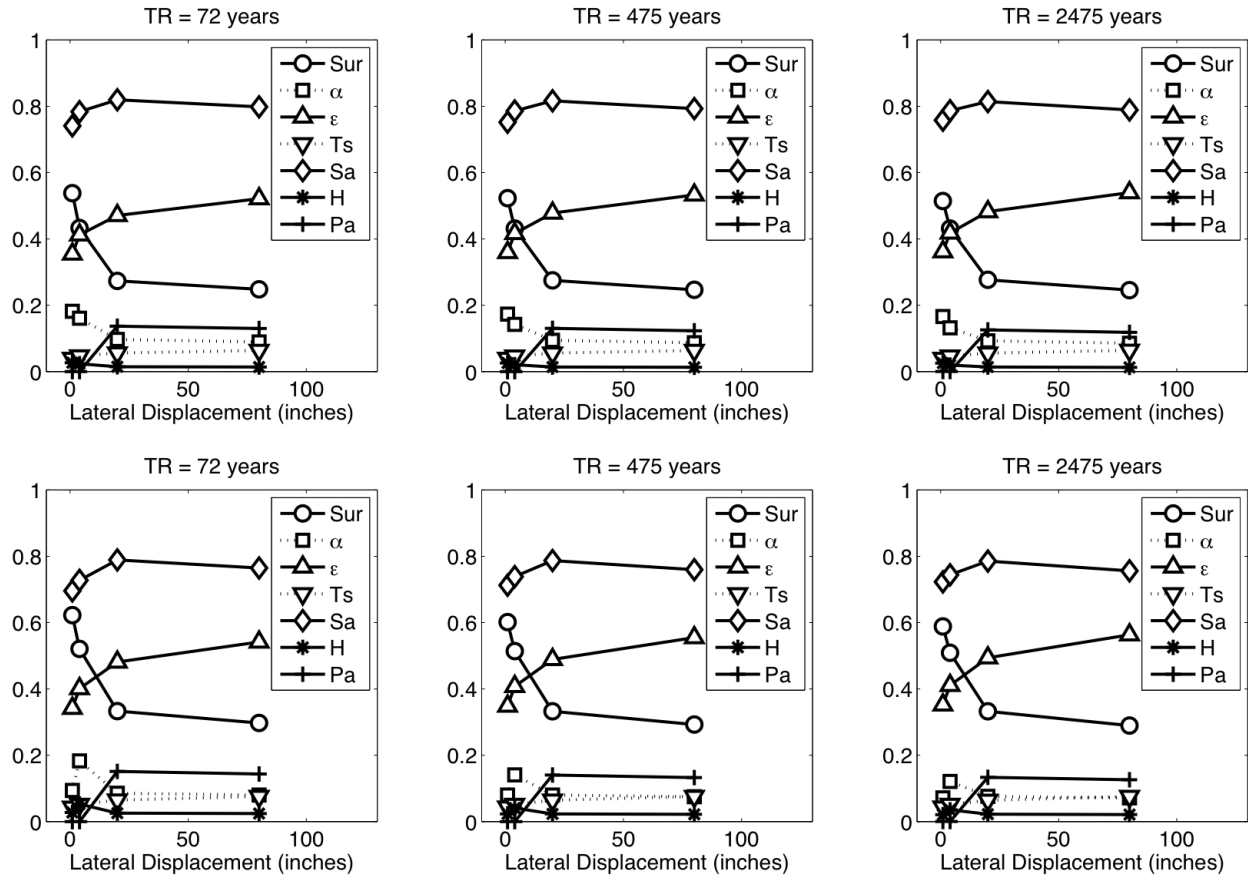


Fig. 7.1 Relative importance of random variables for different hazard and displacement levels. Upper and bottom figures correspond to results for left and right abutments, respectively.

The sensitivity of the “failure” probability, $p_f = P(D > d)$, to variations in the distribution parameters of the random variables can be quantified through the vectors $\underline{\delta}$ and $\underline{\eta}$ (Der Kiureghian 1999). Vectors $\underline{\delta}$ and $\underline{\eta}$ indicate the sensitivity of p_f to variations in the mean and the standard deviation of the random variables, respectively, i.e., the i -th term in the vector $\underline{\delta}$ is related to $\partial p_f / \partial \mu_i$, where μ_i is the mean of the i -th random variable, and the i -th term in the vector $\underline{\eta}$ is related to $\partial p_f / \partial \sigma_i$, where σ_i is the standard deviation of the i -th random variable.

To facilitate the comparison, the vectors $\underline{\delta}$ and $\underline{\eta}$ were normalized to have a unit length. Figures 7.2 and 7.3 show the absolute value of the terms in the normalized vectors $\hat{\underline{\delta}}$ and $\hat{\underline{\eta}}$, respectively, for each level of displacement and hazard level. The probability $p_f = P(D > d)$ is most sensitive to the parameters (mean or standard deviation) of the variables Sa , ϵ , and S_w ,

and least sensitive to the parameters of the variables α , T_s , H , or P_a . For small to moderate displacements, $P(D > d)$ was more sensitive to variations in the mean of S_a than to the mean of the other parameters; but for large displacement, variations in the mean of ϵ and S_{ur} had an important effect on $P(D > d)$.

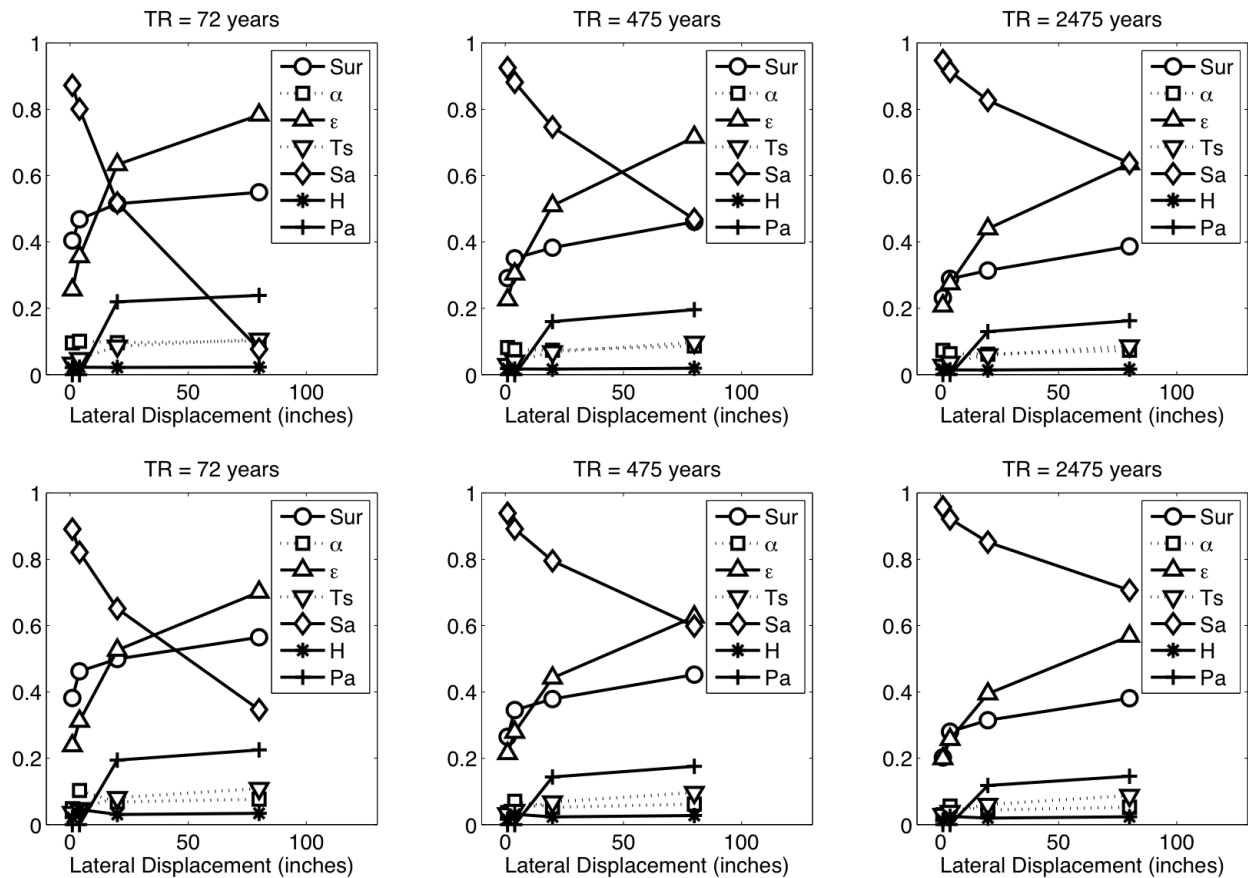


Fig. 7.2 Normalized relative sensitivity ($\hat{\delta}$) of probability $p_f = P(D > d)$ to variations in mean of random variables for different hazard and displacement levels. Upper and bottom figures correspond to results for left and right abutments, respectively.

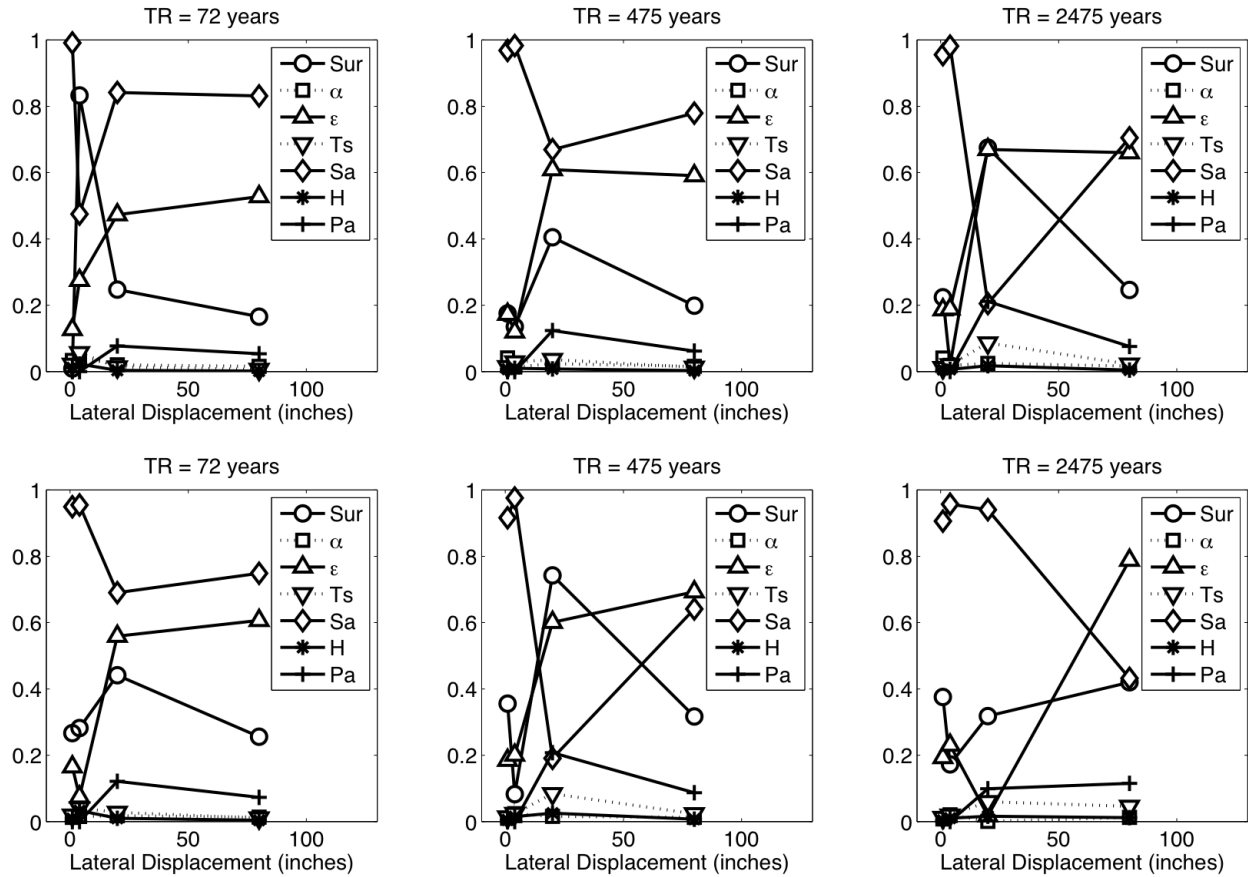


Fig. 7.3 Normalized relative sensitivity ($\hat{\eta}$) of probability $p_f = P(D > d)$ to variations in standard deviation of random variables for different hazard and displacement levels. Upper and bottom figures correspond to results for left and right abutments, respectively.

The previous results show that the most relevant parameters in the estimation of the residual lateral displacement are S_a , ϵ , and S_{ur} . The effect of these random variables on the estimation of bridge repair cost ratios or downtimes was also assessed. Each variable was scaled up and down one standard deviation, and their effect on the mean estimates of these decision variables (DVs) was recorded. The result was that all three variables were almost equally important, i.e., each parameter had essentially the same effect on the estimated DVs, however, S_a and ϵ had a slightly larger influence on the estimated decision variables for higher hazard levels.

7.2 COMMENTS

The results of this analysis indicate that the most influential parameters in this problem are the intensity of the ground motion (S_a), followed by the error term in the estimation of the residual lateral displacements induced by liquefaction (ε), and the residual undrained shear strength of the liquefiable material (S_{ur}). The contribution of the other four variables to the overall uncertainty, and their effect on the calculated probability, is relatively small for the problem studied.

8 Validation of Simplified Approach

8.1 LANDING ROAD BRIDGE DURING 1987 EDGE CUMBE EARTHQUAKE

This section presents the application of the proposed simplified approach to the case of the Landing Road bridge, Whakatane, which suffered moderate damage due to lateral ground displacement induced by the 1987 Edgecumbe, New Zealand, earthquake.

8.1.1 1987 Edgecumbe Earthquake

The $M_w = 6.6$ earthquake of March 2, 1987, occurred on a normal fault, and the nearest strong motion accelerograph was at the Matahina dam site, 16 km away from the rupture area (see Fig. 8.1). The strike, dip, and rake of the fault rupture were 235° , 39° , and -110° , respectively, which means that the strike of the fault is, approximately, in the SW/NE direction, and that it dips toward the northwest. According to the PEER NGA Database (NGA Database 2007), the site at Matahina dam can be classified as a Site C using the Bray and Rodriguez-Marek SGS classification, i.e., weathered soft rock/shallow stiff soil, and since $V_{s,30} \approx 425$ m/s, as a Site C using the NEHRP classification. The NGA database indicates that the peak ground acceleration at the Matahina dam site was $PGA = 0.29g$ (Berrill et al. 2001 indicate that $PGA = 0.33g$). Figure 8.2 shows the acceleration time series and the 5%-damping response spectrum of the Matahina dam station.



Fig. 8.1 Epicenter of 1987 Edgcumbe earthquake, Landing Road bridge, and Matahina dam.

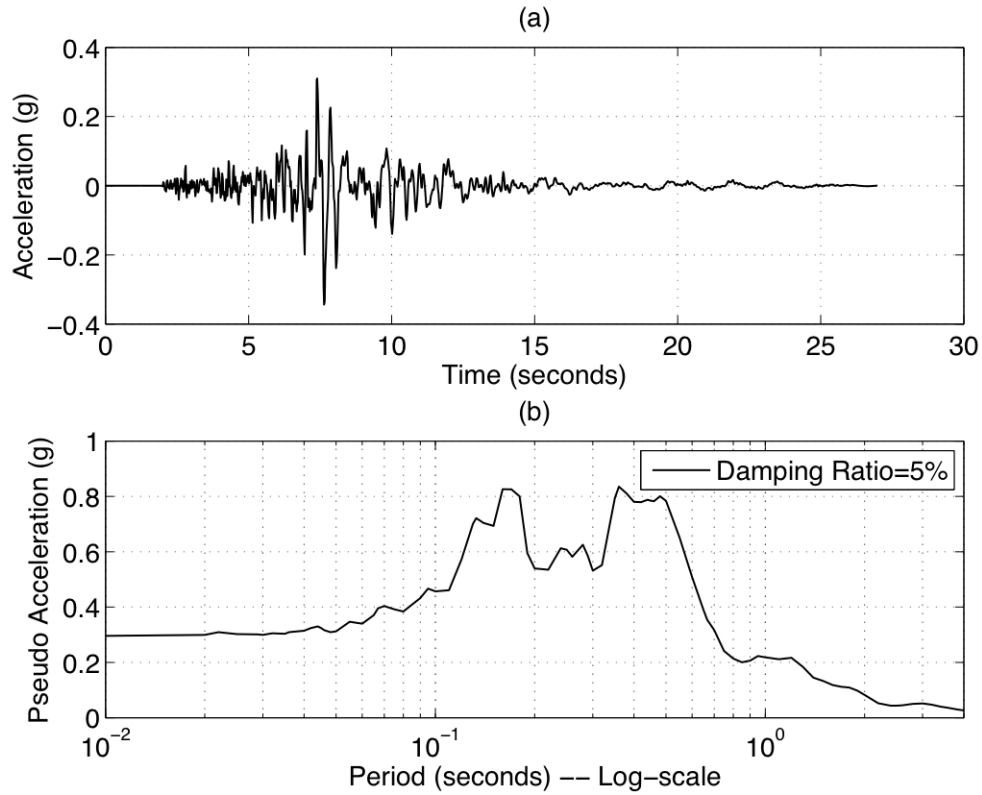


Fig. 8.2 Acceleration time series and 5%-damping response spectrum of Matahina dam station (Source: PEER NGA database).

The Landing Road bridge site is located, approximately, 19 km away from the rupture area. Figure 8.3(a) shows the measured SPT values near the pier (Berrill et al. 2001), and a simplified SPT profile from those measurements. Considering that $G_{\max} = 325(N_{60})^{0.68}$ (ksf) (Imai and Tonouchi 1982), that $N \approx N_{60}$, and that $\gamma \approx 17 \text{ kN/m}^3$, the shear wave velocity profile shown in Figure 8.3(b) was estimated. From the simplified profile a value of $V_{s,30} \approx 230 \text{ m/s}$ was estimated.

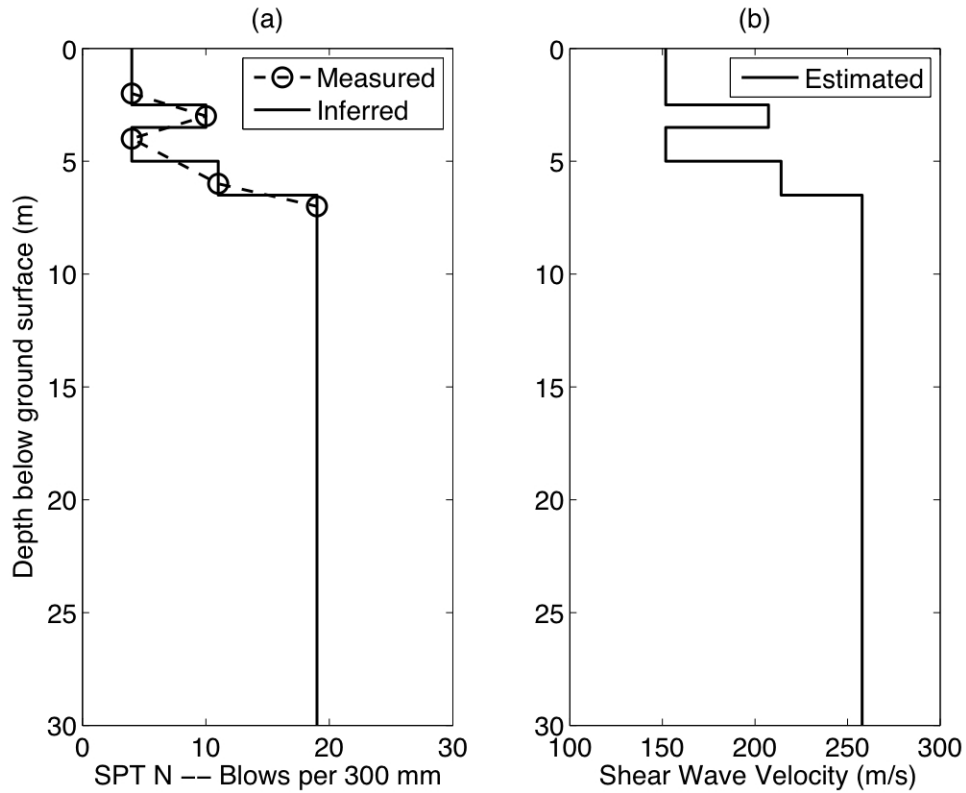


Fig. 8.3 Landing Road bridge—simplified SPT and shear wave velocity profiles.

Given that the Matahina dam site and the Landing Road bridge site are at a different distance from the rupture area (16 km versus 19 km, respectively), and that the site conditions are also different ($V_{s,30} \approx 425$ m/s versus $V_{s,30} \approx 230$ m/s, respectively) the response spectrum shown in Figure 8.2 should be adjusted for distance and site conditions. To estimate the required modifications to the spectrum, the NGA models by Chiou and Youngs (2006) and Campbell and Bozorgnia (2007) were considered. Most of the input parameters for these models were taken from the NGA database: $M_w = 6.6$ (moment magnitude), $R_{rup} = R_{JB} = 16$ or 19 km (distance to rupture area), $V_{s,30} = 425$ or 230 m/s, $W = 13$ km (rupture width), $\delta = 39^\circ$ (rupture dip), $Z_{TOR} = 0$ km (depth to top of rupture), and $Z_{2.5} \approx 1.3$ km (depth of 2.5 km/s shear-wave velocity horizon, from Hodder and Graham (1993)). The spectra were estimated for the Matahina dam and Landing Road bridge sites using the Excel spreadsheets provided in the NGA website, and the ratio between the two spectra was calculated at each period. Figure 8.4 shows the results of these calculations for a period range appropriate for this case.

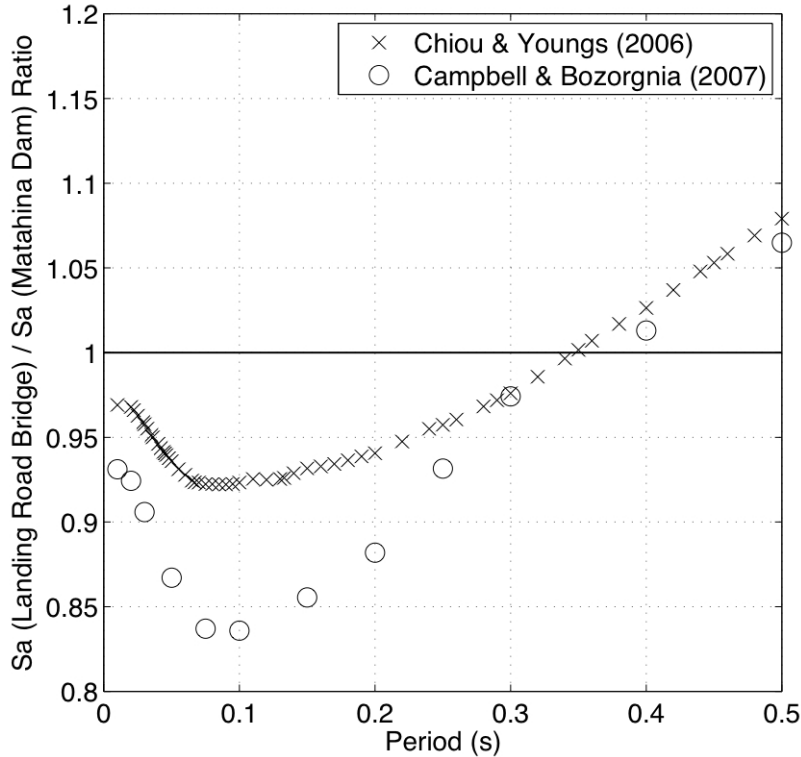


Fig. 8.4 Distance and site condition correction factor as function of period.

As Figure 8.4 shows, for periods of vibration between 0 and ~0.3 sec, an estimation of the spectra at the Landing Road bridge site can be obtained by reducing the one at the Matahina dam site by ~5% to ~12%. Given the uncertainties involved in this estimation, and the order of magnitude of the uncertainties of the rest of the parameters present in this problem, it was decided not to modify the spectra from the Matahina dam site.

8.1.2 Landing Road Bridge

SI units will be used for this case history because data were provided in SI units. As Figure 8.5 shows, the Landing Road bridge comprises 13 simply supported spans 18.3 m (60 ft) long, carrying a two-lane, cast-in-place concrete deck and two foot-paths. Each span consists of five precast post-tensioned concrete I-beams. The spans are not separated but are bolted together and to the abutments, and the beams are bolted down to the piers. The substructure comprises concrete slab piers running the full width of the superstructure, each supported by eight 406 mm (16 in) square pre-stressed concrete piles raked at 1:6 (Berrill et al. 2001). In the preliminary analysis that follows, the shear force in the piles was estimated assuming that the piles were

vertical. Preliminary elastic analysis show that for cases where the rotation and vertical displacement of the pile cap is negligible, this assumption introduces an error of less than 10% in the estimation of the shear force in the piles.

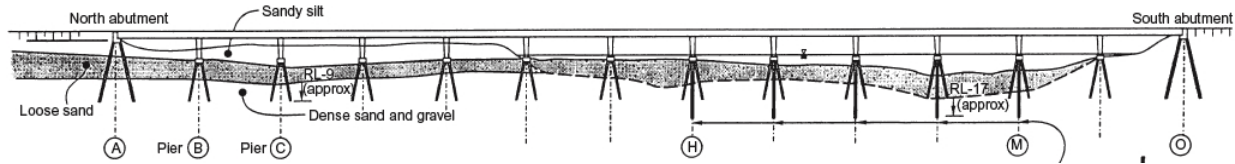


Fig. 8.5 Schematic elevation of Landing Road bridge (after Berrill et al. 2001).

8.1.3 Soil Profile

The soil properties used by Kashighandi and Brandenburg (2006) have been adopted. Table 8.1 shows the location, unit weight, friction angle, and cohesion of the three soils layers that were considered.

Table 8.1 Soil Properties (after Kashighandi and Brandenburg 2006).

Soil Layer	Depth to Top of Layer	Unit Weight, γ	Friction Angle, ϕ	Cohesion, c
Crust	0	12.5 kN/m ³ (~80 pcf)	42°	8 kPa (~165 psf)
Loose sand	1.2 m (~4 ft)	17 kN/m ³ (~110 pcf)	35°	0
Dense sand	6.2 m (~20 ft)	18 kN/m ³ (~115 pcf)	38°	0

8.1.4 Preliminary Calculations

The stability of the north abutment (see Fig. 8.5) is studied.

8.1.4.1 Passive Reaction at Abutment

From the drawings in Berrill et al. (2001) it is estimated that the backwall has dimensions $8 \times 1.4 = 11.2 \text{ m}^2$ (width \times height). Using the expression given in the manual design by Caltrans (2006), the passive reaction at the abutment is:

$$\begin{aligned} F_p (kN) &= A_e (m^2) \times 239 \text{ kPa} \times \frac{h(m)}{1.7} \\ F_p &= (8 \times 1.4) \times 239 \times \frac{1.4}{1.7} \\ F_p &= 2200 \text{ kN } (\sim 495 \text{ kips}) \end{aligned} \quad (8.1)$$

8.1.4.2 Shear Force in Piles

There are eight piles at the abutment, and each one has a yield bending moment of $M_y = 230 \text{ kN}\cdot\text{m}$. The thickness of the liquefiable layer is about 5 meters, and the piles are 0.406 m square piles, then

$$\begin{aligned} V_p &\approx \frac{2(8 \times 230)}{5 + 2(3.5 \times 0.406)} \\ V_p &= 470 \text{ kN } (\sim 105 \text{ kips}) \end{aligned} \quad (8.2)$$

8.1.4.3 Residual Undrained Shear Strength of Liquefied Soil

Assuming that the ground water table is at the top of the liquefied material, the effective vertical stress at the center of the liquefiable material is:

$$\begin{aligned} \sigma_v' &= 12.5 \times 1.2 + (17 - 9.81) \times 2.5 \\ \sigma_v' &= 33 \text{ kPa } (\sim 690 \text{ psf}) \end{aligned} \quad (8.3)$$

From Berrill et al. (2001), $N \approx 6$ bpf. Assuming that $N_{55} \approx N$, then $N_{60} \approx 6 \times (55/60) \approx 5.5$, and since $C_N = \min\{1.70, \sqrt{101.3/33}\} = 1.70$, then $N_{1,60} \approx 1.70 \times 5.5 = 9$ bpf. According to Berrill et al. (2001) the sands were relatively clean, then $N_{1,60-CS} \approx 9$ bpf, and considering that:

$$\mu_{S_{ur}/\sigma_v'} = \exp\left(\frac{N_{1,60-CS}}{8} - 3.5\right) \left(1 + \frac{(0.3N_{1,60-CS})^2}{128}\right) \quad (8.4)$$

then $\mu_{S_{ur}/\sigma_v'} \approx 0.0983$, and $\mu_{S_{ur}} \approx 3.2$ kPa (~ 65 psf).

8.1.4.4 Equivalent Undrained Shear Strength from Passive Reaction and Piles Shear Force

The stability analysis of the slope shows that the base length of the sliding mass is about 30 meters. Assuming that one half of the slide slope masses must be restrained by the piles, and a transverse slope of 2:1 (H:V), the base width of the sliding mass would be about 9.4 meters. Then, the base area of the sliding mass is about 280 m² and the maximum additional strength provided by the passive reaction and the shear force in the piles would be $\Delta S_{ur} = (2200 + 470) / 280 = 9.5$ kPa. This means that if liquefaction occurs and the passive reaction and shear force in the piles are fully mobilized, the equivalent undrained shear strength of the liquefiable material would be about $S_{ur,eq} = 12.7$ kPa (~ 265 psf).

8.1.4.5 Stability Analysis

Considering the properties shown in Table 8.1, and assuming that for the liquefiable layer (loose sand) $S_{ur,eq} = 12.7$ kPa, the stability analysis of the slope indicates that $k_y = 0.082$. Figure 8.6 schematically shows the results of the stability analysis at the north abutment.

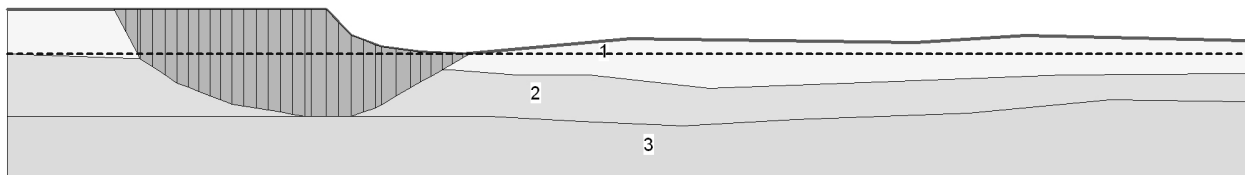


Fig. 8.6 Potential failure mass at north abutment, considering contribution of passive reaction and pile shear force.

8.1.5 Results Using Simplified Approach

8.1.5.1 Initial Fundamental Period of Potential Sliding Mass

Based on Figure 8.6, it is assumed that the representative soil column comprises the upper crust plus $\sim 3/4$ of the liquefiable layer.

The upper crust (silty material) has $\phi=42^\circ$ which means that $N_{60}\approx 50$ bpf, and since $G_{\max}=325(N_{60})^{0.68}$ (ksf), then $G_{\max}(\text{crust}) = 4647$ ksf = 222500 kPa. Since $\chi(\text{crust})=12.5$ kN/m³, then $V_s(\text{crust}) = \text{sqrt}(G_{\max} / \rho) = \text{sqrt}(222500/(12.5/9.81)) = 420$ m/s (~ 1400 ft/s).

The loose sand has $\phi=35^\circ$ which means that $N_{60}\approx 18$ bpf, and since $G_{\max}=325(N_{60})^{0.68}$ (ksf), then $G_{\max}(\text{loose sand}) = 2320$ ksf = 111100 kPa. Since $\chi(\text{loose sand})=17$ kN/m³, then $V_s(\text{loose sand}) = \text{sqrt}(G_{\max} / \rho) = \text{sqrt}(111100/(17/9.81)) = 250$ m/s (~ 820 ft/s).

The average shear wave velocity within the representative soil columns is:

$$\begin{aligned}\bar{V}_s &= \frac{H_1 + H_2}{\frac{H_1}{V_{s1}} + \frac{H_2}{V_{s2}}} \\ \bar{V}_s &= \frac{1.2 + 5 \times 0.75}{\frac{1.2}{420} + \frac{5 \times 0.75}{250}} \\ \bar{V}_s &= 275 \text{ m/s } (\sim 900 \text{ ft/s})\end{aligned}\tag{8.5}$$

Then, the initial fundamental period of the potential sliding mass is:

$$\begin{aligned}T_s &= \frac{4(H_1 + H_2)}{\bar{V}_s} \\ T_s &\approx 0.07 \text{ s}\end{aligned}\tag{8.6}$$

The 5%-damping spectral acceleration at $1.5T_s=0.11$ sec is about 0.46g (see Fig. 8.2). With these parameters an approximate result may be obtained. From Bray and Travararou (2007):

$$\begin{aligned}\ln(D) &= -1.10 - 2.83 \ln(k_y) - 0.333 (\ln(k_y))^2 + 0.566 \ln(k_y) \ln(Sa) + 3.04 \ln(Sa) + \dots \\ &\quad - 0.244 (\ln(Sa))^2 + 1.5T_s + 0.278(M_w - 7) \pm \epsilon\end{aligned}\tag{8.7}$$

then:

$$\begin{aligned} \ln(D) &= 2.48 \pm 0.66 \\ D &= 12 \text{ cm, (6 cm to 23 cm)} \end{aligned} \quad (8.8)$$

Since the estimated residual lateral displacement of the abutment is about 5 in., and in the context of a simplified estimation, this would mean that the bridge should have suffered small to moderate damage, which is consistent with the observations made after the earthquake. Note that if the sliding mass is considered to be rigid, then $S_a(1.5T_s) = PGA = 0.30g$ and

$$\begin{aligned} \ln(D) &= \\ \ln(D) &= 2.35 \pm 0.66 \\ D &= 10 \text{ cm, (5 cm to 20 cm)} \end{aligned} \quad (8.9)$$

The last required component of the simplified approach is the relationship between the equivalent residual undrained shear strength versus the yield coefficient. The yield coefficient was calculated for a suite of S_{ur} values, and the results are shown in Figure 8.7. As this figure shows, the relation between these two parameters is strongly linear and it can be expressed as:

$$k_y \approx 0.01362 \times S_{ur} \text{ (kPa)} - 0.09406 \quad (8.10)$$

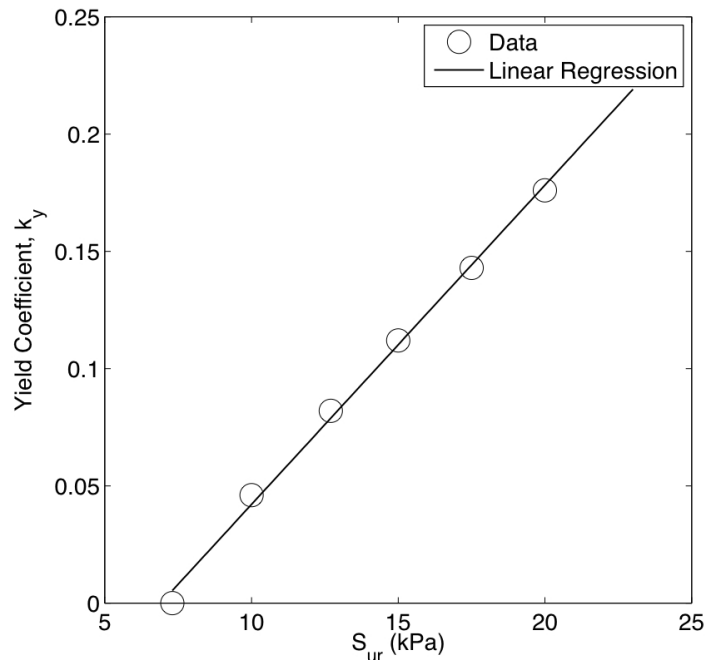


Fig. 8.7 Equivalent residual undrained shear strength versus yield coefficient.

8.1.6 Results

Using the simplified approach, the probability of exceeding different levels of displacements can be estimated. Figure 8.8 shows the result of this estimation for the north abutment of the Landing Road bridge given the intensity of the Edgecumbe, New Zealand.

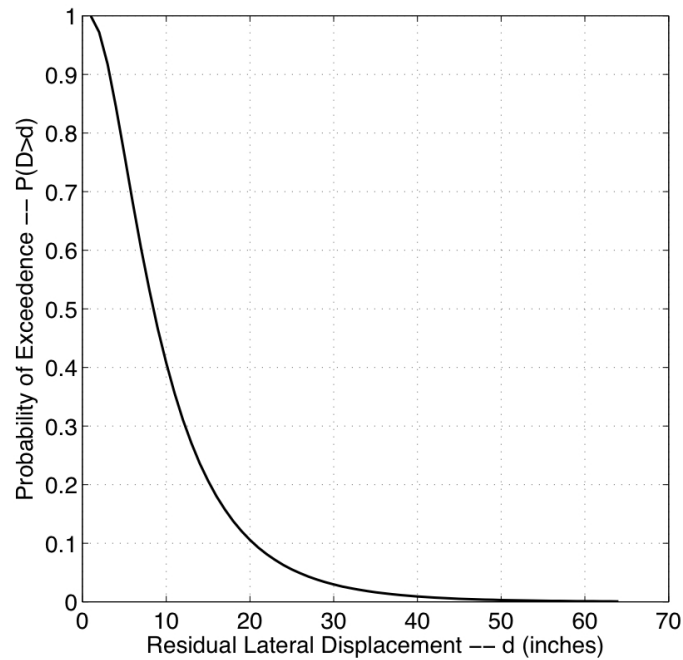


Fig. 8.8 Probability of exceeding a threshold residual lateral displacement (d) at north abutment of Landing Road bridge, given intensity of 1987, $M_w=6.6$ Edgecumbe earthquake in New Zealand.

8.1.6.1 Damage Estimation

The simplified approach described in Section 5.1 is used to estimate damage to the Landing Road bridge. Figure 8.9 shows that, given the characteristics of the Edgecumbe earthquake, the Landing Road bridge should have experienced moderate damage (probability of 74%). This figure also shows that the probabilities of reaching small and large damage states were rather small—15% and 11%, respectively—and that there were negligible probabilities of having either no damage or collapse. These results are consistent with the observations made to the bridge after the earthquake.

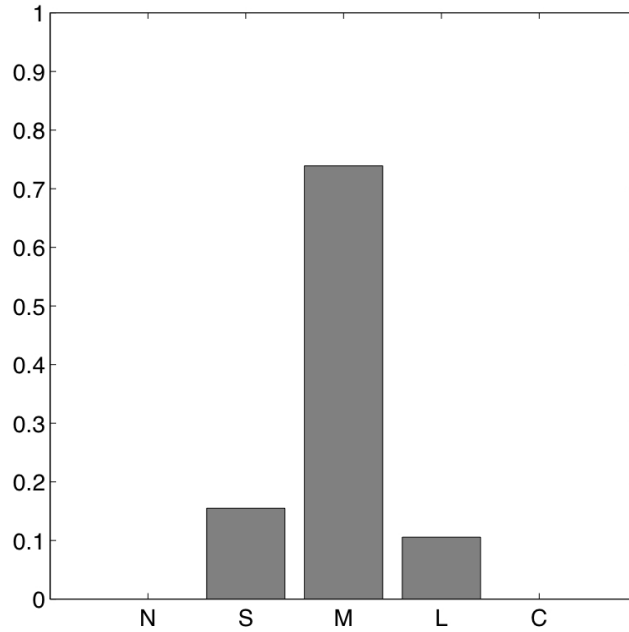


Fig. 8.9 Probability of bridge being in damage states of Negligible (N), Small (S), Moderate (M), Large (L), and Collapse (C).

The analyses performed by Kashighandi and Brandenburg (2006) predict a 18% probability of having less than moderate damage; a 40% chance of having more than moderate, but less than extensive, damage; a 37% chance of having more than extensive damage, but no collapse; and a 5% chance of having collapse, for pile cap lateral displacements in the order of 8 cm.

8.1.6.2 Sensitivity Analysis

As indicated in Chapter 7, the order of importance of the random variables is defined by their contribution to the variance of the linearized limit-state function. This contribution is reflected in the unit vector $\hat{\underline{\gamma}}$, which is different for each threshold level of lateral displacement. Figure 8.10(a) shows the absolute value of the terms in $\hat{\underline{\gamma}}$ as a function of the level of displacement. As this figure shows, the most important random variable in this case is ε , followed by S_{ur} (dash-dotted and continuous lines, respectively).

Vector $\underline{\delta}$ indicates the sensitivity of $P(D > d)$ to variations in the means of the random variables. To make a direct comparison, the vector $\underline{\delta}$ was normalized to have a unit length.

Figure 8.10(b) shows the absolute value of the terms in the normalized vector $\hat{\delta}$ as a function of the level of displacement. As this figure shows, ε is again the most significant random variable, followed by S_{ur} .

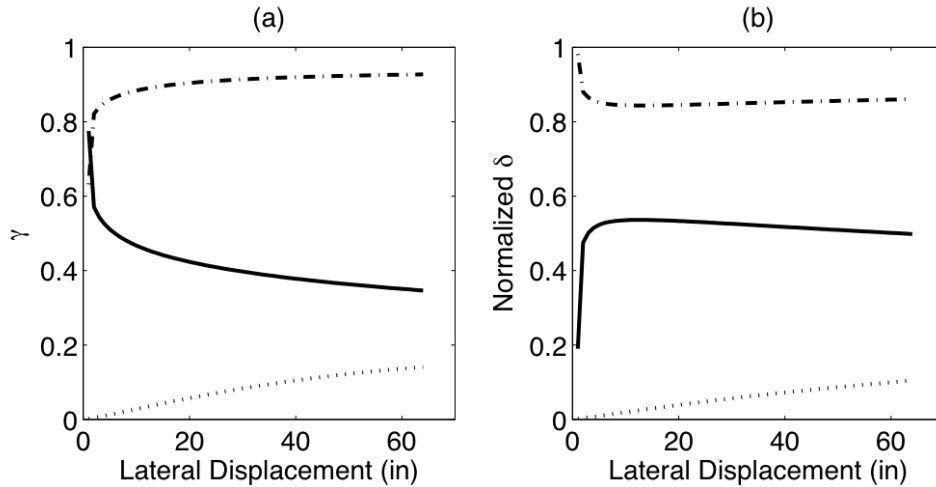


Fig. 8.10 Relative importance of, and $P(D > d)$'s sensitivity with respect to, three random variables, as function of expected level of residual lateral displacement. Continuous line is for S_{ur} , dotted line for α , and dash-dotted line for ε .

8.2 SHOWA BRIDGE DURING 1964 NIIGATA, JAPAN, EARTHQUAKE

This section presents the application of the proposed simplified approach to the case of the Showa bridge, which collapsed due to lateral spreading induced by the 1964 Niigata earthquake in Japan.

8.2.1 1964 Niigata, Japan, earthquake

The 1964 Niigata earthquake—caused by faulting along an almost vertical plane—had a moment magnitude of $M_w = 7.6$ (IRIS website 2007), its epicenter was under the sea, about 55 km north from Niigata city, and its hypocentral depth was about 20–30 km (see Fig. 8.11).

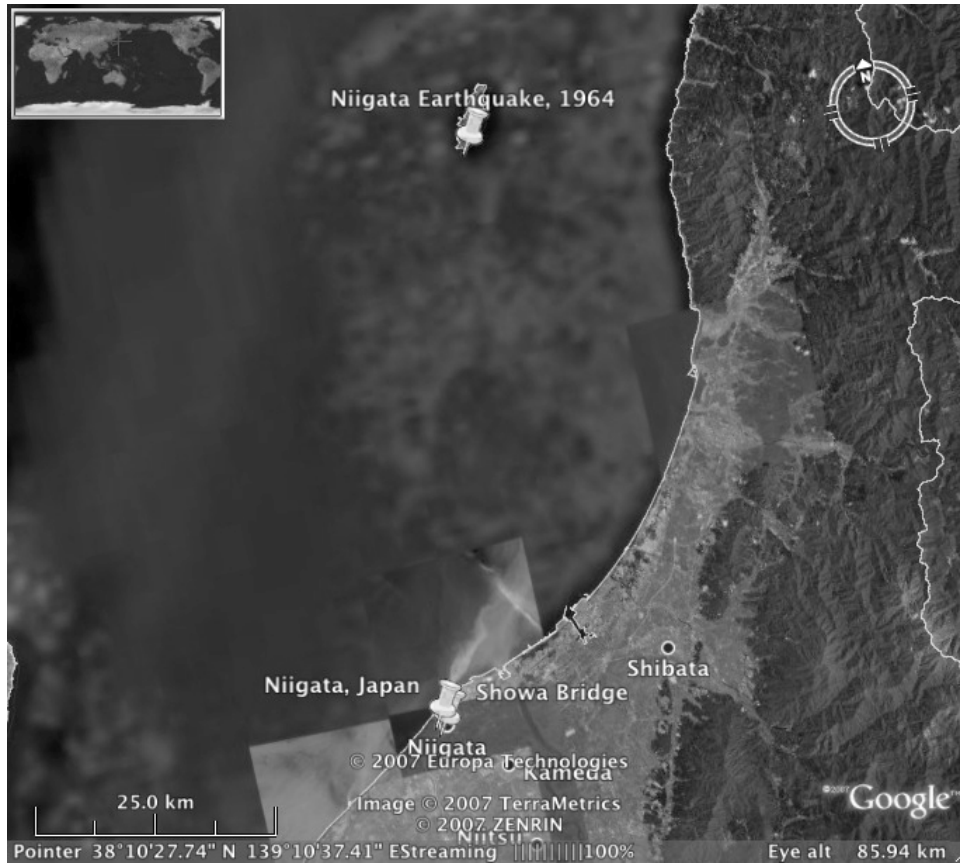


Fig. 8.11 Epicenter of 1964 Niigata earthquake, and Showa bridge.

The earthquake caused a peak ground acceleration at the south bank of the Showa bridge of 159 gals (0.16g) (Orense 2005). Figure 8.12 shows accelerograms at the roof and the base of a 4-story building located along the Shinano River.

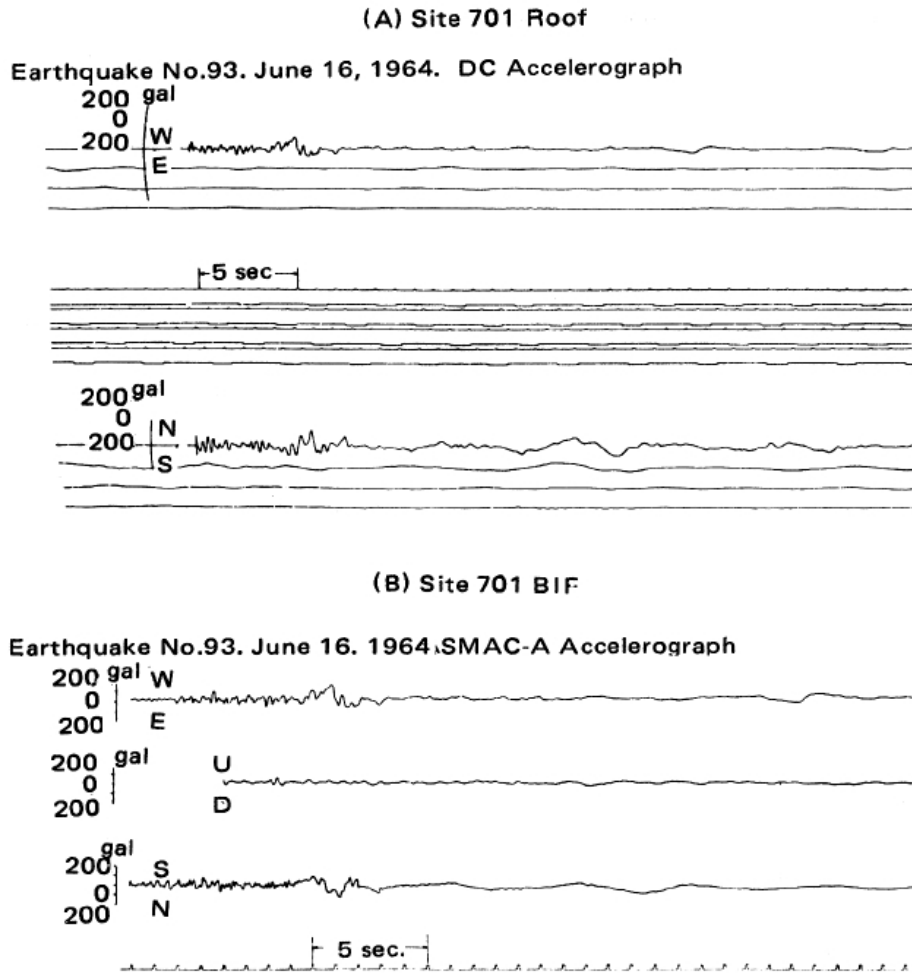


Fig. 8.12 Strong-motion earthquake records during Niigata earthquake; (A) Roof, (B) Basement of 4-story apartment building (after Iwasaki 1974).

8.2.2 Showa Bridge

The construction of the Showa bridge over the Shinano river was completed a month before the Niigata earthquake hit Japan (Iwasaki 1974). The abutments were of pile bents (nine single-row piles with a diameter of 609 mm and a length of 22 m), and the piers were also of pile bents (nine single-row piles of the same diameter and length of 25 m, see Fig. 8.13) with collar braces and cap beams. The design seismic coefficient for the substructures was 0.2 horizontally. The superstructures were of 12-span steel composite girders with simple supports. The total length was 303.9 m (= 13.75 + 10 @ 27.64 + 13.75), and the width was 24 m.

Due to the Niigata earthquake the bridge sustained severe damage (see Figs. 8.13–8.14). According to Iwasaki (1974) the left-bank abutment moved about 1 m toward the center of the

river, and the approach road subsided considerably. On the other hand, the right-bank abutment and the approach road sustained no significant damage. The first to fourth piers from the left-bank tilted toward the right-bank. The fifth and sixth piers collapsed completely into the river bed. The seventh to eleventh piers, however, suffered only slight damage. Five girders, the third to the seventh from the left-bank, out of a total of twelve girders, fell down into the river bed (see Fig. 8.14). The sixth span fell down on both its ends due to the failure of the fifth and sixth piers, which had supported the span.



Fig. 8.13 Collapse of Showa bridge (Photo by Penzien, J., 1964; Source: Earthquake Engineering Online Archive, NISEE, <http://nisee.berkeley.edu/elibrary/>).

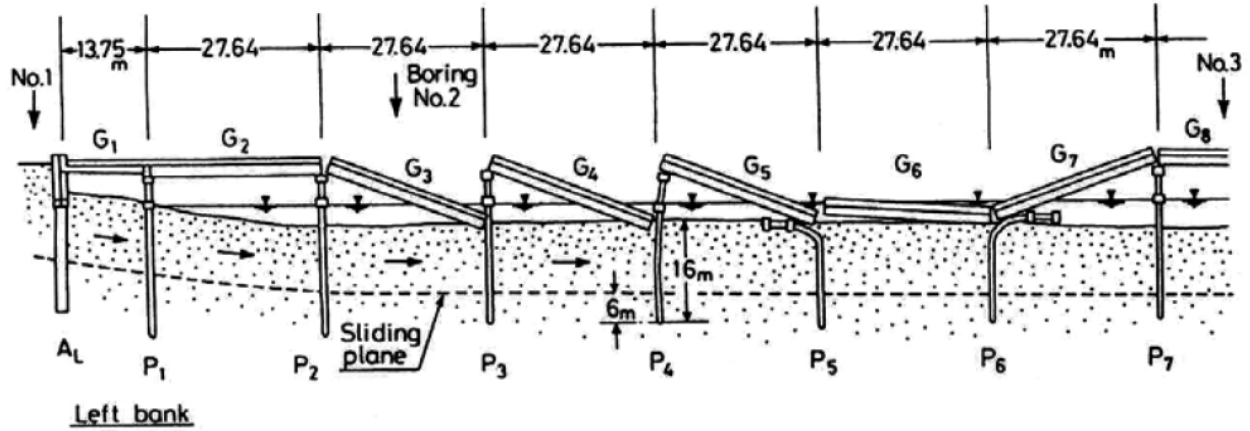
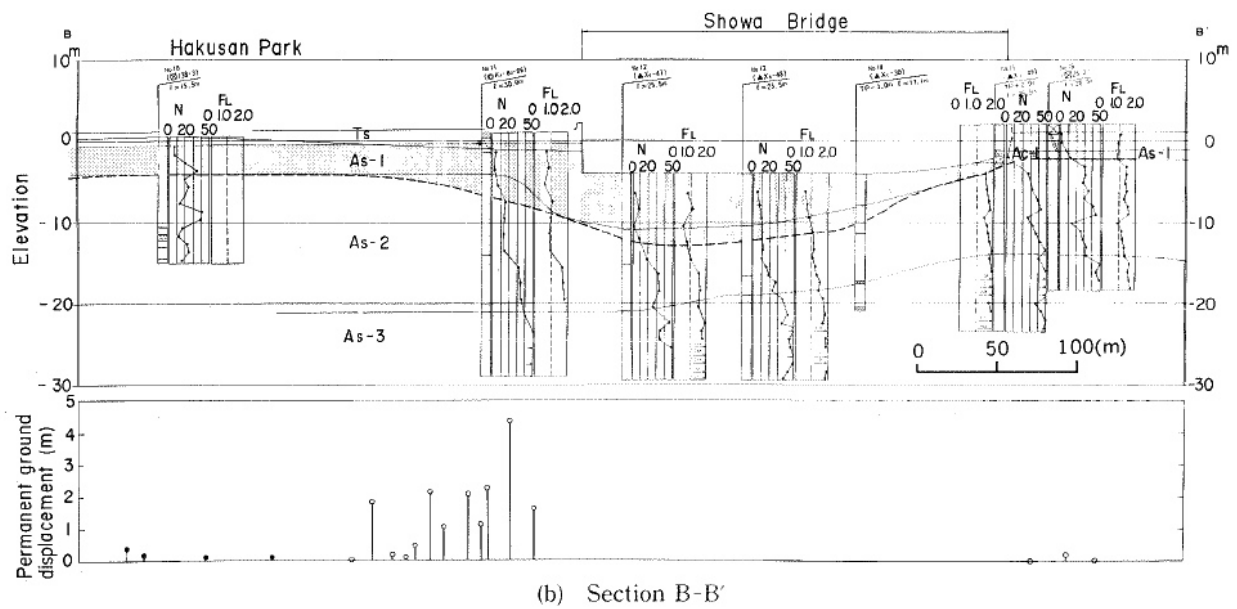


Fig. 8.14 Schematic diagram of collapse of Showa bridge (after Takata et al. 1965).

8.2.3 Soil Profile

The ground conditions at the site were of sandy soils, comparatively loose near the left bank and comparatively dense near the right bank (Iwasaki 1974). As Figure 8.15 shows, the liquefied layer at the left bank was more than 10 meters thick, while at the right bank it was very thin.



LEGEND

Ts	Surface Soil (Fill)	FL : Liquefaction Resistance Factor	○ : Displacement in Right Direction
As-1	Alluvial Sandy Soil	— : Estimated Liquefied Layer	● : Displacement in Left Direction
As-2			
As-3		- - - : Lower Boundary of Estimated Liquefied Layer	
Ac-1	Alluvial Clayey Soil		
Ac-2			

Fig. 8.15 Soil profile and estimated liquefied layer (after Hamada et al. 1986).

8.2.4 Results Using Simplified Approach

As Figures 8.15 and 8.16 show, in the case of the Showa bridge there was no upper non-liquefiable crust. In situations like this, it is recommended to check the design of the piles assuming that the liquefied soil will push the piles with a pressure distribution like the one shown in Figure 8.17.

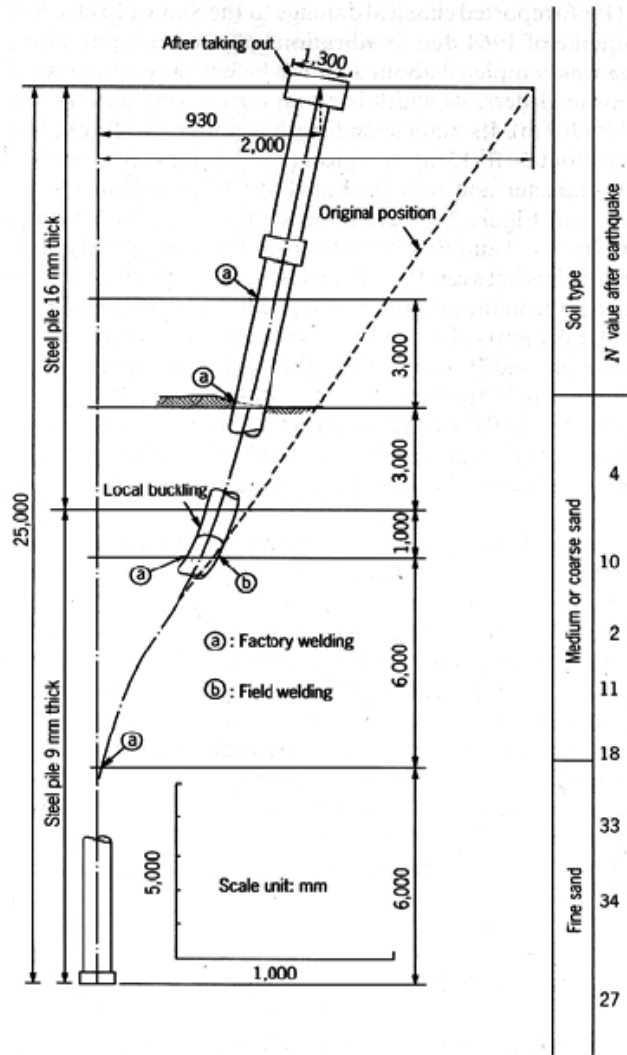


Fig. 8.16 Post-earthquake recovery and deformation of pile from Showa bridge. Note absence of upper non-liquefiable crust (after Fukuoka 1966).

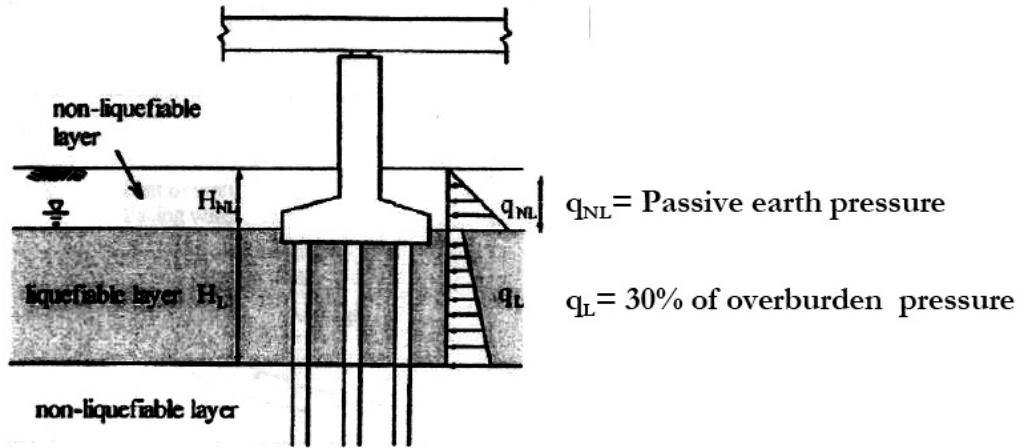


Fig. 8.17 Idealized pressure distribution for pile foundations affected by liquefaction-induced lateral ground displacement (after JRA 1996).

A modified version of the model used by Bhattacharya (2003) (see Fig. 8.18), is considered for this analysis. The point of fixity at the bottom of the piles was assumed to be located 3.5 diameters below the bottom of the liquefied layer, instead of directly below it. The external and internal diameters of the steel pile were set to 609 mm and 591 mm, respectively, and the Young's Modulus was assumed to be 210 GPa. Figure 8.19 shows the deformed shape of the pile and the respective bending moment diagram.

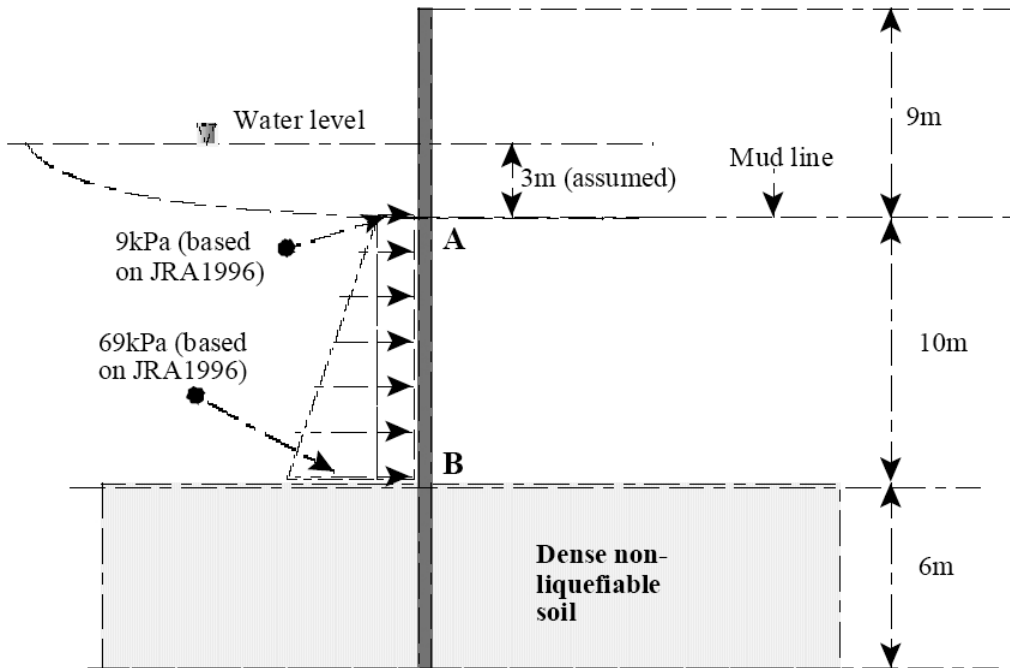


Fig. 8.18 Schematic diagram showing predicted loading based on JRA code (after Bhattacharya 2003).

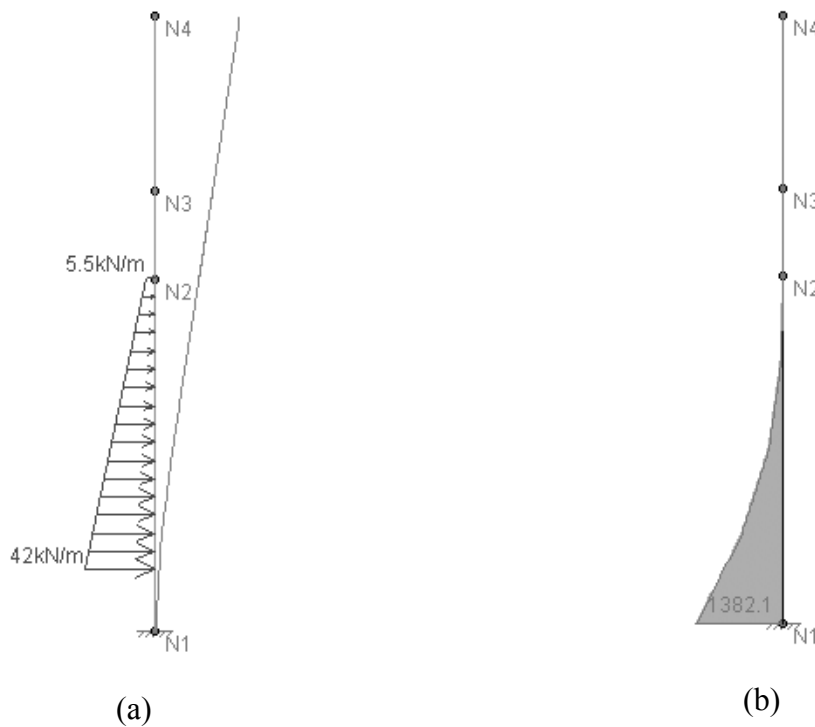


Fig. 8.19 Deformed shape and bending moment diagram (units are kN and m).

The maximum bending moment is below the plastic limit ($FS = 1620/1380 = 1.17$), which means that, according to this analysis, the piles did not fail in bending. This result is consistent with the results by Bhattacharya (2003). However, according to Iwasaki (1974), “... *it seems probable that the girders would fall down into the river bed if the relative displacement increases above 50 cm between the two adjoining piers. This is due to the fact that the width of the crest of each pier, which supports a fixed shoe and a movable shoe, was 50 cm and that there are no devices to prevent the fall of the girders.*” Based on the analysis shown in Figure 8.19, the lateral displacement at the top of the piles was estimated in ~60 cm, i.e., large enough to cause the collapse of the bridge girders.

8.3 CENTRIFUGE TESTS

8.3.1 Introduction

Brandenberg et al. (2005) performed eight dynamic centrifuge tests on the 9 m radius centrifuge at the Center for Geotechnical Modeling at the Univ. of California, Davis to study the behavior of pile foundations in liquefiable and laterally spreading ground. The models were tested in a flexible shear beam container at centrifugal accelerations ranging from 36.2g to 57.2g. Figure 8.20 shows a schematic model and partial instrumentation layout of their centrifuge tests.

Test SJB03 was selected to validate the simplified approach proposed in this study. As Figure 8.20 shows, the soil profile consisted of a non-liquefiable crust overlying loose sand overlying dense sand. All of the layers sloped gently toward a river channel carved in the crust at one end of the model. The non-liquefiable crust consisted of reconstituted Bay mud. The sand layers beneath the crust consisted of uniformly graded Nevada Sand. Water was used as a pore fluid for all of the models. Properties in this section are specified in prototype units.

8.3.2 Foundation Properties

The foundation consisted of a 2×3 pile group with a cap 2.2 m high, 9.2 m wide, and 14.3 m long. The piles had an outside diameter of 1.17 m, a thickness of 63 mm, and material properties of $E = 68.9$ GPa (Young’s modulus) and $\sigma_y = 216$ MPa (yield stress).

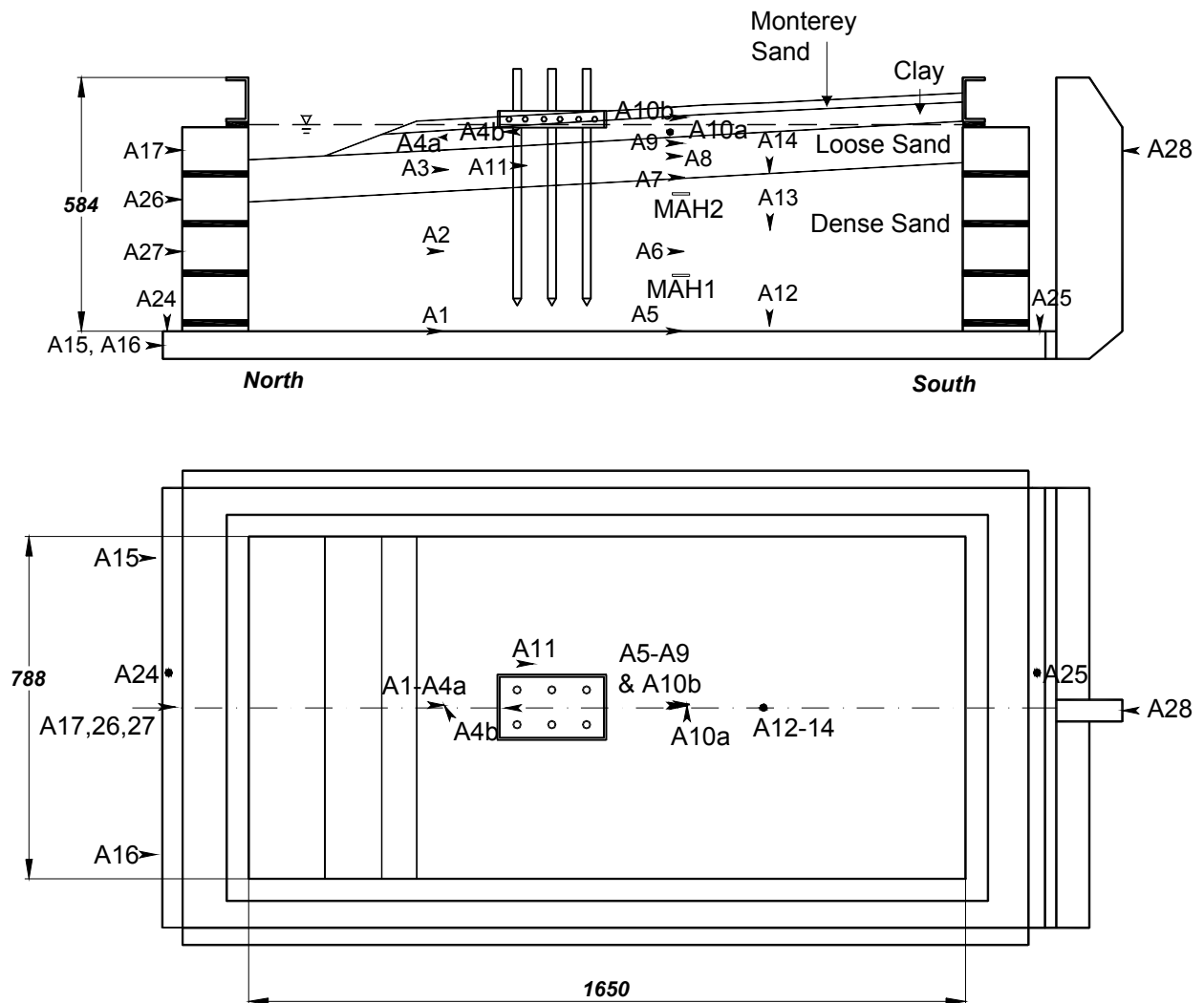


Fig. 8.20 SJB03 model layout–accelerometer instrumentation. Dimensions in mm (after Brandenburg et al. 2003).

8.3.3 Soil Properties

The soil profile consisted of 1.4 m of Monterey sand underlain by 2.7 m of clay ($S_u \approx 44$ kPa) and 5.4 m of loose sand ($D_r \approx 35\%$) over dense sand ($D_r \approx 75\%$). Based on these properties the unit weights were estimated as 17, 19, and 21 kN/m³ for the clay, loose sand, and dense sand layers, respectively.

8.3.4 Input Motions

A series of four simulated earthquake events were applied to Model SJB03. The first was a small Santa Cruz motion¹ with a peak acceleration of 0.13g. The subsequent motions were a medium Santa Cruz ($a_{max,base} = 0.35g$), a large Santa Cruz ($a_{max,base} = 0.67g$), and a large Kobe² ($a_{max,base} = 0.67g$) (Brandenberg et al. 2005). Figure 8.21 shows several time histories of raw and processed data illustrating the behavior of the soil and the pile group during the medium Santa Cruz motion. In this section, the results after this motion will be analyzed.

8.3.5 Results Using Simplified Approach

First, the passive soil resistance is compared against the ultimate structural capacity. The passive soil resistance against the pile cap can be estimated using the $\phi = 0$ sliding wedge method (Mokwa 1999):

$$P_{ult, cap} = \frac{S_u b H}{2} \left(4 + \frac{\gamma H}{S_u} + 0.25 \frac{H}{b} + 2\alpha \right) \quad (8.11)$$

where $S_u = 44$ kPa, $b = 9.2$ m, $H = 2.2$ m, $\gamma = 17$ kN/m³, and $\alpha = 0.75$. Then:

$$P_{ult, cap} = \frac{44 \times 9.2 \times 2.2}{2} \left(4 + \frac{17 \times 2.2}{44} + 0.25 \frac{2.2}{9.2} + 2 \times 0.75 \right) \quad (8.12)$$

$$P_{ult, cap} \approx 2850 \text{ kN}$$

The passive pressures below the pile cap can be estimated using the pressure distributions proposed in JRA (1996). The passive force between the clay layer and the piles would be $P_{ult, clay} = 0.5(37 + 70) \times 6 \times 1.9 \times 1.17 \approx 715 \text{ kN}$, and the resultant force of the liquefied sand reacting against the piles would be $P_{ult, loose sand} = 0.5(21 + 52) \times 6 \times 5.4 \times 1.17 \approx 1385 \text{ kN}$. Then, the total passive reaction of the soil against the foundation would be $P_{ult, soil} \approx 4950 \text{ kN}$.

¹ Univ. of California, Santa Cruz, CA. UCSC/Lick Lab, Channel 1, during the Loma Prieta earthquake.

² Port Island (83 m depth, north-south direction) during the Kobe earthquake.

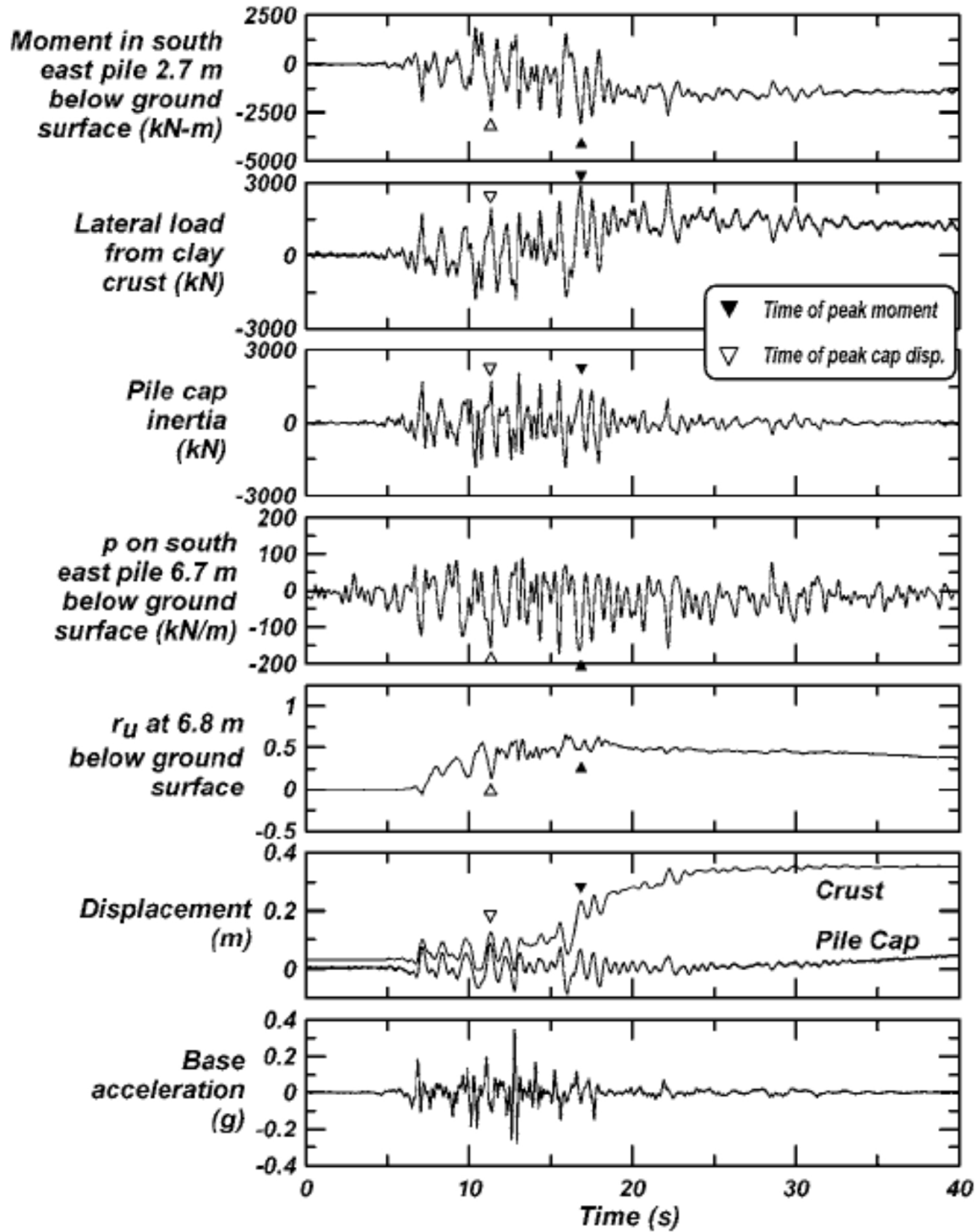


Fig. 8.21 Representative time series from SJB03 for medium Santa Cruz motion (after Brandenburg et al. 2005).

On the other hand, the plastic moment of the pile section is $M_p = \sigma_y Z_p$, where $Z_p = \pi(D_o^4 - D_i^4)/(32D_o)$, then $Z_p = \pi(1.17^4 - 1.044^4)/(32 \times 1.17)$, $Z_p = 0.0576 \text{ m}^3$, and $M_p = 216000 \times 0.0576 = 12440 \text{ kN} \cdot \text{m}$. Assuming that the points of fixity of the six piles are 3.5 diameters away from the liquefied layer, then $P_{ult, str} \approx 6 \times (2 \times M_p / L_{eq})$, i.e., $P_{ult, str} \approx 6 \times (2 \times 12440 / 11.4) = 13100 \text{ kN} > P_{ult, soil}$. Since the soil capacity is smaller than the structural one, the soil should have flown around the foundation. As Figure 8.22 shows, this is consistent to what was observed during the test.

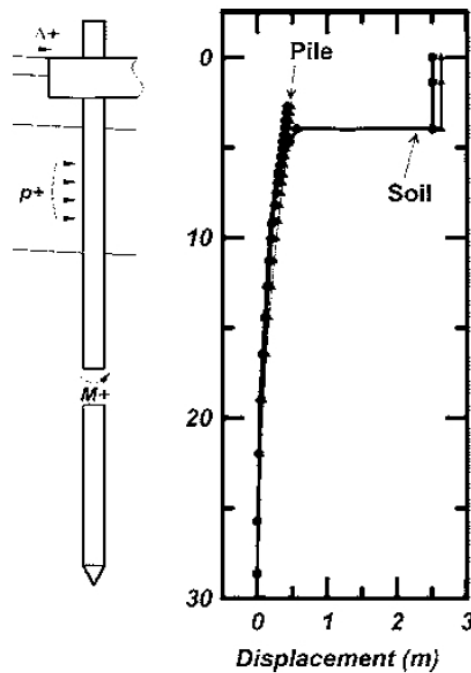


Fig. 8.22 Soil displacement versus pile cap displacement for SJB03 test.

In situations like this, it is proposed to follow the recommendation given in the MCEER/ATC (2003) document, i.e., to design the foundation to resist the passive pressures created by the soil flowing around the structure. Assuming a distance between the ts of fixity of $L_{eq} = 11.4 \text{ m}$, and using a simple structural model (see Fig. 8.23), the residual pile cap displacement and residual bending moment in the piles (at the location where it was measured during the test) were estimated as $\sim 0.04 \text{ m}$ and $\sim 3300 \text{ kN} \cdot \text{m}$, respectively. As Figure 8.21 shows, the residual pile cap lateral displacement in the test was $\sim 0.03 \text{ m}$, and the residual bending moment was $\sim 1250 \text{ kN} \cdot \text{m}$. When comparing these results, it is important to note that the

MCEER/ATC (2003) document is for design, so its estimations are likely to be conservative. Also, as Brandenburg et al. (2005) have indicated, the sequence of shaking events likely induced changes in the soil properties, including densification of the sand layers due to post-shaking consolidation, and cyclic degradation of the stress-strain behavior in the clay. The rather large (~ 0.3 m) relative displacement between the pile cap and the upper crust would generally be considered sufficient to mobilize the passive resistance of the clay crust against the pile cap; however, the peak crust load (estimated from the test) for the medium Santa Cruz motion was less than 50% of the peak load observed during the large shakes. According to Brandenburg et al. (2005), the softer load-displacement response observed in the centrifuge tests compared with static load tests can be attributed in part to cyclic degradation of the clay stress. If half of the full passive reaction is used in the simple analysis shown in Figure 8.23, the residual lateral displacement and pile bending moment would have been ~ 0.02 m and ~ 1650 kN·m, respectively, which are reasonably similar to the results from the test, ~ 0.03 m and ~ 1250 kN·m, respectively.

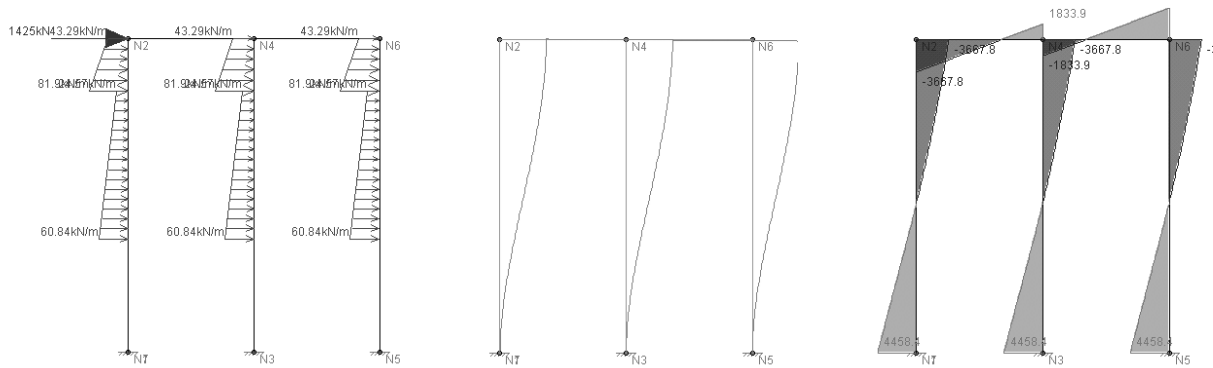


Fig. 8.23 Simplified foundation structural model.

Finally, it is important to realize that inertial effects can play an important role in the response of these systems. As Figure 8.21 shows, the maximum lateral displacement and pile bending moment are $\sim 150\%$ larger than the residual ones. However, the extrapolation of this type of result to real cases is not straightforward.

9 Other Issues

9.1 COMPARISON WITH RESULTS FROM ADVANCED FINITE ELEMENT ANALYSIS

Shin (2007) developed a detailed finite element model of the bridge example described in Chapter 6, putting emphasis in an accurate characterization of the structural and soil behavior, including modeling of bridge components such as piles, pile caps, abutments, and backwall structure. Figure 9.1 shows the finite element mesh developed by Shin, and Figure 9.2 presents some of the main components of this model.

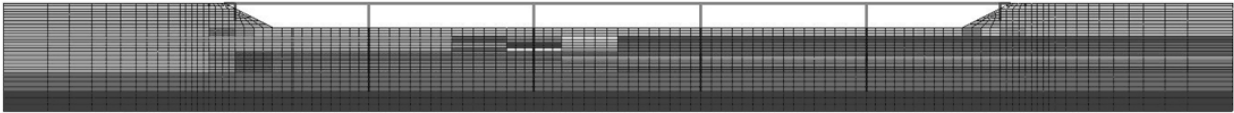


Fig. 9.1 Bridge example finite element mesh (after Shin 2007).

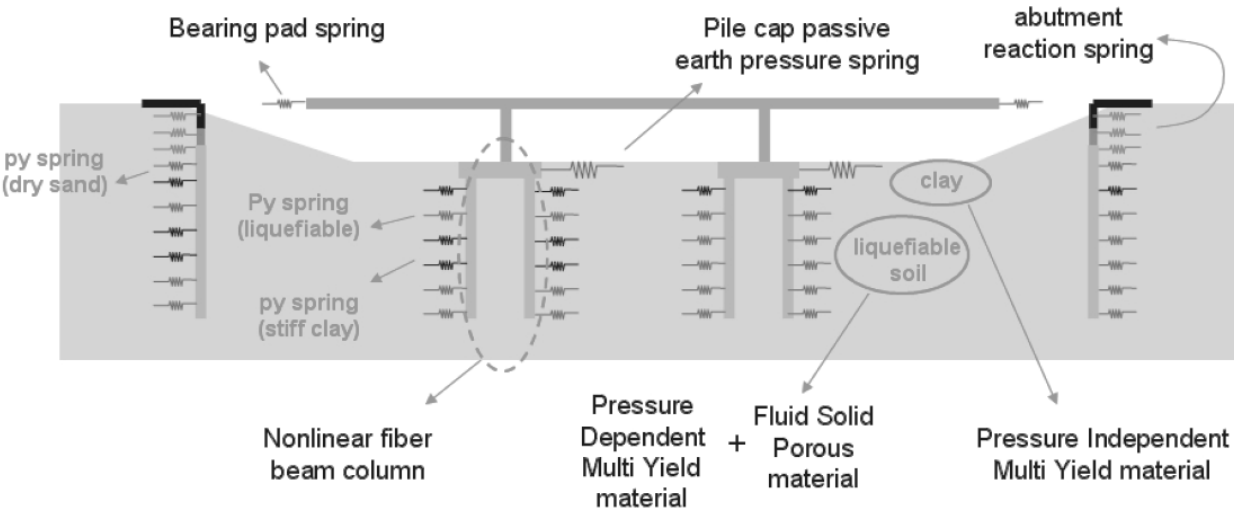


Fig. 9.2 Main components of analytical model (after Shin 2007).

Forty ground motions were applied to this model: ten motions for each hazard level corresponding to return periods of 29, 72, 475, and 2475 years. Scaled versions of the ground motions developed by Somerville and Collins (2000) were used for this purpose. From these analyses, several engineering demand parameters (EDPs) versus intensity measures (IMs) were identified.

Figures 9.3–9.6 show how the EDP-IM plots from the results of the advanced FE analyses compare with the results of the simplified coupled model described in Section 3.2.2. Peak Ground Velocity (PGV) was selected as IM, and four of the most relevant EDPs were chosen to make the comparison. It was assumed that the PGV was 51, 89, and 149 cm/s for return periods of 72, 475, and 2475 years, respectively. The selected EDPs were: residual pile cap longitudinal displacement at the abutments and at the intermediate columns, residual tangential column drift, and residual longitudinal relative deck-end/abutment displacement. As Figures 9.3–9.6 show, the proposed simplified coupled model captures reasonably well the response of the bridge for the different hazard levels.

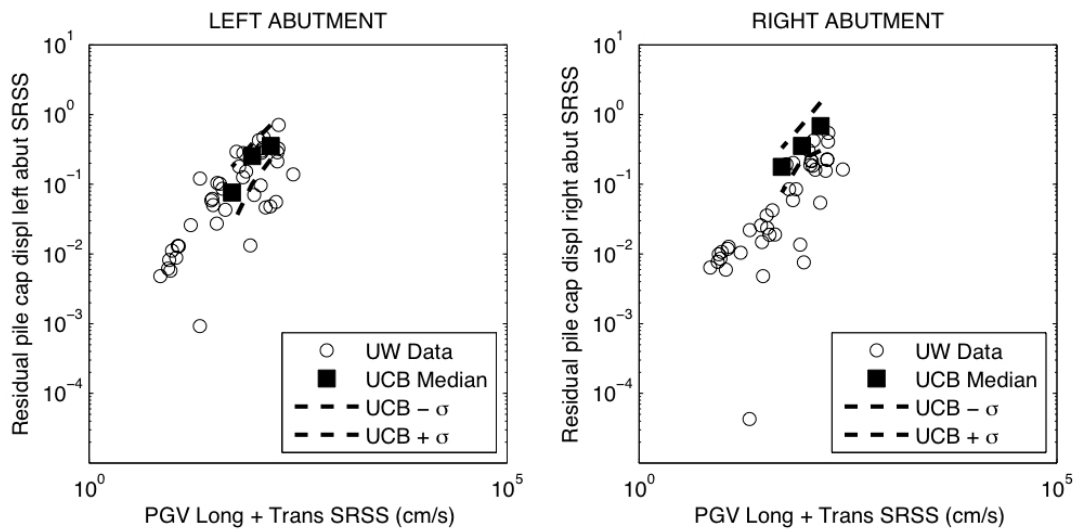


Fig. 9.3 Comparison of results—residual pile cap displacement at abutments.

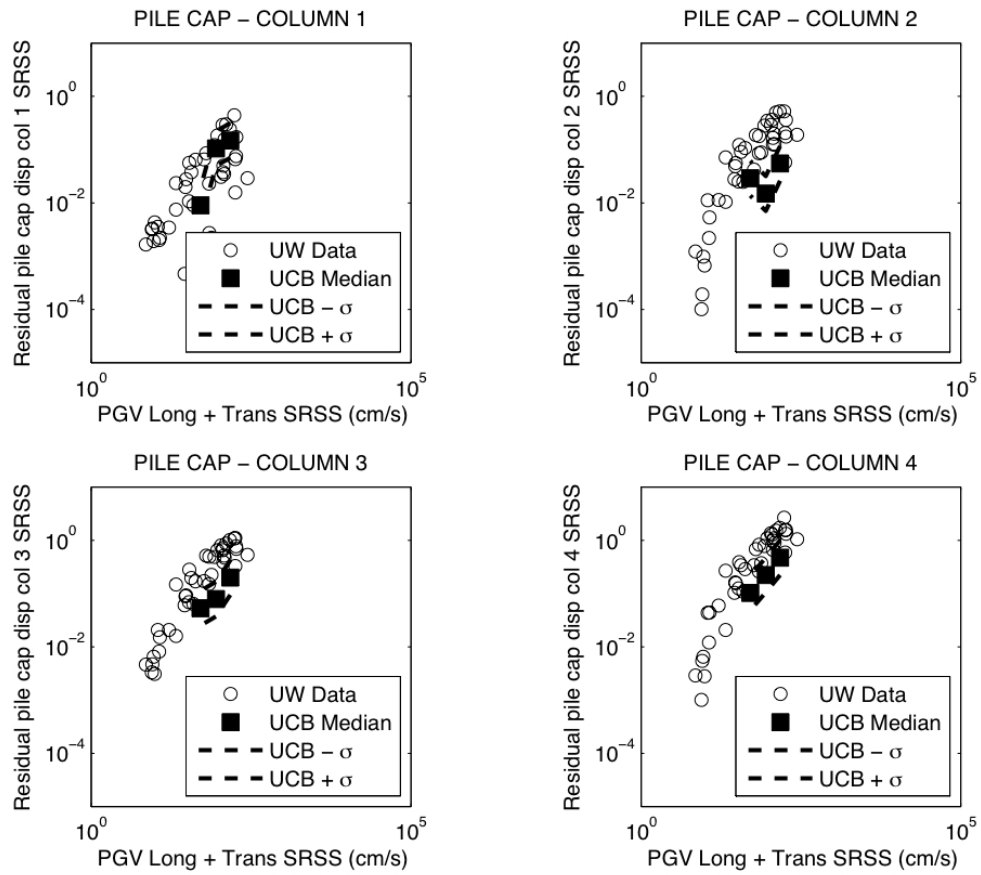


Fig. 9.4 Comparison of results—residual pile cap displacement at piers.

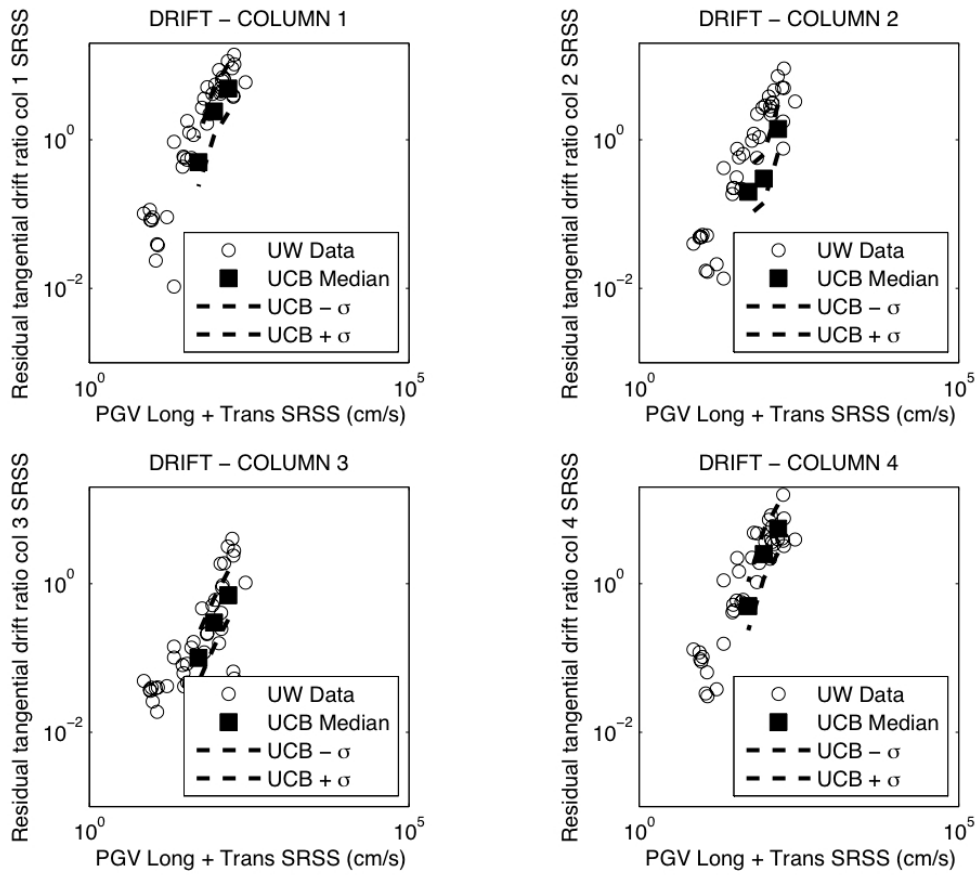


Fig. 9.5 Comparison of results—residual tangential drift ratio at columns.

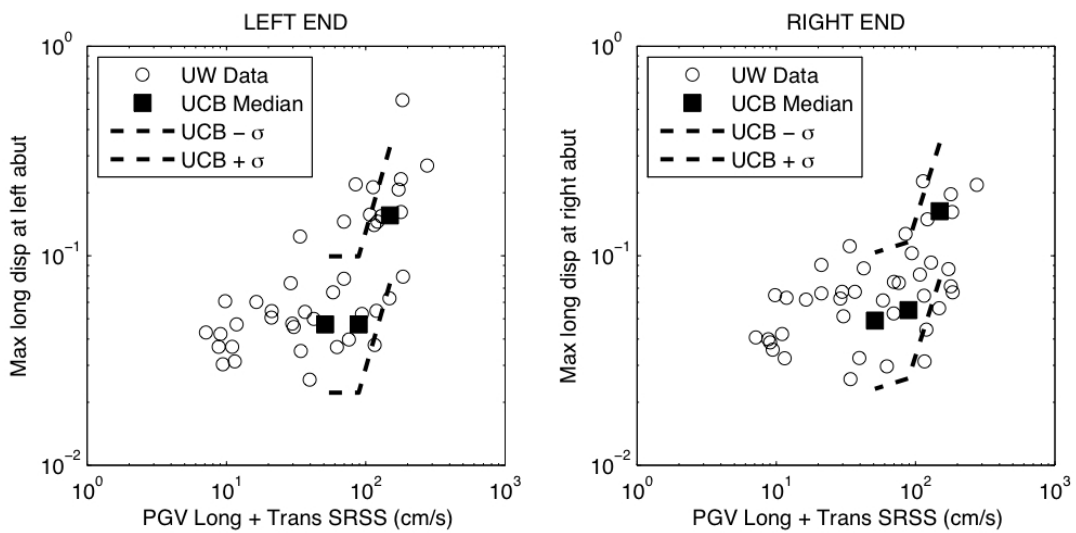


Fig. 9.6 Comparison of results—residual long. relative deck-end/abutment displacement.

9.2 INCORPORATION OF GROUND MOTION TIME HISTORIES

In the simplified approach described in Section 3, the probability that the residual longitudinal displacement at the abutments exceeded a certain threshold, given an intensity measure, was estimated using the expression proposed by Bray and Travararou (2007). However, in some cases, a more refined analysis may be desired. One alternative is to use a fully-coupled nonlinear finite element model like the one developed by Shin (2007) for the bridge example described in Section 6. Although this type of detailed analyses can be useful in illustrating important seismic response mechanisms, its implementation may not be feasible in all but the most critical projects due to economic or time constraints. A second alternative is to use a simplified analytical model that captures the key components of the problem to estimate the required seismic response. Figure 9.7 shows a range of simplified models that are possible, from a rigid Newmark sliding block to a nonlinear lumped mass coupled sliding model. For example, Bray and Travararou (2007) used an iterative procedure with an equivalent-linear sliding block model that had been shown to capture the nonlinear response of a potential sliding mass to develop their recommended expression. If a site-specific set of ground motions is provided, models like those shown in Figure 9.7 can be used to estimate the mean response and to characterize the uncertainty around that mean. At least seven ground motions should be used to estimate the mean residual lateral displacement, and a larger set should be used to estimate the dispersion around that mean. Alternatively, the uncertainty can be conservatively estimated using the error term ε given in the expression by Bray and Travararou (2007). To perform the analyses, and to be consistent with the results by Bray and Travararou (2007), the suite of ground motions should be scaled to match the respective 5%-damped spectral acceleration at the degraded period of vibrations of the potential sliding mass ($1.5T_s$) for each hazard level.

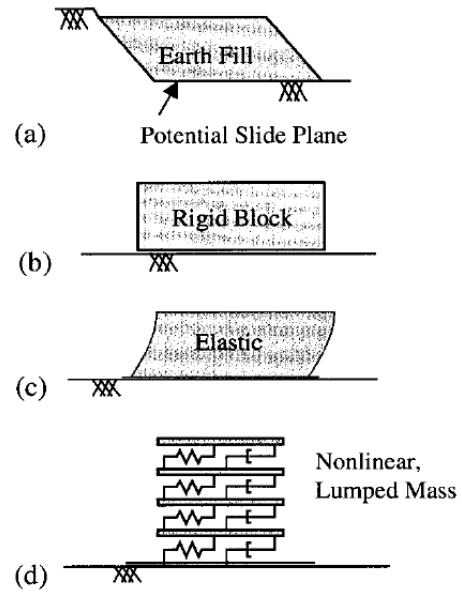


Fig. 9.7 (a) Problem analyzed; (b) Newmark rigid model; (c) Linear elastic, modal, coupled sliding model; (d) Nonlinear, lumped mass, coupled sliding model (after Rathje and Bray 2000).

10 Conclusions

10.1 SUMMARY

Based on the general concepts delineated in the MCEER/ATC-49-1 document, a simplified probabilistic procedure for assessing bridge damage due to liquefaction-induced lateral ground displacement has been developed. Some of the key factors that have been incorporated in this procedure are the “pile-pinning” effect, and characterizations of the uncertainty in parameters such as the residual undrained shear strength of liquefiable soils, the error term in the estimation of the abutments’ seismically induced deviatoric permanent displacement, and the distance to the points of pile fixity in the firm soil layers above and below the liquefiable soil. The use of the proposed approach was illustrated through its application to a detailed bridge example, as well as to a few representative well-documented case histories and a centrifuge model experiment. The estimated results using the simplified procedure agreed reasonably well with the post-earthquake shaking observations in these cases.

10.2 PRINCIPAL FINDINGS

- Liquefaction of the foundation soils dramatically affects the structural response and resulting performance of a bridge system. It is critical that ground conditions at a bridge site be adequately characterized and evaluated in terms of potential for liquefaction or severe strength loss.
- The “pile-pinning” effect is a critical element of the seismic performance of a bridge system that is founded on piles that pass through a potentially liquefiable soil layer with

firm soil layers both above and below the liquefiable soil layer. It is important to include this effect in the estimation of the dynamic resistance of the bridge-foundation-soil system.

- Based on the cases analyzed in this study, the residual longitudinal displacement of the abutments is judged to be an appropriate index of the overall seismic performance of pile-founded bridges affected by liquefaction-induced lateral ground displacement. Large residual displacements of the abutments are typically associated with large deformations of the foundation system, which results in large deformations and forces being developed in the bridge superstructure. Significant deformations and forces in the bridge can lead to severe damage or even the collapse of the bridge.
- Performance-based earthquake engineering (PBEE) provides a practical methodological for evaluating the likely seismic performance of existing and new bridges. Although its formulation may at first appear to be complex, there are now standard analytical tools that facilitate its application to actual projects. Most importantly, it takes advantage of recent advances in probabilistic seismic hazard assessment techniques, tracks the uncertainty associated with key parameters of the analysis, and documents the application of engineering judgment and decisions during the design and evaluation process.
- One of the most important steps in the PEER-PBEE methodology is also one of the most challenging ones, i.e., to define a robust relationship between seismic response, damage condition, and repair actions. Analytical models combined with engineering judgment based on recommendations from a panel of experts are currently the most reliable ways to estimate these types of relationships. The lack of robust relationships that connect the calculated response of engineered systems and the consequences of these responses in terms of death, dollars, and downtimes remains one of the most significant limitations to wider use of this methodology.
- The characterization of the ground motion hazard is an important step in the PEER-PBEE approach. For a selected ground motion hazard level, the most important parameters in this problem were the error term in the estimation of the residual lateral displacement at the abutments and the residual undrained shear strength of the potentially liquefiable layers. Overall, however, the most dominant factor was the spectral acceleration at the degraded period of vibration of the potentially sliding mass. No other parameter was

more important than the ground motion parameter that was used to define the seismic hazard at the site.

- The combination of engineering judgment and simple analytical models can lead to reasonable estimates of the seismic performance of bridge systems undergoing liquefaction-induced lateral ground displacement. The results of these simple models can guide the decision of whether the use of more advanced analyses is required or not.

10.3 FUTURE RESEARCH

- Development of an enhanced, yet still simple, analytical model suitable for dynamic analysis of a bridge-foundation-soil system is required. This model could be a combination of the nonlinear lumped mass coupled sliding model proposed by Rathje and Bray (2000) and the current simplified coupled model.
- Ground motion selection is an important topic warranting additional attention for cases where the bridge evaluation requires more site-specific analysis. Given the importance of the characteristics of the ground motion, the development of guidelines for ground motion selection is of great importance.
- Although it is possible to quantify the consequences of a seismic event in terms other than repair costs, such as downtimes, repair times, or number of deaths, the database available to calibrate these models is still lacking. Hence, it is difficult to make reliable estimations in these terms. More robust relationships are required between engineering demand parameters, damage measures, and decision variables. Gathering sufficient real data is a critical next step.
- Improved evaluation procedures that incorporate the effects that inertial loads have in cases where the bridge deck is present are required. This would include development of guidelines of when and how these inertial loads should be incorporated in the analysis.
- Incorporation of the bridge's transverse response in the seismic performance evaluation is required.

REFERENCES

- Abrahamson, N.A. and Silva, W.J., 1997, "Empirical Response Spectral Attenuation Relations for Shallow Crustal Earthquakes," *Seismological Research Letters*, Vol. 68, No. 1, 94-127.
- Abrahamson, N.A., 2000. "State of the practice of seismic hazard evaluation," *GEOENG 2000 Conference Proceedings*, Melbourne, Australia.
- ATC/MCEER Joint Venture, "MCEER/ATC-49-1, Liquefaction Study Report, Recommended LRFD Guidelines for the Seismic Design of Highway Bridges," Prepared under NCHRP Project 12-49, FY '98, 2003.
- ATC/MCEER Joint Venture, 2003. "NCHRP 12-49, Recommended LRFD Guidelines for the Seismic Design of High-way Bridges, Part I: Specifications."
- Berrill, J.B., Christensen, S.A., Keenan, R.P., Okada, W., and Pettinga, J.R., 2001. "Case study of lateral spreading forces on a piled foundation." *Geotechnique*, 51(6). 501-517.
- Bhattacharya, S., 2003. "Pile Instability During Earthquake Liquefaction," Ph.D. thesis, Cambridge University, 2003.
- Bilge, H.T., and Cetin, K.O., "Probabilistic Models for the Assessment of Cyclic Soil Deformations," *Proceedings of the 8th U.S. National Conference on Earthquake Engineering*, April 18-22, 2006, San Francisco, California, U.S.A., Paper No. 1822.
- Boulanger, R. W., Chang, D., Gulerce, U., Brandenburg, S., and Kutter, B. L., 2006. "Evaluating pile-pinning effects on abutments over liquefied ground." *Seismic Performance and Simulation of Pile Foundations in Liquefied and Laterally Spreading Ground*, *Geotechnical Special Publication No. 145*, ASCE, 306-318.
- Brandenberg, S. J., Boulanger, R. W., Kutter, B. L., and Chang, D., 2005. "Behavior of piles in laterally spreading ground during centrifuge tests," *J. of Geotech. and Geoenviron. Eng.*, ASCE. 131(11).
- Brandenberg, S.J., Chang, D., Boulanger, R.W., and Kutter, B.L., 2003. "Behavior of piles in laterally spreading ground during earthquakes – centrifuge data report for SJB03." *UCD/CGMDR-03/03*, Center for Geotechnical Modeling, Department of Civil Engineering, University of California, Davis.
- Bray, J.D. and Travasarou, T., 2007. "Simplified Procedure for Estimating Earthquake-Induced Deviatoric Slope Displacements," *J. of Geotech. and Geoenviron. Engrg.*, ASCE, April 2007, Vol. 133, No. 4, pp. 381-392.

- Caltrans, 2006. "Seismic Design Criteria."
- Campbell, K.W. and Bozorgnia, Y., 2007. "Campbell-Bozorgnia NGA Ground Motion Relations for the Geometric Mean Horizontal Component of Peak and Spectral Ground Motion Parameters." Report PEER 2007/2, Pacific Earthquake Engineering Research (PEER), Center, Richmond, CA.
- Chiou, B.S.-J. and Youngs, Y., 2006. "Chiou and Youngs PEER-NGA Empirical Ground Motion Model for the Average Horizontal Component of Peak Acceleration and Pseudo-Spectral Acceleration for Spectral Periods of 0.01 to 10 Seconds." Interim Report for USGS Review. June 14, 2006.
- Christian, J. T. and Baecher G. B., 1999, "Point-Estimate Method as Numerical Quadrature," *Journal of Geotechnical and Geoenvironmental Engineering*, Vol. 125, No. 9, pp. 779-786.
- Cornell, C. A., and Krawinkler, H., 2000. "Progress and challenges in seismic performance assessment." PEER Center News, Spring 2000. <http://peer.berkeley.edu/news/2000spring/index.html>
- Cornell, C.A., 1968. "Engineering seismic hazard analysis," *Bull. Seismol. Soc. Am.* 59 (1968) (5), pp. 1583–1606.
- Der Kiureghian, A. "Introduction to Structural Reliability: Class Notes for CE229-Structural Reliability" (Spring, 1999).
- Der Kiureghian, A., 2005. "Probability Concepts for Performance-Based Earthquake Engineering," Paper presented at Symposium Honoring Luis Esteva, Mexico City, September 2005.
- Duncan, J. M., 2000. "Factors of Safety and Reliability in Geotechnical Engineering." *Journal of Geotechnical and Geoenvironmental Engineering*, Volume 126, Issue 4, pp. 307-316 (April 2000).
- Eddy, M. A., Gutierrez, M. S., and Lumbantoruan, M. "Probabilistic Liquefied Shear Strength". *GeoCongress 2006, Geotechnical Engineering in the Information Technology Age, Proceedings of GeoCongress 2006, February 26–March 1, 2006, Atlanta, Georgia, USA.*
- Finn, W.D.L., Ledbetter, R.H., and Stacy, S.T., 1991. "Dam on Liquefiable Foundation: Safety Assessment and Remediation." *Proc., 17th Inter. Conf. on Large Dams, Vienna*, pp. 531-553.
- Finn, W.D.L., Ledbetter, R.H., and Wu, G., 1997. "The Stabilization of the Upstream Slope of Sardis Dam Using Driven Prestressed Concrete Piles: Methods of Analysis." *Proc., 9th Inter.*

- Conf. on Computer Methods and Adv. in Geomechanics, Wuhan, China, J.X. Yuan (Ed.), A.A. Balkema/Rotterdam/Brookfield, pp. 141-150.
- GEO-SLOPE/W International, Ltd., 2004. "Stability Modeling with SLOPE/W." GEOSLOPE/W International, Ltd., Calgary, Alberta, Canada.
- Hamada, M., 1992. "Large ground deformations and their effects on lifelines: 1964 Niigata earthquake. Case Studies of Liquefaction and Lifeline Performance During Past Earthquake, Vol. 1." Technical Rep. NCEER-92-0001, National Center for Earthquake Engineering Research, Buffalo, N.Y., 3-1-3-123.
- Hodder, A.P.W. and Graham, M.Z., 1993. "Earthquake Microzoning from Soil Properties," *Earthquake Spectra* 9, 209.
- Hynes, M. E. and Olsen, R. S., 1999. "Influence of confining stress on liquefaction resistance." Proc., Int. Workshop on Phys. and Mech. Of Soil Liquefaction, Balkema, Rotterdam, The Netherlands, 145-152.
- Idriss, I. M. and Boulanger, R. W., 2007. "SPT- and CPT-based Relationships for the Residual Shear Strength of Liquefied Soils." *Earthquake Geotechnical Engineering*, 4th International Conf. on Earthquake Geotechnical Engineering – Invited Lectures, K. D. Pitilakis, ed., Springer, The Netherlands, 1-22.
- Imai, T., and Tonouchi, K., 1982. "Correlation of N-value with S-wave velocity." *Proceedings of 2nd European Symposium on Penetration Testing*, 67-72.
- Iwasaki, T., 1974. "Response Analysis of Civil Engineering Structures Subjected to Earthquake Motions." Ground Vibration Section, Public Works Research Institute, Ministry of Construction, Japan.
- Jones, A.L., Kramer, S.L., and Arduino P., 2002. "Estimation of Uncertainty in Geotechnical Properties for Performance-Based Earthquake Engineering." Report PEER 2002/16, Pacific EQ Engineering Research (PEER), Center, Richmond, CA.
- JRA, 1996. Japanese Road Association, Specification for Highway Bridges, Part V, Seismic Design.
- Kashighandi, P., and Brandenburg, S.J., 2006. "Fragility Curves for Lateral-Spreading Induced Damage to the Landing Road Bridge." Draft Paper. Personal Communication.
- Kramer, S. L., 1996. "Geotechnical Earthquake Engineering," Prentice Hall, Upper Saddle River, NJ, 653 pp.
- Kramer, S. L., 2007. Personal Communication.

- Liao, S., and Whitman, R. V., 1986. "Overburden correction factors for SPT in sand." *J. Geotech. Engrg., ASCE*, 112(3), 373–377.
- Mackie, K. "Quick (updated) summary of Bridges Types 1 & 11" (November 11, 2005).
- Mackie, K., and Stojadinovic, B. "PEER Methodology Digest" (February 18, 2005)
- Mackie, K., and Stojadinovic, B., 2006. "Seismic vulnerability of typical multi-span California highway bridges." In *Proceedings of the 5th National Seismic Conference on Bridges and Highways*, September 18-20, 2006. San Francisco, CA.
- Mackie, K., Wong, J-M., and Stojadinovic, B., 2007. "Comparison of post-earthquake highway bridge repair costs." In *Proceedings of ASCE Structures Congress*.
- Marcuson, W.F., 1978. "Definition of terms related to liquefaction." *J Geotech Eng Div ASCE* 104(9): 1197–1200.
- Martin, G.R., and Lam, I.P., 2000. "Earthquake Resistant Design of Foundations: Retrofit of Existing Foundations." *Proc. Int. Conf. on Geotech. and Geol. Engrg., Melbourne*, Vol. 1, pp. 1025-1047.
- Martin, G. R., March, M. L., Anderson, D. G., Mayes, R. L., and Power, M. S., 2002. "Recommended Design Approach for Liquefaction Induced Lateral Spreads." *Proc. Third National Seismic Conference and Workshop on Bridges and Highways*, MCEER-02-SP04, Buffalo, N.Y.
- Martin, G. R., 2004. "The Seismic Design of Bridges-Geotechnical and Foundation Design Issues." *Geotechnical Engineering for Transportation Projects (GSP No. 126)*. *GeoTrans* 2004. July 27–31, 2004, Los Angeles, California, USA. Mishac K. Yegian, Edward Kavazanjian, Editors.
- Mokwa, R.L., 1999, "Investigation of the Resistance of Pile Caps to Lateral Loading." Ph.D. thesis, Virginia Polytechnic Institute.
- Moss, R. E. S., Seed, R. B., Kayen, R. E., Stewart, J. P., and Tokimatsu, K., 2005. "Probabilistic Liquefaction Triggering Based on the Cone Penetration Test." *GeoFrontiers 2005*, E. M. Rathje, ed.
- Newmark, N. M., 1965, "Effects of Earthquakes on Dams and Embankments", *Geotechnique*, v. 15, p. 139-160.
- NGA Database, 2007. Next Generation Attenuation (NGA) of Ground Motions Project, <http://peer.berkeley.edu/nga>

- Olson, S. M. and Stark, T. D., 2002, "Liquefied Strength Ratio from Liquefaction Flow Failure Case Histories," *Can. Geotech. J.* 39: 629–647.
- Orense, R.P., 2005. "Assessment of Liquefaction Potential based on Peak Ground Motion Parameters," *Soil Dynamics and Earthquake Engineering*, 25, 225 – 240.
- Rathje, E. M. and Bray J. D., 1999. "An examination of Simplified Earthquake-Induced Displacement Procedures for Earth Structures." *Canadian Geotechnical Journal* 1999; 36(1): 72-87.
- Rathje, E.M. and Bray, J.D., 2000. "Nonlinear Coupled Seismic Sliding Analysis of Earth Structures," *Journal of Geotechnical and Geoenvironmental Engineering*, ASCE, Vol. 126, No. 11, pp. 1002-1014.
- Reese, L. C., Wang, S. T., Isenhower, W. M., Arrelaga, J.A., and Hendrix, J. A., 2000. "LPILE Plus Version 4.0M," Ensoft, Inc. Austin, TX.
- Rosenblueth, E., 1975, "Point Estimates for Probability Moments." *Proc. Nat. Acad. Sci. USA*, Vol. 72, No. 10, pp. 3812-3814.
- SAC Joint Venture for the Federal Emergency Management Agency (FEMA), "FEMA 351-Recommended Seismic Evaluation and Upgrade Criteria for Existing Welded Steel Moment-Frame Buildings"
- Seed, H. B. and Idriss, I. M., 1971. "Simplified procedure for evaluating soil liquefaction potential." *J. Geotech. Engrg. Div., ASCE*, 97(9), 1249–1273.
- Seed, H. B. and Idriss, I. M., 1982. "Ground motions and soil liquefaction during earthquakes." *Earthquake Engineering Research Institute Monograph*, Oakland, Calif.
- Seed, H. B., 1983. "Earthquake-resistant design of earth dams." *Proc., Symp. Seismic Des. of Earth Dams and Caverns*, ASCE, New York, 41–64.
- Seed, R.B. and Harder, L. F., 1990, "SPT-based analysis of cyclic pore pressure generation and undrained residual strength." *Proceedings of H. Bolton Seed Memorial Symposium*, volume 2, pages 351-376.
- Seed, R.B., Cetin, K.O., Moss, R.E.S., Kammerer, A., Wu, J., Pestana, J.M., Riemer, M.F., Sancio, R.B., Bray, J.D., Kayen, R.E., and Faris, A., "Recent Advances in Soil Liquefaction Engineering: A Unified and Consistent Framework," *Keynote Address*, 26th Annual Geotechnical Spring Seminar, Los Angeles Section of the GeoInstitute, American Society of Civil Engineers, H.M.S. Queen Mary, Long Beach, California, April 30, 2003.

- Shin, H-S, 2007. "Numerical Modeling of a Bridge System and Its Applications for Performance-Based Earthquake Engineering," Ph.D. thesis, University of Washington.
- Somerville, P., and Collins, N., 2002. "Ground Motion Time Histories for the 1880 Bridge, Oakland."
- Somerville, P.G., Smith, N.F., Graves, R.W., and Abrahamson, N.A., 1997. "Modification of empirical strong ground motion attenuation relations to include the amplitude and duration effects of rupture directivity," *Seismological Research Letters* 68, 199-222.
- Travasarou, T., Bray, J., and Der Kiureghian, A., "A probabilistic methodology for assessing seismic slope displacements," *Proceedings, 13th World Conference on Earthquake Engineering, Vancouver, Canada, August 1-6, 2004 (CD-ROM), 2004, 15 pp.*
- Weiler, W.A. (1988). "Small strain shear modulus of clay". *Earthquake Engineering and Soil Dynamics II – Recent Advances in Ground-Motion Evaluation, Geotechnical Special Publication No. 20, ASCE, p331.*
- Youd, T.L., I. M. Idriss, Ronald D. Andrus, Ignacio Arango, Gonzalo Castro, John T. Christian, Richardo Dobry, W. D. Liam Finn, Leslie F. Harder Jr., Mary Ellen Hynes, Kenji Ishihara, Joseph P. Koester, Sam S. C. Liao, William F. Marcuson III, Geoffrey R. Martin, James K. Mitchell, Yoshiharu Moriwaki, Maurice S. Power, Peter K. Robertson, Raymond B. Seed, and Kenneth H. Stokoe II, 2001. "Liquefaction Resistance of Soils: Summary Report from the 1996 NCEER and 1998 NCEER/NSF Workshops on Evaluation of Liquefaction Resistance of Soils." *Journal of Geotechnical and Geoenvironmental Engineering*, 124(10).

Appendix A: Representative MATLAB Routines

This section presents the MATLAB routines that were used to estimate the probability of exceeding a certain level of residual longitudinal displacement at the abutments due to liquefaction-induced lateral ground displacement, for a given intensity measure of the ground motion.

The main routine is called “master.m.” In that routine the user needs to specify the set of displacement at which the required probability is going to be calculated, and also appropriate input values for the parameters T_s , μ_{Sur} , σ_{Sur} , Sa , and M_w . For the evaluation of the sensitivity parameters it is also necessary to input the standard deviation of the random variables S_{ur} , α , and ε along the diagonal of the diagonal matrix \underline{D} . The main routine then calls the toolbox FERUM with input file “inputfile_*.m,” which in turns makes use of the function “GetD_*.m.” The latter function calculates the amount of lateral displacement for given values of S_{ur} , α , ε , T_s , Sa , and M_w using the expression developed by Bray and Travasarou (2007).

```

%
% Routine master.m
%

close all
clear all
clc

dlist=[0.5 1]; % inches

Ts = 0.14;      % -- LEFT (May17.07)
muSur = 649;    % psf -- LEFT (Jun29.07)
sdSur = 260;    % psf -- LEFT (Jun29.07)

% Ts = 0.16;      % -- RIGHT (May17.07)
% muSur = 512;    % psf -- RIGHT (Jun29.07)
% sdSur = 205;    % psf -- RIGHT (Jun29.07)

% Ts = 0.13;      % -- NoLiq -- LEFT & RIGHT
% muSu = 975;     % psf -- Upper Clay -- LEFT & RIGHT
% sdSu = 244;     % psf -- Upper Clay -- LEFT & RIGHT

% LEFT
%sa = 0.346; Mw = 6.6; % New (9/7/07)
%sa = 0.879; Mw = 6.6;
sa = 1.591; Mw = 6.8;
%sa = 2.333; Mw = 7.0;

% RIGHT
%sa = 0.334; Mw = 6.6; % New (9/7/07)
%sa = 0.869; Mw = 6.6;
%sa = 1.580; Mw = 6.8;
%sa = 2.326; Mw = 7.0;

% NoLiq -- LEFT & RIGHT
%sa = 0.348; Mw = 6.6; % New (9/7/07)
%sa = 0.874; Mw = 6.6;
%sa = 1.579; Mw = 6.8;
%sa = 2.309; Mw = 7.0;

D=zeros(3,3);

%D(1,1)=sdSur; % Liq case
D(1,1)=sdSu; % NonLiq case
D(2,2)=0.86603;
D(3,3)=0.66;

k=1;
for i=1:length(dlist)
    d=dlist(i);
    run inputfile_liqLEFT
%    run inputfile_liqRIGHT
%    run inputfile_noliq
    ferumFORM
    p(k)=formresults.pf1;
    impt_gamma(:,k)=formresults.imptg;
    impt_delta(:,k)=D*formresults.beta_sensi_thetaf(:,1);
    impt_eta(:,k)=D*formresults.beta_sensi_thetaf(:,2);
    k=k+1;
end

```

```

%
% Routine inputfile_liqLEFT.m
%
output_filename = 'outputfile_liqLeft.txt';

probddata.marg(1,:) = [ 2 muSur sdSur muSur 0.0 0.0 0.0 0.0]; % Sur (lognormal)
probddata.marg(2,:) = [ 6 3.5 0.86603 3.5 0.0 0.0 0.0 0.0]; % alpha (uniform)
probddata.marg(3,:) = [ 1 0.00 0.66 0.00 0.0 0.0 0.0 0.0]; % epsilon (normal)

probddata.parameter = distribution_parameter(probddata.marg);

probddata.correlation = [1.0 0.0 0.0;
                        0.0 1.0 0.0;
                        0.0 0.0 1.0];

analysisopt.ig_max = 100; % Maximum number of global iterations allowed in the
search algorithm
analysisopt.il_max = 5; % Maximum number of line iterations allowed in the
search algorithm
analysisopt.e1 = 0.001; % Tolerance on how close design point is to limit-
state surface
analysisopt.e2 = 0.001; % Tolerance on how accurately the gradient points
towards the origin
analysisopt.step_code = 0; % 0: step size by Armijo rule, otherwise: given value
(0 < s <= 1) is the step size.
analysisopt.grad_flag = 'FFD'; % 'DDM': direct differentiaclotion, 'FFD': forward
finite difference

%analysisopt.sim_point = 'origin';
analysisopt.sim_point = 'dspt';
analysisopt.stdv_sim = 1;
analysisopt.num_sim = 10000;
analysisopt.target_cov = 0.05;

femodel = 0;
randomfield = 0;

for i = 1:length(d)
    gfundata(i).evaluator = 'basic';
    gfundata(i).type = 'expression';
    gfundata(i).parameter = 'no';
    gfundata(i).expression = [num2str(d(i)) '-' ...
                             'GetD_Left(x(1),x(2),x(3),' ...
                             num2str(Ts) ',' ...
                             num2str(Mw) ',' ...
                             num2str(sa) ')];
end

system.system=length(d);
system.scis_max = 20000;
system.scis_min = 1000;
system.cov_max = 0.05;

```

```

function [D] = GetD_Left(Sur,alpha,epsilon,Ts,Mw,sa)

% function [D] = GetD_Left(Sur,alpha,epsilon,Ts,Mw,sa)
%
% Input      Sur:      Post-liquefaction undrained shear strength (psf)
%            alpha:    Number of diameters, above and below liquefiable
%                    layer, to points of fixity
%            epsilon:  Error term in Bray an Travasarou (2007)
%            Ts:       Initial fundamental period of the potential
%                    sliding mass
%            Mw:       Moment magnitude
%            Sa:       Spectral acceleration at 1.5Ts
% Output     D:        Residual displacement of abutment in longitudinal
%                    direction (inches)

% Parameters for FPiles (lbf)
Es = 29000000;      % Young's modulus of steel (lbf/in^2)
Ip = 2549;          % Moment of inertia of one pile (in^4)
H = 2.5;            % Thickness of liquefiable layer (feet) -- LEFT
N = 6;              % Number of Piles
My = 1381;          % Plastic moment of one pile (kips*ft)
R = 1;              % Radius of one pile (feet)

% Parameters for FPassive (lbf)
g_abut = 4;         % inches (10 cm)
k_abut = 21.8;      % kips/in/ft
p_abut = 32.7;      % kips/ft
W = 43;             % Width of back wall (feet)

% Other parameters
A = 55*71;          % Base area of potential failure surface (ft^2) -- LEFT

% Calculations
syms d real

assignin('base','H',H); assignin('base','alpha',alpha); assignin('base','R',R);
assignin('base','N',N); assignin('base','Es',Es); assignin('base','Ip',Ip);
assignin('base','My',My);
FPiles = subs('GetFPilesSmooth(0.5*d,H,alpha,R,N,Es,Ip,My)');      % lbf
FPiles = vpa(FPiles);

assignin('base','g_abut',g_abut); assignin('base','k_abut',k_abut);
assignin('base','p_abut',p_abut); assignin('base','W',W);
FPassive = subs('GetFPassiveSmooth(0.5*d,g_abut,k_abut,p_abut,W)'); % lbf
FPassive = vpa(FPassive);

assignin('base','Sur',Sur); assignin('base','FPiles',FPiles);
assignin('base','FPassive',FPassive); assignin('base','A',A);
S = subs('Sur + (FPiles + FPassive)/A'); S = vpa(S); % psf

ky = GetKySmooth(S,'1'); % ky(S) -- LEFT

% From Bray and Travasarou (2007)
eqn = log(d) - ( -1.10 - 2.83*log(ky) - 0.333*(log(ky)).^2 + ...
    0.566*log(ky)*log(sa) + 3.04*log(sa) - 0.244*(log(sa))^2 + ...
    1.50*Ts + 0.278*(Mw-7) + epsilon );
eqn = char(vpa(eqn)); % char() is required for Matlab 7

if feval(inline(eqn),1)<0
    dsol = fzero(inline(eqn),[1 1e6]); % cm
    dsol = dsol/2.54; % inches
else
    dsol = 1/2.54; % inches
end

D = dsol;

```

```

function [F] = GetFPilesSmooth(d,H,alpha,R,N,Es,Ip,My)
% function [F] = GetFPilesSmooth(d,H,alpha,R,N,Es,Ip,My)
%
% Input      d:      Displacement (inches)
%
% Parameteres H:      Thickness of liquefiable layer (feet)
%             alpha:  Number of diameters, above and below liquefiable
%                   layer, to points of fixity
%             R:      Radius of one pile (feet)
%             N:      Number of piles
%             Es:     Young's modulus of steel (lbf/in^2)
%             Ip:     Moment of inertia of one pile (in^4)
%             My:     Plastic moment of one pile (kips*ft)
%
% Ouput      F:      Total shear force in piles system (lbf)

ft2in = 12;
kips2lbf = 1000;

L = H + 2*(alpha*2*R); % feet
L = L*ft2in;          % inches
My = My*kips2lbf*ft2in; % lbf*in
Vy = (2*My/L)*N;     % lbf
dy = My*L^2/(6*Es*Ip); % inches

b = 0;
RR = 10;

deq = d/dy;

Feq = b*deq + (1-b)*deq./((1+deq.^RR).^ (1/RR));
F = Feq*Vy;

return

```

```

function [F] = GetFPassiveSmooth(d,g_abut,k_abut,p_abut,W)
% function [F] = GetFPassiveSmooth(d,g_abut,k_abut,p_abut,W)
%
% Input      d:      Displacement (inches)
%
% Parameteres  g_abut: Abutment gap (inches) -- Caltrans units
%              k_abut: Abutment linear stiffness (kips/in/foot)
%                  Caltrans units
%              p_abut: Abutment total passive capacity (kips/foot)
%                  Caltrans units
%              W:      Width of back wall (feet)
%
% Output      F:      Passive reaction at the abutment (lbf)

RR = 10;

dy = 0.5*p_abut/k_abut; % inches
Vy = p_abut*1000*W/2; % lbf

deq = (d-g_abut-dy)/dy;

% b=0
Feq = 1 + deq./((1+deq.^RR).^ (1/RR));
F = Feq*Vy;

return

```

```

function [ky] = GetKySmooth(S,side)

% function [ky] = GetKySmooth(S,side)
%
% Input          S:      Total equivalente shear strength of liquefiable layer %
                  (includes passive reaction,piles reaction)
                  (psf)
%               side:  'l' or 'r' (left or right)
%
% Ouput          ky:      Yield coefficient

RR = 200;

if side == 'l'
    Sy = 0.5*50000;      % psf
    kys = 0.0004*Sy;    % --
    Sys = 0.0895/0.0004; % psf
    Seq = (S-Sys-Sy)/Sy;
    % b=0
    kyeq = 1 + Seq./((1+Seq.^RR).^(1/RR));
    ky = kyeq*kys;
elseif side == 'r'
    Sy = 0.5*50000;      % psf
    kys = 0.0004*Sy;    % --
    Sys = 0.1132/0.0004; % psf
    Seq = (S-Sys-Sy)/Sy;
    % b=0
    kyeq = 1 + Seq./((1+Seq.^RR).^(1/RR));
    ky = kyeq*kys;
elseif side == 'nl'    % No Liquefaction Case - LEFT & RIGHT
    Sy = 0.5*50000;      % psf
    kys = 0.0004*Sy;    % --
    Sys = 0.1473/0.0004; % psf
    Seq = (S-Sys-Sy)/Sy;
    % b=0
    kyeq = 1 + Seq./((1+Seq.^RR).^(1/RR));
    ky = kyeq*kys;
end

```

Appendix B: Pile Design

This section presents the design of the piles under the abutments and piers of the example described in Chapter 6.

PEER Bridge Piles Design Report

Christian A. Ledezma Jonathan D. Bray

April 27, 2006

1 Design Loads

The design loads for the piles system are a function of the characteristics of the bridge pier that it supports. In this report, the case of *Bridge Type 1* (height=22 feet) and *Column Type A* (i.e. a circular reinforced concrete column with a diameter of 4 feet and 2% of steel reinforcement) will be analyzed. The loads in this case are (Ketchum, 2004)

$$\begin{aligned}P_{DL} &= 1796 \text{ kips} \\P_{LL} &= 418 \text{ kips} \\M_p &= 5674 \text{ kips ft} \Rightarrow M_o = 1.2M_p = 6809 \text{ kips ft} \\V_p &= 516 \text{ kips} \Rightarrow V_o = 1.2V_p = 619 \text{ kips}\end{aligned}$$

where P_{DL} and P_{LL} correspond, respectively, to the dead and live axial loads at the bottom of each pier section, M_p is the plastic moment of the pier based on the average of the axial dead and earthquake loads, V_p is the shear force associated with M_p , and M_o and V_o are the overstrength moment and shear capacities of each pier, respectively.

2 Subsurface Characterization

Figure 1 shows the soil properties that will be considered.

3 Foundation Type

A group of 3×2 circular open-ended steel piles (PP 24×0.5 , $f_y = 60$ ksi), with a center-to-center spacing of 6 ft and a length of 60 ft, have been pre-selected for design. The dimensions and properties of each pile are (Coduto, 2001):

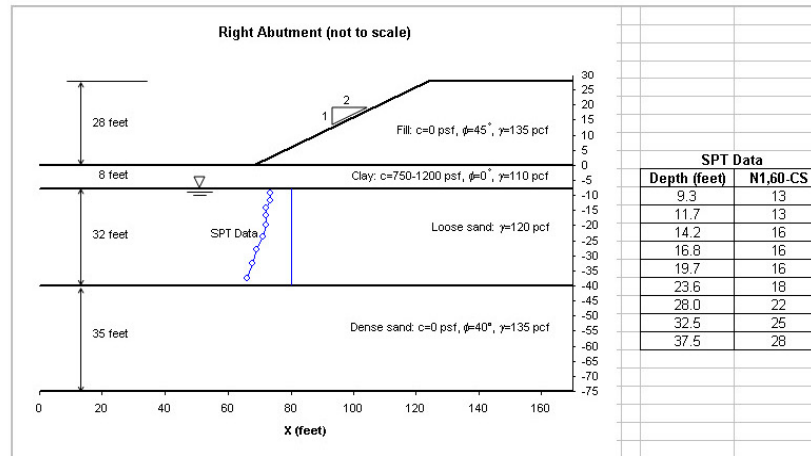


Figure 1: Soil profile at the right abutment

External diameter: $D = 24$ in
 Thickness: $t = 0.5$ in
 Area: $A = 36.91$ in²
 Moment of inertia: $I = 2549$ in⁴
 Section modulus $S = 212.4$ in³
 Weight $w = 126$ lbf/ft

4 Axial Loads

4.1 Structural Capacity

The axial load in a pile should not exceed the factored axial structural capacity (Barker et al., 1991), i.e.

$$r\phi_a P_n \geq \gamma_D P_D + \gamma_L P_L$$

For steel pipes the eccentricity factor is $r = 0.87$ and the performance factor is $\phi_a = 0.85$, the nominal structural capacity of the pile is $P_n = f_y A_y = 60 \text{ ksi} \times 36.91 \text{ in}^2 = 2214.6 \text{ kips}$, the load factors are $\gamma_D = 1.3 \times 1.0 = 1.30$ and $\gamma_L = 1.3 \times 2.2 = 2.86$, and the axial loads are $P_D = P_{DL}/6 = 1796 \text{ kips}/6 = 299.3 \text{ kips}$ and $P_L = P_{LL}/6 = 418 \text{ kips}/6 = 69.7 \text{ kips}$, then

$$\begin{aligned} 0.87 \times 0.85 \times 2214.6 \text{ kips} &\geq 1.30 \times 299.3 \text{ kips} + 2.86 \times 69.7 \text{ kips} \\ 1637.7 \text{ kips} &\geq 588.4 \text{ kips} \end{aligned}$$

which implies that the structural axial capacity is appropriate.

4.2 Soil Capacity

The ultimate bearing capacity of a pile is the sum of the skin and point resistances minus the weight of the pile

$$Q_{ult} = Q_s + Q_p - W$$

The tip resistance can be estimated as

$$Q_p = A_p q_p$$

Since the penetration-to-diameter ratio is $60/2 = 30$, the soil plug may be considered rigidly embedded (Paikowsky and Whitman, 1990) which means that $A_p = \pi 2^2/4 = 3.14 \text{ ft}^2$.

In cohesionless soils, like sand, the drained ultimate tip resistance may be approximated as (Kulhawy et al., 1983)

$$q_p = \sigma'_v N_q s_q d_q r_q$$

where the term $N_q s_q d_q r_q$ can be estimated from the friction angle, $\phi' = 40^\circ$, and the rigidity index I_r , where for dense sands (Kulhawy et al., 1983)

$$I_r \approx \frac{110}{(\sigma'_v)^{0.5} \tan \phi'}$$

with σ'_v is in tsf. At the bottom of the pile we have that

$$\sigma'_v = 110 \times 8 + 120 \times 32 + 135 \times 20 - 62.428 \times (32 + 20)$$

$$\sigma'_v = 4173.7 \text{ psf} \Rightarrow \sigma'_v = 2.09 \text{ tsf}$$

$$\Rightarrow I_r \approx \frac{110}{(2.09)^{0.5} \tan 40^\circ} = 90.7$$

For $\phi' = 40^\circ$ and $I_r = 90.7$, $N_q s_q d_q r_q \approx 94$, then $q_p = \sigma'_v N_q s_q d_q r_q = 4173.7 \text{ psf} \times 94 = 392.3 \text{ ksf}$ and

$$Q_p = 3.14 \text{ ft}^2 \times 392.3 \text{ ksf} = 1231.8 \text{ kips}$$

The ultimate load carried by the pile shaft is

$$Q_s = A_s q_s$$

The surface area of the pile shaft is $A_s = \pi \times 2 \times 60 = 376.99 \text{ ft}^2$. The skin friction of piles in cohesionless soils can be estimated using the following equation (Meyerhof, 1976)

$$q_s = \frac{\bar{N}}{50} \text{ in tsf}$$

The weighted average of the uncorrected SPT blow counts along the pile shaft is¹ $\bar{N} \approx 17.1$, then $q_s \approx 0.34 \text{ tsf} = 680 \text{ psf}$, and

$$Q_s = 376.99 \text{ ft}^2 \times 680 \text{ psf} = 256.4 \text{ kips}$$

The weight of the pile W is (neglecting the weight of the soil plug)

$$\begin{aligned} W &= 126 \frac{\text{lb}}{\text{ft}} \times 60 \text{ ft} \\ W &= 7.6 \text{ kips} \end{aligned}$$

Then, the ultimate bearing capacity of one pile is

$$\begin{aligned} Q_{ult} &= 256.4 \text{ kips} + 1231.8 \text{ kips} - 7.6 \text{ kips} \\ Q_{ult} &= 1480.6 \text{ kips} \end{aligned}$$

What needs to be verified is that

$$\phi_q Q_{ult} \geq \gamma_D P_D + \gamma_L P_L$$

where, for the methods that were used to estimate q_s and q_p , the performance factor is $\phi_q = 0.45$, then

$$\begin{aligned} 0.45 \times 1480.6 \text{ kips} &\geq 588.4 \text{ kips} \\ 666.3 \text{ kips} &\geq 588.4 \text{ kips} \end{aligned}$$

which shows that the soil capacity for axial loads is appropriate. The ultimate bearing capacity of the group is also appropriate since, in the case of sands, the group capacity can be estimated by adding the capacities of all the piles in the group and conservatively considering a group efficiency of one.

5 Settlement

The settlement ρ can be estimated as (Meyerhof, 1976)

$$\rho = \frac{2q\sqrt{XI}}{N_{corr}}$$

where ρ is in inches, q is the net foundation pressure (in tsf) applied at $2D_b/3$, X is the width of pile group (in ft), and I is the influence factor of the effective group embedment.

¹Since in this last version of the soil profile the blow counts are higher than in the original profile, this value of \bar{N} is now a bit conservative. However, since this is an end-bearing pile, this change has a very small effect in the end result.

The depth of embedment in the dense sand is $D_b = 20 \text{ ft} \Rightarrow \frac{2D_b}{3} = 13.3 \text{ ft}$,
 $X = 8 \text{ ft}$, and

$$\begin{aligned} q &= \frac{P_D + P_L}{8 \times 14} \\ &= \frac{(1796 + 418) \times 1000 \text{ lbf}}{8 \times 14 \text{ ft}^2} \\ &= 19768 \text{ psf} \\ \Rightarrow q &= 9.88 \text{ tsf} \end{aligned}$$

also

$$I = 1 - \frac{D'}{8X} = 1 - \frac{13.3}{8 \times 8} = 0.79 \geq 0.5$$

and, since $\phi' = 40^\circ \Rightarrow N \approx 30$, and

$$\begin{aligned} \sigma'_v &\approx 110 \times 8 + 120 \times 32 + 135 \times (13.3 + 0.5 \times (35 - 13.3)) \\ &\quad - 62.428 \times (32 + 13.3 + 0.5 \times (35 - 13.3)) \\ \sigma'_v &\approx 4474.9 \text{ psf} = 2.24 \text{ tsf} \end{aligned}$$

then

$$\begin{aligned} N_{corr} &= (0.77 \log_{10} (20/\sigma'_v)) N \\ &= (0.77 \log_{10} (20/2.24)) 30 \\ \Rightarrow N_{corr} &= 22.0 \end{aligned}$$

and

$$\begin{aligned} \rho &= \frac{2q\sqrt{XI}}{N_{corr}} = \frac{2 \times 9.88\sqrt{8} \times 0.79}{22.0} \\ \Rightarrow \rho &= 2.0 \text{ in} \end{aligned}$$

The typical allowable total settlement for bridges is 2 in (Coduto, 2001).

6 Lateral Deformations

6.1 Single Pile Deflection

The Evans and Duncan (1982) procedure will be used.

First, we need to determine the characteristic load P_c which in the case of sands is

$$P_c = 1.57D^2 (E_p R_I) (\gamma' D \phi' K_p / (E_p R_I))^{0.57}$$

where

$$\begin{aligned}
D &= \text{Diameter of Pile} = 2 \text{ ft} = 24 \text{ in} \\
E_p &= \text{Young's modulus of steel} = 29000000 \text{ lbf/in}^2 \\
I_p &= \text{Moment of inertia of pile} = 2549 \text{ in}^4 \\
I_{solid} &= \frac{\pi D^4}{64} = 16286 \text{ in}^4 \\
R_I &= \text{Moment of inertia ratio} = \frac{I_p}{I_{solid}} = 0.16 \\
\gamma' &\approx 120 - 62.428 = 57.6 \text{ pcf} = 0.0333 \text{ lbf/in}^3 \\
\phi' &\approx 35^\circ \text{ (since } N_{ave} \approx 10 \text{ in the zone of interest)} \\
K_p &= \tan^2(45^\circ + \phi'/2) = 3.69
\end{aligned}$$

then

$$\begin{aligned}
P_c &= 1.57 \times 24^2 (29000000 \times 0.16) \times (0.0333 \times 24 \times 35 \times 3.69 / (29000000 \times 0.16))^{\frac{1}{2}} \\
P_c &= 9348938.5 \text{ lbf} = 9349 \text{ kips}
\end{aligned}$$

Then, we need to calculate the load ratio P_{sp}/P_c , where P_{sp} is the unfactored lateral load. The ultimate lateral load is $V_o = 1.2V_p = 619$ kips. Let us *assume* that the the unfactored total lateral load is $619 \text{ kips} / 3 = 206.3$ kips, then, in average, each pile experiments an unfactored lateral load of $P_{sp} \approx 206.3 \text{ kips} / 6 = 34.4$ kips. The load ratio is then $P_{sp}/P_c = 0.00368$.

Since $P_{sp}/P_c = 0.00368$, the Y_{sp}/D ratio is about 0.0063, then the single pile deflection is $Y_{sp} \approx 0.0063 \times 24 = 0.2$ in.

6.2 Pile Group Deflection

The lateral deflection of a group of piles can be estimated using the empirical equation (Barker et al., 1991)

$$Y_g = \frac{A + N_{pile}}{B \sqrt{\frac{S}{D} + \frac{P_{sp}}{C P_N}}} Y_{sp}$$

where

$$\begin{aligned}
A &= 9 \text{ for sand} \\
N_{pile} &= \text{Number of piles in group} = 6 \\
B &= 3 \text{ for sand} \\
S &= \text{Average spacing of piles} = 6 \text{ ft} \\
D &= \text{Pile Diameter} = 2 \text{ ft} \\
P_{sp} &\approx 34.4 \text{ kips (from previous sub-section)} \\
C &= 16 \text{ for sand} \\
P_N &= K_p \gamma D^3 = 3.69 \times 120 \times 2^3 = 3.5 \text{ kips}
\end{aligned}$$

then

$$\begin{aligned}
 Y_g &= \frac{9 + 6}{3\sqrt{\frac{6}{2} + \frac{34.4}{16 \times 3.5}}} Y_{sp} \\
 &= 2.63 Y_{sp} \\
 Y_g &\approx 0.5 \text{ in}
 \end{aligned}$$

Coduto (2001) indicates that

Building, bridges, and other similar structures typically tolerate no more than 5 to 20 mm (0.25 in to 0.75 in) of lateral deflection in the foundation.

7 Combined Axial Loads and Bending Moments

From the previous section we know that $P_c = 9349$ kips. The factored lateral load per pile is $\gamma_h P_{sp} = 1.3 P_{sp} = 1.3 \times 34.4$ kips = 44.7 kips, then $(\gamma_h P_{sp}) / P_c = 0.005 \Rightarrow M_{sp} / M_c \approx 0.003$.

For sands, the characteristic moment M_c is defined as

$$M_c = 1.33 D^3 (E_p R_I) (\gamma' D \phi' K_p / (E_p R_I))^{0.4}$$

then

$$\begin{aligned}
 M_c &= 1.33 \times 24^3 (29000000 \times 0.16) (0.0333 \times 24 \times 35 \times 3.69 / (29000000 \times 0.16)) \\
 &= 1.175 \times 10^9 \text{ lbf in} \\
 \Rightarrow M_c &= 97917 \text{ kips ft}
 \end{aligned}$$

and the bending moment in a single pile is $M_{sp} \approx 0.003 \times 97917$ kips ft $\Rightarrow M_{sp} = 293.8$ kips ft.

The maximum bending moment in a pile within a pile group M_g can be estimated as (Barker et al., 1991)

$$M_g = \left(\frac{Y_g}{Y_{sp}} \right)^n M_{sp}$$

The Y_g / Y_{sp} ratio is 2.63 and, for sands

$$n = \frac{\gamma_h P_{sp}}{300 P_N} + 0.3 = \frac{44.7 \text{ kips}}{300 \times 3.5 \text{ kips}} + 0.3 \approx 0.34$$

then

$$\begin{aligned}
 M_g &= 2.63^{0.34} M_{sp} \\
 &= 1.39 M_{sp} \\
 \Rightarrow M_g &= 408 \text{ kips ft}
 \end{aligned}$$

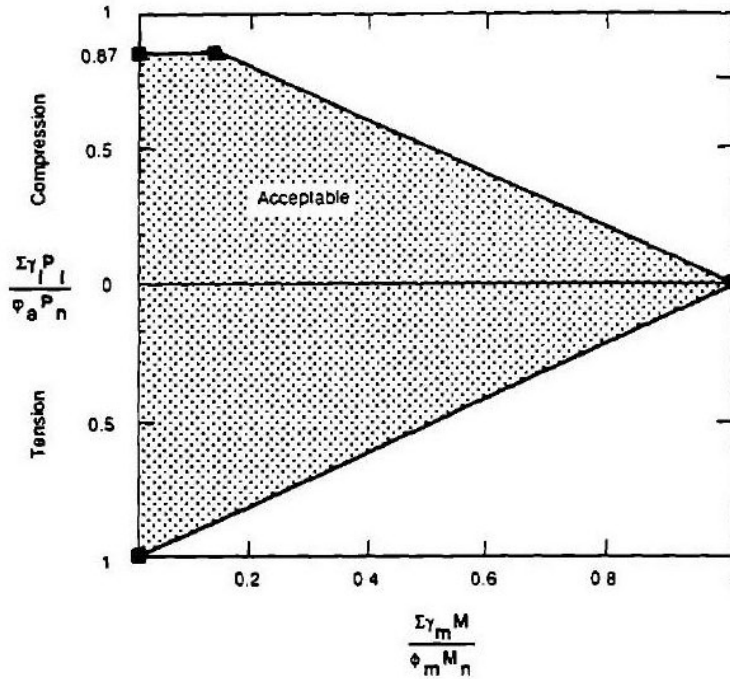


Figure 2: Normalized load-moment interaction curve for steel pipe piles (after Barker et al., 1991)

The normalized load-moment interaction curves shown in Figure 2 will be used to check the structural adequacy of the piles.

Let us *assume* that the unfactored flexural moment is $M_o/3 = 6809 \text{ kips ft} / 3 = 2270 \text{ kips ft}$. Then, the maximum axial load per pile due to the earthquake load is $P_{EQ} = 2270 \text{ kips ft} / 12 \text{ ft} / 2 = 95 \text{ kips}$. The combined axial load per pile is $1.3 (P_D + P_{EQ}) = 1.3 (1796/6 + 95) = 513 \text{ kips}$. On the other hand, the nominal axial structural capacity of the pile is $P_n = 2214.6 \text{ kips}$, and the performance factor for P_n is $\phi_a = 0.85$. Then $\phi_a P_n = 1882 \text{ kips}$.

The factored design bending moment is $\gamma_m M = 1.3 \times 408 \text{ kips ft} = 530 \text{ kips ft}$. The nominal structural moment capacity of the pile is $M_n = f_y Z_p$, where Z_p is the plastic section modulus ($Z_p = 276.2 \text{ in}^3$), then $M_n = 60 \text{ ksi} \times 276.2 \text{ in}^3 = 16572 \text{ kips in} = 1381 \text{ kips ft}$. The performance factor for M_n is $\phi_m = 0.9$. Then $\phi_m M_n = 1243 \text{ kips ft}$.

The ratios $\sum \gamma_i P_i / \phi_a P_n$ and $\sum \gamma_m M / \phi_m M_n$ are $513 / 1882 = 0.27$ and $530 / 1243 = 0.43$, respectively. The point at the coordinate values $(0.27 \quad 0.43)$ falls *inside* the acceptable range on the normalized load-moment interaction diagram, which means that the pile is adequate.

References

- [1] Barker, R. M., Duncan, J. M., Rojiani, K. B., Ooi, P. S. K., Tan, C. K. and Kim, S. G., "Manuals for Design of Bridge Foundations", NCHRP Report 343, Transportation Research Board, Washington, 1991.
- [2] Coduto, D., "Foundation Design, Principles and Practices", Second Edition, 2001.
- [3] Evans Jr., L.T., and Duncan, J.M., "Simplified Analysis of Laterally Loaded Piles", UC Berkeley Rept. No. UCB/GT/82-04, July, 1982, 245 pp.
- [4] Ketchum, M. et al., "Influence of Design Ground Motion Level on Highway Bridge Costs", November, 2004.
- [5] Kulhawy, F. H., Trautmann, C. H., Beech, J. F., O'Rourke, T. D., and McGuire, W., "Transmission Line Structure Foundations for Uplift-Compression Loading." EPRI Rept. EL-2870, Electric Power Research Institute, 1983.
- [6] Meyerhof, G.G., "Bearing Capacity and Settlement of Pile Foundations", ASCE JGED, Vol. 102, No. GT3, March 1976, pp 196-228.
- [7] Paikowsky, S.G., and Whitman, R.V., "The Effects of Plugging on Pile Performance and Design", Canadian Geotechnical Journal, Vol. 27, pp 429-440.

PEER Bridge

Design of Piles Under the Abutment

Christian A. Ledezma Jonathan D. Bray

May 3, 2006

Remark 1 *In the design of the piles under the abutment, some of the results from the design of the piles under the piers were used.*

1 Subsurface Characterizations

Figure 1 shows the soil properties that will be considered.

2 Abutment Details

Figures 2 and 3 show the dimensions of the abutment. Please note that the piles will be designed considering only *one row* of them.

3 Foundation Type

One row of open-ended steel piles (PP 24 × 0.5, $f_y = 60$ ksi), with a length of 70 ft, will be considered for design. The dimensions and properties of each pile are:

External diameter:	$D = 24$ in
Thickness:	$t = 0.5$ in
Area:	$A = 36.91$ in ²
Moment of inertia:	$I = 2549$ in ⁴
Section modulus	$S = 212.4$ in ³
Weight	$w = 126$ lbf/ft

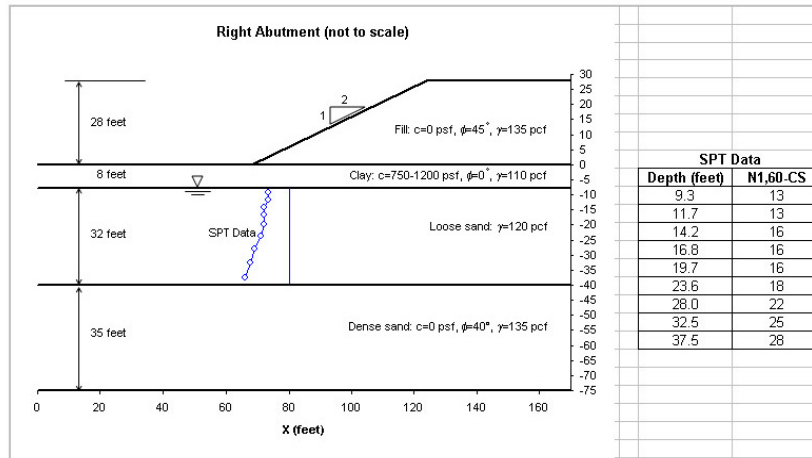


Figure 1: Soil Profile at the Right Abutment

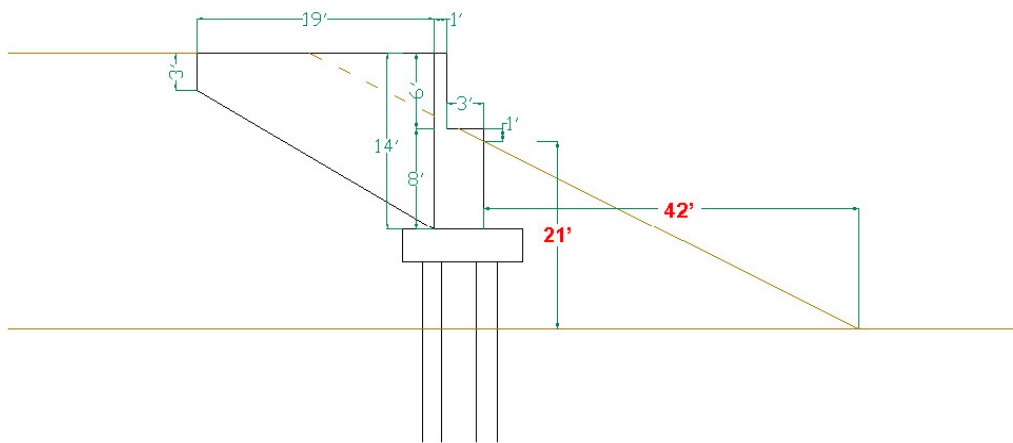


Figure 2: Abutment-Side View

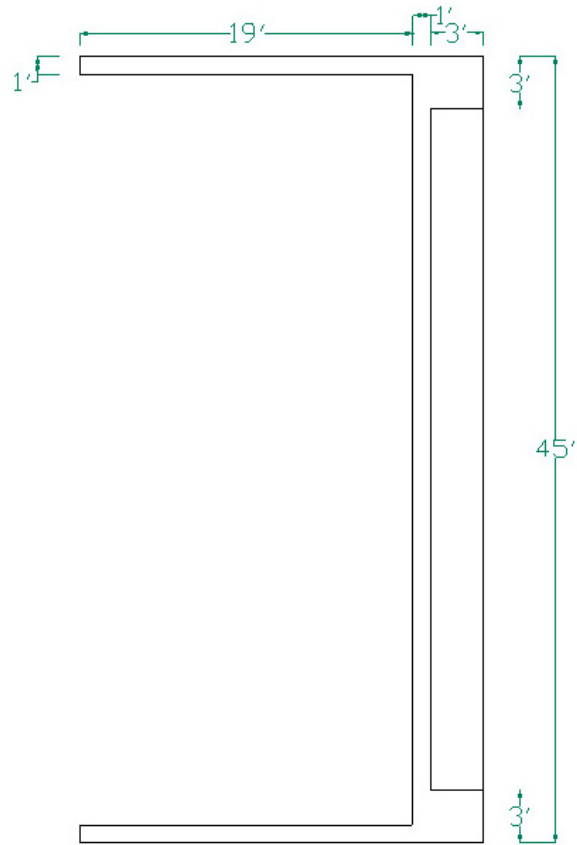


Figure 3: Abutment-Plan View

4 Design Loads

4.1 Loads from the superstructure

The vertical loads at the abutment P_{abutment} can be estimated as

$$P_{\text{abutment}} = P_{\text{column}} \frac{L_2}{L_1 + L_2}$$

where P_{column} is the vertical load acting on any column, L_1 is the horizontal distance between columns, and L_2 is the horizontal distance between the center of the last column and the abutment. In our case $P_{\text{column}} = P_{DL}$ or P_{LL} and $L_1 = 150$ ft and $L_2 \approx 120$ ft, then the vertical dead and live loads at the abutment are

$$\begin{aligned} P_{DL} &= 1796 \text{ kips} \frac{120}{150 + 120} = 798 \text{ kips} \\ P_{LL} &= 418 \text{ kips} \frac{120}{150 + 120} = 186 \text{ kips} \end{aligned}$$

4.2 Loads from earth pressures

If the thickness of the footing is assumed to be $T = 3$ ft, the earth pressure will act over a height $H = 14 + 3 = 17$ ft. The earth pressure must be investigated for 75% of the active earth pressure (i.e., $K_a = 0.75 \times 0.3 = 0.225$) (Caltrans, 1988). The lateral force is $p_a = \frac{1}{2} K_a \gamma H^2 = \frac{1}{2} \times 0.225 \times 135 \times 17^2 = 4.4 \frac{\text{kips}}{\text{ft}}$. Since the width is 45 ft, then the total lateral force is $P_a = 4.4 \times 45 = 198$ kips. This lateral force will induce a moment of $M = 198 \text{ kips} \times \frac{1}{3} \times 17 \text{ ft} = 1122 \text{ kips ft}$ (clockwise).

4.3 Dead load from abutment structure

Assuming a unit weight for the concrete of $\gamma_c = 155$ pcf, the loads coming from the weight of the concrete structure at the abutment, and the weight of the blocks of soils that are supported by the pile cap, are

$$\begin{aligned} P &= 698 \text{ kips} \\ M &= -862 \text{ kips ft (counterclockwise)} \end{aligned}$$

5 Design

Let N be the number of required piles.

5.1 Axial Loads

Structural Capacity

The requirement is (Barker et al., 1991)

$$r\phi_a P_n \geq \gamma_D P_D + \gamma_L P_L$$

In our case $P_D = 798 + 698 = 1496$ kips, $P_L = 186$ kips, then

$$\begin{aligned} 0.87 \times 0.85 \times 2214.6 \text{ kips} &\geq \frac{1.30 \times 1496 \text{ kips} + 2.86 \times 186 \text{ kips}}{N} \\ N &\geq \frac{2477 \text{ kips}}{1638 \text{ kips}} = 1.5 \\ \Rightarrow N &\geq 2 \end{aligned} \quad (1)$$

Soil Capacity

The requirement is ¹ (Barker et al., 1991)

$$\begin{aligned} \phi_q Q_{ult} &\geq \gamma_D P_D + \gamma_L P_L \\ 0.45 \times 1480.6 \text{ kips} &\geq \frac{1.30 \times 1496 \text{ kips} + 2.86 \times 186 \text{ kips}}{N} \\ N &\geq \frac{2477 \text{ kips}}{666 \text{ kips}} = 3.7 \\ \Rightarrow N &\geq 4 \end{aligned} \quad (2)$$

5.2 Settlement

The requirement is (Barker et al., 1991, Shantz, T., 2006)

$$\rho = \frac{2q\sqrt{X}I}{N_{corr}} \leq 0.5 \text{ in}$$

If the center-to-center spacing between piles is $3D = 6$ ft, then

$$\begin{aligned} q &= \frac{(798 + 186) \times 1000}{2 \times (2N + 4(N - 1))} \frac{1}{2000} = \frac{492}{12N - 8} \text{ tsf}, \text{ and} \\ X &= 2 \text{ ft} \\ I &= 1 - \frac{D'}{8X} = 1 - \frac{13.3}{8 \times 2} = 0.17 \geq 0.5 \Rightarrow I = 0.5 \\ N_{corr} &= 22 \end{aligned}$$

¹This value of Q_{ult} comes from the piles under the columns of the bridge. Since this is an end-bearing pile, and the tip resistance of all piles is the same, this value of Q_{ult} is a bit conservative.

then

$$\begin{aligned} \frac{2 \frac{492}{(12N-8)} \sqrt{20.5}}{22} &\leq 0.5 \\ N &\geq 5.9 \\ \Rightarrow N &\geq 6 \end{aligned} \tag{3}$$

From equations (1), (2), and (3), the required number of piles is $N = 6$. This is the number of piles that will be assumed for the remaining sections of this report.

5.3 Lateral Deformations

The manual by Barker et al. (1991) was used for this section.

Single pile deflection

Since $P_c = 9349$ kips, and $P_{sp} = 198/N = 198/6 = 33$ kips, then $P_{sp}/P_c = 0.0035 \Rightarrow Y_{sp}/D \approx 0.006 \Rightarrow Y_{sp} \approx 0.14$ in.

Pile group deflection

The lateral deflection of the group of piles can be estimated using the empirical equation

$$Y_g = \frac{A + N_{pile}}{B \sqrt{\frac{S}{D} + \frac{P_{sp}}{C P_N}}} Y_{sp}$$

where

$$\begin{aligned} A &= 9 \text{ for sand} \\ N_{pile} &= \text{Number of piles in group} = 6 \\ B &= 3 \text{ for sand} \\ S &= \text{Average spacing of piles} = 6 \text{ ft} \\ D &= \text{Pile Diameter} = 2 \text{ ft} \\ P_{sp} &\approx 33 \text{ kips (from previous sub-section)} \\ C &= 16 \text{ for sand} \\ P_N &= K_p \gamma D^3 = 3.69 \times 120 \times 2^3 = 3.5 \text{ kips} \end{aligned}$$

then

$$\begin{aligned}
Y_g &= \frac{9 + 6}{3\sqrt{\frac{6}{2} + \frac{33}{16 \times 3.5}}} Y_{sp} \\
&= 2.64 Y_{sp} \\
Y_g &\approx 0.4 \text{ in}
\end{aligned}$$

Please note that in this estimation it has been assumed that the bridge deck does not contribute to control the lateral deformation of the abutment. Also, Coduto (2001) indicates that

Building, bridges, and other similar structures typically tolerate no more than 5 to 20 mm (0.25 in to 0.75 in) of lateral deflection in the foundation.

5.4 Combined Axial Loads and Bending Moments

We know that $P_c = 9349$ kips. The factored lateral load per pile is $\gamma_h P_{sp} = 1.3 P_{sp} = 1.3 \times 33$ kips = 42.9 kips, then $(\gamma_h P_{sp})/P_c = 0.0046 \Rightarrow M_{sp}/M_c \approx 0.0026$.

Since $M_c = 97917$ kips ft the bending moment in a single pile due to the shear force is $M_{sp} \approx 0.0026 \times 97917$ kips ft $\Rightarrow M_{sp} = 254.6$ kips ft. Additionally, the loads from the earth pressures, and the dead loads from the abutment structure, apply a bending moment of $(1122$ kips ft -862 kips ft) $/6 = 43.3$ kips ft. Then, the total factored bending moment in a single pile is $M_{sp} = 254.6 + 1.3 \times 43.3 = 311$ kips ft.

The maximum bending moment in a pile within a pile group M_g can be estimated as (Barker et al., 1991)

$$M_g = \left(\frac{Y_g}{Y_{sp}} \right)^n M_{sp}$$

The Y_g/Y_{sp} ratio is 2.64 and, for sands

$$n = \frac{\gamma_h P_{sp}}{300 P_N} + 0.3 = \frac{42.9 \text{ kips}}{300 \times 3.5 \text{ kips}} + 0.3 \approx 0.34$$

then

$$\begin{aligned}
M_g &= 2.64^{0.34} M_{sp} \\
&= 1.39 M_{sp} \\
\Rightarrow M_g &= 432 \text{ kips ft}
\end{aligned}$$

The normalized load-moment interaction curves shown in Figure 4 will be used to check the structural adequacy of the piles.

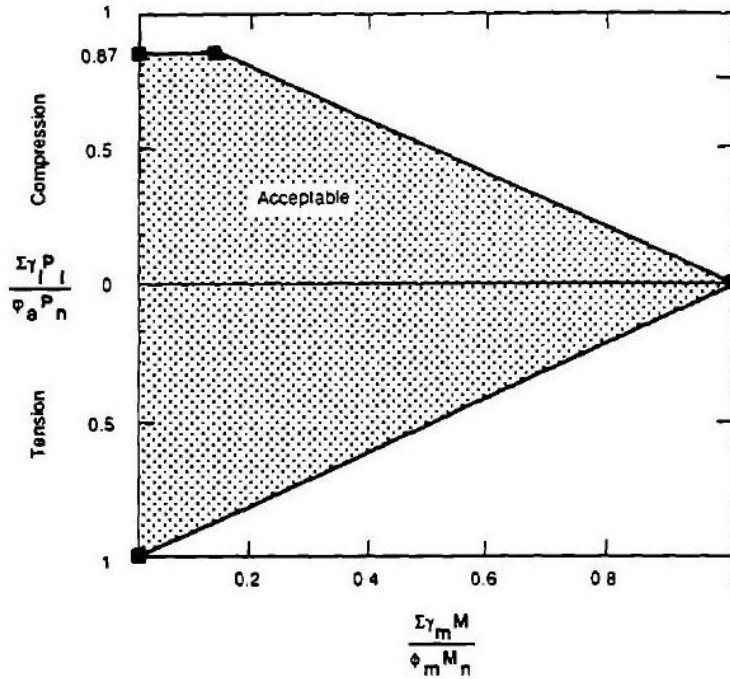


Figure 4: Normalized load-moment interaction curve for steel pipe piles (after Barker et al., 1991)

The combined axial load per pile is $(1.30 \times 1496 \text{ kips} + 2.86 \times 186 \text{ kips}) \div N = 413 \text{ kips}$. On the other hand, the nominal axial structural capacity of the pile is $P_n = 2214.6 \text{ kips}$, and the performance factor for P_n is $\phi_a = 0.85$. Then $\phi_a P_n = 1882 \text{ kips}$.

The factored design bending moment is 432 kips ft. The nominal structural moment capacity of the pile is $M_n = f_y Z_p$, where Z_p is the plastic section modulus ($Z_p = 276.2 \text{ in}^3$), then $M_n = 60 \text{ ksi} \times 276.2 \text{ in}^3 = 16572 \text{ kips in} = 1381 \text{ kips ft}$. The performance factor for M_n is $\phi_m = 0.9$. Then $\phi_m M_n = 1243 \text{ kips ft}$.

The ratios $\sum \gamma_i P_i / \phi_a P_n$ and $\sum \gamma_m M / \phi_m M_n$ are $413 / 1882 = 0.22$ and $432 / 1243 = 0.35$, respectively. The point at the coordinate values $(0.22 \quad 0.35)$ falls *inside* the acceptable range on the normalized load-moment interaction diagram, which means that the pile is adequate.

6 Summary

Under the abutment, one row of *six* open-ended steel piles (PP 24×0.5 , $f_y = 60 \text{ ksi}$), with a length of 70 ft, and with a center-to-center spacing of 6 ft is required. However, the total width of the abutment in plan view is 45 ft, and

six piles installed at the required spacing of 6 ft will only span a distance of 32 ft. Hence, in the final design, the pile spacing is increased to 8 ft so that the pile foundation now spans a distance of 42 ft under the abutment.

References

- [1] Barker, R. M., Duncan, J. M., Rojiani, K. B., Ooi, P. S. K., Tan, C. K. and Kim, S. G., "Manuals for Design of Bridge Foundations", NCHRP Report 343, Transportation Research Board, Washington, 1991.
- [2] Caltrans-Bridge Design Aids: Abutment Investigation. January 1988.
- [3] Caltrans-Bridge Design Practice. Section 5: Substructure & Retaining Walls. January 1982.
- [4] Coduto, D., "Foundation Design, Principles and Practices", Second Edition, 2001.
- [5] Evans Jr., L.T., and Duncan, J.M., "Simplified Analysis of Laterally Loaded Piles", UC Berkeley Rept. No. UCB/GT/82-04, July, 1982, 245 pp.
- [6] Ketchum, M. et al., "Influence of Design Ground Motion Level on Highway Bridge Costs", November, 2004.
- [7] Kulhawy, F. H., Trautmann, C. H., Beech, J. F., O'Rourke, T. D., and McGuire, W., "Transmission Line Structure Foundations for Uplift-Compression Loading." EPRI Rept. EL-2870, Electric Power Research Institute, 1983.
- [8] Meyerhof, G.G., "Bearing Capacity and Settlement of Pile Foundations", ASCE JGED, Vol. 102, No. GT3, March 1976, pp 196-228.
- [9] Paikowsky, S.G., and Whitman, R.V., "The Effects of Plugging on Pile Performance and Design", Canadian Geotechnical Journal, Vol. 27, pp 429-440.
- [10] Shantz, T., 2006, Personal Communication.

Appendix C: Ultimate Capacity Calculation Sheet—PYCAPSI

Below is a snapshot of the Excel spreadsheet developed by Professors Mokwa and Duncan to estimate the ultimate passive reaction against pile caps. The electronic file can be obtained by contacting Prof. Mokwa at: rmokwa@ce.montana.edu.

The screenshot shows the PYCAPSI Excel spreadsheet with the following data:

Ultimate Capacity Calculation Sheet - PYCAPSI			
Created by R.L. Mokwa and J.M. Duncan - August 1999			
Date:	10,10,2007		
Description:	Bulkhead in natural soil		
Engineer:	RLM		
Input Values (red)			
cap width, b (m) =			14.63
cap height, H (m) =			1.52
embedment depth, z (m) =			0.00
surcharge, q_s (kN/m ²) =			0.0
cohesion, c (kN/m ²) =			0.00
soil friction angle, ϕ (deg.) =			45.00
wall friction, δ (deg.) =			0
initial soil modulus, E_s (kN/m ²) =			42613
poisson's ratio, ν =			0.33
soil unit weight, γ_w (kN/m ³) =			21.21
adhesion factor, α =			0.00
Δ_{pc}/H , (0.04 suggested, see notes) =			0.04
Calculated Values (blue)			
K_d (Rankine) =			0.17
K_p (Rankine) =			5.83
K_c (Coulomb) =			5.83
K_{qs} (Log Spiral, soil weight) =	Rankine K_p		
K_{qs} (Log Spiral, surcharge) =	Rankine K_p		
K_{cc} (Log Spiral, cohesion) =	Rankine K_p		
E_p (kN/m) =			143.5
Ovesen's 3-D factor, R =			1.10
k_{pc} , elastic stiffness (kN/mm) =			644.2
P_{ur} (kN) =			2317.7
P_u (kips) =			521.0

LPILE		
p-y values for pile cap		
Depth (in) ==>	y (mm)	p (kN/mm)
0	10	<=== No. of data points
0.00	0.000	definig p-y curves
0.20	0.080	
0.80	0.280	
2.00	0.555	
6.00	0.987	
10.00	1.169	
15.00	1.288	
20.00	1.357	
40.00	1.475	
200.00	1.521	
1524	10	<=== No. of data points
0.00	0.0	definig p-y curves

The diagram shows a pile cap of width b and height H embedded in soil. A surcharge q_s is applied to the ground surface above the cap. The vertical axis is labeled z . A button labeled "Press to calculate P_{ur} " is shown next to the diagram.

PEER REPORTS

PEER reports are available from the National Information Service for Earthquake Engineering (NISEE). To order PEER reports, please contact the Pacific Earthquake Engineering Research Center, 1301 South 46th Street, Richmond, California 94804-4698. Tel.: (510) 665-3405; Fax: (510) 665-3420.

- PEER 2008/05** *Performance-Based Earthquake Engineering Design Evaluation Procedure for Bridge Foundations Undergoing Liquefaction-Induced Lateral Ground Displacement.* Christian A. Ledezma and Jonathan D. Bray. August 2008.
- PEER 2008/04** *Benchmarking of Nonlinear Geotechnical Ground Response Analysis Procedures.* Jonathan P. Stewart, Annie On-Lei Kwok, Youssef M. A. Hashash, Neven Matasovic, Robert Pyke, Zhiliang Wang, and Zhaohui Yang. August 2008.
- PEER 2008/02** *Treatment of Uncertainties in Seismic-Risk Analysis of Transportation Systems.* Evangelos Stergiou and Anne S. Kiremidjian. July 2008.
- PEER 2008/01** *Seismic Performance Objectives for Tall Buildings.* William T. Holmes, Charles Kircher, William Petak, and Nabih Youssef. August 2008.
- PEER 2007/12** *An Assessment to Benchmark the Seismic Performance of a Code-Conforming Reinforced Concrete Moment-Frame Building.* Curt Haselton, Christine A. Goulet, Judith Mitrani-Reiser, James L. Beck, Gregory G. Deierlein, Keith A. Porter, Jonathan P. Stewart, and Ertugrul Taciroglu. August 2008.
- PEER 2007/11** *Bar Buckling in Reinforced Concrete Bridge Columns.* Wayne A. Brown, Dawn E. Lehman, and John F. Stanton. February 2008.
- PEER 2007/10** *Computational Modeling of Progressive Collapse in Reinforced Concrete Frame Structures.* Mohamed M. Talaat and Khalid M. Mosalam. May 2008.
- PEER 2007/09** *Integrated Probabilistic Performance-Based Evaluation of Benchmark Reinforced Concrete Bridges.* Kevin R. Mackie, John-Michael Wong, and Božidar Stojadinović. January 2008.
- PEER 2007/08** *Assessing Seismic Collapse Safety of Modern Reinforced Concrete Moment-Frame Buildings.* Curt B. Haselton and Gregory G. Deierlein. February 2008.
- PEER 2007/07** *Performance Modeling Strategies for Modern Reinforced Concrete Bridge Columns.* Michael P. Berry and Marc O. Eberhard. April 2008.
- PEER 2007/06** *Development of Improved Procedures for Seismic Design of Buried and Partially Buried Structures.* Linda Al Atik and Nicholas Sitar. June 2007.
- PEER 2007/05** *Uncertainty and Correlation in Seismic Risk Assessment of Transportation Systems.* Renee G. Lee and Anne S. Kiremidjian. July 2007.
- PEER 2007/04** *Numerical Models for Analysis and Performance-Based Design of Shallow Foundations Subjected to Seismic Loading.* Sivapalan Gajan, Tara C. Hutchinson, Bruce L. Kutter, Prishati Raychowdhury, José A. Ugalde, and Jonathan P. Stewart. May 2008.
- PEER 2007/03** *Beam-Column Element Model Calibrated for Predicting Flexural Response Leading to Global Collapse of RC Frame Buildings.* Curt B. Haselton, Abbie B. Liel, Sarah Taylor Lange, and Gregory G. Deierlein. May 2008.
- PEER 2007/02** *Campbell-Bozorgnia NGA Ground Motion Relations for the Geometric Mean Horizontal Component of Peak and Spectral Ground Motion Parameters.* Kenneth W. Campbell and Yousef Bozorgnia. May 2007.
- PEER 2007/01** *Boore-Atkinson NGA Ground Motion Relations for the Geometric Mean Horizontal Component of Peak and Spectral Ground Motion Parameters.* David M. Boore and Gail M. Atkinson. May. May 2007.
- PEER 2006/12** *Societal Implications of Performance-Based Earthquake Engineering.* Peter J. May. May 2007.
- PEER 2006/11** *Probabilistic Seismic Demand Analysis Using Advanced Ground Motion Intensity Measures, Attenuation Relationships, and Near-Fault Effects.* Polsak Tothong and C. Allin Cornell. March 2007.
- PEER 2006/10** *Application of the PEER PBEE Methodology to the I-880 Viaduct.* Sashi Kunnath. February 2007.
- PEER 2006/09** *Quantifying Economic Losses from Travel Forgone Following a Large Metropolitan Earthquake.* James Moore, Sungbin Cho, Yue Yue Fan, and Stuart Werner. November 2006.
- PEER 2006/08** *Vector-Valued Ground Motion Intensity Measures for Probabilistic Seismic Demand Analysis.* Jack W. Baker and C. Allin Cornell. October 2006.
- PEER 2006/07** *Analytical Modeling of Reinforced Concrete Walls for Predicting Flexural and Coupled-Shear-Flexural Responses.* Kutay Orakcal, Loenardo M. Massone, and John W. Wallace. October 2006.

- PEER 2006/06** *Nonlinear Analysis of a Soil-Drilled Pier System under Static and Dynamic Axial Loading.* Gang Wang and Nicholas Sitar. November 2006.
- PEER 2006/05** *Advanced Seismic Assessment Guidelines.* Paolo Bazzurro, C. Allin Cornell, Charles Menun, Maziar Motahari, and Nicolas Luco. September 2006.
- PEER 2006/04** *Probabilistic Seismic Evaluation of Reinforced Concrete Structural Components and Systems.* Tae Hyung Lee and Khalid M. Mosalam. August 2006.
- PEER 2006/03** *Performance of Lifelines Subjected to Lateral Spreading.* Scott A. Ashford and Teerawut Juirnarongrit. July 2006.
- PEER 2006/02** *Pacific Earthquake Engineering Research Center Highway Demonstration Project.* Anne Kiremidjian, James Moore, Yue Yue Fan, Nesrin Basoz, Ozgur Yazali, and Meredith Williams. April 2006.
- PEER 2006/01** *Bracing Berkeley. A Guide to Seismic Safety on the UC Berkeley Campus.* Mary C. Comerio, Stephen Tobriner, and Ariane Fehrenkamp. January 2006.
- PEER 2005/16** *Seismic Response and Reliability of Electrical Substation Equipment and Systems.* Junho Song, Armen Der Kiureghian, and Jerome L. Sackman. April 2006.
- PEER 2005/15** *CPT-Based Probabilistic Assessment of Seismic Soil Liquefaction Initiation.* R. E. S. Moss, R. B. Seed, R. E. Kayen, J. P. Stewart, and A. Der Kiureghian. April 2006.
- PEER 2005/14** *Workshop on Modeling of Nonlinear Cyclic Load-Deformation Behavior of Shallow Foundations.* Bruce L. Kutter, Geoffrey Martin, Tara Hutchinson, Chad Harden, Sivapalan Gajan, and Justin Phalen. March 2006.
- PEER 2005/13** *Stochastic Characterization and Decision Bases under Time-Dependent Aftershock Risk in Performance-Based Earthquake Engineering.* Gee Liek Yeo and C. Allin Cornell. July 2005.
- PEER 2005/12** *PEER Testbed Study on a Laboratory Building: Exercising Seismic Performance Assessment.* Mary C. Comerio, editor. November 2005.
- PEER 2005/11** *Van Nuys Hotel Building Testbed Report: Exercising Seismic Performance Assessment.* Helmut Krawinkler, editor. October 2005.
- PEER 2005/10** *First NEES/E-Defense Workshop on Collapse Simulation of Reinforced Concrete Building Structures.* September 2005.
- PEER 2005/09** *Test Applications of Advanced Seismic Assessment Guidelines.* Joe Maffei, Karl Telleen, Danya Mohr, William Holmes, and Yuki Nakayama. August 2006.
- PEER 2005/08** *Damage Accumulation in Lightly Confined Reinforced Concrete Bridge Columns.* R. Tyler Ranf, Jared M. Nelson, Zach Price, Marc O. Eberhard, and John F. Stanton. April 2006.
- PEER 2005/07** *Experimental and Analytical Studies on the Seismic Response of Freestanding and Anchored Laboratory Equipment.* Dimitrios Konstantinidis and Nicos Makris. January 2005.
- PEER 2005/06** *Global Collapse of Frame Structures under Seismic Excitations.* Luis F. Ibarra and Helmut Krawinkler. September 2005.
- PEER 2005/05** *Performance Characterization of Bench- and Shelf-Mounted Equipment.* Samit Ray Chaudhuri and Tara C. Hutchinson. May 2006.
- PEER 2005/04** *Numerical Modeling of the Nonlinear Cyclic Response of Shallow Foundations.* Chad Harden, Tara Hutchinson, Geoffrey R. Martin, and Bruce L. Kutter. August 2005.
- PEER 2005/03** *A Taxonomy of Building Components for Performance-Based Earthquake Engineering.* Keith A. Porter. September 2005.
- PEER 2005/02** *Fragility Basis for California Highway Overpass Bridge Seismic Decision Making.* Kevin R. Mackie and Božidar Stojadinović. June 2005.
- PEER 2005/01** *Empirical Characterization of Site Conditions on Strong Ground Motion.* Jonathan P. Stewart, Yoojoong Choi, and Robert W. Graves. June 2005.
- PEER 2004/09** *Electrical Substation Equipment Interaction: Experimental Rigid Conductor Studies.* Christopher Stearns and André Filiatrault. February 2005.
- PEER 2004/08** *Seismic Qualification and Fragility Testing of Line Break 550-kV Disconnect Switches.* Shakhzod M. Takhirov, Gregory L. Fenves, and Eric Fujisaki. January 2005.
- PEER 2004/07** *Ground Motions for Earthquake Simulator Qualification of Electrical Substation Equipment.* Shakhzod M. Takhirov, Gregory L. Fenves, Eric Fujisaki, and Don Clyde. January 2005.
- PEER 2004/06** *Performance-Based Regulation and Regulatory Regimes.* Peter J. May and Chris Koski. September 2004.

- PEER 2004/05** *Performance-Based Seismic Design Concepts and Implementation: Proceedings of an International Workshop.* Peter Fajfar and Helmut Krawinkler, editors. September 2004.
- PEER 2004/04** *Seismic Performance of an Instrumented Tilt-up Wall Building.* James C. Anderson and Vitelmo V. Bertero. July 2004.
- PEER 2004/03** *Evaluation and Application of Concrete Tilt-up Assessment Methodologies.* Timothy Graf and James O. Malley. October 2004.
- PEER 2004/02** *Analytical Investigations of New Methods for Reducing Residual Displacements of Reinforced Concrete Bridge Columns.* Junichi Sakai and Stephen A. Mahin. August 2004.
- PEER 2004/01** *Seismic Performance of Masonry Buildings and Design Implications.* Kerri Anne Taeko Tokoro, James C. Anderson, and Vitelmo V. Bertero. February 2004.
- PEER 2003/18** *Performance Models for Flexural Damage in Reinforced Concrete Columns.* Michael Berry and Marc Eberhard. August 2003.
- PEER 2003/17** *Predicting Earthquake Damage in Older Reinforced Concrete Beam-Column Joints.* Catherine Pagni and Laura Lowes. October 2004.
- PEER 2003/16** *Seismic Demands for Performance-Based Design of Bridges.* Kevin Mackie and Božidar Stojadinović. August 2003.
- PEER 2003/15** *Seismic Demands for Nondeteriorating Frame Structures and Their Dependence on Ground Motions.* Ricardo Antonio Medina and Helmut Krawinkler. May 2004.
- PEER 2003/14** *Finite Element Reliability and Sensitivity Methods for Performance-Based Earthquake Engineering.* Terje Haukaas and Armen Der Kiureghian. April 2004.
- PEER 2003/13** *Effects of Connection Hysteretic Degradation on the Seismic Behavior of Steel Moment-Resisting Frames.* Janise E. Rodgers and Stephen A. Mahin. March 2004.
- PEER 2003/12** *Implementation Manual for the Seismic Protection of Laboratory Contents: Format and Case Studies.* William T. Holmes and Mary C. Comerio. October 2003.
- PEER 2003/11** *Fifth U.S.-Japan Workshop on Performance-Based Earthquake Engineering Methodology for Reinforced Concrete Building Structures.* February 2004.
- PEER 2003/10** *A Beam-Column Joint Model for Simulating the Earthquake Response of Reinforced Concrete Frames.* Laura N. Lowes, Nilanjan Mitra, and Arash Altoontash. February 2004.
- PEER 2003/09** *Sequencing Repairs after an Earthquake: An Economic Approach.* Marco Casari and Simon J. Wilkie. April 2004.
- PEER 2003/08** *A Technical Framework for Probability-Based Demand and Capacity Factor Design (DCFD) Seismic Formats.* Fatemeh Jalayer and C. Allin Cornell. November 2003.
- PEER 2003/07** *Uncertainty Specification and Propagation for Loss Estimation Using FOSM Methods.* Jack W. Baker and C. Allin Cornell. September 2003.
- PEER 2003/06** *Performance of Circular Reinforced Concrete Bridge Columns under Bidirectional Earthquake Loading.* Mahmoud M. Hachem, Stephen A. Mahin, and Jack P. Moehle. February 2003.
- PEER 2003/05** *Response Assessment for Building-Specific Loss Estimation.* Eduardo Miranda and Shahram Taghavi. September 2003.
- PEER 2003/04** *Experimental Assessment of Columns with Short Lap Splices Subjected to Cyclic Loads.* Murat Melek, John W. Wallace, and Joel Conte. April 2003.
- PEER 2003/03** *Probabilistic Response Assessment for Building-Specific Loss Estimation.* Eduardo Miranda and Hesameddin Aslani. September 2003.
- PEER 2003/02** *Software Framework for Collaborative Development of Nonlinear Dynamic Analysis Program.* Jun Peng and Kincho H. Law. September 2003.
- PEER 2003/01** *Shake Table Tests and Analytical Studies on the Gravity Load Collapse of Reinforced Concrete Frames.* Kenneth John Elwood and Jack P. Moehle. November 2003.
- PEER 2002/24** *Performance of Beam to Column Bridge Joints Subjected to a Large Velocity Pulse.* Natalie Gibson, André Filiatrault, and Scott A. Ashford. April 2002.
- PEER 2002/23** *Effects of Large Velocity Pulses on Reinforced Concrete Bridge Columns.* Greg L. Orozco and Scott A. Ashford. April 2002.
- PEER 2002/22** *Characterization of Large Velocity Pulses for Laboratory Testing.* Kenneth E. Cox and Scott A. Ashford. April 2002.

- PEER 2002/21** *Fourth U.S.-Japan Workshop on Performance-Based Earthquake Engineering Methodology for Reinforced Concrete Building Structures.* December 2002.
- PEER 2002/20** *Barriers to Adoption and Implementation of PBEE Innovations.* Peter J. May. August 2002.
- PEER 2002/19** *Economic-Engineered Integrated Models for Earthquakes: Socioeconomic Impacts.* Peter Gordon, James E. Moore II, and Harry W. Richardson. July 2002.
- PEER 2002/18** *Assessment of Reinforced Concrete Building Exterior Joints with Substandard Details.* Chris P. Pantelides, Jon Hansen, Justin Nadauld, and Lawrence D. Reaveley. May 2002.
- PEER 2002/17** *Structural Characterization and Seismic Response Analysis of a Highway Overcrossing Equipped with Elastomeric Bearings and Fluid Dampers: A Case Study.* Nicos Makris and Jian Zhang. November 2002.
- PEER 2002/16** *Estimation of Uncertainty in Geotechnical Properties for Performance-Based Earthquake Engineering.* Allen L. Jones, Steven L. Kramer, and Pedro Arduino. December 2002.
- PEER 2002/15** *Seismic Behavior of Bridge Columns Subjected to Various Loading Patterns.* Asadollah Esmaeily-Gh. and Yan Xiao. December 2002.
- PEER 2002/14** *Inelastic Seismic Response of Extended Pile Shaft Supported Bridge Structures.* T.C. Hutchinson, R.W. Boulanger, Y.H. Chai, and I.M. Idriss. December 2002.
- PEER 2002/13** *Probabilistic Models and Fragility Estimates for Bridge Components and Systems.* Paolo Gardoni, Armen Der Kiureghian, and Khalid M. Mosalam. June 2002.
- PEER 2002/12** *Effects of Fault Dip and Slip Rake on Near-Source Ground Motions: Why Chi-Chi Was a Relatively Mild M7.6 Earthquake.* Brad T. Aagaard, John F. Hall, and Thomas H. Heaton. December 2002.
- PEER 2002/11** *Analytical and Experimental Study of Fiber-Reinforced Strip Isolators.* James M. Kelly and Shakhzod M. Takhirov. September 2002.
- PEER 2002/10** *Centrifuge Modeling of Settlement and Lateral Spreading with Comparisons to Numerical Analyses.* Sivapalan Gajan and Bruce L. Kutter. January 2003.
- PEER 2002/09** *Documentation and Analysis of Field Case Histories of Seismic Compression during the 1994 Northridge, California, Earthquake.* Jonathan P. Stewart, Patrick M. Smith, Daniel H. Whang, and Jonathan D. Bray. October 2002.
- PEER 2002/08** *Component Testing, Stability Analysis and Characterization of Buckling-Restrained Unbonded Braces™.* Cameron Black, Nicos Makris, and Ian Aiken. September 2002.
- PEER 2002/07** *Seismic Performance of Pile-Wharf Connections.* Charles W. Roeder, Robert Graff, Jennifer Soderstrom, and Jun Han Yoo. December 2001.
- PEER 2002/06** *The Use of Benefit-Cost Analysis for Evaluation of Performance-Based Earthquake Engineering Decisions.* Richard O. Zerbe and Anthony Falit-Baiamonte. September 2001.
- PEER 2002/05** *Guidelines, Specifications, and Seismic Performance Characterization of Nonstructural Building Components and Equipment.* André Filiatrault, Constantin Christopoulos, and Christopher Stearns. September 2001.
- PEER 2002/04** *Consortium of Organizations for Strong-Motion Observation Systems and the Pacific Earthquake Engineering Research Center Lifelines Program: Invited Workshop on Archiving and Web Dissemination of Geotechnical Data, 4–5 October 2001.* September 2002.
- PEER 2002/03** *Investigation of Sensitivity of Building Loss Estimates to Major Uncertain Variables for the Van Nuys Testbed.* Keith A. Porter, James L. Beck, and Rustem V. Shaikhutdinov. August 2002.
- PEER 2002/02** *The Third U.S.-Japan Workshop on Performance-Based Earthquake Engineering Methodology for Reinforced Concrete Building Structures.* July 2002.
- PEER 2002/01** *Nonstructural Loss Estimation: The UC Berkeley Case Study.* Mary C. Comerio and John C. Stallmeyer. December 2001.
- PEER 2001/16** *Statistics of SDF-System Estimate of Roof Displacement for Pushover Analysis of Buildings.* Anil K. Chopra, Rakesh K. Goel, and Chatpan Chintanapakdee. December 2001.
- PEER 2001/15** *Damage to Bridges during the 2001 Nisqually Earthquake.* R. Tyler Ranf, Marc O. Eberhard, and Michael P. Berry. November 2001.
- PEER 2001/14** *Rocking Response of Equipment Anchored to a Base Foundation.* Nicos Makris and Cameron J. Black. September 2001.
- PEER 2001/13** *Modeling Soil Liquefaction Hazards for Performance-Based Earthquake Engineering.* Steven L. Kramer and Ahmed-W. Elgamal. February 2001.

- PEER 2001/12** *Development of Geotechnical Capabilities in OpenSees.* Boris Jeremi . September 2001.
- PEER 2001/11** *Analytical and Experimental Study of Fiber-Reinforced Elastomeric Isolators.* James M. Kelly and Shakhzod M. Takhirov. September 2001.
- PEER 2001/10** *Amplification Factors for Spectral Acceleration in Active Regions.* Jonathan P. Stewart, Andrew H. Liu, Yoojoong Choi, and Mehmet B. Baturay. December 2001.
- PEER 2001/09** *Ground Motion Evaluation Procedures for Performance-Based Design.* Jonathan P. Stewart, Shyh-Jeng Chiou, Jonathan D. Bray, Robert W. Graves, Paul G. Somerville, and Norman A. Abrahamson. September 2001.
- PEER 2001/08** *Experimental and Computational Evaluation of Reinforced Concrete Bridge Beam-Column Connections for Seismic Performance.* Clay J. Naito, Jack P. Moehle, and Khalid M. Mosalam. November 2001.
- PEER 2001/07** *The Rocking Spectrum and the Shortcomings of Design Guidelines.* Nicos Makris and Dimitrios Konstantinidis. August 2001.
- PEER 2001/06** *Development of an Electrical Substation Equipment Performance Database for Evaluation of Equipment Fragilities.* Thalia Agnanos. April 1999.
- PEER 2001/05** *Stiffness Analysis of Fiber-Reinforced Elastomeric Isolators.* Hsiang-Chuan Tsai and James M. Kelly. May 2001.
- PEER 2001/04** *Organizational and Societal Considerations for Performance-Based Earthquake Engineering.* Peter J. May. April 2001.
- PEER 2001/03** *A Modal Pushover Analysis Procedure to Estimate Seismic Demands for Buildings: Theory and Preliminary Evaluation.* Anil K. Chopra and Rakesh K. Goel. January 2001.
- PEER 2001/02** *Seismic Response Analysis of Highway Overcrossings Including Soil-Structure Interaction.* Jian Zhang and Nicos Makris. March 2001.
- PEER 2001/01** *Experimental Study of Large Seismic Steel Beam-to-Column Connections.* Egor P. Popov and Shakhzod M. Takhirov. November 2000.
- PEER 2000/10** *The Second U.S.-Japan Workshop on Performance-Based Earthquake Engineering Methodology for Reinforced Concrete Building Structures.* March 2000.
- PEER 2000/09** *Structural Engineering Reconnaissance of the August 17, 1999 Earthquake: Kocaeli (Izmit), Turkey.* Halil Sezen, Kenneth J. Elwood, Andrew S. Whittaker, Khalid Mosalam, John J. Wallace, and John F. Stanton. December 2000.
- PEER 2000/08** *Behavior of Reinforced Concrete Bridge Columns Having Varying Aspect Ratios and Varying Lengths of Confinement.* Anthony J. Calderone, Dawn E. Lehman, and Jack P. Moehle. January 2001.
- PEER 2000/07** *Cover-Plate and Flange-Plate Reinforced Steel Moment-Resisting Connections.* Taejin Kim, Andrew S. Whittaker, Amir S. Gilani, Vitelmo V. Bertero, and Shakhzod M. Takhirov. September 2000.
- PEER 2000/06** *Seismic Evaluation and Analysis of 230-kV Disconnect Switches.* Amir S. J. Gilani, Andrew S. Whittaker, Gregory L. Fenves, Chun-Hao Chen, Henry Ho, and Eric Fujisaki. July 2000.
- PEER 2000/05** *Performance-Based Evaluation of Exterior Reinforced Concrete Building Joints for Seismic Excitation.* Chandra Clyde, Chris P. Pantelides, and Lawrence D. Reaveley. July 2000.
- PEER 2000/04** *An Evaluation of Seismic Energy Demand: An Attenuation Approach.* Chung-Che Chou and Chia-Ming Uang. July 1999.
- PEER 2000/03** *Framing Earthquake Retrofitting Decisions: The Case of Hillside Homes in Los Angeles.* Detlof von Winterfeldt, Nels Roselund, and Alicia Kitsuse. March 2000.
- PEER 2000/02** *U.S.-Japan Workshop on the Effects of Near-Field Earthquake Shaking.* Andrew Whittaker, ed. July 2000.
- PEER 2000/01** *Further Studies on Seismic Interaction in Interconnected Electrical Substation Equipment.* Armen Der Kiureghian, Kee-Jeung Hong, and Jerome L. Sackman. November 1999.
- PEER 1999/14** *Seismic Evaluation and Retrofit of 230-kV Porcelain Transformer Bushings.* Amir S. Gilani, Andrew S. Whittaker, Gregory L. Fenves, and Eric Fujisaki. December 1999.
- PEER 1999/13** *Building Vulnerability Studies: Modeling and Evaluation of Tilt-up and Steel Reinforced Concrete Buildings.* John W. Wallace, Jonathan P. Stewart, and Andrew S. Whittaker, editors. December 1999.
- PEER 1999/12** *Rehabilitation of Nonductile RC Frame Building Using Encasement Plates and Energy-Dissipating Devices.* Mehrdad Sasani, Vitelmo V. Bertero, James C. Anderson. December 1999.
- PEER 1999/11** *Performance Evaluation Database for Concrete Bridge Components and Systems under Simulated Seismic Loads.* Yael D. Hose and Frieder Seible. November 1999.

- PEER 1999/10** *U.S.-Japan Workshop on Performance-Based Earthquake Engineering Methodology for Reinforced Concrete Building Structures.* December 1999.
- PEER 1999/09** *Performance Improvement of Long Period Building Structures Subjected to Severe Pulse-Type Ground Motions.* James C. Anderson, Vitelmo V. Bertero, and Raul Bertero. October 1999.
- PEER 1999/08** *Envelopes for Seismic Response Vectors.* Charles Menun and Armen Der Kiureghian. July 1999.
- PEER 1999/07** *Documentation of Strengths and Weaknesses of Current Computer Analysis Methods for Seismic Performance of Reinforced Concrete Members.* William F. Cofer. November 1999.
- PEER 1999/06** *Rocking Response and Overturning of Anchored Equipment under Seismic Excitations.* Nicos Makris and Jian Zhang. November 1999.
- PEER 1999/05** *Seismic Evaluation of 550 kV Porcelain Transformer Bushings.* Amir S. Gilani, Andrew S. Whittaker, Gregory L. Fenves, and Eric Fujisaki. October 1999.
- PEER 1999/04** *Adoption and Enforcement of Earthquake Risk-Reduction Measures.* Peter J. May, Raymond J. Burby, T. Jens Feeley, and Robert Wood.
- PEER 1999/03** *Task 3 Characterization of Site Response General Site Categories.* Adrian Rodriguez-Marek, Jonathan D. Bray, and Norman Abrahamson. February 1999.
- PEER 1999/02** *Capacity-Demand-Diagram Methods for Estimating Seismic Deformation of Inelastic Structures: SDF Systems.* Anil K. Chopra and Rakesh Goel. April 1999.
- PEER 1999/01** *Interaction in Interconnected Electrical Substation Equipment Subjected to Earthquake Ground Motions.* Armen Der Kiureghian, Jerome L. Sackman, and Kee-Jeung Hong. February 1999.
- PEER 1998/08** *Behavior and Failure Analysis of a Multiple-Frame Highway Bridge in the 1994 Northridge Earthquake.* Gregory L. Fenves and Michael Ellery. December 1998.
- PEER 1998/07** *Empirical Evaluation of Inertial Soil-Structure Interaction Effects.* Jonathan P. Stewart, Raymond B. Seed, and Gregory L. Fenves. November 1998.
- PEER 1998/06** *Effect of Damping Mechanisms on the Response of Seismic Isolated Structures.* Nicos Makris and Shih-Po Chang. November 1998.
- PEER 1998/05** *Rocking Response and Overturning of Equipment under Horizontal Pulse-Type Motions.* Nicos Makris and Yiannis Roussos. October 1998.
- PEER 1998/04** *Pacific Earthquake Engineering Research Invitational Workshop Proceedings, May 14–15, 1998: Defining the Links between Planning, Policy Analysis, Economics and Earthquake Engineering.* Mary Comerio and Peter Gordon. September 1998.
- PEER 1998/03** *Repair/Upgrade Procedures for Welded Beam to Column Connections.* James C. Anderson and Xiaojing Duan. May 1998.
- PEER 1998/02** *Seismic Evaluation of 196 kV Porcelain Transformer Bushings.* Amir S. Gilani, Juan W. Chavez, Gregory L. Fenves, and Andrew S. Whittaker. May 1998.
- PEER 1998/01** *Seismic Performance of Well-Confined Concrete Bridge Columns.* Dawn E. Lehman and Jack P. Moehle. December 2000.

ONLINE REPORTS

The following PEER reports are available by Internet only at http://peer.berkeley.edu/publications/peer_reports.html

- PEER 2008/101** *Seismic Performance Objectives for Tall Buildings*. William T. Holmes, Charles Kircher, William Petak, and Nabih Youssef. August 2008.
- PEER 2007/101** *Generalized Hybrid Simulation Framework for Structural Systems Subjected to Seismic Loading*. Tarek Elkhoraibi and Khalid M. Mosalam. July 2007.
- PEER 2007/100** *Seismic Evaluation of Reinforced Concrete Buildings Including Effects of Masonry Infill Walls*. Alidad Hashemi and Khalid M. Mosalam. July 2007.

